Characterization of the interactions between Caspase-9 and phosphatases PP1A and PP2A in apoptosis: applications as therapeutic target in cancer

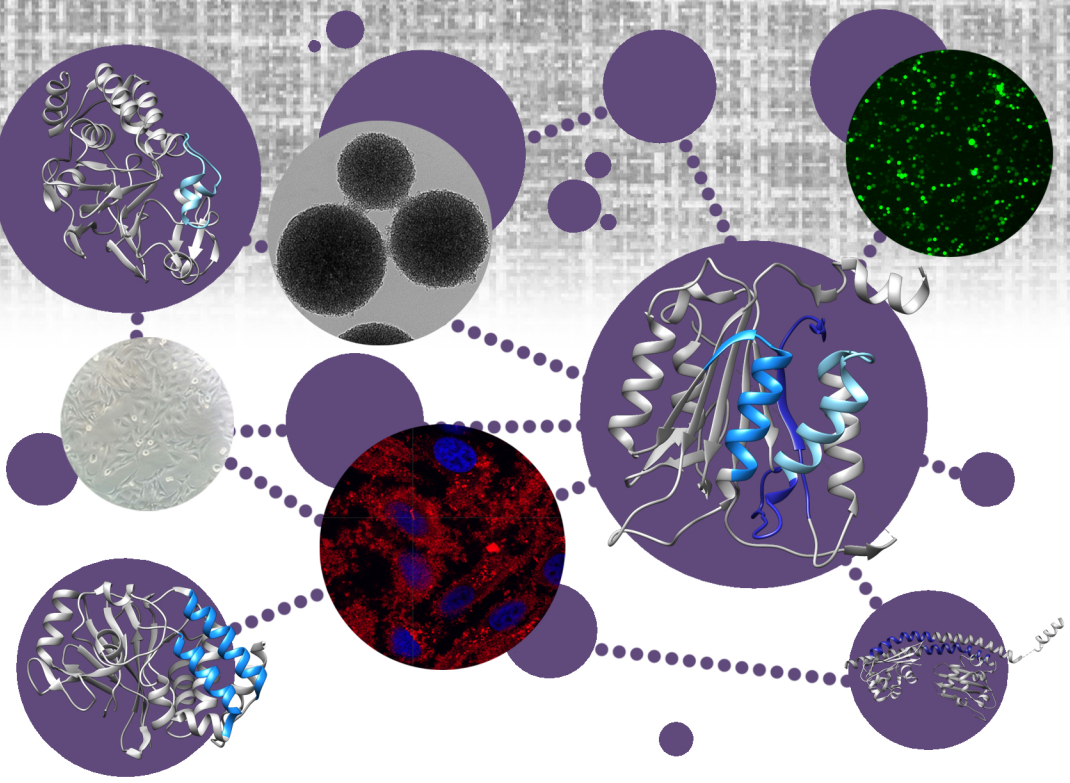

Leticia Domínguez Berrocal

Tesis doctoral 2015

VNiVERSiDAD D SALAMANCA
CAMPUS OF INTERNATIONAL EXCELLENCE

ibv INSTITUTO DE BIOMEDICINA DE VALENCIA CSIC

CSIC
CONSEJO SUPERIOR DE INVESTIGACIONES CIENTÍFICAS

Characterization of the interactions between Caspase-9 and phosphatases PP1A and PP2A in apoptosis: applications as therapeutic target in cancer

Leticia Domínguez Berrocal

A dissertation presented to the Faculty of the Graduate School of the University of Salamanca in candidacy for the degree of Doctor of Philosophy.

November 2015

Caracterización de las interacciones entre Caspasa-9 y las fosfatasas PP1A y PP2A en apoptosis: aplicaciones como diana terapéutica en cáncer

Leticia Domínguez Berrocal

Memoria presentada en la Escuela de Doctorado de la Universidad de Salamanca para optar al grado de Doctor.

Noviembre 2015

Dr. Jerónimo Bravo Sicilia, Científico Titular del Consejo Superior de Investigaciones Científicas (CSIC) en el Instituto de Biomedicina de Valencia (IBV-CSIC)

CERTIFICA:

Que Dña. Leticia Domínguez Berrocal, licenciada en Biología por la Universidad de Salamanca, ha realizado bajo su dirección el trabajo de Tesis Doctoral que lleva por título "**Characterization of the interactions between Caspase-9 and phosphatases PP1A and PP2A in apoptosis: applications as therapeutic target in cancer"**, y considera que éste reúne originalidad y contenidos suficientes para que sea presentada ante el Tribunal correspondiente y optar al Grado de Doctor por la Universidad de Salamanca.

Y para que así conste a los efectos oportunos, expide el presente certificado en Valencia, a de Noviembre de 2015.

Dr. Jerónimo Bravo Sicilia
Director de la tesis

To my parents.

To my grandmother Orfe.

A mis padres.

A mi abuela Orfe.

ACKNOWLEDGEMENTS / AGRADECIMIENTOS

In this section I don’t want to skip the opportunity to express my gratitude to all the people who have supported this work in one way or another. The thesis is written in English, as it is the language of science, but I also consider that my feelings have to be written in my native language, Spanish.

En primer lugar quiero agradecer a Jero, mi director de tesis, por darme la oportunidad de satisfacer mi motivación por la investigación y permitirme hacer la tesis en tu laboratorio, a pesar de que mi cometido inicial en el grupo fuera totalmente diferente, y confiar en mí para embarcarme en este proyecto. Gracias también por todo lo que he podido aprender durante estos años.

GRACIAS con mayúsculas a mis compañeros de laboratorio; sin vosotros esto habría sido muchísimo más duro todavía. Gracias Marcin, por tu motivación contagiosa, por tus ideas siempre útiles, por tu bendita locura, por las noches de “Polonia” y por las de Benimaclet, por estar siempre ahí, por crear una amistad para toda la vida. Gracias Sara, por acogerme en el lab con los brazos abiertos, por guiarme en los comienzos en un campo totalmente nuevo para mí, por la “música de trabajar”, por las idas de pinza y los gafes que nos alegran el día y por compartir tantos consejos y opiniones en esta etapa final que estamos viviendo a la par. Espero seguir compartiendo muchas cosas contigo. Gracias Nada, you taught me babaganoush, but more importantly, you taught me how to be a better person and more open-minded, to love people and to love animals, but not enough to quit jamón and polish sausages. I’m proud of you; you have a friend on me wherever we may be.

Gracias también a las que ya no están en el laboratorio, como Sandrea, gracias por tus conversaciones, por tus ataques de risa, por los vídeos de Bollywood en los días de oscurantismo científico y por ser un ejemplo en el laboratorio. Te deseo lo mejor en tu nueva vida y espero volver a verte pronto. Gracias Isa, por aportar un punto de sensatez en la locura predoctoral y ser tan buena compañera.

Gracias a Susana, a Jéssica y al resto de técnicos que han pasado por el laboratorio durante estos años y que nos han facilitado el trabajo y siempre han aportado algo al grupo.

Gracias a Miriam Guillén, mi pequeño saltamontes, por ayudarme tanto en el tiempo que compartimos, por tu entrega y por darme el empujoncito de motivación que necesitaba para acabar. Amiga, llegarás lejos y espero que volvamos a trabajar juntas, somos un gran equipo. Gracias también a Miriam Valera y al resto de estudiantes en prácticas a los que he formado, porque de todos vosotros he aprendido algo.

Gracias a mis colaboradores, sin vosotros gran parte de este trabajo no habría sido posible. Gracias a Angelita, por la estrecha colaboración que hemos tenido estos años, por los skypes, por los envíos de péptido, muestras o cualquier cosa que necesitara, por estar disponible para atender mis mensajes y por confiar en mí para el futuro. Gracias a Jesús, por tus grandes ideas, tus sabios consejos y tu generosa ayuda; cada vez que hablo contigo aprendo algo. Me gustaría seguir trabajando contigo mucho tiempo.

Gracias a Cristina de la Torre por sintetizar las nanopartículas y participar activamente para que esta parte del proyecto salga adelante, y a José Ramón Murguía por habernos puesto en contacto. Gracias también a Pablo Luján y al fallecido Quique Pérez-Payá por cedernos sus equipos y ayudarnos con los experimentos que necesitábamos hacer en sus instalaciones.

Gracias a la gente del IBV, por mantener un buen ambiente de trabajo y hacer que todo el mundo se sienta bienvenido en el instituto. Especialmente quiero agradecer a los vecinos, los Albertos, por estar siempre disponibles a ayudarnos y dejarnos cualquier cosa que necesitemos y por ser tan majos. También tienen mi gratitud los compañeros de la sala de cultivos, que me han dado buenos consejos y buenos ratos. También quiero agradecer especialmente a algunas de las chicas del IBV, porque desde vuestra experiencia siempre tenéis disponible una sonrisa, palabras de ánimo y ayuda, gracias Ada, Libia, Nadine, Belén, Patri y Elisa por animarme a seguir adelante.

GRACIAS a Pablo, también gracias con mayúsculas, por tu amor sin condiciones, por tu apoyo y comprensión infinitos, a pesar de no trabajar en ciencia. Por haber estado a mi lado todo este tiempo y creer en mí hasta en los momentos más difíciles. Las palabras se quedan pequeñas…

Gracias a mis amigos de Madrid, por haberme sentido una más del grupo desde el primer día, por recibirme siempre con los brazos abiertos y contar siempre conmigo aunque no nos veamos en persona todo lo que me gustaría y por vuestras visitas a Valencia que me cargan las pilas. Gracias especialmente a Raúl por intentar salvar mis viejos ordenadores por inoportuno que fuera el momento y a Irene por ayudarme a hacer que esta tesis sea un poco más bonita.

Gracias también a mis amigos de la carrera, Gustavo, Laura y Lucía. A pesar de que nuestros caminos se van separando seguís ahí y da gusto volvernos a encontrar y compartir cómo vamos creciendo. Gracias también a María y Pul, por vuestra amistad intemporal.

Por supuesto, gracias a mis padres, sin los cuales no estaría aquí. Gracias por darme la oportunidad de estudiar y por inculcarme valores como el esfuerzo, el trabajo duro, la austeridad, el respeto y la capacidad de ayudar a los demás que tanto me han servido durante todos estos años. Gracias a la abuela Orfe, por enseñarme tantas cosas de la vida y por interesarte siempre en lo que hago. Gracias Ofelia, por estar siempre ahí y haber compartido tantas cosas buenas desde que andaba a gatas.

Gracias a todos, sin vosotros mi vida y mi tesis no habrían sido posibles.

INDEX

ÍNDICE

INDEX OF FIGURES

INDEX OF TABLES

ABBREVIATIONS

AOBS acoustic optical beam splitter

Apaf-1 apoptosis protease-activating factor-1

ATP adenosine triphosphate

BAD Bcl-2-associated death promoter

Bcl-2 B-cell lymphoma 2

BID BH3 interacting-domain death agonist

BLI biolayer interferometry

BSA bovine serum albumin

CARD caspase activation and recruitment domain

CD5, 19, 20, 22, 23, 79b cluster of differentiation 5, 19, 20, 22, 23, 79b

CDK1 cyclin-dependent kinase 1

cDNA complementary DNA

CHES *N*-Cyclohexyl-2-aminoethanesulfonic acid

CK2 casein kinase 2

CLL chronic lymphocytic leukemia

CPPs cell-penetrating peptides

CTAB hexadecyltrimethyl ammonium bromide

dATP deoxyadenosine triphosphate

DED death effector domain

DEPC diethylpyrocarbonate

DISC death-inducing signaling complex

DMEM Dulbecco’s modified Eagle medium

DMSO dimethyl sulfoxide

DNA deoxyribonucleic acid

dNTPs deoxynucleotides triphosphate

DPT phosphatase-derived drug technology

DR4 death receptor 4

DR5 death receptor 5

DTT dithiothreitol

DYRK1A dual specificity tyrosine-phosphorylation-regulated kinase 1A

ECL enhanced chemiluminiscence

EDTA ethylenediaminetetraacetic acid

ERK extracellular-signal-regulated kinase

FACS fluorescence-activated cell sorting

FADD Fas-associated protein with death domain

FBS fetal bovine serum

FFT fast Fourier transform

FITC fluorescein isothiocyanate

Fmoc 9-fluorenylmethyloxycarbonyl

FRM fast rotational method

GAPDH glyceraldehyde 3-phosphate dehydrogenase

GST glutathione S-transferase

HD healthy donor

HPLC high-performance liquid chromatography

HRP horseradish peroxidase

HTS high-throughput screening

ICAD inhibitor of caspase activated DNAse

IgV_H immunoglobulin variable-region heavy chain

IgV_L immunoglobulin variable-region light chain

IL-2 interleukin 2

IPTG isopropyl β-D-1-thiogalactopyranoside

ITC isothermal titration calorimetry

K_D dissociation constant

kDa kilodaltons

LIC ligation independent cloning

m.o.i. multiplicity of infection

MBP maltose binding protein

Mcl-1 Induced myeloid leukemia cell differentiation protein

MCM-41 mobil composition of matter No. 41

mRNA messenger ribonucleic acid

MSNs mesoporous silica nanoparticles

MyPhoNE myosin phosphatase N-terminal element

NHL B-cell non-Hodgkin lymphoma

Ni-NTA nickel-nitrilotriacetic acid

NK natural killer

NSCLC non small cell lung cancer

PBMC peripheral blood mononuclear cells

PBS phosphate-buffered saline

PCR polymerase chain reaction

PDB protein data bank

PEG polyethylene glycol

PI propidium iodide

PI-3K Phosphatidylinositol-4,5-bisphosphate 3-kinase

PIPs PP1-interacting proteins

PKA protein kinase A

PKB protein kinase B

PKCζ protein kinase Cζ

PME-1 protein phosphatase methyl esterase-1

PO peroxidase

PP1 protein phosphatase 1

PP2A protein phosphatase 2A

PP5 protein phosphatase 5

PPP phosphoprotein phosphatases

RIP receptor-interacting protein

RIPK1 receptor-interacting serine/threonine-protein kinase 1

RIPK3 receptor-interacting serine/threonine-protein kinase 3

RNA ribonucleic acid

ROS reactive oxygen species

RPMI Roswell park memorial institute medium

RT-PCR reverse transcription polymerase chain reaction

SDS sodium dodecyl sulfate

SDS-PAGE sodium dodecyl sulfate polyacrylamide gel electrophoresis

SE size exclusion

SF3B1 splicing factor 3B subunit 1

siRNA small interfering ribonucleic acid

snRNP small nuclear ribonucleic protein

TBST Tris-buffered saline Tween 20

TCEP tris (2-carboxyethyl) phosphine

TEOS tetraethylorthosilicate

TFE trifluoroethanol

TNFR1 tumor necrosis factor receptor 1

TNFα tumor necrosis factor α

TRADD tumor necrosis factor receptor type 1-associated DEATH domain protein

TRAIL tumor necrosis factor related apoptosis inducing ligand

XIAP X-linked inhibitor of apoptosis protein

SUMMARY

"Science is organized knowledge. Wisdom is organized life." "The story of philosophy", (1924), Will Durant.

SUMMARY

Apoptosis is the major mechanism of regulated cell death, having a crucial role not only upon cell damage or stress, but also during normal development, morphogenesis, maintenance of tissue homeostasis and for an effective immune system. Therefore, its disturbance is implicated in numerous pathologies, as neurodegenerative disorders, ischemic damage, autoimmune diseases and cancer. The intracellular apoptotic machinery relies on a family of proteases that present cysteine at their active site and cleave their target proteins through specific aspartate residues, termed caspases, which are necessary for apoptosis and inflammatory response. Caspases are regulated at the posttranslational level by phosphorylation/dephosphorylation events that affect the conformation of the target protein and/or its interaction with other proteins, as well as its activity, function, half-life, stability, substrate affinity or subcellular localization. This mechanism is controlled by two big families of proteins: protein kinases and protein phosphatases.

In the present work we have given a step further in the characterization of the interaction between procaspase-9 and the Ser/Thr protein phosphatase 1α (PP1cα), confirming that PP1cα binds to both the CARD and the catalytic domain of procaspase-9 with a K_D of 10^{-7}M in a transient interaction.

We have also described and characterized the direct interaction between Caspase-9 and the catalytic domain of Ser/Thr protein phosphatase 2A (PP2Acα), determining the binding sites and the key residues of the interaction, as mutants that disrupt the association were found. This interaction seems to be also transient, as the K_D of the binding is in the micromolar range. Moreover, in this work we have obtained preliminary evidences for a ternary complex formed by Caspase-9, PP1cα and PP2Acα.

These findings have allowed us to generate bifunctional peptides fusing the cell-penetrating peptide DPT to Caspase-9 and PP2Acα derived peptides corresponding to the binding sites. DPT-C9h has shown to be very efficient inducing apoptosis in cancer cell lines, primary human cells and primary human breast cancer xenograft models. In addition, DPT-C9h has a specific effect on transformed B cells isolated from chronic lymphocytic leukemia patients without any effect on primary

healthy cells, confirming its tumor specificity. Besides, DPT-C9h is also specific for B cells, not inducing any apoptotic effect on T-cells, NK-cells or monocytes.

With the aim of facing preclinical trials, this bifunctional peptide has been optimized removing a serum protease cleavage site in the DPT sequence. Furthermore, in the present work the efficiency of mesoporous silica nanoparticles has been evaluated as a tool for drug delivery. In this sense, MCM-41 nanoparticles have provided promising results that suggest the possibility of a up to 10-fold dose reduction in cancer treatment with C9h.

Chronic lymphocytic leukemia (CLL) patients and healthy donors were analyzed to study the relative abundance of aberrant spliced variants of Caspase-9 (Caspase-9b) and PP2Acα (PP2Acα2). 40% of CLL patients presented moderately or highly dysregulated Caspase-9b but we couldn't correlate this data with other parameters of the disease. More importantly, PP2Acα2 was dysregulated in 88% of the patients and it has been associated with Binet B and C stages of the disease. Therefore, we postulate in this work the use of PP2Acα2 overexpression as a biomarker for CLL diagnose.

In other part of the study, we have characterized the binding sites between Caspase-9 and SET, suggesting a direct interaction between them, although it couldn't be characterized *in vitro*. The bifunctional peptides derived of binding site 1 of Caspase-9 and binding site 1 of SET resulted in a very effective drug to induce apoptosis in breast cancer cells.

In sum, the present work has addressed multidisciplinary approaches to better characterize the interactions between Ser/Thr phosphatases PP1 and PP2A and Caspase-9, as well as its association with the PP2A inbitor SET, which has allowed us to get efficient peptide-based drugs for cancer therapy.

RESUMEN

RESUMEN

La apoptosis es el principal mecanismo regulado de muerte celular, que tiene un papel crucial no sólo en condiciones de daño celular o estrés, sino también durante el desarrollo normal, la morfogénesis, el mantenimiento de la homeostasis de los tejidos y para un sistema inmune efectivo. Por ello, su alteración está implicada en numerosas patologías, como enfermedades neurodegenerativas, daño isquémico, enfermedades autoinmunes y cáncer.

La maquinaria apoptótica intracelular está controlada por una familia de proteasas que presentan cisteína en el sitio activo y procesan a sus proteínas diana a través de residuos específicos de aspartato, denominadas caspasas, que son necesarias para la apoptosis y la respuesta inflamatoria. Las caspasas están reguladas a nivel posttraduccional por eventos de fosforilación/desfosforilación que afectan a la conformación de la proteína diana y/o a su interacción con otras proteínas, así como a su actividad, función, vida media, estabilidad, afinidad de sustrato o localización subcelular. Este mecanismo está controlado por dos grandes familias de proteínas: las proteín kinasas y las proteín fosfatasas.

En este trabajo hemos abordado el estudio de las interacciones entre Caspasa-9 y las fosfatasas PP1 y PP2A, así como la interacción entre Caspasa-9 y el inhibidor 2 de PP2A, SET. Además, hemos estudiado la abundancia relativa de las variantes de empalme alternativo aberrante de Caspasa-9 y PP2Acα en pacientes de CLL y hemos podido aplicar el conocimiento de la interacción Caspasa-9 – PP2Acα para desarrollar un péptido capaz de inducir apoptosis específicamente en células B de CLL y otro tipo de células tumorales, así como en modelos de xenotransplantes de cáncer de mama. Con el objetivo de llevar a cabo ensayos preclínicos para desarrollar este péptido como fármaco, hemos evaluado el uso de nanopartículas como vehículos para transportar este péptido a las céulas diana. En conjunto, los resultados obtenidos en este trabajo se agrupan en los siguientes capítulos:

1. Caracterización de la interacción Caspasa-9 – PP1α.
   En este trabajo hemos dado un paso más en la caracterización de la interacción entre procaspasa-9 y la proteín fosfatasa de Ser/Thr 1α (PP1cα). Para ello hemos clonado varias construcciones de Caspasa-9, correspondientes al dominio CARD,

dominio ΔCARD-Caspasa-9 con mutaciones para formar el dímero en la estructura, dominio ΔCARD-Caspasa-9 C287A, con la mutación en el sitio activo para evitar su autoprocesamiento y Caspasa-9 C287A completa. Todas estas construcciones llevan en su extremo N-terminal una etiqueta de GST para facilitar su purificación. Asímismo, produjimos PP1cα recombinante siguiendo un protocolo basado en la coexpresión con chaperonas, incubación a 10ºC y un paso posterior de replegamiento *in vitro* para conseguir la proteína correctamente plegada. Con las proteínas puras se hicieron ensayos pull-down y western blot, donde se vio que PP1cα se unía tanto al dominio CARD como al ΔCARD, además de a Caspasa-9 completa. Los ensayos de interferometría de biocapa nos permitieron confirmar que PP1cα se une tanto al dominio CARD como al dominio catalítico de procaspasa-9 con una K_D de 10^{-7}M en una interacción transitoria.

2. Caracterización de la interacción Caspasa-9 – PP2Acα.
   Hemos descrito y caracterizado la interacción directa entre Caspasa-9 y el dominio catalítico de la proteín fosfatasa de Ser/Thr 2A (PP2Acα), determinando los sitios de unión entre ellas, que corresponden con los residuos 363-380 de Caspasa-9 y los residuos 173-194 de PP2Acα. El diseño de mutantes dentro de las regiones de unión nos ha permitido definir los residuos clave de la interacción, puesto que la mutación en el residuo W374 de Caspasa-9 y las mutaciones simples en los residuos L177 y R185 de PP2Acα impiden esta asociación.
   El análisis *in silico* del residuo W374 de Caspasa-9 con FoldX no proporcionó un cambio significativo en la energía libre al mutar este residuo a alanina, lo que indicó que este triptófano no está implicado en la estabilidad estructural de la proteína. La comparación del péptido de Caspasa-9 de la zona de unión a PP2Acα con la secuencia de tipo silvestre y la secuencia con la mutación W374A no mostró diferencias significativas en el porcentaje de formación de hélice α, confirmando que este residuo no tiene una importancia estructural pero sí resulta clave para que tenga lugar la interacción con PP2Acα.
   La caracterización biofísica de la interacción entre Caspasa-9 y el péptido YPP2Ah, correspondiente a la zona de PP2Acα de unión a Caspasa-9, indicó que esta interacción también podría ser transitoria, con una K_D de la unión en el

rango de micromolar según los ensayos de fluorimetría diferencial de barrido y de calorimetría isoterma de titulación. Sin embargo, el péptido YPP2Ah no presenta la capacidad de activar Caspasa-9 *in vitro* según pudimos comprobar en el ensayo de activación de Caspasa-9 basado en la detección del procesamiento del sustrato fluorogénico Ac-LEHD-AFC.

La aproximación a la sobreexpresión de PP2Acα en células de insecto infectadas con baculovirus nos permitió optimizar la cantidad de virus amplificado y aumentar el rendimiento de sobreexpresión de la proteína. Sin embargo, las condiciones de purificación todavía no han sido optimizadas y hasta el momento sólo se ha podido obtener la proteína en forma de agregados solubles, lo que ha supuesto un factor limitante en este proyecto para continuar con la caracterización biofísica y estructural del complejo Caspasa-9 – PP2Acα.

3. Potencial terapéutico del péptido C9h para la terapia anticáncer.

   El conocimiento de la interacción Caspasa-9 – PP2Acα nos ha permitido generar péptidos bifuncionales fusionando el péptido penetrante DPT a los péptidos derivados de los sitios de unión de Caspasa-9 y PP2Acα. DPT-C9h proporcionó mejores resultados que DPT-PP2Ah induciendo apoptosis en líneas celulares. DPT-C9h ha demostrado ser muy eficiente induciendo apoptosis en líneas celulares de cáncer, células primarias humanas y modelos de xenotransplantes de cáncer de mama primario humano. A su vez, DPT-C9h presenta un efecto específico en células B transformadas aisladas de pacientes de leucemia linfocítica crónica sin mostrar ningún efecto en células sanas primarias, confirmando su especificidad por tumores. Además, DPT-C9h también es específico de células B, ya que no induce ningún efecto apoptótico en células T, NK ni monocitos.

   Con el objetivo de afrontar ensayos preclínicos, este péptido bifuncional se ha optimizado eliminando un sitio de corte de una proteasa del suero en la secuencia del DPT. Además, en el presente trabajo se ha evaluado la eficiencia de dos tipos de nanopartículas mesoporosas de sílice como herramienta para la liberación de drogas. Las MSNs de 400nm de diámetro presentaron problemas de agregación y sólo fueron capaces de producir una reducción en la viabilidad celular de en torno al 10-20%; sin embargo, demostraron no ser tóxicas en ensayos de

viabilidad celular y entrar en el citoplasma de las células, como se observó por microscopía confocal. Por otra parte, las nanopartículas MCM-41, de 100nm de diámetro, han proporcionado resultados prometedores reduciendo la viabilidad celular e induciendo apoptosis, analizada por citometría de flujo, lo que sugiere la posibilidad de una reducción de la dosis de hasta 10 veces en el tratamiento de cáncer con C9h.

4. Evidencias preliminares del complejo ternario Caspasa-9 – PP1cα – PP2Acα.
   Los ensayos de Far Western Blot basado en péptidos identificaron nuevos sitios de unión a Caspasa-9 cuando tanto PP1cα como PP2Acα estaban presentes. El sitio de unión 1 a PP1cα no se mantenía en el complejo triple, pero sí el sitio de unión 2 a PP1cα y el sitio de unión a PP2Acα, además de la aparición de nuevos sitios de unión que son coherentes con la posibilidad de la formación de un complejo ternario cuando se observan en la estructura de Caspasa-9.

5. Estudio de las variantes de empalme alternativo de Caspasa-9 y PP2Acα.
   Se analizaron pacientes de leucemia linfocítica crónica (CLL) y donantes sanos para estudiar la abundancia relativa de las variantes de empalme alternativo aberrantes de Caspasa-9 (Caspasa-9b) y PP2Acα (PP2Acα2). El 40% de los pacientes de CLL presentaron una desregulación moderada o alta de Caspasa-9b pero no hemos podido correlacionar estos datos con otros parámetros de la enfermedad. Pero lo que es más importante, PP2Acα2 estaba desregulada en el 88% de los pacientes y se ha asociado con los estadíos de la enfermedad Binet B y C. En este trabajo se relaciona por primera vez la expresión de PP2Acα2 con un estado patológico, concretamente asociado a CLL. Sólo hay un artículo publicado donde se describe la existencia de esta variante aberrante de empalme alternativo y hasta el momento no se conoce su función y se considera una proteína inactiva. Por ello, en este trabajo postulamos la utilización de la sobreexpresión de PP2Acα2 como biomarcador para el diagnóstico de CLL.

6. Caracterización de la interacción directa entre Caspasa-9 y el inhibidor 2 de PP2A (SET).

   En este trabajo hemos descrito los sitios de unión entre Caspasa-9 y SET, indicando una interacción directa entre ellos, a través de 3 sitios de unión en la

secuencia de Caspasa-9, todos localizados en el dominio catalítico, y de 2 sitios de unión en la secuencia de SET. Sin embargo, esta interacción no ha podido ser caracterizada *in vitro* ni por ensayos pull-down ni por técnicas biofísicas como interferometría de biocapa o calorimetría isoterma de titulación. A partir de la información obtenida de los ensayos de Far Western Blot basado en péptidos, hemos diseñado péptidos bifuncionales derivados del sitio de unión 1 de Caspasa-9 y del sitio de unión 1 de SET, que han resultado ser una droga muy eficiente para inducir apoptosis en células de cáncer de mama.

En definitiva, el presente trabajo ha llevado a cabo aproximaciones multidisciplinares para caracterizar mejor las interacciones entre las fosfatasas de Ser/Thr PP1 y PP2A y Caspasa-9, así como su asociación al inhibidor de PP2A SET, lo que nos ha permitido obtener drogas eficientes basadas en péptidos para la terapia anticáncer, utilizando para su liberación bien péptidos penetrantes o nanopartículas como vehículos para llevar el péptido a las células diana.

INTRODUCTION

"Equipped with his five senses, man explores the Universe around him and calls the adventure science". "Nature of science" (1954) Edwin Powell Hubble.

1. INTRODUCTION

1.1. Programmed cell death and apoptosis

The cells of a multicellular organism are members of a highly organized community. The number of cells in this entity is tightly regulated, not only by the control of cell division rate but also by the cell death rate. When the cells are no longer necessary, they commit suicide activating an intracellular program, generally termed programmed cell death (Alberts et al., 2004). Three major types of programmed cell death have been described: apoptosis, necroptosis and autophagy. In the last years it has been known that these pathways are interconnected in a complex interplay. Several death initiator and effector molecules, signaling pathways and subcellular sites constitute common elements between apoptosis and necroptosis or act as a switch between these two processes. Furthermore, autophagy, despite being a predominantly cytoprotective process, has been related to apoptosis and necroptosis, presenting either a prosurvival or prodeath function (Nikoletopoulou et al., 2013).

Among these pathways, apoptosis is the most intensively studied since it was described by (Kerr et al., 1972) and it comprises the major mechanism of regulated cell death, having a crucial role not only upon cell damage or stress, but also during normal development and morphogenesis. When a cell suffers apoptosis, it dies in a clean way without damaging neighbor cells. Mitochondrial membrane permeabilizes, chromatin condenses, cytoskeleton collapses, nuclear membrane disassembles and nuclear DNA breaks in fragments. In turn, the cell surface is altered, leading to a rounded cell and the shedding of apoptotic bodies. The dying cell will be rapidly phagocyted, either by a neighbor cell or a macrophage, before any escape of its content takes place, what allows the recycling of the organic components of the dead cell by the cell that engulfs it (Alberts et al., 2004).

Apoptosis is crucial for normal development (Arya and White, 2015), maintenance of tissue homeostasis and for an effective immune system. Therefore, its disturbance is implicated in numerous pathologies, as neurodegenerative disorders, ischemic damage, autoimmune diseases and cancer (Fernald and Kurokawa, 2013; Hassan et al., 2014).

1.2. Caspase-dependent and independent apoptotic pathways

The caspase-dependent apoptotic signaling cascade can be mainly activated either through an extrinsic or an intrinsic pathway; however, there is evidence that the two pathways are connected and the molecules in one route can influence the other one. Eventually, both pathways trigger the activation of a family of cysteine aspartyl proteases, called caspases, which will be described in detail below (Elmore, 2007).

The extrinsic pathway receives stimuli through cell surface death receptors, such as TNFα (tumor necrosis factor α), Fas (CD95/APO1) and TRAIL (TNF related apoptosis inducing ligand) receptors. Upon ligand binding, cytoplasmic adapter proteins are recruited and exhibit their death domains that bind with the receptors. The binding of Fas ligand to TNF receptor results in the binding of the adapter protein TRADD with recruitment of FADD and RIP, and then FADD associates with procaspase-8. A death-inducing signaling complex is formed (DISC), leading to the autocatalytic activation of caspase-8, which in turn triggers the execution phase of apoptosis (Hsu et al., 1995; Kischkel et al., 1995; Locksley et al., 2001; Wajant, 2002).

The intrinsic pathway is activated through inner stimuli, which trigger the opening of the mitochondrial permeability transition pore, loss of mitochondrial transmembrane potential and release of proteins to cytosol, as cytochrome c, Smac/DIABLO and the serine protease HtrA2/Omi, which in turn activate the caspase-dependent mitochondrial pathway (Chinnaiyan, 1999; Du et al., 2000; Garrido et al., 2006; Saelens et al., 2004). In the cytoplasm, hydrolysis of ATP/dATP by Apaf-1 and its binding to cytochrome c promote Apaf-1 oligomerization, forming a multimeric Apaf-1 – cytochrome c complex, which is sufficient to recruit and activate procaspase-9 (Zou et al., 1999) . In a further study it was also demonstrated that caspase recruitment domains of Apaf-1 and procaspase-9 form a CARD-CARD disc, which is flexibly attached to the apoptosome (Yuan et al., 2011, 2010).

The extrinsic and intrinsic pathways converge at the level of executioner caspases, where mature Caspase-9 cleaves and activates Caspase-3 and -7 to execute the apoptotic event (Salvesen and Ashkenazi, 2011). Procaspase-9 and mature Caspase-3 present overlapping binding sites on the central hub of the apoptosome;

however, procaspase-3 doesn't bind to the apoptosome. These shared binding sites may play a role in procaspase-3 activation, as procaspase-9 apoptosomes cleave procaspase-3, creating Caspase-3/procaspase-3 dimers and fully active Caspase-3 dimers, but only this active mature protein is binding to the apoptosome. This scenario suggests the formation of hybrid apoptosomes with procaspase-9 and Caspase-3 proteolytic activities, which allow Caspase-3 to downregulate procaspase-9 activity in the apoptosome (Yuan et al., 2011).

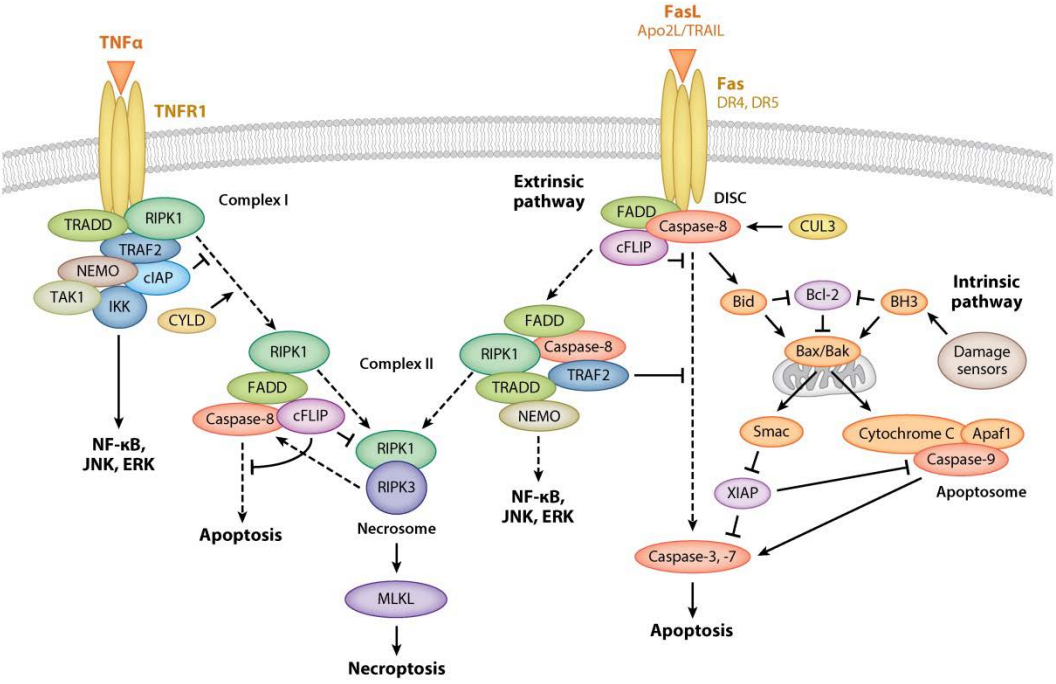

Figure 1. Scheme of death-receptor control of cell death. In the extrinsic pathway, upon ligation, the death receptors Fas, DR4 or DR5 assemble a primary DISC at the plasma membrane, thereby activating Caspase-8, which directly stimulates the executioner caspases -3 and -7. This route is connected with the intrinsic pathway by processing the BH3-only protein BID, which further activates BAX and BAK to induce release of cytochrome c and Smac/DIABLO from mitochondria. Cytochrome C then associates with Apaf 1 to form an apoptosome that drives Caspase-9 activation and subsequent Caspase-3 and -7 stimulation. In a rough outline of the necroptotic pathway, upon ligation by TNFα, TNFR1 assembles Complex I at the plasma membrane. A second complex, Complex II is also assembled by the same receptors as the extrinsic pathway. Inhibition of Caspase-8 allows RIPK1 to recruit RIPK3 and form a third complex, the necrosome complex, triggering necroptosis. Taken from (Ashkenazi and Salvesen, 2014).

There is a third apoptotic pathway that involves T-cell mediated cytotoxicity and perforin-granzyme-dependent killing of the cell, inducing apoptosis via either granzyme B or A. Granzyme B cleaves procaspase-10 and factors like ICAD (inhibitor of caspase activated DNAse), utilize the mitochondrial pathway by specific cleavage of Bid and induction of cytochrome c release and it can also directly activate Caspase-3 (Barry and Bleackley, 2002; Russell and Ley, 2002). The granzyme A pathway activates a caspase-independent cell death pathway via single stranded DNA damage as well as rapid loss of cell membrane integrity and mitochondrial transmembrane potential, thereby generating ROS (reactive oxygen species) that drive the SET complex into the nucleus (Lieberman, 2010; Martinvalet et al., 2005). Granzyme A protease cleaves the SET complex, releasing inhibition of the tumor suppressor NM23-H1, leading to DNA degradation. In addition, the SET complex plays an important role in chromatin structure and DNA repair and the members of this complex (the nucleosome assembly protein SET, the base excision repair endonuclease Ape1, the tumor suppressor pp32 and the DNA bending protein HMG2) seem to work together to protect chromatin and DNA structure. Moreover, cleavage of Ape1 by Granzyme A interferes with its oxidative repair functions and then the cell loses its ability of self-reparation. Thus, when Granzyme A inactivates this complex it also contributes to apoptosis, blocking the maintenance of DNA and chromatin structure integrity (Fan et al., 2003; Lieberman and Fan, 2003).

1.3. Caspases in apoptosis

The intracellular machinery responsible for apoptosis seems to be similar in all animal cells. This machinery relies on a family of proteases that present cysteine at their active site and cleave their target proteins through specific aspartate residues. The term initially used to designate this family was cysteine-dependent aspartate-directed proteases, which was afterwards shortened to caspases (Alnemri et al., 1996). Caspases are necessary for apoptosis and inflammatory response. There are 14 different types of caspases in mammals, but only 11 of them are present in humans. Caspases are produced in cells as inactive zymogens and they are constituted by a large subunit and a small subunit, showing all crystallographic structures solved from caspases the same basic fold (Denault and Salvesen, 2002a).

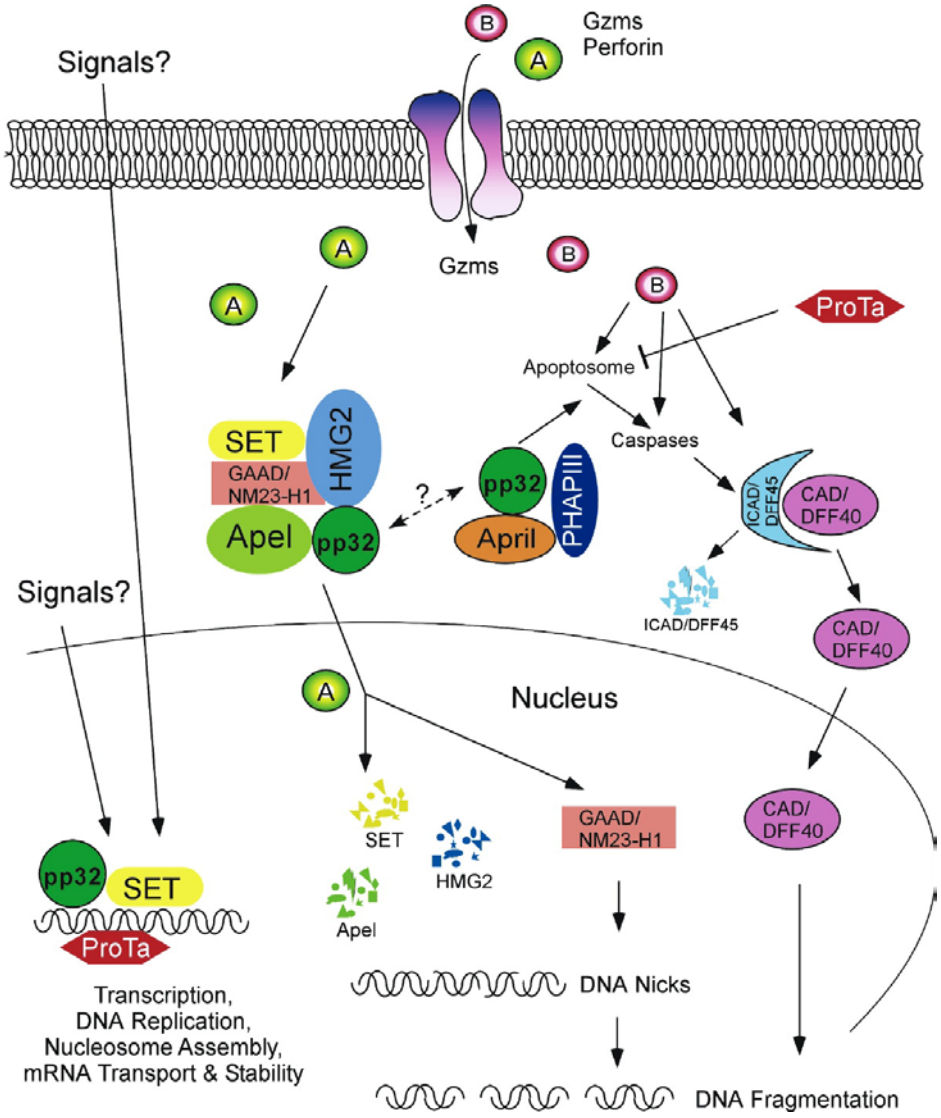

Figure 2. Granzyme A and B apoptotic pathway. Granzyme A cleaves SET, HMG2 and Ape1, but not PP32, to activate NM23-H1 DNAse function and to induce DNA nicking. Granzyme B induces caspase-dependent apoptosis. Also PP32 and its homologs April and PHAPIII promote apoptosome formation and caspase activities, thus connecting the caspase-dependent and caspase-independent pathways of apoptosis. Taken from (Chakravarti and Hong, 2003).

Active caspases are generally found as dimers of catalytic domains, mainly bound through hydrophobic interactions. The subunits of each catalytic domain are αβα sandwiches, folded into a compact cylinder with six-stranded β sheets in the center, surrounded by 5 helices placed on opposing sides of the plane formed by the β sheets. The catalytic dimer possesses monomers arranged by two-fold symmetry, with the two active sites at opposite ends of the dimer. The C-terminal end of the large subunit and the N-terminal end of the small subunit are close to each other. The catalytic pair His^{237}/Cys^{285}, which is highly conserved among caspases, is found in the large subunit.

The variation in the aminoacid sequence of the small subunit is responsible of the variability in the substrate specificity of caspases. The main chain of the substrate forms an antiparallel β sheet with the main chain of the residues 339-341, in the case of Caspase-3, but it is similar in other caspases. This mode of substrate alignment strongly differs from what is found in other families of cysteine-proteases, but it is shared with the serine-protease family of chymotrypsins.

The catalytic domains of caspases, of around 30kDa, are well conserved and contain all the enzymatic machinery. In addition, other two types of domains are found in the amino-terminal region of several caspases: CARD (caspase activation and recruitment domain) and DED (death effector domain). Both domains are implicated in homophilic interactions with other proteins, which allow that the respective caspase zymogens will be recruited to protein complexes to promote their activation. The activation of caspases that contain CARD and DED domains usually leads to the cleavage of these domains and release of the active catalytic portion, with the exception of Caspase-9, as it will be explained below. Caspase-3, -6 and -7 have a short N-peptide of 27-28 residues that is removed during activation.

An effector caspase is activated by an initiator caspase through the proteolytic processing of the first at internal specific aspartate residues, to separate the large and small subunits of the mature caspase. Once activated, effector caspases can act over a wide range of cellular targets, finally causing cell death (Parrish et al., 2013).

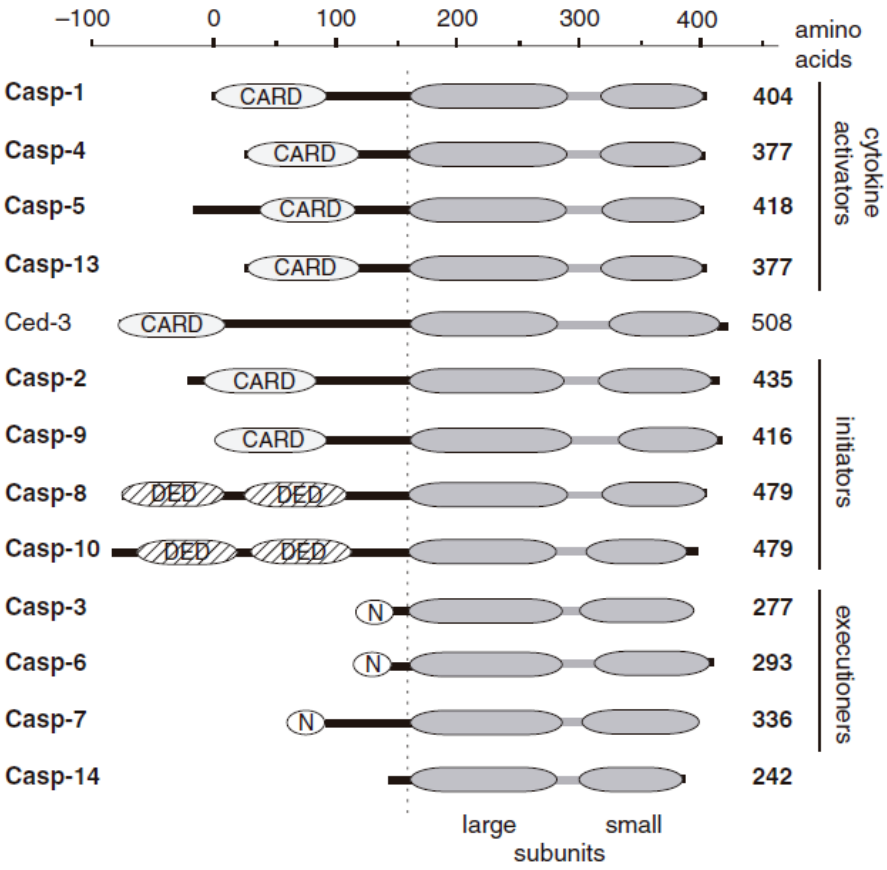

Figure 3. Scheme of domain organization of Caspases and *C. elegans* Ced-3 family members. The CARD domain is represented in light grey, the DED domain is stripped and the N corresponds to the small N peptide of the executioner caspases. The scale has been established according to Caspase-1 residue numbers. The dotted line indicates the start of the large subunit. Taken from (Denault and Salvesen, 2002a).

1.4. Caspase-9

Caspase-9 is an apoptotic initiator caspase, whose activation by dimerization requires loops rearrangement to position the catalytic machinery and the substrate binding sites (Denault and Salvesen, 2002b). Procaspases activation normally requires the scission of a specific internal aspartate residue present in interdomain linkers between the prodomain and the catalytic region and between both catalytic

subunits. This cleavage releases the prodomain and generates the large and small subunit to form a dimeric catalytical entity. Caspase-9 has two potential processing sites, aspartic residues 315 and 330, and the active site, cysteine 287. It has been demonstrated that the mutation of the active site prevents the autoprocessing of Caspase-9 that will give rise to both subunits (Srinivasula et al., 1998).

From the structural point of view, mature Caspase-9 is a heterotetramer composed by two antiparallel heterodimers, each one formed by a p20 subunit (20kDa) and a p10 subunit (10kDa). As for other caspases, the dimer is formed through interactions between strands 8 of the small subunits. Nevertheless, there are two characteristics unique for Caspase-9. First of all, in other caspases a small β sheet is observed between the C-terminal residues of the large subunit and the N-terminal residues of the small subunit that is not present in Caspase-9, due to the disorder at the C-terminal part of the large subunit inactive domain. Moreover, the large subunit possesses a seven-residue loop inserted at position 240 between strands 3 and 3A, which interacts across the dimer interface (Renatus et al., 2001).

At concentrations in the micromolar range, Caspase-9 is an inactive monomer, and its complete form *in vivo* is also a monomer (Renatus et al., 2001). Caspase-9 is not activated by proteolysis, but by homophilic interactions between the CARD domain of Caspase-9 and the cofactor Apaf-1, in the presence of cytochrome-c and ATP, to generate a completely functional apoptosome, as it was previously described. This apoptosome controls the cellular suppression during the central nervous system development and the apoptotic response to lethal agents for the cell, as ionizing radiation or chemotherapeutic drugs.

The function of Caspase-9 is to generate the active forms of Caspase-3 and Caspase-7 by limited proteolysis, thereby transmitting the apoptotic signal to the execution phase (Riedl et al., 2001).

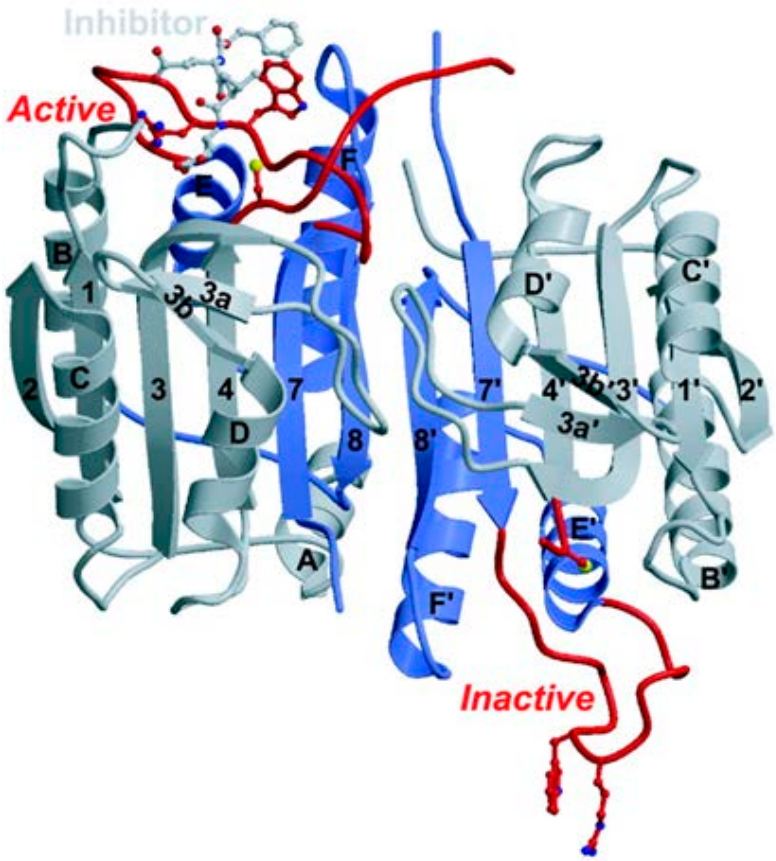

Figure 4. Scheme of ΔCARD Caspase-9 structure. The large subunit is colored in grey and the small subunit is colored in blue. The inhibitor Z-EVD-DCBMK that was crystallized with Caspase-9 is shown in light grey and the side chains of the catalytic residue Cystein 285 as well as the specificity determining residues Arginine 341 and Tryptophan 340 are represented in the highlighted balls and sticks. Taken from (Renatus et al., 2001).

1.5. Caspases regulation

As caspases play a key role in apoptosis, their activation and activity is tightly regulated to avoid unplanned cellular demise. This control is of crucial importance, avoiding pathological processes as an aberrant or untimely apoptotic cell death, potentially leading to carcinogenesis, autoimmunity, neurodegeneration and

immunodeficiency. Either before or after activation, caspases can be regulated through a variety of mechanisms that may inhibit or enhance enzymatic activity or may affect activity towards particular cellular substrates (Parrish et al., 2013).

The first point of regulation is at the synthesis level, as caspases are initially produced as inactive zymogens, lacking protease activity; this way they will only be activated upon certain stimuli (Earnshaw et al., 1999). A subsequent form of regulation is proteolysis, in which the N-terminal prodomain has an important role. This region contains well-conserved domains: CARD for caspases -1, -2, -4, -5, -9, -11 and -12, and DED found in Caspase-8 and -10. Both domains are distantly related and are implicated in homophilic interactions with other proteins, allowing caspase zymogens to be recruited to protein complexes to promote their activation. Caspases containing CARD or DED domains are usually activated by proteolytic cleavage with the exception of Caspase-9, as described before (Denault and Salvesen, 2002a). Initiator caspases are activated through limited proteolysis when adaptor proteins interact with the N-terminal prodomains and promote caspase dimerization. Nevertheless, effector caspases exist in the cell as inactive homodimers, which are activated by prodomain cleavage mediated by an initiator caspase.

Caspase-9 regulation at posttranslational level is the best characterized among the family. Several phosphorylation sites have been reported, resulting in most of the cases in a reduction of activation and/or cleavage of the protein (Allan and Clarke, 2009). This mechanism is controlled by two big families of proteins: protein kinases and protein phosphatases. Phosphorylation/dephosphorylation events affect the conformation of the target protein and/or its interaction with other proteins, as well as its activity, function, half-life, stability, substrate affinity or subcellular localization (Bononi et al., 2011). Threonine 125 is known to be the phosphorylation site of Erk kinase, but also of cdk1, DYRK1A and p38α (Allan et al., 2003; Seifert and Clarke, 2009). Other phosphorylation sites have been also described, as Serine 144, phosphorylated by PKCζ in response to hyperosmotic stress, Serines 99, 183 and 195 by PKA, Serine 196 by PKB/Akt, Serine 348 by CK2 and Tyrosine 153 by c-Abl after DNA damage (Brady et al., 2005; Cardone et al., 1998; Martin et al., 2005; McDonnell et al., 2008; Raina et al., 2005). Caspase-9 can also be modified by nitrosylation in the presence of high levels of nitric oxide (Török et al., 2002).

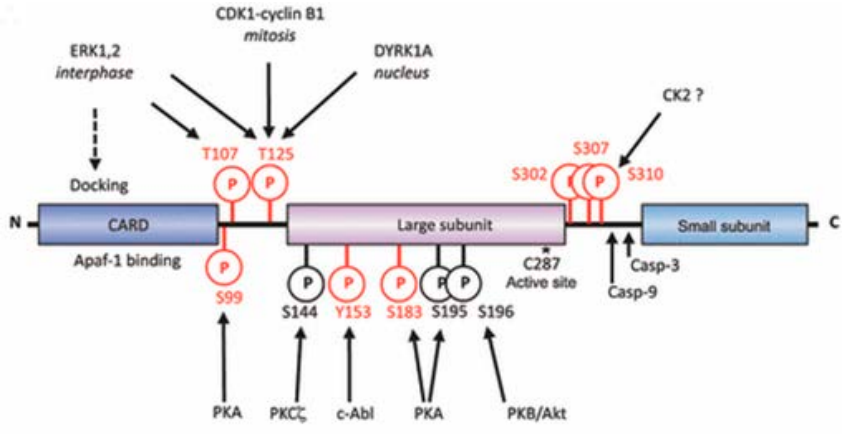

Figure 5. Caspase-9 phosphorylation sites. Linear representation of Caspase-9 with the position of phosphorylation sites and the proteinkinases responsible for phosphorylation at each site. Taken from (Allan and Clarke, 2009).

Regarding the protein stability level, Caspase-9 can be regulated through ubiquitylation mediated by XIAP (X-linked inhibitor of apoptosis protein) E3 ubiquitin ligase, which only polyubiquitylate the large subunit of active Caspase-9 but not the inactive procaspase-9 (Silke and Meier, 2013).

1.6. Serine/threonine protein phosphatases in apoptosis

In eukaryotes, the most commonly modified residues are serine and threonine. In fact, 98% of dephosphorylation events occurs at these two amino acids and there are two major proteins named Protein Phosphatase 1 (PP1) and Protein Phosphatase 2A (PP2A) of the family of Phosphoprotein Phosphatases (PPP) termed Serine/threonine protein phosphatases that account for 90% of serine/threonine dephosphorylation (Xiao et al., 2010). PP1 and PP2A are in fact important regulators at several levels of the apoptotic pathway and they are two of the most abundant enzymes in many cell types. They are part of a complicated interplay between kinases and phosphatases in the execution of apoptosis, in which caspases are the major drivers.

Serine/threonine phosphatases PP1 and PP2A have a key role in the regulation of Bcl-2 family members and caspases in the cell decision of living or dying. PP1 and PP2A are implicated in the cell death induction through Bad dephosphorylation (a member of the proapoptotic family Bcl-2) (Ayllón et al., 2002, 2000), stimulation of cytochrome-c release from mitochondria and dephosphorylation of retinoblastoma protein (Ray et al., 2005; Rubin et al., 2001). Nevertheless, PP1 and PP2A can present both an apoptotic and anti-apoptotic function, as the inhibition of PP1α or PP2A can trigger apoptosis (Kang and Choi, 2001; Singh et al., 2000).

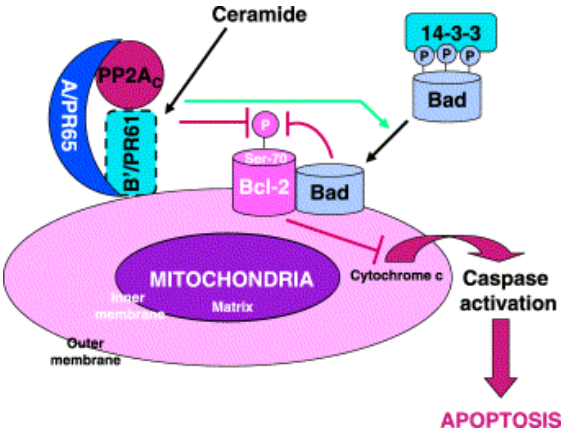

Figure 6. Regulatory role of PP2A in the apoptotic signal transduction pathway upstream Bcl-2. PP2A dephosphorylates and inactivates Bcl-2 at Ser 70. PP2A is also a Bad phosphatase, maintaining this protein dephosphorylated and localized at the mitochondria. The net result is cytochrome-c release, necessary for apoptotic response. Taken from (Van Hoof and Goris, 2003).

PP1 and PP2A can also control apoptosis through negative regulation of anti-apoptotic partners, modulating Akt function as regulator of cell survival, differentiation and gene expression by directly dephosphorylating Thr 450 and Thr 308 and Ser 473, respectively (Kuo et al., 2008; Xiao et al., 2010). These two phosphatases also play an important role in the regulation of Caspase-9 phosphorylation state, thus controlling its activation under certain stimuli, as it will be detailed below (Arrouss et al., 2013; Dessauge et al., 2006).

1.7. Protein phosphatase 1A

Protein phosphatase 1 (PP1) is a ubiquitous serine/threonine phosphatase that regulates different important cellular processes such as cell progression, cytokinesis, transcription, protein synthesis, carbohydrate metabolism, muscle contraction and neuronal signaling. In mammals, three different genes encode four catalytic subunits of PP1: PP1α, PP1β/γ and the splice variants PP1γ_1 and PP1γ_2, showing higher sequence differences among them at the C-terminal extreme. PP1α is a highly conserved 38 kDa protein that dephosphorylates hundreds of crucial biological targets, and its apoenzyme associates with more than 200 regulatory proteins to form specific holoenzymes (Bollen et al., 2010). In fact, the specificity of the catalytic domain for certain residues near the target phosphorylation site appears to be limited. For this reason, the action of PP1 is directed in time and space by these regulatory proteins. However, PP1 has shown to possess interaction domains which are conserved among its interacting partners. The most common is the RVxF motif, which is present in most PP1-interacting proteins (PIPs). The consensus sequence described by (Bollen et al., 2010) is K/R/H/N/S-V/I/L-x-F/W/Y, being x any residue except Phe, Ile, Met, Tyr, Asp or Pro. Although it brings about little conformational changes on the catalytic subunit of PP1, the binding to this motif is crucial for the partner proteins to become anchored to PP1. This docking site helps to bring closer interacting proteins, thereby making additional interactions possible, thus determining the activity and substrate specificity of the holoenzyme. The disruption of just a single motif can be enough to weaken or even break the interaction. Other common PIPs interaction motifs are SILK and MyPhoNE, both usually N-terminal to the RVxF motif (Hendrickx et al., 2009).

PP1 catalytic site is at the intersection of three potential substrate binding regions: the hydrophobic, acidic and C-terminal grooves. Two metals placed at the active site of PP1 mediate a single step dephosphorylation reaction. These metal ions enhance the nucleophilicity of a water molecule that is bound at the active site, leading to nucleophilic substitution with the phosphate moiety. When PP1 is expressed *in vitro*, it is produced in the presence of $MnCl_2$, and two Mn^{2+} ions remain bound to the active site (Dancheck et al., 2011; Goldberg et al., 1995).

All PP1 structures solved present an invariant conformation, showing to be independent of the interaction partner, as represented in **Figure 7** (Peti et al., 2013). PP1 is folded into a single elliptical domain comprising a central β-sandwich of two mixed β-sheets surrounded on one side by seven α-helices and on the other side by a subdomain formed by three α-helices and a three-stranded mixed β-sheet.

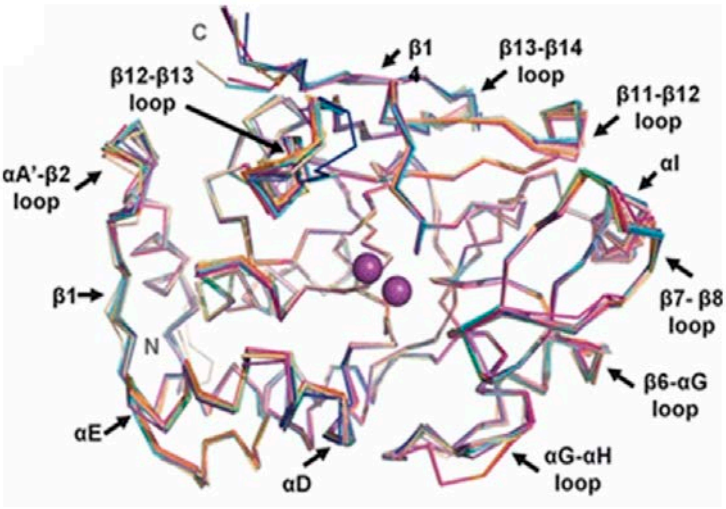

Figure 7. Overlay of PP1 structures showing that its conformation is invariant independently of the ligands bound to the protein. The structures represented correspond to PDB codes 1FMJ (dark blue), 1IT6 (cyan), 1JK7 (magenta), 1S70 (beige), 2BCD (salmon), 2BDX (orange), 2O8G (slate), 3E7A (grey), 3E7B (lime green), 2EGG (teal), 3HVQ (pink), 3N5U (yellow-orange) and 3EGH (purple-blue). The regions of PP1 that present conformational changes are labeled. Taken from (Peti et al., 2013).

The interface of the three β-sheets at the top of the β-sandwich generates a shallow catalytic site channel. A β-α-β-α-β motif is present in sheet 1 that along with loops from the opposite β-sheet (sheet 2) provide the catalytic site residues (Egloff et al., 1995).

Our collaborators described the direct interaction between PP1 and Caspase-9, showing that upon IL-2 deprivation PP1 dephosphorylation was induced, leading to its activation and further dephosphorylation and activation of Caspase-9. In this study, three Caspase-9 binding sites were detected in PP1, which were separated in the aminoacid sequence but close in the protein structure, as well as exposed in the surface, allowing the interaction with Caspase-9 (**Figure 8**). PP1 catalytic site is

placed on the other side of the molecule. In the same way, two PP1 binding sites were determined in Caspase-9 sequence, covering the first 16 aminoacids of the protein sequence, corresponding to the N-terminal extreme of the CARD domain, and the residues 185-201 of human Caspase-9 (residues 223-239 of mouse Caspase-9), placed in the large subunit of the ΔCARD Caspase-9 domain, the catalytic p20 domain (Dessauge et al., 2006).

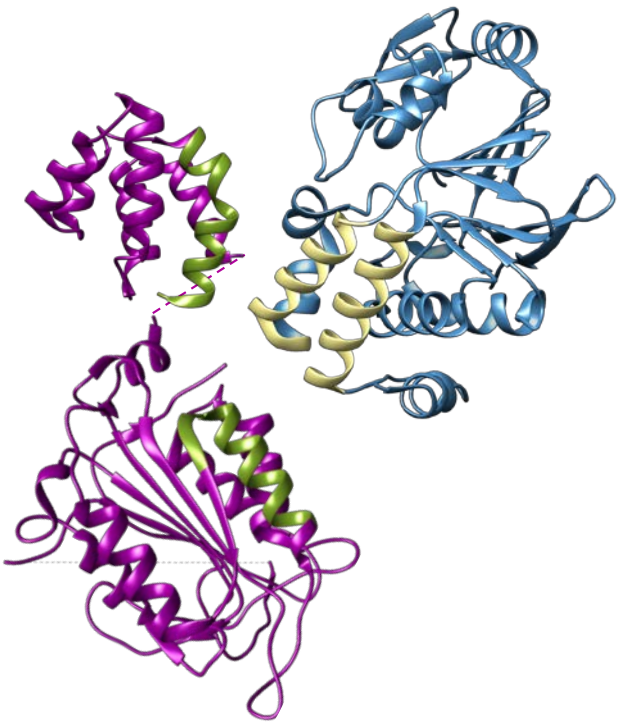

Figure 8. Caspase-9 and PP1cα binding model showing interaction sites. Caspase-9 is represented in purple, showing the CARD domain (PDB 4RHW) up and the ΔCARD domain down (PDB 1JXQ). Both structures are bound by a discontinuous line covering the residues 93-139 corresponding to the flexible linker between both domains. PP1 binding sites are highlighted in green. PP1cα is colored in blue on the right (PDB 3E7A), showing Caspase-9 binding sites in light yellow. The third Caspase-9 binding site corresponding to residues 312-328 is not shown as these residues are not visible in the structure.

1.8. Protein phosphatase 2A

PP2A is a ubiquitously expressed Serine/threonine phosphatase and it is implicated in the regulation of cell homeostasis through the negative regulation of the signaling pathways started by proteinkinases. PP2A is considered an important tumor suppressor (Janssens et al., 2005); in addition, it has been demonstrated that the principal substrates in this suppressor activity are downstream components of the Ras signaling pathway. Additionally, PP2A suppression makes Ras intensify the activity of the oncogenic proteins that are downstream targets of Ras-activated pathway (Mumby, 2007a).

PP2A phosphatase activity has been related with cell cycle regulation and mitosis, cell morphology, differentiation, development, signal transduction, replication, DNA transcription, translation, RNA splicing and apoptosis. PP2A also participates in stress, heat shock and DNA damage responses and in the regulation of calcium channels in cardiac muscle. PP2A alterations can lead to pathological states as Alzheimer disease and oncogenic transformation, as well as enhanced metastasis (Janssens and Goris, 2001). Therefore, a peculiarity of PP2A is that a single phosphatase is responsible for the regulation of several processes activated by different proteinkinases. The distinctive capacity of PP2A to affect the phosphorylation state of a wide variety of substrates derives from its complex structure and regulation.

Structurally, PP2A is a heterodimeric or heterotrimeric complex, composed by a constant core dimerical structure of 65kDa that serves as a scaffold ($PP2A_A$ or PR65/A) and a catalytic subunit of 36kDa ($PP2A_C$, α and β isoforms) (**Figure 9**). This dimeric structure ($PP2A_D$) can be associated or not to a third variable subunit, a family of regulatory B subunits that confer substrate or tissue specificity to the trimeric holoenzymes of PP2A and they are differentially expressed during development in mammals (Lechward et al., 2001). PP2Ac activity can also be modulated by reversible phosphorylation on Tyrosine 307 and methylation on Leucine 309, its last aminoacid at the C-terminal.

The structure of the catalytic subunit of PP2A is very similar to other members of the serine/threonine phosphatase family as PP1, PP2B and PP5, and it contains two metal ions at the active site, determined as manganese. The C-terminal

part (residues 296-309) extends away from the main globular protein and nestles into a surface groove at the interface of the scaffold and regulatory subunits, which is responsible for PP2Ac specificity for the scaffold subunit. The entire PP2AA scaffold subunit is composed by 15 tandem HEAT repeats that adopt a horseshoe or C-shaped conformation in the PP2A holoenzyme. The interaction between A and C subunits is ruled by an extensive network of hydrogen bonds that accounts for the high affinity of this interaction (Cho and Xu, 2007; Mumby, 2007b; Xing et al., 2006).

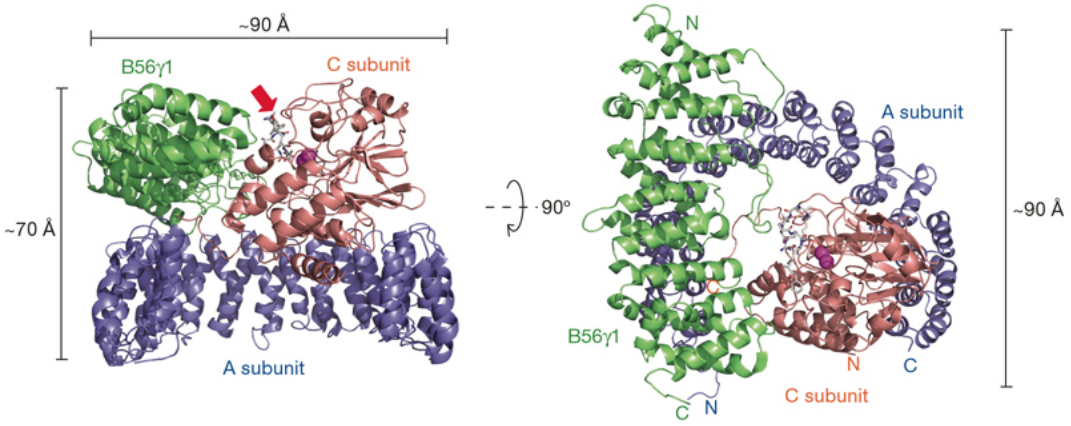

Figure 9. Crystal structure of the heterotrimeric PP2A holoenzyme. The front view is represented on the left and the top view on the right. The A scaffold subunit is colored in blue, the catalytic C subunit is shown in red and the regulatory B56γ1 is marked in green. Taken from (Cho and Xu, 2007).

The catalytic subunit of PP2A is among the best conserved enzymes from yeast to mammals (Cohen et al., 1990). In mammalian cells, A and C subunits have both two isoforms, α and β, which share a high sequence similarity. In both cases, α isoform is much more abundant than β (Arino et al., 1988; Hemmings et al., 1990).

The inactivation of α and β isoforms of PP2A A subunit has been related to cancer (Ruediger et al., 2001; Suzuki and Takahashi, 2003). Mutations in this subunit that negatively affect the binding to the catalytic or regulatory PP2A subunits or a total lack or substantial reduction of A subunit are tightly related to diverse primary tumors in humans (Takagi et al., 2000; Wang et al., 1998). In another study, a truncated form of the PR61/B/γ1 B subunit was associated with resistance to

radiotherapy in metastatic state of melanoma cells (Ito et al., 2003; Koma et al., 2004), although it was also shown that this subunit can act as a tumor suppressor. Furthermore, it has been postulated that the critical point of PP2A role in maintaining the equilibrium between survival and cell death is related with the phosphorylation state of Tyrosine 307 residue of its catalytic domain (Wong et al., 2010).

In a study developed in collaboration with the present work, our colleagues recently described the direct interaction between Caspase-9 and PP2Acα, which constitutes a potential target for anticancer therapy (Arrouss et al., 2013).

1.9. Protein phosphatase 2A inhibitor 2 (SET)

SET, also called TAF-1β, INHAT or I_2PP2A (Inhibitor 2 of PP2A) is a 33.5 kDa (Isoform 1) or 32 kDa (Isoform 2) protein. In the present project, we have worked with isoform 2. SET was firstly described as a translocation breakpoint-encoded protein in a case of acute undifferentiated leukemia (von Lindern et al., 1992), and it has been further characterized as a histone chaperone that interacts with several factors as DNA binding proteins and proteases. SET participates in the regulation of transcription, replication and apoptosis. Furthermore, SET inhibits the activity of histone acetyltransferases, indicating that it regulates the nuclear activity coming from the chemical modifications of core histones.

Structurally, SET forms a dimer that presents a “headphone”-like structure. Each subunit of the dimer consists of an N terminus, a so called backbone helix and an “earmuff” domain. The region of SET responsible of chaperon activity is the bottom surface of the earmuff domain, due to the binding of this surface to core histones and double-stranded DNA (Muto et al., 2007).

SET has been related to serine/threonine protein phosphatases PP1 and PP2A. It has been reported that SET associates with PP1 and modifies its substrate specificity. In the presence of physiological concentrations of Mn^{2+}, SET enhanced PP1 activity by 15-20-fold with myelin basic protein and histone H1 but not with phosphorylase. Furthermore, SET reduced PP1 Mn^{2+} requirement by about 30-fold to 10μM (Katayose et al., 2000). In a doctoral thesis, the interaction between I_2PP2A

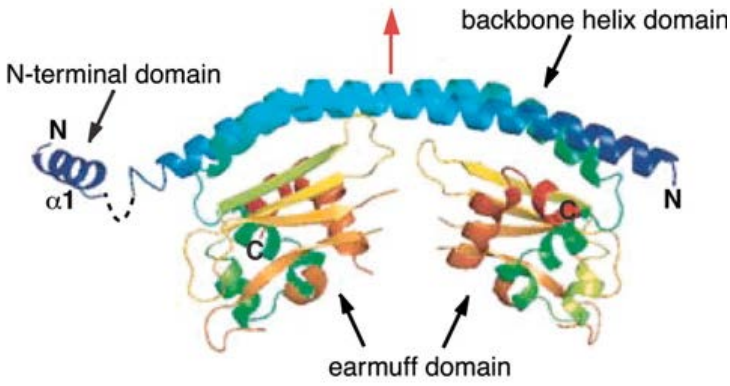

Figure 10. Overall structure of SET dimer, with the pseudo twofold axis represented with a red arrow. Taken from (Muto et al., 2007).

and PP1 from *Plasmodium falciparum* was characterized by yeast two hybrid, observing that only diploid yeasts expressing PfPP1 and PfI_2PP2A were capable of growing in a selective –LWH medium, showing an interaction between these two proteins. In a further phosphatase assay, they observed that low concentrations of PfI_2PP2A (100-400nM) activated PfPP1; in contrast, high concentrations of PfI_2PP2A resulted in an inhibition of PfPP1 upon pNPP (para-nitrophenyl phosphate) substrate addition. *Plasmodium falciparum* I_2PP2A and its human ortholog SET share a 26.7% of identity, including a RVxF PP1 binding site (Egloff et al., 1997) that is conserved between humans and this parasite, comprising residues 123-126 of the human protein (Vandomme, 2014).

The interaction between SET and PP2A was first reported in 1996, where SET was a potent and specific inhibitor of PP2A, termed I_2PP2A, provoking an impaired regulation of PP2A that may contribute to acute myeloid leukemogenesis (Li et al., 1996). In a recent study, both N-terminal (residues 1-175) and C-terminal (176-277) SET fragments bound and inhibited PP2Ac, showing that SET Valine 92 residue and also its C-terminal acidic part were indispensable for the interaction to take place. SET full length localized in the nucleus, but after cleavage at residue 175, both fragments were diffused in the cytoplasm, where they inhibited PP2Ac causing abnormal tau hyperphosphorylation in Alzheimer disease brain (Arnaud et al., 2011).

In addition to chronic myelogenous leukemia, SET has been found overexpressed in primary chronic lymphocytic leukemia (CLL) cells and B-cell non-Hodgkin lymphoma (NHL) Raji and Ramos cell lines, showing a correlation between SET overexpression and a higher disease severity. The relative abundance of SET splicing variants was also altered in CLL and NHL cells, presenting similar amounts of α and β isoforms, whereas in healthy cells the β isoform was majority (Christensen et al., 2011a).

1.10. Chronic lymphocytic leukemia

Chronic lymphocytic leukemia (CLL) is the most common B-cell malignancy in Caucasian aging adults, rarely younger than 50 years old. The disease is characterized by the accumulation of CD5+ monoclonal B cells in the blood, bone marrow and peripheral lymphoid organs (Chiorazzi et al., 2005; Ghia et al., 2007; Rozman and Montserrat, 1995). CLL B lymphocytes proliferation also involves CD19, CD20 and CD23 expression and presents low levels of Ig on their surface membranes, as well as low membrane expression of CD79b, CD22 and FMC7 (Batata and Shen, 1992; Inamdar and Bueso-Ramos, 2007; Moreau et al., 1997). Immunoglobulin V_H gene repertoire differs between B-CLL cells and normal peripheral blood CD5+, unlike V_L repertoire, that remains similar in both healthy and CLL B cells (Chiorazzi and Ferrarini, 2003). The lack of somatic mutations of rearranged IgV_H genes has been characterized as the strongest predictor of aggressive disease and poor response to fludarabine chemotherapy (Damle et al., 1999; Hamblin et al., 1999).

CLL is also generally described as a disease of failed apoptosis, as genetic alterations and changes in the expression of many apoptotic regulators have been reported, including Bcl-2, Bcl-x, Mcl-1, p53, PI-3K and SET, among others (Christensen et al., 2011a; Kitada et al., 1998; Klein et al., 2000; Packham and Stevenson, 2005; Ringshausen et al., 2002). Many apoptotic factors are regulated via alternative splicing, allowing the production of several protein isoforms with different functions from the same mRNA precursor. These isoforms often have antagonistic roles that are crucial for the regulation of the apoptotic pathway. In other cases, the mRNA transcript does not code for a functional polypeptide,

preventing the overexpression of the main protein (David and Manley, 2010; Schwerk and Schulze-Osthoff, 2005).

Splicing regulation has become a pathogenetic mechanism of clinical relevance in CLL, especially in cases of chemorefractoriness. Spliceosome machinery has shown to be altered in CLL, as recurrent mutations affecting the C-terminal HEAT-repeat domain of SF3B1, a component of the U2 snRNP spliceosome, appear in 10-15% of cases (Wang et al., 2011). SF3B1 mutations are associated with aggressive forms of the disease since they induce aberrant splicing in several genes (Quesada et al., 2011; Rossi et al., 2011). Besides, the frequency of SF3B1 mutations is significantly higher in CLL patients treated with fludarabine (17%) than in untreated patients (5%), suggesting that chemotherapy may induce SF3B1 mutations or select a population of mutated cells (Rozovski et al., 2013).

1.11. Caspase-9 aberrant splicing

The expression of the mRNA spliced variant of Caspase-9, termed Caspase-9b, confers the opposite effect of the full length protein by inducing resistance to apoptotic stimuli (Seol and Billiar, 1999). This aberrant form can interact with Apaf-1 CARD domain, blocking activation of Procaspase-9 and -3, and therefore inhibiting apoptosis in a dominant-negative manner. The post-transcriptional processing of Caspase-9 pre-mRNA is a complex mechanism involving the inclusion or exclusion of a four exon cassette (exons 3, 4, 5, and 6). Inclusion of these four exons into the mature transcript produces the pro-apoptotic Caspase-9 while exclusion of these exons produces the anti-apoptotic Caspase-9b. This b form of 30.1 kDa contains the first 139 residues (prodomain) fused in frame to the last 127 residues, comprising the linker segment between large and small subunit and small subunit domain, responsible for substrate specificity; nevertheless, it lacks the entire large subunit (140-289 residues), which contains the active site and is responsible for the catalytic activity. Thus, this form is catalytically inactive (Srinivasula et al., 1999). Surprisingly, Caspase-9b seems to show a tolerance to large scale aberration events, presenting an αβα-fold that may have evolved adding αβ-motifs to the edges of the core sheets, allowing this protein to fold into a stable conformation despite lacking large and conserved regions of the protein structure (Birzele et al., 2008).

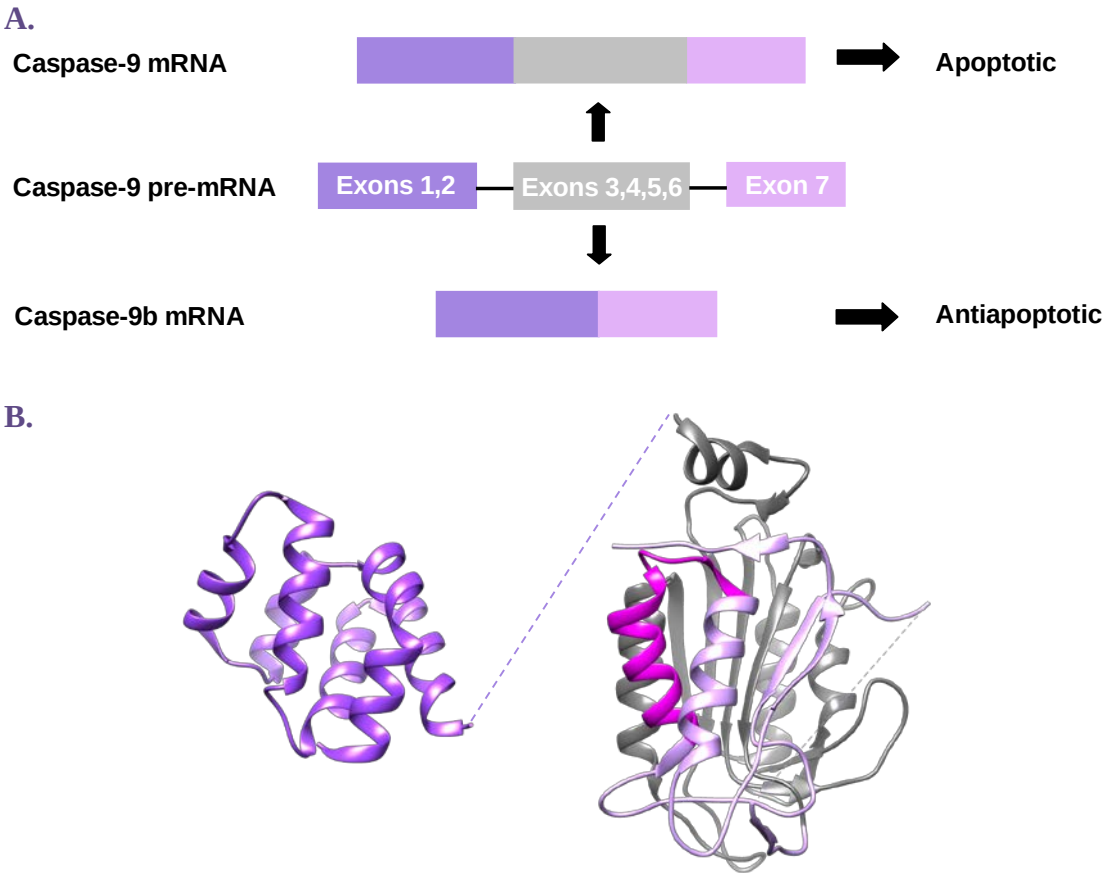

Figure 11. A. Scheme of Caspase-9 alternative splicing, leading to either the apoptotic full length protein if mRNA is formed by exons 1-7 or the aberrant antiapoptotic Caspase-9b protein, whose mRNA lacks exons 3-6. **B. Caspase-9 structure.** CARD domain is represented in purple (PDB 4RHW), the discontinuous line comprising residues 93-140 corresponds to the disordered interdomain linker between CARD domain and the large catalytic subunit, the deleted 3-6 exons in Caspase-9b that coincide with the catalytic large subunit are shown in grey, PP2A binding site is colored in magenta and Caspase-9 small subunit is presented in violet (ΔCARD-Caspase-9 PDB 1JXQ).

In healthy cells, the ratio of Caspase-9/Caspase-9b has been usually reported as 1:0.1. However, when Caspase-9 and Caspase-9b are present at equimolar concentration, only one third of Apaf-1 complexes contain functional procaspase-9 homodimers capable of autoactivation, and therefore proapoptotic. The remaining two thirds of Apaf-1 complexes would contain Caspase-9b homodimers and

procaspase-9/Caspase-9b heterodimers that would be nonfunctional, stopping the apoptotic signal. All in all, Caspase-9b overexpression may establish a threshold to regulate Caspase-9 activation and prevent spontaneous formation of the Apaf-1/Caspase-9 complex, leading to undesired apoptosis (Srinivasula et al., 1999). Caspase-9b is dysregulated in several subtypes of non-small-cell lung cancer (NSCLC) patient tumors, including adenocarcinomas, squamoid carcinomas and large-cell carcinomas. Moreover, the low Caspase-9/Caspase-9b ratio was responsible of maintaining the tumorigenic capacity of NSCLC cells and made cells resistant to erlotinib treatment (Shultz et al., 2011). Targeting the alternative splicing of Caspase-9 would sensitize NSCLC cells to already available chemotherapies, increasing their efficiency and thereby limiting their toxic side-effects (Shultz & Chalfant, 2011).

1.12. PP2Acα aberrant splicing

Little is known about PP2Acα alternative splicing, as the only report about it was recently published. An aberrant isoform of the catalytic C subunit termed PP2Acα2 was described, lacking exon 5, which is closed to the catalytic site. Although it would be expected to give rise to a dominant negative phenotype, the result was a catalytically inactive form, as PP2Acα phosphatase activity was not altered when PP2Acα2 was overexpressed. PP2Acα2 has only been observed overexpressed in PBMC cells incubated in medium without serum or rather starvation conditions during 24h. After this time, cells were still viable and the ratio PP2Acα/PP2Acα2 was reestablished once they were transferred to culture medium. When analyzed in cell lines, PP2Acα2 was present either as mRNA or as protein but at really low levels. In addition, in PBMC cells isolated from healthy donors only PP2Acα could be detected by RT-PCR. Unlike PP2Acα, PP2Acα2 presented an enhanced binding for the α4 regulatory PP2A subunit but no binding for the scaffold PP2A subunit and protein phosphatase methyl esterase-1 (PME-1).

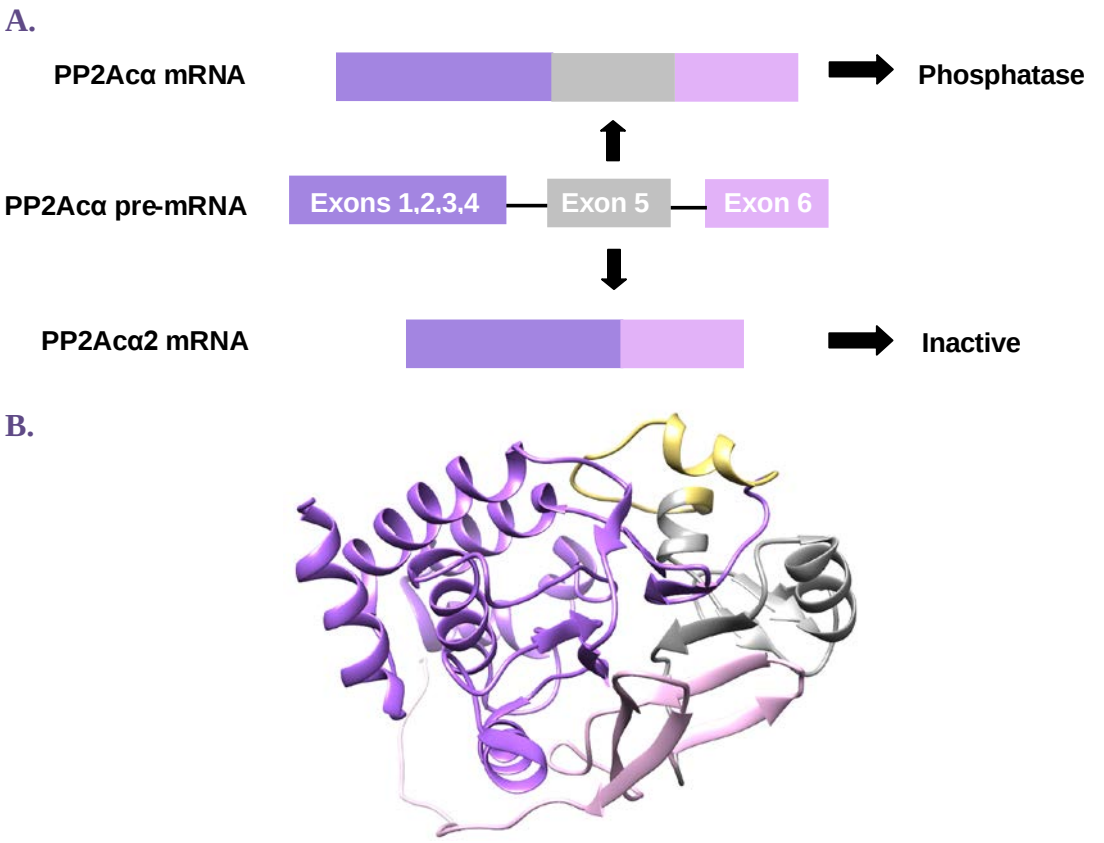

Figure 12. A. Scheme of PP2Acα alternative splicing, leading to either the apoptotic full length protein if mRNA is formed by exons 1-6 or the aberrant inactivePP2Acα2 protein, whose mRNA lacks exon 5. **B. PP2Acα structure** (PDB 2IAE), showing exons 1-4 in purple, the deleted exon 5 in PP2Acα2 is represented in grey, Caspase-9 binding site is colored in yellow and exon 6 is marked in violet.

1.13. Novel strategies for cancer therapy

The understanding of how proteins interact with each other has elucidated the molecular basis of a number of diseases, as cancer. Protein-protein interactions have developed into attractive molecular targets for novel therapies and the modulation of protein-protein interactions regulating signaling cascades is particularly relevant for the discovery of novel therapeutic agents for cancer therapies (Zinzalla and

Thurston, 2009). In this way, many therapeutic approaches have been developed to target protein-protein interactions, as it is the case of the complex SET-PP2A with the use of peptides as a potential treatment for CLL, non-Hodgkin lymphoma (Christensen et al., 2011a), glioblastoma, breast adenocarcinoma (Switzer et al., 2011) and inflammation (Christensen et al., 2011b), as well as small molecules for chronic myeloid leukemia and CLL treatment (Wang et al., 2015; Zonta et al., 2015).

A large number of potential peptide therapeutics have not obtained FDA approval due to their poor physic-chemical characteristics, as they have been considered poor drug candidates because of their low oral bioavailability and instability. Once these have been overcome with new strategies to improve peptide stability, bioavailability and prevent degradation, pharmaceutical companies have recovered their interest in developing these therapeutic peptides, despite the high attrition rates they suffered in the last decade (Goodwin et al., 2012; Kola and Landis, 2004; Vlieghe et al., 2010). Pharmacology of these peptides can be improved with their redesign including cell-penetrating peptides (CPPs) that ameliorate cellular uptake and increase bioavailability as well as providing more effective or safer routes of administration. This therapeutic potential of CPPs has led to the formation of new drug delivery companies exploiting proprietary cell-penetrating technologies (Chen and Harrison, 2007).

Another strategy developed in the last years for therapeutic delivery of different cargos has been the use of nanoparticles as drug carriers, which allow the specific release of active molecules in a controlled manner (Wu et al., 2011). Mesoporous silica nanoparticles constitute a promising tool to overcome the toxic side effects of chemotherapy due to the lack of tumor selectivity, the multi-drug resistance and metastasis occurrence. Notwithstanding, most of the nanomedicines developed based on inorganic nanocarriers are still at preclinical or basic research level (He and Shi, 2014).

1.13.1. Cell-penetrating peptides

In the last years, cell penetrating peptides (CPPs) have constituted a promising tool for therapeutic applications, as they have demonstrated to be efficient

shuttles to introduce different kind of cargoes within a great variety of cells, both *in vitro* and *in vivo* (Dietz *et al*., 2004, Johansson *et al*., 2011), as small organic molecules, nanoparticles, liposomes, peptides, proteins, siRNAs, plasmid DNA and imaging agents (Kersemans *et al*., 2010). The first CPPs derived from proteins, Tat and Antennapedia (Antp), suggested that nature had already foreseen a solution for the transportation of proteins into cells. However, for the majority of proteins and peptides which cannot enter the cells, conjugation to a CPP would facilitate their entry (Bolhassani *et al*., 2011, Hassane *et al*., 2010).

Peptides possess many advantages, as they offer high efficacy, selectivity and specificity. They have small size, ease of synthesis and modification, tumor-penetrating ability and good biocompatibility. Moreover, they lack of toxicity, as their degradation products are aminoacids, and they present low bioaccumulation, as they possess short half-life (Thundimadathil, 2012).

Based on CPPs, a new phosphatase-derived drug technology (DPT) was designed, focused on the concept of blocking the interaction of the Ser/Thr phosphatases PP1 and PP2A core catalytic subunits with their local regulatory partners using intracellular delivery of peptides to prevent specific substrate dephosphorylation. A new cell-penetrating sequence was identified in *Theileria parva* casein kinase 2α and was used as a new nontoxic shuttle for *ex vivo* and *in vivo* intracellular delivery of sequences interfering with PP2A or PP1 holoenzymes (Guergnon *et al*., 2006). Our collaborators generated a peptide containing the DPT penetrating sequence associated to the interaction motif between human Caspase-9 and PP2Acα (DPT-C9h), in order to target their association. DPT-C9h specifically targets Caspase-9/PP2A interaction *in vitro* and *in vivo* and induced Caspase-9-dependent apoptosis in cancer cell lines. DPT-C9h also induced significant tumor growth inhibition in breast cancer xenograft models. The mouse-specific peptide DPT-C9 also induced tumor growth inhibition in lung ($K\text{-}Ras^{LA\text{-}1}$) and breast cancer (Polyoma MiddleT, PyMT) mouse models without showing any toxicity nor immunogenic response (Arrouss et al., 2013). DPT-C9h had a specific effect on transformed B cells isolated from chronic lymphocytic leukemia patients without any effect on T-cells, NK-cells and monocytes but didn’t show any effect on primary B cells from healthy donors (Arrouss et al., 2015).

One concern with using peptides as therapeutics is the potential effects of serum proteases on peptide degradation prior to cellular internalization. Several measures have been performed to stabilize CPPs for *in vivo* applications, as the incubation with SDS or polysialic acid, substitution of L-aminoacids by D-isomers containing peptides, retroinversion, the use of non-natural aminoacids, modification of peptide backbones, cyclization, disulfide bond formation, constrained peptides and stapled peptides among others (Fominaya et al., 2015b). DPT-C9h serum proteolysis resistance was improved performing mutations in a serum protease cleavage site comprised within the CPP sequence. The peptide Mut3DPT-C9h with an Arginine to alanine mutation at the eighth residue of the DPT sequence showed enhanced peptide stability and a better pharmacokinetic profile, also maintaining the same apoptotic effect as the original DPT-C9h (Fominaya et al., 2015a).

1.13.2. Mesoporous silica nanoparticles

Mesoporous silica nanoparticles (MSNs) have been widely used as reservoirs for drug storage and delivery because of their unique mesoporous structure that confers large load capacity, biocompatibility, high thermal stability, homogeneous porosity, inertness and tunable pore sizes. MSNs undergo cellular uptake by endocytosis and they are assembled on their external surface with gates that allow them to show zero-delivery and release their cargo upon external stimuli in a controlled way (Agostini et al., 2012; Li et al., 2012). Mesoporous silica nanoparticles have shown to preferentially accumulate in tumors in biodistribution studies performed in human cancer xenograft models and effectively deliver drugs in the tumors and suppress tumor growth, thus presenting a satisfactory biocompatibility (Lu et al., 2010).

MCM-41 nanoparticles have a size of 100nm of diameter and present a regular pore system formed by an array of unidimensional hexagonally shaped pores, composed of amorphous silica (Kresge et al., 1992). MCM-41 have been successfully applied for the delivery of ibuprofen (Vallet-Regí, 2006; Vallet-Regí et al., 2001), antibacterial drugs (Mas et al., 2013) and cancer chemotherapeutics (de la Torre et al., 2014; Giménez et al., 2015). In the present work, we have used MCM-41 nanoparticles loaded with C9h Caspase-9 peptide and functionalized on the outer

surface with the polymer ε-poly-L-lysine, which showed zero cargo release in water and a high delivery in the presence of pronase protease, due to ε-poly-L-lysine hydrolysis (Mondragón et al., 2014).

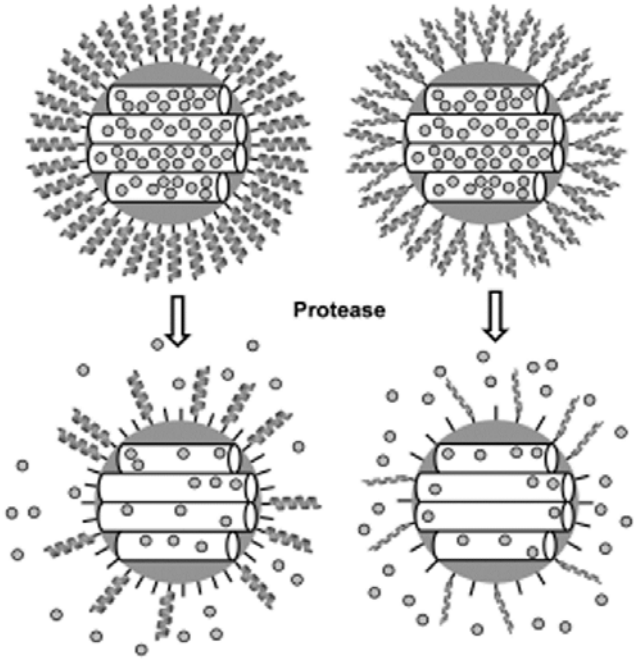

Figure 13. Schematic representation of MCM-41 nanoparticles loaded with the chosen cargo and capped with ε-poly-L-lysine attached specifically through the C-terminal side of the polymer in the left figure and randomly anchored to the nanoparticles through the amino groups in the side chains of the lysine aminoacids in the right side of the figure. In the presence of an intracellular protease, ε-poly-L-lysine amide bonds are hydrolyzed, allowing the delivery of the cargo. Adapted from (Mondragón et al., 2014).

INTRODUCCIÓN

2. INTRODUCCIÓN

2.1. Muerte celular programada y apoptosis

Las células de un organismo multicelular son miembros de una comunidad altamente organizada. El número de células en esta entidad está regulado estrechamente, no sólo por el rango de control de la división celular, sino también por el rango de muerte celular. Cuando las células ya no son necesarias, se suicidan activando un programa intracelular denominado generalmente muerte celular programada (Alberts et al., 2004). Se han descrito tres tipos principales de muerte celular programada: apoptosis, necroptosis y autofagia. En los últimos años se ha conocido que estas tres rutas están interconectadas de manera compleja. Algunas moléculas iniciadoras y efectoras de señales de muerte, rutas de señalización y localizaciones subcelulares constituyen elementos comunes a apoptosis y necroptosis o actúan a modo de interruptor entre estos dos procesos. Además, la autofagia, a pesar de ser un proceso predominantemente citoprotector, se ha relacionado con apoptosis y necroptosis, puesto que presenta tanto una función a favor de la supervivencia como a favor de la muerte celular (Nikoletopoulou et al., 2013).

Entre estas rutas, la apoptosis es la que se ha estudiado más intensamente desde que fue descrita por (Kerr et al., 1972), y comprende el principal mecanismo de muerte celular regulada, que tiene un papel crucial no sólo en situaciones de daño celular o estrés, sino también durante el desarrollo normal y la morfogénesis. Cuando una célula sufre apoptosis, muere de forma limpia sin dañar a las células vecinas. La membrana mitocondrial se permeabiliza, la cromatina se condensa, el citoesqueleto colapsa, la membrana nuclear se desensambla y el ADN nuclear se rompe en fragmentos. A su vez, la superficie celular se altera dando lugar a una célula redondeada y a la formación de cuerpos apoptóticos. La célula que está muriendo será fagocitada rápidamente bien por una célula vecina o por un macrófago antes de que tenga lugar cualquier escape de su contenido, lo que permite el reciclaje de los componentes orgánicos de la célula muerta por parte de la célula que la engulle (Alberts et al., 2004).

La apoptosis es crucial para el desarrollo normal (Arya and White, 2015), el mantenimiento de la homeostasis de los tejidos y para un sistema inmune efectivo.

Por ello, su alteración está implicada en numerosas patologías, como enfermedades neurodegenerativas, daño isquémico, enfermedades autoinmunes y cáncer (Fernald and Kurokawa, 2013; Hassan et al., 2014).

2.2. Rutas de apoptosis dependiente e independiente de Caspasas

La cascada de señalización apoptótica dependiente de caspasas puede activarse principalmente bien a través de una ruta extrínseca o de una ruta intrínseca; sin embargo, existen evidencias que señalan que ambas rutas están conectadas y que las moléculas de una ruta pueden influenciar a las de la otra. Finalmente, ambas rutas desencadenan la activación de una familia de proteasas de cisteína aspartilo, llamadas caspasas, que se describirán en detalle posteriormente (Elmore, 2007).

La ruta extrínseca recibe estímulos a través de los receptores de muerte de la superficie celular, como TNFα (tumor necrosis factor α, factor de necrosis tumoral α), Fas (CD95/APO1) y TRAIL (TNF related apoptosis inducing ligand, ligando inductor de apoptosis relacionado con TNF).

Cuando se une el ligando, las proteínas adaptadoras citoplasmáticas se reclutan y exhiben sus dominios de muerte que se unen a los receptores. La unión del ligando Fas al receptor TNF resulta en la unión de la proteína adaptadora TRADD, junto con el reclutamiento de FADD y RIP, y posteriormente FADD se asocia con procaspasa-8. A continuación se forma un complejo de señalización inductor de muerte (DISC, death-inducing signaling complex, complejo de señalización inductor de muerte), que conduce a la activación autocatalítica de Caspasa-8, que a su vez desencadena la fase de ejecución de apoptosis (Hsu et al., 1995; Kischkel et al., 1995; Locksley et al., 2001; Wajant, 2002).

La ruta intrínseca se activa a través de estímulos internos, que desencadenan la apertura del poro de transición de permeabilidad mitocondrial, la pérdida del potencial transmembrana mitocondrial y la liberación de proteínas al citosol, como citocromo c, Smac/DIABLO y la proteasa de serina HtrA2/Omi, que a su vez activa la ruta mitocondrial dependiente de caspasas (Chinnaiyan, 1999; Du et al., 2000; Garrido et al., 2006; Saelens et al., 2004). En el citoplasma, la hidrólisis de ATP/dATP por parte de Apaf-1 y su unión a citocromo c favorece la

oligomerización de Apaf-1, formando un complejo multimérico Apaf-1 – citocromo c, que es suficiente para reclutar y activar a procaspasa-9 (Zou et al., 1999) . En un estudio posterior se demostró también que los dominios de reclutamiento de caspasas de Apaf-1 y procaspasa-9 forman un disco CARD-CARD, que se une de forma flexible al apoptosoma (Yuan et al., 2011, 2010).

Las rutas extrínseca e intrínseca convergen a la altura de las caspasas ejecutoras, donde Caspasa-9 madura procesa y activa a Caspasa-3 y -7 para ejecutar el evento apoptótico (Salvesen and Ashkenazi, 2011). Procaspasa-9 y Caspasa-3 madura presentan sitios de unión que se superponen en el núcleo central del apoptosoma; sin embargo, procaspasa-3 no se une al apoptosoma. Estos sitios de unión compartidos pueden jugar un papel en la activación de procaspasa-3, puesto que los apoptosomas de procaspasa-9 procesan a procaspasa-3, creando dímeros de Caspasa-3/procaspasa-3 y dímeros totalmente activos de Caspasa-3, pero sólo la proteína madura activa se une al apoptosoma. Esto sugiere la formación de apoptosomas híbridos con las actividades proteolíticas de procaspasa-9 y Caspasa-3, lo que permite a Caspasa-3 regular la actividad de procaspasa-9 en el apoptosoma (Yuan et al., 2011).

Existe una tercera ruta de apoptosis que implica citotoxicidad mediada por células T y la muerte celular dependiente de perforina-granzima, induciendo apoptosis via granzima B o A. Granzima B procesa a procaspasa-10 y a factores como ICAD (inhibitor of caspase activated DNAse, inhibidor de la ADNasa activada por caspasas), utiliza la ruta mitocondrial a través del procesamiento específico de Bid y la inducción de la liberación de citocromo c y también puede activar directamente a Caspasa-3 (Barry and Bleackley, 2002; Russell and Ley, 2002). La ruta de granzima A activa una ruta de muerte celular independiente de caspasas a través del daño de ADN de cadena sencilla así como de una pérdida rápida de la integridad de la membrana celular y el potencial transmembrana mitocondrial, generando con ello especies reactivas de oxígeno, que dirigen al complejo SET hacia el interior del núcleo (Lieberman, 2010; Martinvalet et al., 2005). La proteasa granzima A procesa el complejo SET, liberando la inhibición del supresor de tumores NM23-H1, dando lugar a la degradación del ADN. Además, el complejo SET juega un papel importante en la estructura de la cromatina y la reparación del ADN y los miembros de este complejo (la proteína de ensamblaje del nucleosoma

SET, la endonucleasa de reparación de escisión de bases Ape1, el supresor de tumores pp32 y la proteína de torsión de ADN HMG2) parecen trabajar juntos para proteger a la cromatina y a la estructura del ADN.

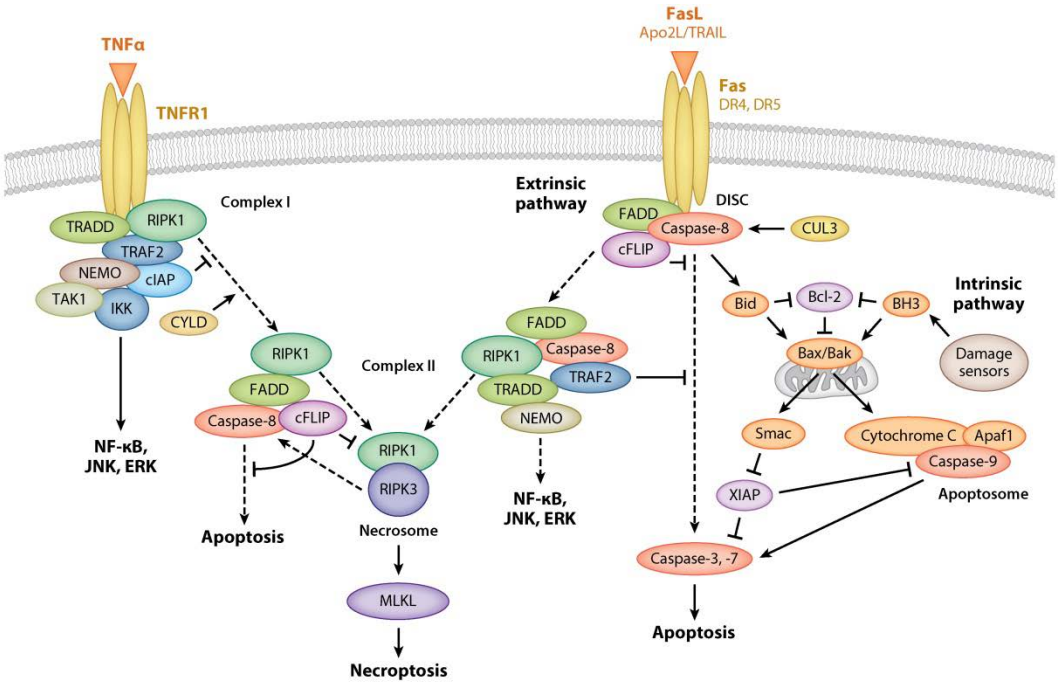

Figura 14. Esquema del control de la muerte celular por parte de los receptores de muerte. En la ruta extrínseca, cuando se une el ligando, los receptores de muerte Fas, DR4 o DR5 se ensamblan en un DISC primario en la membrana plasmática, activando con ello a Caspasa-8, que estimula directamente a las caspasas ejecutoras -3 y -7. Esta ruta está conectada con la ruta intrínseca por el procesamiento de la proteína de sólo-BH3 BID, que posteriormente activa a BAX y a BAK para inducir la liberación de citocromo c y Smac/DIABLO de la mitocondria. Después, citocromo c se asocia con Apaf-1 para formar un apoptosoma, que conduce a la activación de Caspasa-9 y posterior estimulación de Caspasa-3 y -7. En la ruta de necroptosis lo que ocurre a grandes rasgos es que cuando se une el ligando a TNFα, TNFR1 ensambla el Complejo I en la membrana plasmática. Un segundo complejo, Complejo II también es ensamblado por los mismos receptores que en la ruta extrínseca. La inhibición de Caspasa-8 permite a RIPK1 reclutar a RIPK3 y formar un tercer complejo, el complejo de necrosoma, desencadenando la necroptosis. Tomada de (Ashkenazi and Salvesen, 2014).

Además, el procesamiento de Ape1 por parte de granzima A interfiere con sus funciones de reparación oxidativa y en consecuencia la célula pierde su

capacidad de autorreparación. Por eso, cuando granzima A inactiva este complejo también contribuye a la apoptosis, bloqueando el mantenimiento del ADN y la integridad de la estructura de la cromatina (Fan et al., 2003; Lieberman and Fan, 2003).

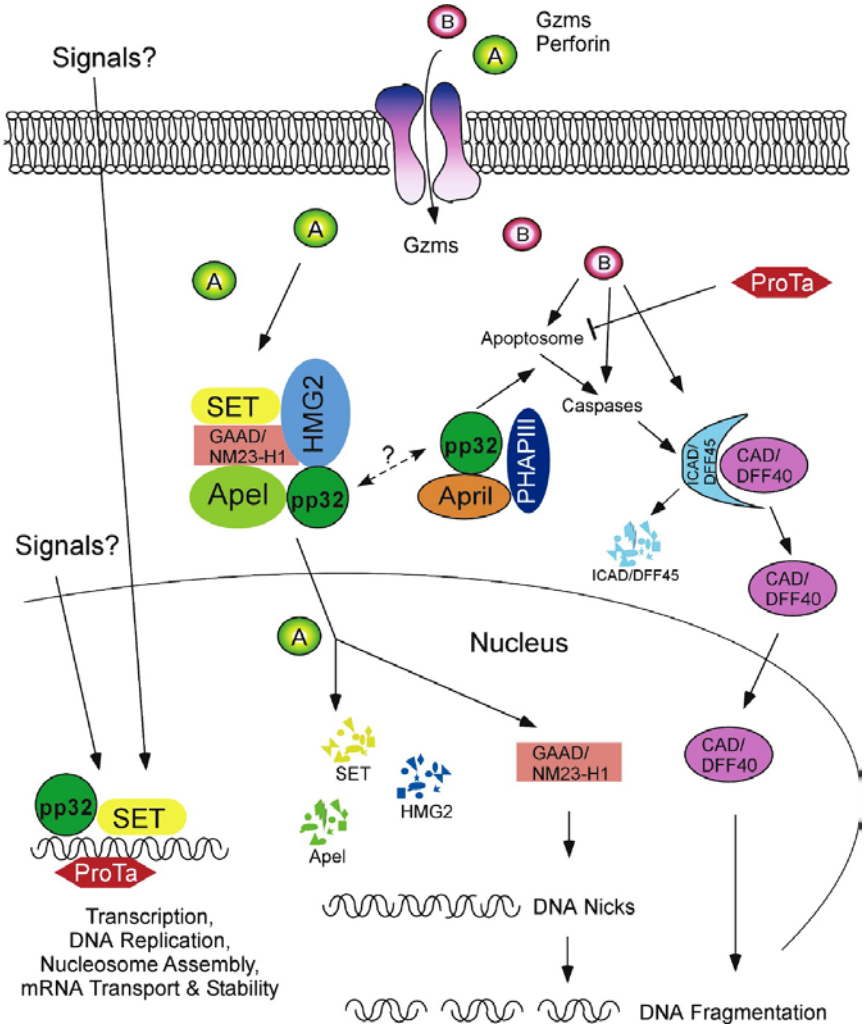

Figura 15. Ruta de apoptosis de granzima A y B. Granzima A procesa a SET, HMG2 y Ape1, pero no a PP32, para activar la función ADNasa de NM23-H1 y para inducir su actividad endonucleasa de ADN. Granzima B induce apoptosis dependiente de caspasas. También PP32 y sus homólogos April y PHAPIII favorecen la formación del apoptosoma y las actividades caspasa, conectando con ello las rutas de apoptosis dependiente e independiente de caspasas. Tomada de (Chakravarti and Hong, 2003).

2.3. Caspasas en apoptosis

La maquinaria intracelular responsable de la apoptosis parece ser similar en todas las células animales. Esta maquinaria se basa en una familia de proteasas que presentan cisteína en el sitio activo y procesan a sus proteínas diana a través de residuos específicos de aspartato. El término que se utilizó inicialmente para designar a esta familia fue el de proteasas dependientes de cisteína específicas de aspartato, que posteriormente se acortó a caspasas (Alnemri et al., 1996). Las caspasas son necesarias para la apoptosis y la respuesta inflamatoria. Hay 14 tipos diferentes de caspasas en mamíferos, pero sólo 11 de ellos están presentes en humanos. Las caspasas se producen en las células como zimógenos inactivos y están constituidas por una subunidad grande y una subunidad pequeña, de modo que todas las estructuras cristalográficas resueltas de caspasas muestran el mismo plegamiento básico (Denault and Salvesen, 2002a). Las caspasas activas generalmente se encuentran como dímeros de dominios catalíticos, principalmente unidos a través de interacciones hidrofóbicas. Las subunidades de cada dominio catalítico son sándwiches αβα, plegados en un cilindro compacto con seis láminas β en el centro, rodeadas por cinco hélices situadas en lados opuestos del plano formado por las láminas β. El dímero catalítico presenta monómeros ordenados según una simetría doble, con los dos sitios activos en extremos opuestos del dímero. El extremo C-terminal de la subunidad grande y el extremo N-terminal de la subunidad pequeña se encuentran próximos entre sí. El par catalítico His237/Cys285, que está muy conservado entre caspasas, se encuentra en la subunidad grande.

La variación en la secuencia de aminoácidos de la subunidad pequeña es la responsable de la variabilidad en la especificidad de sustrato de las caspasas. La cadena principal del sustrato forma una lámina β antiparalela con la cadena principal de los residuos 339-341, en el caso de Caspasa-3, pero es similar en otras caspasas. Esta forma de alineamiento del sustrato difiere fuertemente de lo que se encuentra en otras familias de proteasas de cisteína, pero la comparten con la familia de proteasas de serina de las quimotripsinas.

Los dominios catalíticos de las caspasas, de en torno a 30kDa, están bien conservados y contienen toda la maquinaria catalítica. Además, se encuentran otros dos tipos de dominios en la región aminoterminal de algunas caspasas: CARD

(caspase activation and recruitment domain, dominio de activación y reclutamiento de caspasas) y DED (death effector domain, dominio efector de muerte). Ambos dominios están implicados en interacciones homofílicas con otras proteínas, lo que permite que los respectivos zimógenos de caspasas sean reclutados en complejos de proteínas para facilitar su activación. La activación de caspasas que contienen dominios CARD y DED normalmente conduce al procesamiento de estos dominios y la liberación de la porción catalítica activa, a excepción de Caspasa-9, como se detallará a continuación. Caspasa-3, -6 y -7 presentan un péptido N corto de 27-28 residuos que se elimina durante la activación.

Una caspasa efectora se activa por una caspasa iniciadora a través del procesamiento proteolítico de la primera en residuos de aspartato específicos internos, para separar las subunidades grande y pequeña de la caspasa madura. Una vez activadas, las caspasas efectoras pueden actuar sobre un amplio rango de dianas celulares, causando finalmente la muerte celular (Parrish et al., 2013).

2.4. Caspasa-9

Caspasa-9 es una caspasa apoptótica iniciadora, cuya activación por dimerización requiere un reordenamiento de bucles para posicionar la maquinaria catalítica y los sitios de unión al sustrato (Denault and Salvesen, 2002b). La activación de procaspasas normalmente requiere la escisión de un residuo de aspartato específico interno presente en los conectores interdominio entre el prodominio y la región catalítica y entre ambas subunidades catalíticas. Este procesamiento libera el prodominio y genera las subunidades grande y pequeña para formar una entidad catalítica dimérica. Caspasa-9 tiene dos sitios potenciales de procesamiento, los residuos de aspártico 315 y 330, y el sitio activo, cisteína 287. Se ha demostrado que la mutación en el sitio activo evita el autoprocesamiento de Caspasa-9 que daría lugar a ambas subunidades (Srinivasula et al., 1998).

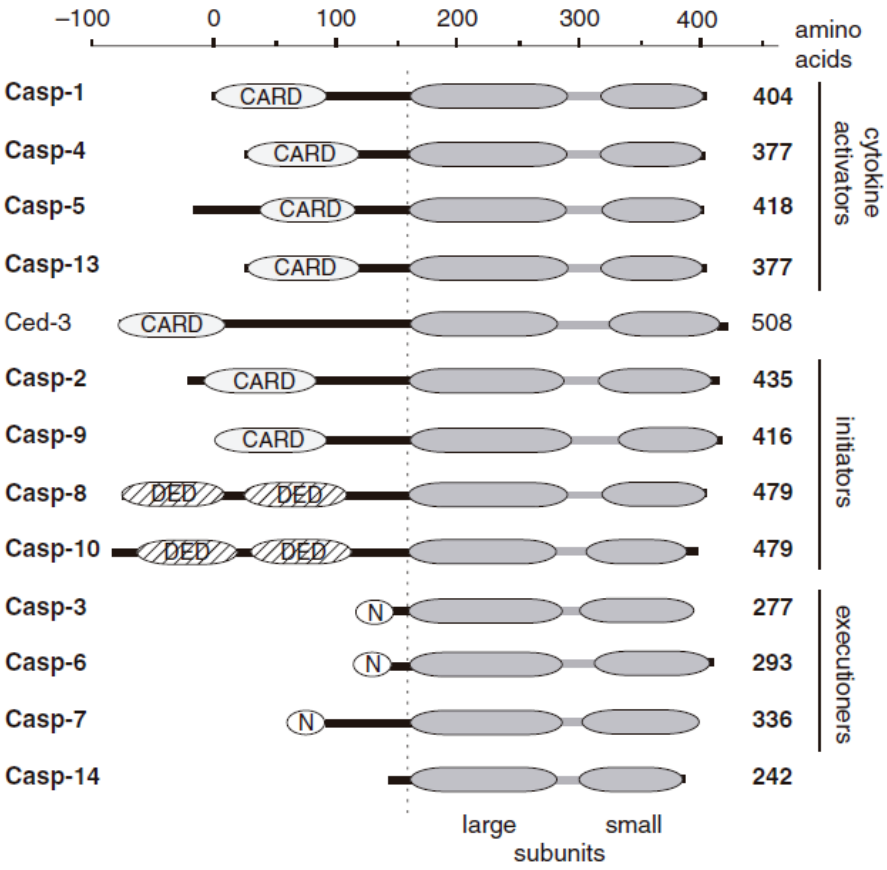

Figura 16. Esquema de la organización de dominos de las caspasas y de los miembros de la familia Ced-3 de *C. elegans*. El dominio CARD está representado en gris claro, el dominio DED a rayas y el N corresponde al péptido pequeño N de las caspasas ejecutoras. La escala se ha establecido de acuerdo a los números de los residuos de Caspasa-1. La línea de puntos indica el inicio de la subunidad grande. Tomada de (Denault and Salvesen, 2002a).

Desde el punto de vista estructural, la Caspasa-9 madura es un heterotetrámero compuesto por dos heterodímeros antiparalelos, cada uno de ellos formado por una subunidad p20 (20kDa) y una subunidad p10 (10kDa). Al igual que para otras caspasas, el dímero está formado a través de interacciones entre las cadenas 8 de las subunidades pequeñas. Sin embargo, hay dos características que son únicas para Caspasa-9. En primer lugar, en otras caspasas se encuentra una lámina β pequeña entre los residuos del C-terminal de la subunidad grande y los residuos del

N-terminal de la subunidad pequeña que no está presente en Caspasa-9, debido al desorden de la parte C-terminal del dominio inactivo de la subunidad grande. A su vez, la subunidad grande posee un giro de 7 residuos insertado en la posición 240 entre las cadenas 3 y 3A, que interacciona a través de la superficie del dímero (Renatus et al., 2001).

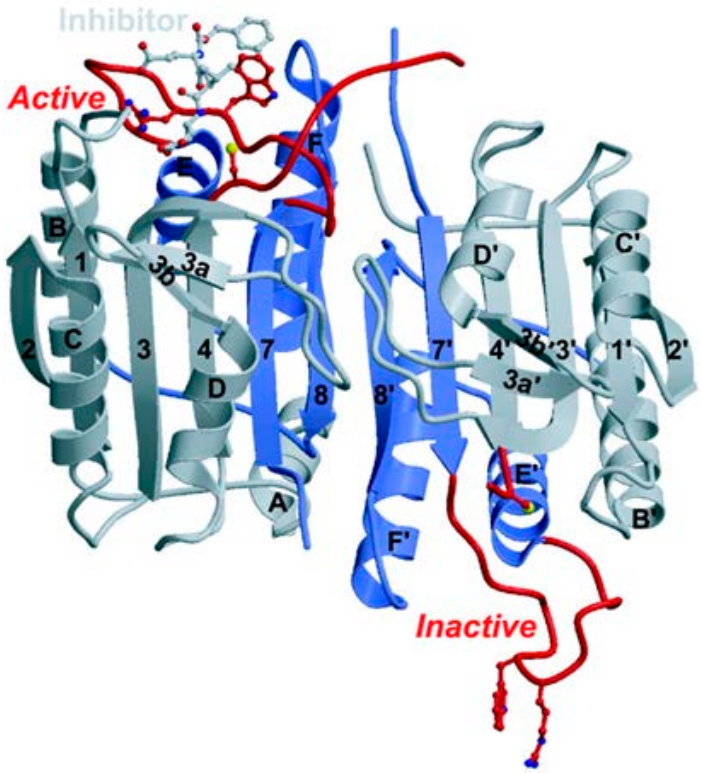

Figura 17. Esquema de la estructura de ΔCARD Caspasa-9. La subunidad grande está coloreada en gris y la subunidad pequeña en azul. El inhibidor Z-EVD-DCBMK que se cristalizó con Caspasa-9 está representado en gris claro y las cadenas laterales del residuo catalítico cisteína 285 así como los residuos determinantes de especificidad arginina 341 y triptófano 340 están representados con esferas y bastones. Tomado de (Renatus et al., 2001).

A concentraciones en el rango de micromolar, Caspasa-9 es un monómero inactivo, y su forma completa *in vivo* es también un monómero (Renatus et al., 2001). Caspasa-9 no se activa por proteólisis, sino por interacciones homofílicas entre el dominio CARD de Caspasa-9 y el cofactor Apaf-1 en presencia de

citocromo c y ATP, para generar un apoptosoma completamente funcional, como se ha descrito previamente. Este apoptosoma controla la supresión celular durante el desarrollo del sistema nervioso central y la respuesta apoptótica a agentes letales para la célula, como la radiación ionizante o drogas quimioterapeúticas.

La función de Caspasa-9 es generar las formas activas de Caspasa-3 y Caspasa-7 por proteólisis limitada, transmitiendo con ello la señal apoptótica a la fase de ejecución (Riedl et al., 2001).

2.5. Regulación de las caspasas

Dado que las caspasas juegan un papel clave en la apoptosis, su activación y actividad están estrechamente reguladas para evitar una muerte celular no planeada. Este control tiene una importancia crucial para esquivar procesos patológicos como una muerte celular apoptótica aberrante o prematura, que conduciría potencialmente a carcinogénesis, autoinmunidad, neurodegeneración e inmunodeficiencia. Bien antes o después de su activación, las caspasas pueden estar reguladas a través de una variedad de mecanismos que pueden inhibir o aumentar la actividad enzimática o afectar a la actividad a través de sustratos celulares determinados (Parrish et al., 2013).

El primer punto de regulación es a nivel de la síntesis, dado que las caspasas se producen inicialmente como zimógenos inactivos que carecen de actividad proteasa, de forma que sólo serán activados por parte de ciertos estímulos (Earnshaw et al., 1999).

Una forma de regulación posterior es por proteólisis, en la que el prodominio N-terminal tiene un papel importante. Esta región contiene dominios bien conservados: CARD para caspasas -1, -2, -4, -5, -9, -11 y -12, y DED en Caspasa-8 y -10. Ambos dominios están vagamente relacionados y están implicados en interacciones homofílicas con otras proteínas, permitiendo a los zimógenos de caspasas ser reclutados en complejos de proteínas para promover su activación. Las caspasas que contienen dominios CARD o DED se activan generalmente por procesamiento proteolítico a excepción de Caspasa-9, como se ha descrito previamente (Denault and Salvesen, 2002a). Las caspasas iniciadoras se activan a

través de proteólisis limitada cuando las proteínas adaptadoras interaccionan con los prodominios N-terminales y favorecen la dimerización de las caspasas. Sin embargo, las caspasas efectoras existen en la célula como homodímeros inactivos, que se activan por el procesamiento del prodominio mediado por una caspasa iniciadora.

La regulación de Caspasa-9 a nivel posttraduccional es la que mejor caracterizada está de la familia. Se han descrito algunos sitios de fosforilación, resultando en la mayoría de los casos en una reducción de la activación y/o del procesamiento de la proteína (Allan and Clarke, 2009). Este mecanismo está controlado por dos grandes familias de proteínas: proteín kinasas y proteín fosfatasas. Los eventos de fosforilación y desfosforilación afectan a la conformación de la proteína diana y/o su interacción con otras proteínas, así como a su actividad, función, vida media, estabilidad, afinidad por el sustrato o localización subcelular (Bononi et al., 2011). Se sabe que la Treonina 125 es el sitio de fosforilación de la kinasa Erk, pero también de cdk1, DYRK1A y p38α (Allan et al., 2003; Seifert and Clarke, 2009). También se han descrito otros sitios de fosforilación, como la Serina 144, fosforilada por PKCζ en respuesta a estrés hiperosmótico, Serinas 99, 183 y 195 por PKA, Serina 196 por PKB/Akt, Serina 348 por CK2 y tirosina 153 por c-Abl después de que se produzca daño en el ADN (Brady et al., 2005; Cardone et al., 1998; Martin et al., 2005; McDonnell et al., 2008; Raina et al., 2005). Caspasa-9 también puede modificarse por nitrosilación en presencia de niveles altos de óxido nítrico (Török et al., 2002).

Según el nivel de estabilidad de la proteína, Caspasa-9 puede ser regulada por ubiquitinación mediada por la ubiquitín ligasa E3 XIAP (X-linked inhibitor of apoptosis protein, proteína unida a X inhibidora de apoptosis), que sólo poliubiquitila la subunidad grande de la Caspasa-9 activa pero no la procaspasa-9 inactiva. Tomada de (Silke and Meier, 2013).

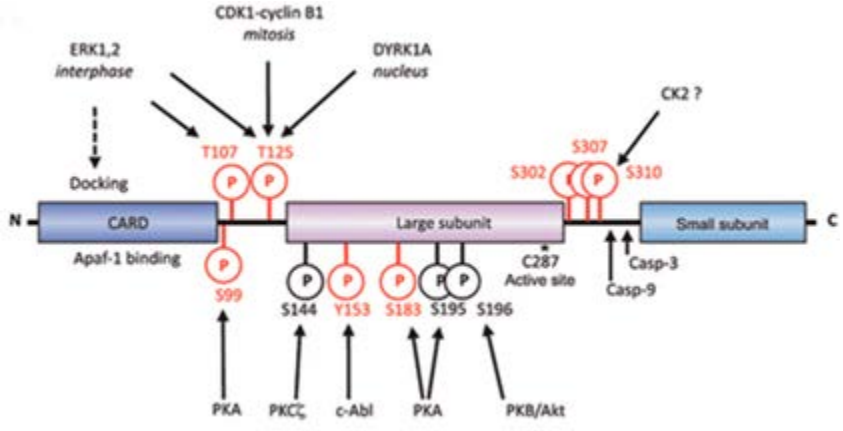

Figura 18. Sitios de fosforilación de Caspasa-9. Representación lineal de Caspasa-9 con la posición de los sitios de fosforilación y la proteín kinasa responsable de la fosforilación en cada sitio. Tomada de (Allan and Clarke, 2009).

2.6. Proteín fosfatasas de serina/treonina en apoptosis

En eucariotas, los residuos más comúnmente modificados son serina y treonina. De hecho, el 98% de los eventos de desfosforilación ocurren en estos dos aminoácidos y hay dos proteínas principales llamadas proteín fosfatasa 1 (PP1) y proteín fosfatasa 2A (PP2A) de la familia de las fosfoproteín fosfatasas (PPP) denominadas proteín fosfatasas de serina/treonina, que engloban el 90% de las desfosforilaciones de serina/treonina (Xiao et al., 2010). Además, PP1 y PP2A son reguladores importantes en varios niveles de la ruta de apoptosis y son dos de las enzimas más abundantes en muchos tipos celulares. Estas proteínas son parte de una complicada intercomunicación entre kinasas y fosfatasas en la ejecución de apoptosis, en la que las caspasas son las principales conductoras.

Las protein fosfatasas de serina/treonina PP1 y PP2A tienen un papel clave en la regulación de los miembros de la familia Bcl-2 y de las caspasas en la decisión de la célula de vivir o morir. PP1 y PP2A están implicadas en la inducción de muerte celular a través de la desfosforilación de Bad (un miembro de la familia proapoptótica Bcl-2) (Ayllón et al., 2002, 2000), estimulación de la liberación de citocromo c de la mitocondria y desfosforilación de la proteína retinoblastoma (Ray

et al., 2005; Rubin et al., 2001). No obstante, PP1 y PP2A pueden presentar una función tanto apoptótica como antiapoptótica, dado que la inhibición de PP1α o PP2A puede desencadenar la apoptosis (Kang and Choi, 2001; Singh et al., 2000).

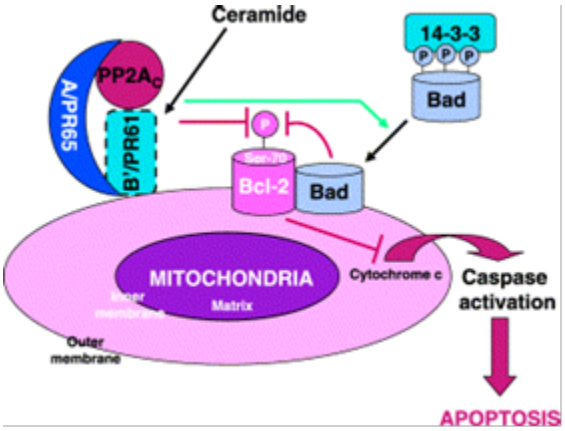

Figura 19. Papel regulador de PP2A en la ruta de transducción de señales de apoptosis aguas arriba de Bcl-2. PP2A desfosforila e inactiva a Bcl-2 en la Serina 70. PP2A también es una fosfatasa de Bad, manteniendo esta proteína desfosforilada y localizada en la mitocondria. El resultado neto es la liberación de citocromo c, necesaria para la respuesta apoptótica. Tomada de (Van Hoof and Goris, 2003).

PP1 y PP2A también pueden controlar la apoptosis a través de la regulación negativa de otras proteínas antiapoptóticas, modulando la función de Akt como regulador de la supervivencia celular, la diferenciación y la expresión de genes desfosforilando directamente la Treonina 450 y la Treonina 308 y Serina 473 respectivamente (Kuo et al., 2008; Xiao et al., 2010). Estas dos fosfatasas también tienen un papel importante en la regulación del estado de fosforilación de Caspasa-9, controlando con ello su activación bajo ciertos estímulos, como se detallará a continuación (Arrouss et al., 2013; Dessauge et al., 2006).

2.7. Proteín fosfatasa 1A

La proteín fosfatasa 1 (PP1) es una fosfatasa de serina/treonina ubicua que regula diferentes procesos celulares importantes como progresión celular, citocinesis, transcripción, síntesis de proteínas, metabolismo de carbohidratos, contracción

muscular y señalización neuronal. En mamíferos hay tres genes que codifican para cuatro subunidades catalíticas de PP1: PP1α, PP1β/γ y las variantes de procesamiento $PP1\gamma_1$ y $PP1\gamma_2$, que muestran mayores diferencias en la secuencia entre ellas en el extremo C-terminal. PP1α es una proteína de 38kDa altamente conservada que desfosforila cientos de sustratos biológicos clave, y su apoenzima se asocia con más de 200 proteínas reguladoras para formar holoenzimas específicas (Bollen et al., 2010). De hecho, la especificidad del dominio catalítico por ciertos residuos cerca del sitio diana de fosforilación parece ser limitada. Por este motivo, la acción de PP1 está dirigida en espacio y tiempo por estas proteínas reguladoras. Sin embargo, PP1 ha demostrado poseer dominios de interacción que están conservados entre las proteínas que interaccionan con ella. El más común es el motivo RVxF, que está presente en la mayoría de las proteínas que interaccionan con PP1 (PIPs, PP1-interacting proteins). La secuencia consenso descrita por (Bollen et al., 2010) es K/R/H/N/S-V/I/L-x-F/W/Y, siendo x cualquier residuo excepto Phe, Ile, Met, Tyr, Asp o Pro. Aunque cause pocos cambios conformacionales en la subunidad catalítica de PP1, la unión a este motivo es crucial para las proteínas que interaccionan con PP1 para anclarse a ella. Este sitio de unión ayuda a atraer proteínas que interaccionen con ella, y de esta manera proporcionar uniones adicionales que determinan la actividad y especificidad de sustrato de la holoenzima. El bloqueo de uno de estos motivos puede ser suficiente para debilitar o incluso romper la interacción. Otros motivos comunes de PIPs son SILK y MyPhoNE, ambos situados normalmente hacia el N-terminal del motivo RVxF (Hendrickx et al., 2009).

El sitio catalítico de PP1 se encuentra en la intersección de tres regiones potenciales de unión de sustrato: los surcos hidrofóbico, acídico y C-terminal. Los dos metales localizados en el sitio activo de PP1 median una reacción de desfosforilación en un único paso. Estos iones metálicos aumentan la nucleofilicidad de la molécula de agua que está unida al sitio activo, dando lugar a la sustitución nucleofílica por el fosfato. Cuando se sobreexpresa PP1 *in vitro*, se produce en presencia de $MnCl_2$ y dos iones Mn^{2+} permanecen unidos al sitio activo (Dancheck et al., 2011; Goldberg et al., 1995).

Todas las estructuras resueltas de PP1 presentan una conformación invariable, que resulta ser independiente de la proteína con la que interacciona, como se representa en la **Figura 20** (Peti et al., 2013). PP1 está plegada en un único

dominio elíptico que comprende un sándwich β central de dos láminas β mixtas, rodeado por un lado por siete hélices α y por el otro lado por un subdominio formado por tres hélices α y una lámina β mixta de tres cadenas. La interfaz de las tres láminas β en la parte superior de sándwich β genera un canal en la superficie del sitio catalítico. En la lámina 1 está presente un motivo β-α-β-α-β que, junto con los bucles de la lámina β opuesta (lámina 2), proporciona los residuos del sitio catalítico (Egloff et al., 1995).

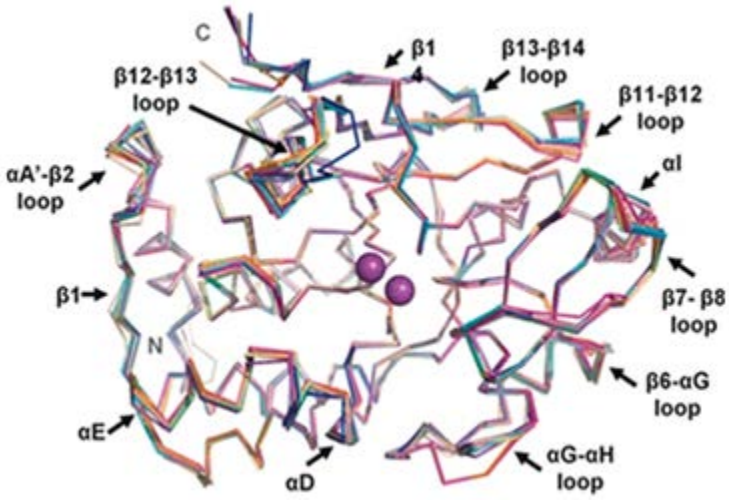

Figura 20. Superposición de las estructuras de PP1 mostrando que su conformación es invariable independientemente de los ligandos que se unan a la proteína. Las estructuras representadas se corresponden con los códigos PDB 1FMJ (azul oscuro), 1IT6 (cián), 1JK7 (magenta), 1S70 (beige), 2BCD (salmón), 2BDX (naranja), 2O8G (azul pizarra), 3E7A (gris), 3E7B (verde lima), 2EGG (verde azulado), 3HVQ (rosa), 3N5U (amarillo anaranjado) and 3EGH (morado - azul). Las regiones de PP1 que presentan cambios conformacionales están señaladas. Tomada de (Peti et al., 2013).

Nuestros colaboradores describieron la interacción directa entre PP1 y Caspasa-9, demostrando que la privación de IL-2 inducía la desfosforilación de PP1, conduciendo a su activación y posterior desfosforilación y activación de Caspasa-9. En este estudio, se detectaron tres sitios de unión a Caspasa-9 en PP1, que estaban separados en la secuencia de aminoácidos pero próximos en la estructura de la proteína, así como expuestos en la superficie, permitiendo la interacción con Caspasa-9. El sitio catalítico de PP1 está situado en el otro lado de la molécula. Del mismo modo, se determinaron dos sitios de unión a PP1 en la secuencia de Caspasa-

9, comprendidos en los 16 primeros aminoácidos de la secuencia de la proteína, que se corresponde con el extremo N-terminal del dominio CARD, y los residuos 185-201 de Caspasa-9 humana (residuos 223-239 de Caspasa-9 de ratón), localizados en la subunidad grande del dominio ΔCARD Caspasa-9, el dominio catalítico p20 (Dessauge et al., 2006).

Figura 21. Modelo de la interacción entre Caspasa-9 y PP1cα mostrando los sitios de unión. Caspasa-9 se ha representado en morado, mostrando el dominio CARD arriba (PDB 4RHW) y el dominio ΔCARD (PDB 1JXQ) abajo. Estas dos estructuras están unidas por una línea discontinua que abarca los residuos 93-139 correspondientes al conector flexible entre ambos dominios. Los sitios de unión de PP1 están resaltados en verde. PP1cα se ha coloreado en azul a la derecha (PDB 3E7A), mostrando los sitios de unión a Caspasa-9 en amarillo. El tercer sitio de unión a Caspasa-9, que se corresponde con los residuos 312-328 no se muestra en la figura, puesto que estos residuos no son visibles en la estructura.

2.8. Proteín fosfatasa 2A

PP2A es una fosfatasa de serina/treonina que se expresa de forma ubicua y está implicada en la regulación de la homeostasis celular a través de la regulación negativa de las rutas de señalización activadas por proteín kinasas. PP2A es considerada como un importante supresor de tumores (Janssens et al., 2005); además, se ha demostrado que los principales sustratos en esta actividad supresora son componentes aguas abajo de la ruta de señalización de Ras. Adicionalmente, la supresión de PP2A hace que Ras intensifique la actividad de las proteínas oncogénicas que son dianas aguas abajo de la ruta activada por Ras (Mumby, 2007a).

La actividad fosfatasa de PP2A se ha relacionado con la regulación del ciclo celular y la mitosis, morfología celular, diferenciación, desarrollo, transducción de señales, replicación, transcripción de ADN, traducción, empalme alternativo de ARN y apoptosis. PP2A también participa en estrés, choque térmico y respuesta a daño en el ADN y en la regulación de canales de calcio en el músculo cardiaco. Las alteraciones en PP2A pueden dar lugar a estados patológicos tales como enfermedad de Alzheimer y transformación oncogénica, así como potenciar la metástasis (Janssens and Goris, 2001). Por ello, la peculiaridad de PP2A es que una única fosfatasa es responsable de la regulación de varios procesos activados por proteín kinasas diferentes. La capacidad distintiva de PP2A de afectar el estado de fosforilación de una amplia variedad de sustratos deriva de su estructura y regulación complejas.

Estructuralmente, PP2A es un complejo heterodimérico o heterotrimérico, compuesto por un núcleo dimérico que permanece constante, formado por una subunidad de 65kDa que sirve como andamio ($PP2A_A$ o PR65/A) y una subunidad catalítica de 36kDa ($PP2A_C$, α and β isoforms) (**Figura 22**). Esta estructura dimérica ($PP2A_D$) puede estar asociada o no a una tercera subunidad variable, una familia de subunidades B reguladoras que confieren especificidad de sustrato o de tejido a las holoenzimas triméricas de PP2A y que se expresan de manera diferencial durante el desarrollo en mamíferos (Lechward et al., 2001). La actividad de PP2Ac también puede estar modulada por fosforilación reversible en la Tirosina 307 y por metilación en la Leucina 309, el último aminoácido del C-terminal.

La estructura de la subunidad catalítica de PP2A es muy similar a la de otros miembros de la familia de fosfatasas de serina/treonina como PP1, PP2B y PP5, y contiene dos iones metálicos en el sitio activo, determinados como manganeso. La parte C-terminal (residuos 296-309) se extiende hacia fuera de la proteína globular e interacciona con surcos en la superficie en la interfaz de las subunidades andamio y reguladora, siendo esta región C-terminal responsable de la especificidad de PP2Ac por la subunidad andamio. La subunidad andamio PP2AA está formada en su totalidad por 15 *HEAT repeats* en tándem que adoptan una conformación en forma de C o herradura en la holoenzima de PP2A. La interacción entre las subunidades A y C está controlada por una extensa red de puentes de hidrógeno, que son los responsables de la alta afinidad de esta interacción (Cho and Xu, 2007; Mumby, 2007b; Xing et al., 2006).

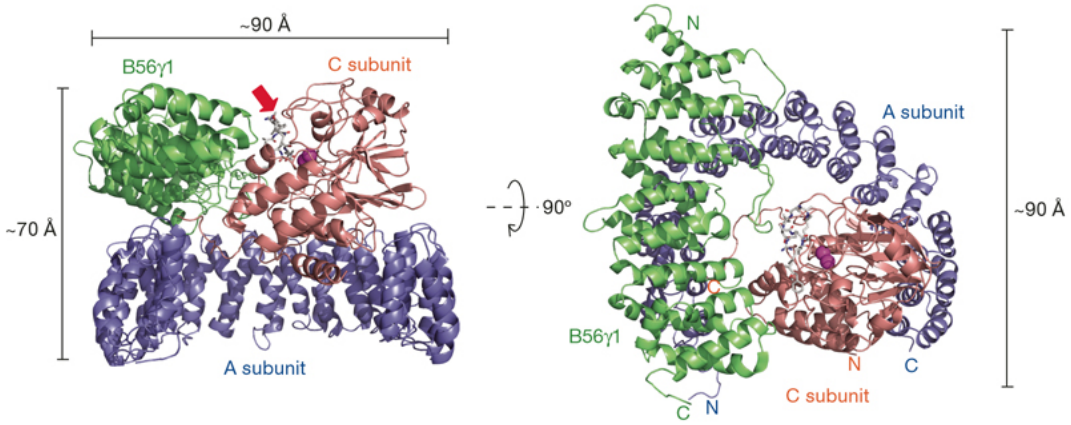

Figura 22. Estructura cristalográfica de la holoenzima heterotrimérica de PP2A. A la izquierda se representa la vista frontal y a la derecha la vista desde arriba. La subunidad A andamio está coloreada en azul, la subunidad C catalítica se muestra en rojo y la subunidad B56γ1 reguladora está marcada en verde. Tomada de (Cho and Xu, 2007).

La subunidad catalítica de PP2A está entre las enzimas más conservadas desde levadura a mamíferos (Cohen et al., 1990). En células de mamífero, las subunidades A y C tienen ambas dos isoformas, α y β, que comparten una alta similaridad de secuencia. En ambos casos, la isoforma α es mucho más abundante que la β (Arino et al., 1988; Hemmings et al., 1990).

La inactivación de las isoformas α y β de la subunidad PP2A A se ha relacionado con cáncer (Ruediger et al., 2001; Suzuki and Takahashi, 2003). Las

mutaciones en esta subunidad que afectan negativamente a la unión a las subunidades catalítica o reguladora de PP2A o bien la carencia total o la reducción sustancial de la subunidad A están estrechamente relacionadas con diversos tumores primaros en humanos (Takagi et al., 2000; Wang et al., 1998). En otro estudio, una forma truncada de la subunidad B PR61/B/γ1 se asoció con la resistencia a la radioterapia en estado metastásico de células de melanoma (Ito et al., 2003; Koma et al., 2004), aunque también se ha demostrado que esta subunidad puede actuar como un supresor de tumores.

Además, se ha postulado que el punto crítico del papel de PP2A en el mantenimiento del equilibrio entre la supervivencia y la muerte celular está relacionado con el estado de fosforilación del residuo Tirosina 307 de su dominio catalítico (Wong et al., 2010).

En un estudio desarrollado en colaboración con el presente trabajo, nuestros colaboradores han descrito recientemente la interacción directa entre Caspasa-9 y PP2Acα, que constituye una diana potencial para la terapia anticáncer (Arrouss et al., 2013).

2.9. Inhibidor 2 de la proteín fosfatasa 2A (SET)

SET, denominada también TAF-1β, INHAT o I_2PP2A (Inhibidor 2 de PP2A) es una proteína de 33.5 kDa (Isoforma 1) o 32 kDa (Isoforma 2). En el presente proyecto, hemos trabajado con la isoforma 2. SET se describió por primera vez como una proteína codificada en un punto de translocación en un caso de leucemia aguda indiferenciada (von Lindern et al., 1992), y posteriormente se ha caracterizado como una chaperona de histonas que interacciona con varios factores como proteínas de unión a ADN y proteasas. SET participa en la regulación de la transcripción, replicación y apoptosis. Además, SET inhibe la actividad de las acetiltransferasas de histonas, regulando la actividad nuclear procedente de las modificaciones químicas de las histonas.

Estructuralmente, SET forma un dímero que presenta una estructura que se asemeja a unos auriculares. Cada subunidad del dímero consiste en un N terminal, un dominio hélice y un dominio globular. La región de SET responsable de la actividad

chaperona es la superficie de abajo del dominio globular, debido a la unión de esta superficie a histonas y a ADN de doble cadena (Muto et al., 2007).

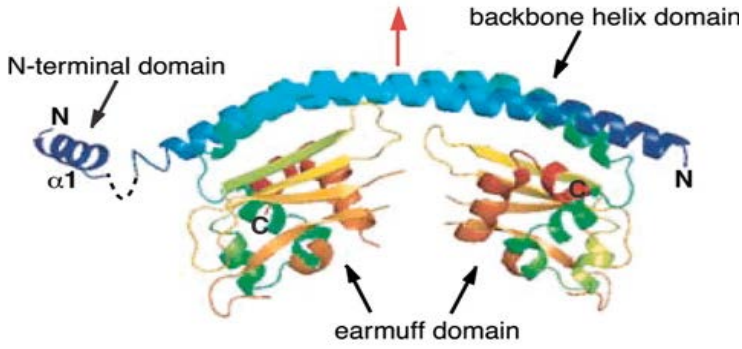

Figura 23. Estructura general del dímero de SET, con el pseudoeje en dos planos representado con la flecha roja.

SET se ha relacionado con las proteín fosfatasas de serina/treonina PP1 y PP2A. Se ha descrito que SET se asocia a PP1 y modifica su especificidad de sustrato. En presencia de concentraciones fisiológicas de Mn^{2+}, SET aumentaba la actividad de PP1 en 15-20 veces sobre la proteína básica de mielina y la histona H1 pero no en el caso de la fosforilasa. Además, SET redujo el requerimiento de Mn^{2+} de PP1 en torno a 30 veces a una concentración de 10µM (Katayose et al., 2000). En una tesis doctoral, se caracterizó la interacción entre I_2PP2A y PP1 de *Plasmodium falciparum* por doble híbrido de levadura, observando que sólo las levaduras diploides que expresaban PfPP1 y PfI_2PP2A fueron capaces de crecer en un medio selectivo –LHW, demostrando la interacción entre estas dos proteínas. En un ensayo fosfatasa, observaron que a bajas concentraciones de PfI_2PP2A (100-400nM) se activaba PfPP1; por el contrario, altas concentraciones de PfI_2PP2A resultaron en una inhibición de PfPP1 cuando se añadía el sustrato pNPP (para-nitrophenyl phosphate, paranitrofenilfosfato). I_2PP2A de *Plasmodium falciparum* y su ortólogo humano SET comparten un 26,7% de identidad, incluyendo un sitio de unión a PP1 RVxF PP1 (Egloff et al., 1997), que está conservado entre humanos y este parásito, y comprende los residuos 123-126 en la proteína humana (Vandomme, 2014).

La interacción entre SET y PP2A se describió por primera vez en 1996, donde se postulaba que SET era un inhibidor específico potente de PP2A,

denominado I_2PP2A, que provocaba una desregulación de PP2A que podría contribuir a la leucemogénesis mieloide aguda (Li et al., 1996). En un estudio reciente, tanto el dominio N-terminal (residuos 1-175) como el C-terminal (176-277) de SET se unían a PP2Ac y la inhibían, demostrando que el residuo de SET Valina 92 y la parte C-terminal acídica eran indispensables para que tuviera lugar la interacción. SET completa se localiza en el núcleo, pero tras el procesamiento en el residuo 175, ambos fragmentos se difunden en el citoplasma, donde inhiben a PP2Ac, causando una hiperfosforilación anormal de tau en cerebros con enfermedad de Alzheimer (Arnaud et al., 2011).

Además de en leucemia mielógena crónica, se ha encontrado sobreexpresión de SET en células primarias de leucemia linfocítica crónica (CLL) y en las líneas celulares Raji y Ramos de linfoma no Hodgkin de células B (NHL), mostrando una correlación entre la sobreexpresión de SET y una mayor severidad de la enfermedad. La abundancia relativa de las variantes de empalme alternativo de SET estaba también alterada en células de CLL y NHL, presentando cantidades similares de las isoformas α y β, mientras que en células sanas la isoforma β es mayoritaria (Christensen et al., 2011a).

2.10. Leucemia linfocítica crónica

La leucemia linfocítica crónica (CLL) es el tumor maligno de células B más común en adultos caucásicos mayores, raramente menores de 50 años. La enfermedad se caracteriza por la acumulación en la sangre, médula ósea y órganos linfoides periféricos de células B monoclonales CD5+ (Chiorazzi et al., 2005; Ghia et al., 2007; Rozman and Montserrat, 1995). La proliferación de linfocitos B de CLL también implica la expresión de CD19, CD20 y CD23 y presenta niveles bajos de Ig en sus superficies de membrana, así como baja expresión de membrana de CD79b, CD22 y FMC7 (Batata and Shen, 1992; Inamdar and Bueso-Ramos, 2007; Moreau et al., 1997). El perfil de expresión génica de la inmunoglobulina V_H difiere entre células B de CLL y células normales de la sangre CD5+, a diferencia del perfil de V_L, que permanece a niveles similares en células sanas y células B de CLL (Chiorazzi and Ferrarini, 2003). La ausencia de mutaciones somáticas en los genes IgV_H se ha caracterizado como el predictor más fuerte de agresividad de la

enfermedad y baja respuesta a la quimioterapia con fludarabina (Damle et al., 1999; Hamblin et al., 1999).

La CLL se ha descrito generalmente como una enfermedad con fallos en apoptosis, puesto que se han observado alteraciones genéticas y cambios en la expresión de muchos reguladores apoptóticos, como Bcl-2, Bcl-x, Mcl-1, p53, PI-3K y SET, entre otros (Christensen et al., 2011a; Kitada et al., 1998; Klein et al., 2000; Packham and Stevenson, 2005; Ringshausen et al., 2002). Muchos factores apoptóticos están regulados a través del empalme alternativo, dando lugar a la producción de varias isoformas de las proteínas con diferentes funciones a partir del mismo precursor de ARNm. Estas isoformas suelen tener funciones antagonistas que son cruciales para la regulación de la ruta de apoptosis. En otros casos, el transcrito de ARNm no codifica para un polipéptido funcional, evitando así la sobreexpresión de la proteína principal (David and Manley, 2010; Schwerk and Schulze-Osthoff, 2005).

La regulación del empalme alternativo es un mecanismo patogénico de relevancia clínica en CLL, especialmente en casos de resistencia a la quimioterapia. Se ha visto que la maquinaria del espliceosoma está alterada en CLL, puesto que hay mutaciones recurrentes que afectan al dominio *HEAT-repeat* C-terminal de SF3B1, un componente del espliceosoma U2 snRNP, que aparece en el 10-15% de los casos (Wang et al., 2011). Las mutaciones en SF3B1 están asociadas con formas agresivas de la enfermedad, dado que inducen un empalme alternativo aberrante en varios genes (Quesada et al., 2011; Rossi et al., 2011). Además, la frecuencia de las mutaciones en SF3B1 es significativamente mayor en pacientes de CLL tratados con fludarabina (17%) que en pacientes no tratados (5%), sugiriendo que la quimioterapia podría inducir mutaciones en Sf3B1 o seleccionar una población de células mutadas (Rozovski et al., 2013).

2.11. Empalme alternativo aberrante de Caspasa-9

La expresión de la variante de empalme alternativo de ARNm de Caspasa-9, denominada Caspasa-9b, confiere el efecto contrario a la proteína completa induciendo resistencia a estímulos apoptóticos (Seol and Billiar, 1999). Esta forma

aberrante puede interaccionar con el dominio CARD de Apaf-1, bloqueando la activación de procaspasa-9 y -3, y con ello inhibiendo la apoptosis de modo dominante negativo. El procesamiento posttranscripcional del pre-ARNm de Caspasa-9 es un mecanismo complejo que implica la inclusión o exclusión de un cassette de cuatro exones (exones 3, 4, 5 y 6). La inclusión de estos cuatro exones en el transcrito maduro produce la Caspasa-9 proapoptótica, mientras que la exclusión de estos exones produce la Caspasa-9b antiapoptótica. Esta forma b de 30,1 kDa contiene los primeros 139 residuos (prodominio), fusionados en fase con los últimos 127 residuos, que comprenden el conector entre las subunidades grande y pequeña y la subunidad pequeña, responsable de la especificidad de sustrato; sin embargo, le falta la subunidad grande entera (residuos 140-298), que contiene el sitio activo y es responsable de la actividad catalítica. Por tanto, esta forma es catalíticamente inactiva (Srinivasula et al., 1999). Sorprendentemente, Caspasa-9b parece mostrar cierta tolerancia a eventos de aberración a gran escala, puesto que presenta un plegamiento αβα que puede haber evolucionado añadiendo motivos αβ en los extremos de las láminas centrales, permitiendo a esta proteína plegarse en una conformación estable a pesar de carecer de regiones grandes conservadas de la estructura de la proteína (Birzele et al., 2008).

En células sanas, la relación Caspasa-9/Caspasa-9b se ha descrito normalmente como 1:0,1. Sin embargo, cuando Caspasa-9 y Caspasa-9b están presentes en concentraciones equimolares, sólo un tercio de los complejos de Apaf-1 contienen homodímeros de procaspasa-9 funcionales capaces de autoactivarse y por tanto proapoptóticos. Los dos tercios restantes de complejos de Apaf-1 contendrían homodímeros de Caspasa-9b y heterodímeros procaspasa-9/Caspasa-9b que no serían funcionales, deteniendo la señal apoptótica. En suma, la sobreexpresión de Caspasa-9b establecería un umbral para regular la activación de Caspasa-9 y evitar la formación espontánea del complejo Apaf-1/Caspasa-9 que daría lugar a una apoptosis no deseada (Srinivasula et al., 1999). Caspasa-9b está desregulada en tumores de pacientes de varios subtipos de cáncer de pulmón de células no pequeñas (NSCLC), incluidos adenocarcinomas, carcinomas escamosos y carcinomas de células grandes.

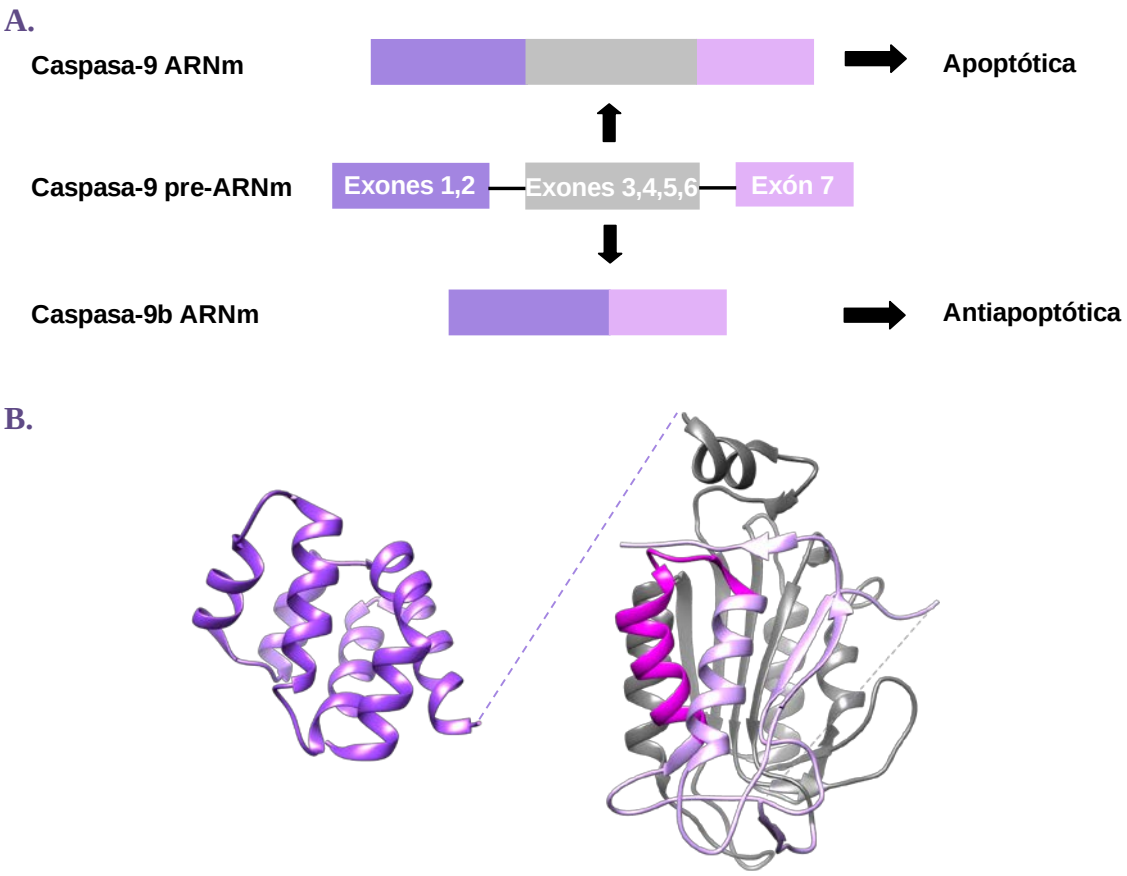

Figura 24. A. Esquema del empalme alternativo de Caspasa-9, que da lugar a la proteína completa apoptótica si el ARNm está formado por los exones 1-7 o la proteína Caspasa-9b antiapoptótica aberrante, cuyo ARNm carece de los exones 3-6. **B. Estructura de Caspasa-9.** El dominio CARD está representado en morado (PDB 4RHW), la línea discontinua comprende los residuos 93-140 correspondientes al conector interdominio desordenado entre el dominio CARD y la subunidad catalítica, los exones 3-6 deleccionados en Caspasa-9b que coinciden con la subunidad catalítica grande se muestran en gris, el sitio de unión a PP2A está coloreado en magenta y la subunidad pequeña de Caspasa-9 se presenta en violeta (ΔCARD-Caspasa-9 PDB 1JXQ).

Además, la baja relación Caspasa-9/Caspasa-9b era la responsable del mantenimiento de la capacidad tumorigénica de las células NSCLC y hacía que las células fueran resistentes al tratamiento con erlotinib (Shultz et al., 2011). La utilización del empalme alternativo de Caspasa-9 como diana sensibilizaría las células de NSCLC a los tratamientos de quimioterapia que ya están disponibles,

aumentando su eficacia y con ello limitando sus efectos secundarios tóxicos (Shultz & Chalfant, 2011).

2.12. Empalme alternativo aberrante de PP2Acα

Se sabe muy poco acerca del empalme alternativo de PP2Acα, puesto que el único artículo donde aparece se ha publicado recientemente. Se ha descrito una isoforma aberrante de la subunidad catalítica C denominada PP2Acα2, que carece del exón 5, que está próximo al sitio catalítico. Aunque cabría esperar que esta isoforma diera lugar a un fenotipo dominante negativo, el resultado es una forma catalíticamente inactiva, dado que la actividad fosfatasa de PP2Acα no se vio alterada cuando se sobreexpresaba PP2Acα2. Esta variante sólo se ha visto sobreexpresada en células mononucleares de sangre periférica (PBMC) incubadas en medio sin suero o en condiciones de ayuno durante 24h. Después de este tiempo, las células todavía eran viables y la relación PP2Acα/PP2Acα2 se veía reestablecida cuando eran transferidas a medio de cultivo. Cuando se analizó en líneas celulares, PP2Acα2 estaba presente tanto a nivel de ARNm como a nivel de proteína pero a niveles muy bajos. Además, en células PBMC aisladas de donantes sanos, sólo pudo detectarse PP2Acα por RT-PCR. A diferencia de PP2Acα, PP2Acα2 presentaba una mayor unión a la subunidad reguladora de PP2A α4 pero no se unía a la subunidad andamio de PP2A ni a la proteín fosfatasa metil esterasa-1 (PME-1) (Migueleti et al., 2012).

2.13. Nuevas estrategias para la terapia anticáncer

El conocimiento de las interacciones de proteínas ha esclarecido las bases moleculares de un gran número de enfermedades, como es el caso del cáncer. Las interacciones proteína-proteína se han desarrollado como dianas moleculares atractivas para nuevas terapias y la modulación de interacciones proteína-proteína que regulan las cascadas de señalización es particularmente relevante para el descubrimiento de nuevos agentes terapéuticos para las terapias anticáncer (Zinzalla and Thurston, 2009).

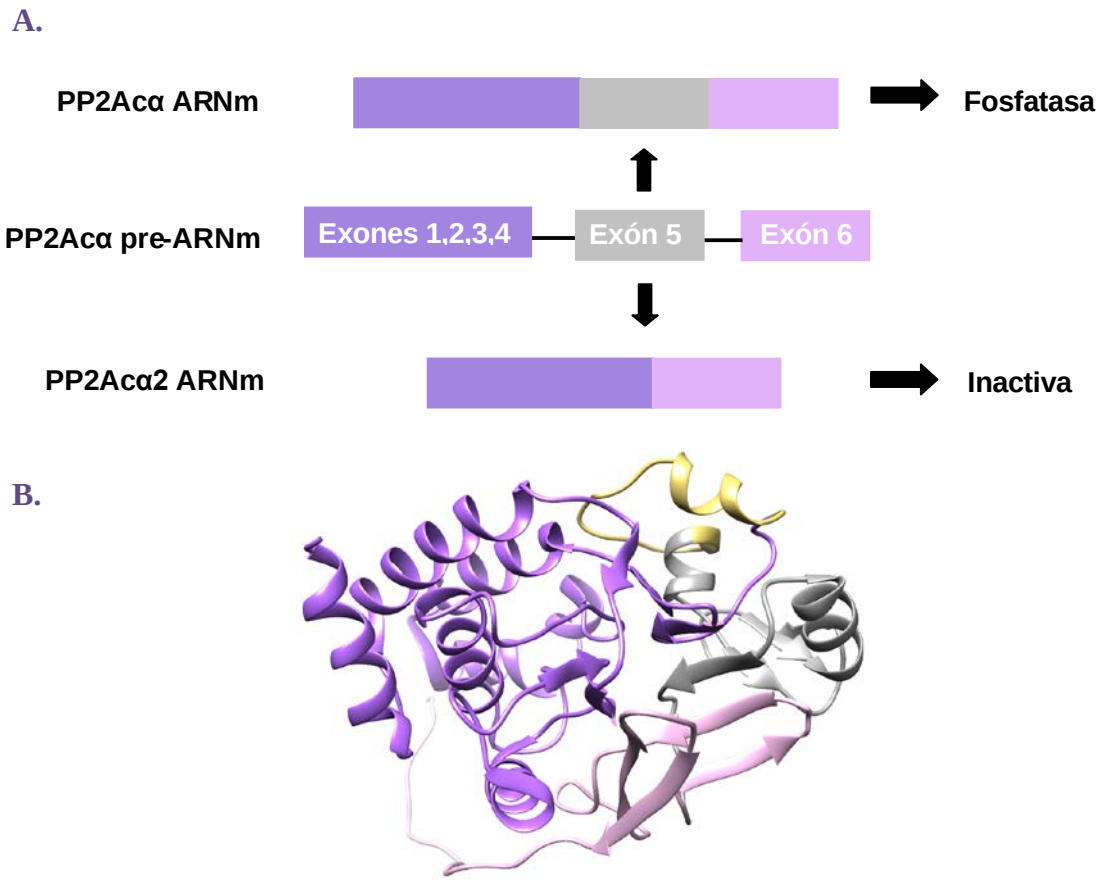

Figura 25. A. Esquema del empalme alternativo de PP2Acα, que da lugar a la proteína entera apoptótica si el ARNm está formado por los exones 1-6 o a la proteína PP2Acα2 inactiva aberrante, cuyo ARNm carece del exón 5. **B. Estructura de PP2Acα** (PDB 2IAE), mostrando los exones 1-4 en morado, el exon 5 deleccionado en PP2Acα2 está representado en gris, el sitio de unión a Caspasa-9 está coloreado en amarillo y el exón 6 está marcado en violeta.

En este sentido, se han desarrollado muchas aproximaciones terapéuticas utilizando interacciones proteína-proteína como diana, como es el caso del complejo SET-PP2A con el uso de péptidos como tratamiento potencial para CLL, linfoma no Hodgkin (Christensen et al., 2011a), glioblastoma, adenocarcinoma de mama (Switzer et al., 2011) e inflamación (Christensen et al., 2011b), así como moléculas pequeñas para el tratamiento de la leucemia mieloide crónica (Wang et al., 2015; Zonta et al., 2015).

Un gran número de péptidos que son terapias potenciales no han obtenido la aprobación de la FDA debido a sus características físico-químicas pobres, puesto que se han considerado candidatos mediocres a drogas debido a su baja biodisponibilidad oral e inestabilidad. Una vez que esto se ha solucionado con nuevas estrategias para mejorar la estabilidad de los péptidos, biodisponibilidad y evitar la degradación, las empresas farmacéuticas han recobrado su interés en desarrollar estos péptidos terapéuticos a pesar de los altos índice de abandono de moléculas durante la última década (Goodwin et al., 2012; Kola and Landis, 2004; Vlieghe et al., 2010). La farmacología de estos péptidos se puede mejorar con su rediseño incluyendo péptidos penetrantes (CPPs) que mejoren la entrada en la célula y aumenten su biodisponibilidad, además de proporcionar rutas de administración más efectivas o más seguras. Este potencial terapéutico de los CPPs ha conducido a la formación de nuevas empresas de liberación de drogas que explotan tecnologías de penetración en la célula (Chen and Harrison, 2007).

Otra estrategia que se ha desarrollado en los últimos años para la liberación terapéutica de diferentes cargos ha sido el uso de nanopartículas como portadores de drogas, lo que permite la liberación específica de moléculas activas de forma controlada (Wu et al., 2011). Las nanopartículas mesoporosas de sílice constituyen una herramienta prometedora para evitar los efectos secundarios tóxicos de la quimioterapia debidos a la falta de selectividad de tumor, la multirresistencia a fármacos y la aparición de metástasis. Sin embargo, la mayoría de las nanomedicinas que se han desarrollado basadas en nanoportadores inorgánicos todavía están a nivel de investigación básica o preclínica (He and Shi, 2014).

2.13.1. Péptidos penetrantes en la célula

En los últimos años, los péptidos penetrantes (CPPs) han constituido una herramienta prometedora para aplicaciones terapéuticas, ya que han demostrado ser lanzaderas eficientes para introducir diferentes tipos de cargos en una gran variedad de células, tanto *in vitro* como *in vivo* (Dietz *et al*., 2004, Johansson *et al*., 2011), de moléculas orgánicas pequeñas, nanopartículas, liposomas, péptidos, proteínas, ARNsis, ADN plasmídico y agentes de imagen (Kersemans *et al*., 2010). Los primeros CPPs derivados de proteínas, Tat y Antennapedia (Antp), parecían indicar

que la naturaleza había encontrado una solución para el transporte de proteínas al interior de las células. Sin embargo, para la mayoría de proteínas y péptidos que no pueden penetrar en las células, la conjugación a un CPP facilitaría su entrada (Bolhassani *et al*., 2011, Hassane *et al*., 2010).

Los péptidos poseen muchas ventajas, puesto que ofrecen alta eficacia, selectividad y especificidad. Presentan tamaño pequeño, facilidad de síntesis y modificación, capacidad de penetración en los tumores y buena biocompatibilidad. Además, carecen de toxicidad, dado que sus productos de degradación son aminoácidos, y presentan baja bioacumulación, puesto que poseen una vida media corta (Thundimadathil, 2012).

Basado en CPPs, se ha diseñado una nueva tecnología de fármacos derivados de fosfatasas (DPT), enfocada al bloqueo de la interacción de las subunidades catalíticas de las fosfatasas de serina/treonina PP1 y PP2A con sus elementos reguladores locales utilizando la liberación intracelular de péptidos para evitar la desfosforilación específica de sustrato. Se ha identificado una nueva secuencia penetrante en la caseín kinasa 2α de *Theileria parva* y se utilizó como una nueva lanzadera no tóxica *ex vivo* e *in vivo* para la liberación intracelular de secuencias que interfieren con las holoenzimas de PP2A o PP1 (Guergnon *et al*., 2006). Nuestros colaboradores generaron un péptido que contenía la secuencia penetrante DPT asociada al motivo de interacción entre Caspasa-9 y PP2Acα humanas (DPT-C9h), para utilizar esta asociación como diana. DPT-C9h actuaba específicamente sobre la interacción Caspasa-9/PP2A *in vitro* e *in vivo* e indujo apoptosis dependiente de Caspasa-9 en líneas celulares de cáncer. DPT-C9h también indujo una inhibición significativa del crecimiento del tumor en modelos de xenotransplantes de cáncer de mama. El péptido específico de ratón DPT-C9 también indujo la inhibición del crecimiento del tumor en modelos murinos de cáncer de pulmón ($K\text{-}Ras^{LA\text{-}1}$) y de mama (Polyoma MiddleT, PyMT) y no mostró ni toxicidad ni respuesta inmunogénica (Arrouss et al., 2013). DPT-C9h tenía un efecto específico en células B transformadas aisladas de pacientes de leucemia linfocítica crónica sin mostrar ningún efecto sobre células T, células NK ni monocitos, ni en células B primarias de donantes sanos (Arrouss et al., 2015).

Un aspecto a tener en cuenta cuando se usan péptidos como terapia son los efectos potenciales de las proteasas del suero en la degradación del péptido antes de la internalización celular. Se han tomado algunas medidas para estabilizar CPPs para aplicaciones *in vivo*, como la incubación con SDS o ácido polisiálico, la sustitución en los péptidos de aminoácidos L por sus isómeros D, la retroinversión, el uso de aminoácidos no naturales, la modificación del esqueleto de los péptidos, la ciclación, la formación de enlaces disulfuro, péptidos constreñidos y péptidos grapados entre otros (Fominaya et al., 2015b). La resistencia a proteólisis en el suero de DPT-C9h se mejoró llevando a cabo mutaciones en un sitio de corte de una proteasa del suero comprendido dentro de la secuencia del CPP. El péptido Mut3DPT-C9h con una mutación de arginina a alanina en el octavo residuo de la secuencia del DPT mostró un aumento en la estabilidad del péptido y un mejor perfil farmacocinético, manteniendo al mismo tiempo el mismo efecto apoptótico que el DPT-C9h original (Fominaya et al., 2015a).

2.13.2. Nanopartículas mesoporosas de sílice

Las nanopartículas mesoporosas de sílice (MSNs) se han utilizado extensamente como reservorios para el almacenamiento y liberación de drogas debido a su estructura mesoporosa única que confiere una gran capacidad de carga, biocompatibilidad, alta estabilidad térmica, porosidad homogénea, naturaleza inerte y tamaño de poro modificable. Las MSNs llevan a cabo la entrada en las células por endocitosis y se ensamblan en su superficie externa con puertas que permiten presentar una liberación cero y liberar su cargo en respuesta a estímulos externos de manera controlada (Agostini et al., 2012; Li et al., 2012). En estudios de biodistribución, las MSNs han mostrado acumularse preferentemente en tumores en modelos de xenotransplantes de tumores humanos y liberar eficazmente drogas en tumores suprimiendo el crecimiento del tumor, presentando una biocompatibilidad satisfactoria (Lu et al., 2010).

Las nanopartículas MCM-41 tienen un tamaño de 100nm de diámetro y presentan un sistema regular de poros formado por una matriz de poros unidimensionales de forma hexagonal, compuestos por sílice amorfo (Kresge et al., 1992). Las MCM-41 se han aplicado con éxito para la liberación de ibuprofeno

(Vallet-Regí, 2006; Vallet-Regí et al., 2001), drogas antibacterianas (Mas et al., 2013) y quimioterapias para cancer (de la Torre et al., 2014; Giménez et al., 2015). En el presente trabajo, hemos utilizado las nanopartículas MCM-41 cargadas con el péptido derivado de Caspasa-9 C9h y las hemos funcionalizado en la superficie externa con el polímero ε-poly-L-lisina, que mostró una liberación cero del cargo en agua y una elevada liberación en presencia de la proteasa pronasa, debido a la hidrólisis de la ε-poly-L-lisina (Mondragón et al., 2014).

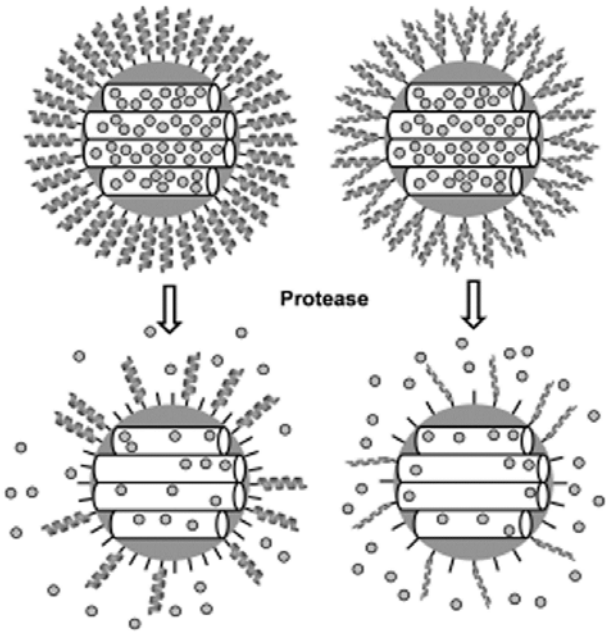

Figura 26. Representación esquemática de las nanopartículas MCM-41 cargadas con la molécula elegida y tapizadas con ε-poly-L-lisina, unidas específicamente a través del extremo C-terminal del polímero en la parte izquierda de la figura y anclados al azar a las nanopartículas a través de los grupos amino de las cadenas laterales de los aminoácidos de lisina en la parte derecha de la figura. En presencia de una proteasa intracelular, los enlaces amida de la ε-poly-L-lisina se hidrolizan, permitiendo la liberación del cargo. Adaptada de (Mondragón et al., 2014).

OBJECTIVES

"The best scientist is open to experience and begins with romance – the idea that anything is possible". Ray Bradbury

3. OBJECTIVES

Apoptosis regulation at Caspase-9 level has a critical role to maintain the equilibrium of the apoptotic signaling pathway. It is known that Caspase-9 undergoes posttranslational modifications as phosphorylation and dephosphorylation reactions, which are capable of enhancing or inhibiting Caspase-9 processing and recruitment to the apoptosome and its further activation (Bratton and Salvesen, 2010). Several years ago, our collaborators described the direct interaction between Caspase-9 and PP1cα, where they could demonstrate that PP1cα dephosphorylated and activated Caspase-9 and they determined the binding sites of the interaction (Dessauge et al., 2006). Nevertheless, the kinetics of this interaction and the dephosphorylation site remain unknown.

The present work has been developed in tight collaboration with Dr. Angelita Rebollo's laboratory at CIMI-UPMC (Paris), who has postulated the direct interaction between Caspase-9 and PP2Acα (Arrouss et al., 2013) and the use of the cell-penetrating peptide DPT bound to Caspase-9 derived peptides as a promising tool for anticancer therapy. With the aim of complementing this work and delve into a deeper knowledge of these phosphatase-caspase interactions as well as the search of the most efficient vehicle for the delivery of our therapeutic peptide C9h, the following objectives were established for this work:

1. Biophysical characterization of the interaction between Caspase-9 and PP1cα.
2. Determination of the binding sites of Caspase-9 / PP2Acα direct interaction.
3. Biophysical characterization of the interaction between Caspase-9 and PP2Acα.
4. Evaluation of MCM-41 nanoparticles efficacy as a vehicle for C9h peptide delivery.
5. Study of the abundance of the aberrant spliced forms of Caspase-9 and PP2Acα in CLL patients and evaluation of its significance for the disease.
6. Characterization of the direct interaction between Caspase-9 and SET.

MATERIAL AND METHODS

"Everything must be made as simple as possible. But not simpler." Albert Einstein.

4. MATERIAL AND METHODS

4.1. Constructs

All plasmid constructs used in this work codify for human proteins. Some of the constructs were engineered by former members of the laboratory, gently transferred by collaborators or purchased at Addgene (https://www.addgene.org/). The characteristics and source of these vectors are detailed in **Table 1**.

Table 1. Constructs transferred or purchased.

Construct name	Protein	Boundaries	Vector	Tag	Protein molecular mass (kDa)	Source
Casp9WTFL	Caspase-9	1-416	pET23b	C-term 6His	46	Dr. Enrique Pérez-Payá (CIPF, Valencia)
CARD	Caspase-9	1-92	p11	N-term 6His	13	Dr. Enrique Pérez-Payá (CIPF, Valencia)
$PP1\alpha_{7-330}$	PP1α	7-330	RP1B	N-term Thio6 (MGSDKI)+ 6His	39	Addgene Cat No. #51768.
PP2A	PP2Acα	1-309	pGEX-4T-2	N-term GST	62	Dr. Angelita Rebollo (CIMI, UPMC, Paris)
SETFL	SET	1-277	ppET28a	N-term 6His	35	In-house construct
SET 1-225	SET	1-225	ppET28a	N-term 6His	29	In-house construct

4.1.1. Cloning of constructs

The rest of the constructs needed for this project were modified from previous constructs or generated with the use of commercial empty plasmids available in the laboratory. pGKI was a gift from Dr. Marcin Węgrecki (IBV, Valencia), engineering an in-house modified version of the pET28-NKI/LIC 6His/3C vector (originally

obtained from Dr A. Perrakis group, NKI, Amsterdam) in which the His tag was substituted by a GST tag. The details of all generated constructs described in this work are listed in **Table 6**. The genes codifying proteins of interest were amplified by PCR from previous constructs or Megaman gene library (Agilent Technologies) using the specific oligonucleotides compiled in **Table 3**. PCR mix and conditions are described in **Table 2**. Tm temperature and extension time were adapted to oligonucleotides and amplicon size for each case.

Table 2. PCR conditions and mix for Kapa HiFi Hot Start PCR kit.

Conditions	Mix
Initial denaturation:	5µL Buffer HiFi 5X
95ºC – 3’	0.75µL dNTPs (10mM each)
30 cycles:	0.75µL Forward primer
98ºC – 20’’	0.75µL Reverse primer
Desired Tm – 20’’	1.25µL DMSO
72ºC – 30’’/kb	0.25µL Template DNA
Final extension:	0.5µL Kapa HiFi DNA polymerase (Nippon Genetics)
72ºC – 5’	15.75µL MilliQ water

PCR products were run on 1% agarose gels (Pronadisa) stained with GelRed (Biotium). The molecular weight marker used was DNA Ladder 1 kb (Nippon Genetics). Electrophoresis was performed at 100V in a Biostep cuvette for 40’ and visualized under UV light. Inserts were further purified with E.Z.N.A. Cycle Pure kit (Omega). DNA concentration was verified with Nanodrop (Thermo Scientific).

Table 3. Primers used for cloning. Specific overhangs designed for ligation are represented in lower case letters.

Primer name	Sequence
CARD1FW	cagggacccggtATGGACGAAGCGGATCGGCGGCTC
CARD92RV	cgaggagaagcccggttagTTAGTTCGCAGAAACGAAGCCAGCATGTCC
ΔCARDC91FW	cagggacccggtGGTGCTCTTGAGAGTTTGAGGGGAAATGCAGATTTG
ΔCARDC9277RV	cgaggagaagcccggttaTGATGTTTTAAAGAAAAGTTTTTTCCGGAGGAAATTAAAGCAACCAGGC
8NdeICASP9FWD	gattcggtcatATGGGTGCTCTTGAGA
XhoCasp9REV	gcgctcgagTGATGTTTTAAAGAAAAGT
C9b FWD	gattcggtgatgtcgAGCAGAAAGACCATGGGTTTGAGGTG
C9b REV	catggtctttctgctCGACATCACCGAATCCTCCAGAAC
PP2ACA2 FWD	gaagttccccatgagGGATATAACTGGTGCCATGACC
PP2ACA2 REV	gcaccagttatatccCTCATGGGGAACTTCTTGTAGG
pGEX_F	GGGCTGGCAAGCCACGTTTGGTG
pGEX_R	CCGGGAGCTGCATGTGTCAGAGG

Depending on the case, the techniques applied for insert ligation into plasmids were the following:

- Complementary cohesive ends were generated after digestion of insert and vector with the same restriction enzymes from Fermentas or New England Biolabs (NEB) and ligated with Quick Ligation kit (NEB). 50ng of vector were mixed with 3-fold molar excess of insert and the final volume was adjusted to 10µL of milliQ water. 10µL of Quick Ligation reaction buffer and 1µL of Quick T4 DNA ligase were added to the mix and incubated at room temperature for 5' before transformation in *E. coli*.
- Ligation Independent Cloning (LIC) (Bonsor et al., 2006). pGKI vector was linearized by digestion with KpnI for 6 h at 37ºC by mixing 30µL of plasmid with 2µL of KpnI (NEB), 4 µL of buffer 1 (NEB), 0.4 µL of BSA (NEB), and 3.6 µL of MilliQ water and further purified with E.Z.N.A. Cycle Pure kit (Omega). Linearized vector and insert were treated separately with T4 DNA polymerase (Fermentas) prior to ligation. 15.3µL of vector or insert were mixed with 4µL of T4 DNA polymerase buffer, 0.2µL of T4 DNA polymerase and 0.5µL of 100mM dATP (insert) or 100mM dTTP (vector)

(Biotools). Reactions were incubated for 10’ at room temperature and 10’ at 70ºC in a Thermomixer comfort (Eppendorf). After that, vector and insert in a 1:1 proportion were incubated for 5’ at room temperature and then 2µL of 50mM EDTA were added and incubated for another 10’ at room temperature, thereafter it was ready for transformation in *E. coli*.

- In-Fusion (Clontech). Linearized pET23b and pFastBacHTb vectors were obtained by PCR amplification of the needed fragment. The genes of interest, codifying for Caspase-9b and PP2Acα2, were amplified by PCR with specific primers that contained 15bp overhangs complementary to the ends of the linearized vectors, pET23b for Caspase-9b and pFastBacHTb for PP2Acα2. PCRs were performed with Kapa HiFi Hot Start PCR kit using the conditions detailed in **Table 2**. Vectors and inserts were purified with Cycle Pure kit (Omega) before setting up the In-Fusion cloning reaction, consisting of 1µL of 5X In-Fusion HD Enzyme premix, 2µL of linearized vector and 2µL of insert. The reaction was incubated for 15’ at 50ºC and then placed on ice prior to transformation in *E. coli*.

When ligation reactions were ready, the mix was transformed by heat shock in DH5α *E. coli* strain (Stratagene). 100µL of chemically competent DH5α cells were thawed on ice for 5’, the ligation reaction was added to the cells and incubated on ice for at least 10’. Cells were incubated for 1’30’’ at 42ºC for heat shock and tubes were placed on ice for 5’ to reduce cell damage. Then, cells were incubated with 200µL of LB medium without antibiotics at 37ºC. After 1h of incubation, cells were plated on a Petri dish containing LB agar supplemented with the required antibiotics and incubated overnight at 37ºC.

The day after, colony PCR was performed following conditions listed in **Table 4** to check whether the colonies had incorporated the vector and the insert was successfully ligated in the plasmid. Positive colonies were cultured in 5mL of LB medium supplemented with the required antibiotics at 37ºC overnight and the plasmid was extracted with QuickGene Plasmid Kit SII (Fujifilm) for sequence analysis at Biomedicine Institute of Valencia sequencing service.

Table 4. Colony PCR conditions using FIREPoL DNA polymerase.

Conditions	Mix
Initial denaturation:	2µL Buffer B 10X
95ºC – 5’	2 µL $MgCl_2$ 25mM
30 cycles:	0.4µL dNTPs (10mM each)
95ºC – 45’’	0.6µL Forward primer
55ºC – 45’’	0.6µL Reverse primer
72ºC –1’/kb	1 colony
Final extension:	0.2µL FIREPoL DNA polymerase (Solis BioDyne)
72ºC – 10’	14.2µL MilliQ water

4.1.2. Site-directed mutagenesis

Mutations in the sequence of the genes of interest were generated following the QuikChange Site-directed mutagenesis kit (Stratagene). Primers were designed to amplify the whole plasmid, including the desired mutations in the central part of their sequence. PCR was performed using Kapa HiFi Hot Start PCR kit using the conditions shown in **Table 5** and **Table 7** and the primers listed in **Table 8.**

Table 5. PCR conditions and mix for Site-directed mutagenesis.

Conditions	Mix
Initial denaturation:	5µL Buffer HiFi 5X
95ºC – 30’’	0.75µL dNTPs (10mM each)
12-18 cycles:(*)	0.75µL Forward primer
95ºC – 30’’	0.75µL Reverse primer
55ºC – 1’	1.25µL DMSO
68ºC – 30’’/kb	0.25µL Template DNA
	0.5µL Kapa HiFi DNA polymerase (Nippon Genetics)
	15.75µL MilliQ water

Table 6. **List of constructs used in the present work.**

Construct	Template	Vector	Tag	Cloning method	Primers	Insert size (bp)	Boundaries	Protein MW (kDa)	Mutations
GST-CARD	CARD in p11	pGKI	N-term GST	LIC	CARD1FW CARD92REV	276	1-92	26+12.5	-
ΔCARDC9C 287A	C9C287AFL in pET23b	pET21b	C-term 6His	Quick Ligation	8NdeICASP9 FWD XhoCasp9REV	831	140-416	30	C287A
GST-ΔCARDC9C 287A	ΔCARDC9C 287A in pET21b	pGKI	N-term GST	LIC	ΔCARDC91FW ΔCARDC9277 REV	831	140-416	26+30	C287A
ΔCARDC94 QC	C9WTFL in pET23b	pET21b	C-term 6-His	Quick Ligation	8NdeICASP9 FWD XhoCasp9REV QC304A FWD QC304A REV QC304B FWD QC304B REV QC315 FWD QC315 REV QC330 FWD QC330 REV	831	140-416	30	D304A, D315A, D330A
GST-ΔCARDC94 QC	ΔCARD4QC in pET21b	pGKI	N-term GST	LIC	ΔCARDC91FW ΔCARDC9277 REV	831	140-416	26+30	D304A, D315A, D330A

Construct	Template	Vector	Tag	Cloning method	Primers	Insert size (bp)	Boundaries	Protein MW (kDa)	Mutations
GST-C9WTFL	C9WTFL in pET23b	pGKI	N-term GST	LIC	CARD1FW ΔCARDC9277 REV	1269	1-416	26+46	-
C9C287AFL	C9WTFL in pET23b	pET23b	C-term 6His	Site-directed mutagenesis	CASP9C287A_FWD CASP9C287A_REV	1269	1-416	46	C287A
GST-C9C287AFL	C9C287AFL in pET23b	pGKI	N-term GST	LIC	CARD1FW ΔCARDC9277 REV	1269	1-416	26+46	C287A
Caspase-9b	C9WTFL in pET23b	pET23b	C-term 6His	In-Fusion	C9b FWD C9b REV	816	1-139,290-416	31	-
PP2AD88N	PP2A in pGEX-4T-2	pGEX-4T-2	N-term GST	Site-directed mutagenesis	QCD88N FWD QCD88N REV	1433	1-309	62	D88N
HAPP2AD88N	PP2AD88N in pGEX-4T-2	pFastBacHTb	N-term HA, N-term 6His	Quick Ligation	pGEX_F pGEX_R	1041	1-309	40	D88N
PP2Ac α2	HAPP2AD88N in pFastBacHTb	pFastBacHTb	N-term HA, N-term 6His	In-Fusion	PP2ACA2 FWD PP2ACA2 REV	879	1-193, 248-309	34	-

Table 7. (*) Number of cycles required for PCR depending on the number of mutations introduced.

Type of mutation desired	Number of cycles
Point mutations	12
Single aminoacid changes	16
Multiple aminoacids deletions or insertions	18

Table 8. Primers used for Site-directed mutagenesis.

Primer name	Sequence
CASP9C287A_FWD	CTTTTTCATCCAGGCCGCTGGTGGGGAGCAGAAAG
CASP9C287A_REV	CTTTCTGCTCCCCACCAGCGGCCTGGATGAAAAAG
QC304A FWD	CCACTTCCCCTGCAGCCGAGTCCCCTGGC
QC304A REV	TACTGCCAGGGGACTCGGCTGCAGGGGAA
QC304B FWD	CCCCTGCAGCCGCGTCCCCTGGCAG
QC304B REV	CTGCCAGGGGACGCGGCTGCAGGGG
QC315A FWD	CCCCGAGCCAGCTGCCACCCCG
QC315A REV	CGGGGTGGCAGCTGGCTCGGGG
QC330A FWD	CGACCAGCTGGCCGCCATATCTAG
QC330A REV	CTAGATATGGCGGCCAGCTGGTCG
QCD88NFWD	GTTTATGGGAGATTATGTTAACAGAGGATATTATTCAGTTG
QCD88NREV	CAACTGAATAATATCCTCTGTTAACATAATCTCCCATAAAC

PCR amplification was verified on 0.8% agarose gel. PCR product was digested with 2µL of DpnI for 2h at 37ºC to remove parent DNA and transformed in DH5α as previously described. Positive colonies were sequenced at IBV sequencing service to check if the mutation was correctly performed.

4.2. Protein overexpression

4.2.1. Caspase-9 overexpression in *E.coli*

For all Caspase-9 constructs the plasmid of interest was transformed in BL21 (DE3) Codon Plus RIPL chemically competent *E.coli* cells (Stratagene) as

previously described for DH5α with the exception of 45'' of heat shock incubation. Finally, 150µL of cells were seeded in a culture plate containing the required antibiotics and incubated overnight at 37 ºC.

The expression protocol was optimized from Current Protocols in Protein Science, Unit 21.13 (Denault and Salvesen, 2002a) including some modifications. For new constructs, small-scale overexpression trials were performed and further verified with small-scale affinity purification. If soluble protein was obtained, we proceeded to Caspase-9 overexpression at large scale.

For small scale overexpression, an isolated colony was inoculated in 5mL of 2xTY medium (16g tryptone (Pronadisa), 10g yeast extract (Pronadisa), 5g NaCl (Panreac) and 1L distilled water) supplemented with antibiotics and incubated overnight at 37ºC in continuous shaking (180rpm). Then, this preculture was inoculated in 20mL of 2xTY medium supplemented with antibiotics and incubated at 37ºC until the OD_{600} was 0.6. Absorbance was measured with a cellular densitometer Ultrospec 10 (Amersham Biosciences). To induce Caspase-9 overexpression, culture was inoculated with a final concentration of 0.4mM IPTG (CalBiochem) and incubated for 4h at 30ºC. Cultures were centrifuged (Sorvall ST16R, rotor 75003629 TX-400) at 4ºC and 4000 rpm for 30'. Supernatants were discarded and cells were resuspended in 1mL 1X PBS for each culture. Finally, cells were harvested again by centrifugation at 4ºC and 4000 rpm for 20', supernatants were discarded and pellets were frozen at -80ºC.

For large scale Caspase-9 overexpression, an isolated colony was inoculated in 50mL of 2xTY medium supplemented with antibiotics and incubated overnight at 37ºC in continuous shaking (180rpm). This preculture was inoculated in 1L of 2xTY medium supplemented with antibiotics and was incubated at 37ºC until the OD_{600} was 0.6. Overexpression was induced with 0.4mM IPTG and incubated for 4h at 30 ºC. Cultures were centrifuged at 4ºC and 9000rpm for 30' (Sorvall RC6, rotor SLA-3000), supernatants were discarded and cells were resuspended in 40mL 1xPBS for each liter of culture pellet. Finally, cells were harvested again by centrifugation at 4ºC and 4000rpm for 30' in a Sorvall ST16R with rotor 75003629 TX-400 and pellets were frozen at -80ºC.

4.2.2. PP1Acα overexpression in *E. coli*

RP1B vector containing PP1α_{7-330} sequence in frame with an N-terminal Thio6-His6 expression and purification tag (MGSDKIHHHHHH) and a TEV cleavage site (ENLYFQGH) (Addgene plasmid #51768) (Peti and Page, 2007) was cotransformed with pGRO7 vector encoding GroEl-GroEs chaperones (Chaperone plasmid set, Takara) by heat shock bacterial transformation into chemically competent BL21 (DE3) *E.coli* cells as described above and plated in LB Agar (Pronadisa) with 33µg/mL kanamycin and 33µg/mL chloramphenicol.

The bottleneck for PP1 structural studies was to have an abundant source and a sufficient amount of the active, pure and homogeneous enzyme. Nevertheless, the production of PP1 in *E.coli* has shown important difficulties: it is highly insoluble, exhibits phosphotyrosine phosphatase activity and it is insensitive to regulation by several targeting subunits (reviewed by (Peti et al., 2013)). In order to solve the problem of insolubility there are two main strategies. The first one is to fuse PP1 with a tag that increases solubility and the second one is an *in vivo* refolding. Recently, (Peti et al., 2013) developed and optimized a novel PP1 expression protocol that achieves a 10-fold increase in PP1 yield, a 100-fold increase in PP1 activity and the possibility to form holoenzymes with high affinity. This chaperone-assisted PP1 expression protocol was the one used in the present work.

According to (Kelker et al., 2009) protocol, co-transformed cells were inoculated in LB medium (Pronadisa) supplemented with 33µg/mL kanamycin, 33µg/mL chloramphenicol and 1mM $MnCl_2$ and incubated overnight at 37ºC. Each 950mL of LB were inoculated with 50mL of preculture and supplemented with 33 µg/mL of kanamycin and 33 µg/mL chloramphenicol and 1mM $MnCl_2$. Cells were cultured at 37ºC until they reached an OD_{600} of 0.5. At that moment, the culture was induced with 2g/L of arabinose to induce the expression of GroEL/GroES chaperones. At OD_{600}=1, temperature was lowered to 10ºC and PP1 overexpression was induced with 0.1mM IPTG. After 20h of expression, cells were harvested and resuspended in fresh LB supplemented with 1mM $MnCl_2$ and 200µg/ml of chloramphenicol to stop ribosomal activity. For the final *in vivo* refolding step, cells were cultured at 10ºC for 2h, what increased the yield of active and well-folded PP1.

Finally, cells were harvested as described above for Caspase-9 and frozen at -80ºC for further use.

4.2.3. SET overexpression in *E. coli*

SET full length (1-277) and SET 1-225 constructs cloned in ppET28a were available in the plasmid collection of the laboratory. Plasmids were transformed in BL21 (DE3) Codon Plus RIPL chemically competent *E.coli* cells (Stratagene) as previously described. Finally, 150µL of cells were seeded in a culture plate containing the required antibiotics and incubated overnight at 37 ºC.

For small scale overexpression, an isolated colony was inoculated in 5mL of LB medium (Pronadisa), supplemented with 33µg/mL kanamycin and 33µg/mL chloramphenicol and incubated overnight at 37ºC in continuous shaking (180rpm). Then, this preculture was inoculated in 20mL of LB medium supplemented with antibiotics and incubated at 37ºC until the OD_{600} was 0.6. Absorbance was measured with a cellular densitometer Ultrospec 10 (Amersham Biosciences). To induce SET overexpression, culture was inoculated with a final concentration of 1mM IPTG and incubated for 4h at 30 ºC. Cultures were centrifuged (Sorvall ST16R, rotor 75003629 TX-400) at 4ºC and 4000 rpm for 30'. Supernatants were discarded and cells were resuspended in 1mL 1X PBS for each culture. Finally, cells were harvested again by centrifugation at 4ºC and 4000 rpm for 20', supernatants were discarded and pellets were frozen at -80ºC.

For large scale overexpression, an isolated colony was inoculated in 50mL of LB medium supplemented with 33µg/mL kanamycin and 33µg/mL chloramphenicol and incubated overnight at 37ºC in continuous shaking (180rpm). This preculture was inoculated in 950mL of LB medium supplemented with 33µg/mL kanamycin and 33µg/mL chloramphenicol and was incubated at 37ºC until the OD_{600} was 0.6. Overexpression was induced with 1mM IPTG and incubated at 20ºC overnight. Cultures were centrifuged at 4ºC and 3400rpm for 40' in a Beckman Coulter J6-HC centrifuge, supernatants were discarded and cells were resuspended in 40mL 1X PBS for each liter of culture pellet. Finally, cells were harvested again by

centrifugation at 4ºC and 4000rpm for 30’ in a Sorvall ST16R, with rotor 75003629 TX-400, and pellets were frozen at -80ºC.

4.2.4. PP2Acα overexpression in insect cells

PP2Acα D88N was cloned in pFastBacHTb donor vector as described in (Cho and Xu, 2007). The mini-att site containing the sequence of PP2Acα was transposed into a bacmid contained in DH10Bac *E.coli* competent cells, according to Bac-to-Bac Baculovirus Expression System protocol (Life Technologies). 5µL of bacmid were transfected into 500.000 Sf9 insect cells in Sf900II medium (Gibco) with 4µL FuGene (Promega) in a final volume of 2mL and were incubated at 27ºC for one week. Virus was amplified inoculating 500µL of transfected cells in 30mL of $1.5 \cdot 10^6$ Sf9 cells and incubating it at 27ºC for one week. Virus yield was titrated infecting Sf9-ET insect cells at a density of $0{,}8 \cdot 10^6$ with serial dilutions of virus in a 96-well plate. After 5 days of incubation, fluorescence of infected cells expressing GFP was observed in a confocal microscope Leica TCS SL with I3 filter to determine the amount of virus in the stock. High Five insect cells at a density of $2 \cdot 10^6$ in Express Five medium (Gibco) were infected with fresh recombinant virus at a m.o.i. of 2 and incubated at 27ºC for 72h. Cell pellets were harvested at 1100 rpm for 15’, washed with 1X PBS and centrifuged at 600g for 30’. Pellets were stored at -80ºC until use.

The same protocol was followed to overexpress PP2Acα2 construct.

4.3. Protein purification

Depending on the construct, the proteins used for this work had different buffer requirements for purification steps. The buffers applied in each case are detailed in **Table 9**.

Table 9. **Buffers used for protein purification.**

Constructs	Purification step	Buffer composition
C9WTFL SETFL SET 1-225	Lysis buffer	100 mM Tris pH 8, 100 mM NaCl, 0.5% Triton X-100, half tablet of Complete EDTA-free protease inhibitor cocktail (Roche)
	Buffer A	100 mM Tris pH 8, 100 mM NaCl
	Buffer B	100 mM Tris pH 8, 100 mM NaCl, 200mM Imidazole
	Size-exclusion buffer	20mM Tris pH8, 100mM NaCl, 1mM β-mercaptoethanol
GST-CARD GST-ΔCARDC94QC GST- ΔCARDC9C287A GST-C9C287AFL	Lysis buffer	100 mM Tris pH 8, 200 mM NaCl, 5% glycerol, 0.5% Triton X-100, half tablet of Complete EDTA-free protease inhibitor cocktail (Roche)
	Buffer A	100 mM Tris pH 8, 200 mM NaCl, 5% glycerol
	Buffer B	100 mM Tris pH 8, 200 mM NaCl, 5% glycerol, 20mM Reduced Glutathione
	Size-exclusion buffer	20mM Tris pH8, 200mM NaCl, 5% glycerol, 1mM β-mercaptoethanol
Caspase-9b	Lysis buffer	100mM Tris pH8.8, 150mM NaCl, 5% Glycerol, 0,5% Triton X100, half tablet of Complete EDTA-free protease inhibitor cocktail (Roche)
	Buffer A	100mM Tris pH8.8, 150mM NaCl, 5% Glycerol
	Buffer B	100mM Tris pH8.8, 150mM NaCl, 5% Glycerol, 200mM Imidazole
	Size-exclusion buffer	20mM Tris pH 8.8, 150mM NaCl, 5% Glycerol, 1mM β-mercaptoethanol
$PP1\alpha_{7-330}$	Lysis buffer	50mM Tris pH 8, 700 mM NaCl, 1mM $MnCl_2$, 5% Glycerol, 10 mM Imidazole, 0.5% Triton x-100, half complete EDTA-free protease inhibitor cocktail tablet (Roche)
	Buffer A	50mM Tris pH 8, 700 mM NaCl, 1mM $MnCl_2$, 5% Glycerol,10 mM Imidazole
	Buffer B	50mM Tris pH 8, 700 mM NaCl, 1mM

		$MnCl_2$, 5% Glycerol,250 mM Imidazole
	Size-exclusion buffer	50mM Tris pH 8, 500mM NaCl, 0.5mM TCEP, 5% glycerol
PP2AD88N PP2Acα2	Lysis buffer	50mM Tris pH 8, 100 mM NaCl, 5mM β-mercaptoethanol, 0.5% Triton x-100, half complete EDTA-free protease inhibitor cocktail tablet (Roche)
	Buffer A	50mM Tris pH 8, 100 mM NaCl, 3mM β-mercaptoethanol
	Buffer B	50mM Tris pH 8, 100 mM NaCl, 3mM β-mercaptoethanol, 300 mM Imidazole
	Size-exclusion buffer	25mM Tris pH8, 50mM NaCl, 1mM DTT

4.3.1. Small scale purification

To verify soluble protein overexpression, cell pellets from 20mL of culture were lysed with 300µL of lysis buffer and the lysate was sonicated using Standard B01010005 (Diagenode) bioruptor at medium intensity (200W) for 30' at 30'' intervals at 4ºC. Sample was centrifuged at 4ºC at 14800 rpm during 30' and supernatant was kept on ice. Depending on the tag fused to the protein of interest, different type of resin was used for purification. Gluthathione sepharose 4B beads (GE Healthcare) were used for GST-tagged proteins, Ni-NTA beads (ABT beads) for His-tagged proteins and amylose beads (New England Biolabs) for MBP-tagged ones. 80µL of beads in each tube were centrifuged at 7000g for 1' with Sorvall Legend micro 21R (Thermo Scientific) to remove preservative solution (20% ethanol). Beads were washed and equilibrated with 1mL MilliQ water and then with the same volume of buffer A. Supernatant of sample was incubated with the beads in a nutator for 30' at 4ºC. After centrifugation for 5' at 5000 rpm, beads were washed with 1mL of buffer A three times. The bound protein was eluted with 100µL of buffer B. After elution, samples were prepared for SDS-PAGE electrophoresis: 40µL of pellet, supernatant, flow-through and wash as controls, and 40µL of elution were mixed with 15µL SDS-PAGE loading buffer 6X. Samples were incubated at 95ºC in a Multi Blok dry block heater (Thermo Scientific) for 10' and loaded into a 10%

polyacrylamide gel adding a sample of molecular weight Blue Star Prestained Protein Marker (Nippon) or Precision Plus Protein Dual Color Standards (BioRad). The gel was run for 40' at 200V in a Mini-Protean tetra cell electrophoresis (Biorad) cuvette filled with NuPAGE MES 1X (Invitrogen). The gel was dyed with a Coomassie Blue solution (1g Coomassie Blue, 40% methanol, 10 % glacial acetic acid and 50% distilled water) for 5' and destained with Coomassie blue destaining solution (10% methanol, 10% glacial acetic acid, 80% H_2O) until the protein bands were visible. The presence of the purified protein in the elution allowed us to continue with large scale overexpression and purification experiments.

4.3.2. Affinity chromatography

Cell pellets from 1-2L of large scale overexpression cultures were thawed on ice and resuspended in 50 mL of lysis buffer. The dissolved pellet was sonicated for 15' (1'' On-1'' Off) in a Bioblock scientific Vibra Cell 75042 sonicator and further centrifuged at 17000 rpm for 40' at 4ºC (Sorvall RC6, SS-34 rotor). Supernatant was filtered through a syringe filter of 0.45µm diameter and loaded into the column required in each case using a Gilson Minipuls 3 peristaltic pump.

4.3.2.1. Affinity chromatography of His-tagged proteins

A 5mL Ni-NTA column (ABT Agarose Beads Technologies) was equilibrated with 5 column volumes of Milli Q water and 5 column volumes of buffer A with a Gilson Minipuls 3 peristaltic pump before loading the sample containing the protein of interest. With the help of Äkta purifier (GE Healthcare), the column was washed with 40mL of buffer A to remove unspecific bound proteins and elution was performed in 5mL fractions applying an increasing gradient of Buffer B during at least 7 column volumes.

4.3.2.2. Affinity chromatography of GST-tagged proteins

A 5mL GSTrap column (GE Healthcare) was equilibrated with 5 column volumes of MilliQ water and 5 column volumes of buffer A with a Gilson Minipuls 3 peristaltic pump before loading the sample. Once the sample was loaded, the column was initially washed with approximately 20 mL of buffer A and the sample was eluted with a syringe adding 12 mL of 100% buffer B containing 20mM reduced Glutathione.

4.3.2.3. SDS-PAGE electrophoresis

For both affinity chromatography cases three samples were used as controls: the discarded pellet obtained after lysate centrifugation (to check if the protein was expressed insoluble), the flow-through of the column (to check that the protein of interest had been retained in the column) and a fraction of the subsequent wash step. These samples and the elution fractions were mixed with SDS-PAGE loading buffer 6X and run in a 10% polyacrylamide gel as described in section 4.3.1.

According to the electrophoresis results, the fractions containing the desired pure protein were concentrated by centrifugation (Eppendorf Sorvall ST16R) at 4000 rpm and 4ºC using Amicon Ultracel 30K, 10K or 3K cutoff concentrators, until the sample reached a final volume of 2.5 mL.

4.3.3. Size exclusion chromatography

Size exclusion chromatography was performed using Äkta Prime (GE Healthcare) with a Superdex 200 26/60, Superdex 200 16/60 or Superdex 75 16/60 column (Pharmacia Biotech). The column was equilibrated with 360 mL of water and 360mL of SE buffer for 26/60 column and 180mL in each step for 16/60 columns. 2.5 mL of the eluted protein from affinity chromatography were injected into the system to perform separation. The fractions containing a peak in the chromatogram were run in a 10% polyacrylamide gel as described before and the fractions containing the desired protein were concentrated using a new Amicon

Ultracel concentrator, until protein concentration was enough to perform biophysical assays. Protein concentration was measured diluting 1µL of pure protein in 499µL of guanidine hydrochloride in a Precision Cell Synthetic Quartz Glass 10mm path cuvette (Hellma Analytics). Absorbance at 280nm was measured in a UV Visible spectrophotometer Ultrospec 2000 (Pharmacia Biotech) and concentration was calculated with Lambert-Beer law equation.

As Caspase-9 and PP1A cannot be frozen without losing its stability, these purification protocols were repeated every time an interaction assay was performed.

4.4. Characterization of binding sites

4.4.1. Pep-scan-based Far Western Blot

To determine the PP2Acα sequence that bound Caspase-9 (PP2Ah), overlapping dodecapeptides (shift of 2 aminoacids) covering the whole PP2Acα sequence were synthesized into an amino-derivatized cellulose membrane at Centro Nacional de Biotecnología (Madrid) or by GL Biochem (Shangai), using an automated multiple peptide synthesizer with solid phase procedure and standard Fmoc chemistry. The purity and composition of the peptides were confirmed by reverse phase HPLC and aminoacid analysis. The membrane was blocked with 3% BSA and 3% non-fat powder milk, incubated overnight with 4µg/mL of purified Caspase-9 protein and after several washing steps with 1x PBS-Tween, it was incubated during 4h with anti-Caspase-9 followed by 1h of incubation with PO-conjugated secondary antibody. Interaction sites were visualized using ECL system (Amersham).

C9h and PP2Ah mutants were designed and synthesized and the interaction with PP2A and Caspase-9 respectively was analyzed by pep-scan-based Far Western Blot in the same way as described for PP2Acα overlapping peptides.

With the aim of mapping the triple interaction Caspase-9/PP2Acα/PP1cα interaction, overlapping dodecapeptides covering murine Caspase-9 sequence were synthesized as described for PP2Acα, and the amino-derivatized cellulose membrane was incubated first with PP1α and after washing steps, with PP2Acα. After that, the membrane was incubated during 4h with anti-PP2A followed by 1h of incubation of

PO-conjugated secondary antibody. Interaction sites were visualized using ECL system (Amersham).

To determine Caspase-9 and SET binding sites, overlapping dodecapeptides covering human SET sequence were synthesized as described for PP2Acα. The membrane was blocked with 3% BSA and 3% non-fat powder milk, incubated overnight with 4µg/mL purified Caspase-9 protein and after several washing steps with 1x PBS-Tween, it was incubated during 4h with anti-Caspase-9 followed by 1h of incubation with PO-conjugated secondary antibody. In the same way, overlapping dodecapeptides covering human Caspase-9 sequence were synthesized, the membrane was blocked and incubated with purified SET protein and after several washing steps it was incubated with anti-SET followed by PO-conjugated secondary antibody. In both cases interaction sites were visualized using ECL system.

4.4.2. Synthetic peptides

Caspase-9 derived peptide C9h was designed and synthesized as described in (Arrouss et al., 2013). The rest of synthetic peptides used in this work (**Table 10**) were synthesized by SynPeptide (China) using an automated multiple peptide synthesizer with solid phase procedure and standard Fmoc chemistry. The purity and composition of the peptides were confirmed by reverse phase HPLC and by aminoacid analysis.

4.4.3. Molecular docking

To validate the interaction site detected by pep-scan-based Far Western Blot, a molecular docking analysis was performed using the algorithm implemented in Frodock software, an approach to fast rotational protein-protein docking (http://chaconlab.org/frodock/index.html), to get predictions of the interaction between Caspase-9 and PP2Acα from their 3D coordinates in the free state (Garzon et al., 2009). This software was run in Linux Red Hat and a rigid docking was modeled. The PDB files submitted were 2IE3 for PP2Acα and 1JXQ for Caspase-9. The model obtained was analyzed using PyMOL software.

Table 10. Synthetic peptides used in this work.

Peptide name	Amino acid sequence
C9h	YVETLDDIFEQWAHSEDL
C9h mut	YVETLDDIFEQAAHSEDL
DPT-C9h	VKKKKIKREIKI- YVETLDDIFEQWAHSEDL
DPTmut3-C9h	VKKKKIKAEIKI- YVETLDDIFEQWAHSEDL
DPTmut3-C9hS4	VKKKKIKAEIKI-QMPGCFNFLRKKLFFKTS
DPTmut3-C9hS5	VKKKKIKAEIKI- TFPGFVSWRDPKSGSWYV
C9h-Rhodamine B	YVETLDDIFEQWAHSEDLK-Rhodamine B
C9h-C	YVETLDDIFEQWAHSEDLC
YPP2Ah	YDTLDHIRALDRLQEVPHE
DPT-PP2Ah	VKKKKIKREIKI-DTLDHIRALDRLQEVPHE
DPTmut3-SET-S1	VKKKKIKAEIKI-ILKVEQKYNKLRQPFFQKRSEL
DPTmut3-SET-S2	VKKKKIKAEIKI-RSSQTQNKASRKRQHEEP

4.4.4. Effect of mutations on Caspase-9 stability

FoldX 3.0 algorithm (http://foldx.crg.es/), executed in Windows XP, was applied to evaluate the contribution of Caspase-9 point mutations to protein stability. Firstly, the protein structure (PDB 1JXQ) was optimized using the Repair PDB command. Then, two calculations were executed:

- Stability analysis: the most basic analysis, which provided free energy calculation, generating as a result the free Gibbs energy of folding in kcal/mol decomposed in the different energy terms used by FoldX.

- Alascan: a virtual Alanine residues scan in the protein evaluated the direct effect that each point mutation had in the global stability of the protein. All positions except Glycine residues were changed to Alanine and the position of the adjacent side chains was optimized. The results brought by FoldX is the energy difference (ΔΔG, in kcal/mol) between the wild type and the mutant structures, decomposed in energy terms (Schymkowitz et al., 2005).

4.4.5. Circular dichroism

Wild type and W374A Caspase-9 derived synthetic peptides covering PP2Acα binding site (corresponding to residues 363-380) were synthesized. Both peptides were analyzed with a Jasco J-010 spectropolarimeter to study the differences among them in the secondary structure and the percentage of α helix.

Peptides were dissolved in 10mM Sodium phosphate pH 7.5 prepared from 10mL solution A + 84mL solution B in a final volume of 200mL.

Solution A: 2.76 g $NaH_2PO_4 \cdot 3H_2O$. (0.0552g / 20mL) (AppliChem)

Solution B: 5.365 g $Na_2HPO_4 \cdot 7H_2O$. (0.5365g / 100mL) (Sigma - Aldrich)

Final pH of the mix was adjusted to 7.65.

To induce α helix formation in the peptides, a titration with trifluoroethanol (TFE) (Sigma – Aldrich) was performed. Samples were prepared with 50µM of peptide dissolved in a final volume of 300µL with increasing concentrations of TFE (20%, 40%, 60% and 80%). Samples were introduced in the spectropolarimeter in a Quartz Suprasil Precission cell 0,1cm cuvette (Hellma), using 300µL of buffer solution as blank. Measurements were repeated 10 times for each sample and 5 times for each blank and they were performed at 20ºC.

Data were processed with spectropolarimeter software to substract blank from sample spectra and millidegrees units were further converted to molar elipticity.

4.5.*In vitro* binding assays

4.5.1. Pull-down assays

Caspase 9 and PP1 constructs were expressed according to the protocols described above. 20 mL of Caspase-9 and PP1 cultures were processed as described for low-scale purification protocol. After lysate centrifugation, aliquots of pellet and supernatant of each construct were kept as controls. The supernatant of Caspase-9 constructs (CARD, ΔCARDC94QC, ΔCARDC9C287A, CASP9C287AFL), as baits, was incubated for 30' with Glutathione sepharose 4B beads in a nutator at 4ºC. In the same way, the supernatant of PP1$\alpha_{7\text{-}330}$ was incubated with Glutathione sepharose 4B beads to perform a negative control. After bait incubation, beads were centrifuged for 5' at 5000g. The flow-through containing the unbound proteins was separated and kept as a control. Beads were washed three times with buffer A (100 mM Tris pH 8, 200mM NaCl) to eliminate the unspecifically bound material. In a further step, the supernatant of PP1$\alpha_{7\text{-}330}$ was added as prey protein and incubated for 30' in a nutator at 4ºC. The mixture was centrifuged again and beads were washed three times with 1mL of buffer A. Finally, the protein-protein complex was eluted with 100µL of buffer B (100mM Tris pH8, 200mM NaCl, 20mM reduced Glutathione). Samples were run in a SDS-PAGE as previously described and a western blot was performed to confirm the presence of the two proteins in the elution.

The pull down assay between Caspase-9 and SET was performed following the same protocol, using GST-Caspase-9 constructs as bait protein and SET full length or SET 1-225 as prey protein.

4.5.2. Western Blot

Protein samples previously eluted from the pull-down assay were separated by SDS-PAGE at 200V for 30'. Two 10% polyacrylamide gels were run in parallel in order to perform two western blots with different antibodies. Polyacrylamide gels were transferred to two nitrocellulose membranes (Hybond-ECL) using a Trans-Blot SD Semi-Dry Electrophoretic Transfer Cell (BioRad) at 16V during 1h. After transference, membranes were blocked in 10mL of blocking solution: 5% non-fat dry

milk in TBST 1X (50 mM Tris HCl pH 7.4, 150mM NaCl, 0.1% Tween 20) for 1h. One membrane was incubated for 1h with Anti-His6-Peroxidase antibody (Roche), conjugated to horseradish peroxidase. The other membrane was incubated for 1h with Anti-GST antibody (Anti-GST HRP Conjugate. GE Healthcare Life Sciences). Finally, membranes were washed with TBST 1X three times for 8'. Protein detection was performed using 1mL of Pierce ECL Western Blotting Substrate (Life Technologies) and visualized in an Image Quant LAS 4000 mini (GE Healthcare).

4.5.3. Differential scanning fluorimetry

Caspase-9 stability was measured by differential scanning fluorimetry, also termed thermal shift assay or Thermofluor, in the presence of increasing concentrations of YPP2Ah peptide, corresponding to Caspase-9 binding site of PP2Acα. Purified ΔCARD Caspase-9 C287A was diluted to 1mg/mL in 198µL of size exclusion buffer and 2µL of Sypro Orange (Sigma – Aldrich) were added to the sample. The experiment was performed in a 96 wells Micro Amp Fast Optical reaction plate (Applied Biosystems). 36µL of YPP2Ah were shared into each well from A to D, performing serial dilutions in size exclusion buffer. Then, 4µL of ΔCARD Caspase-9 C287A were added to each well and 20µL of the mix were taken to do a replicate in wells from E to H. Thermal cycles were performed in a Real Time Fast 7500 device (Applied Biosystems), increasing 1ºC/cycle during 65 cycles.

4.5.4. Biolayer interferometry

BLItz (FortéBio, Pall Life Sciences) was used with Ni-NTA biosensors charged with Tris-NTA groups for the capture of His-tagged molecules or anti-GST biosensors for binding of GST-tagged proteins, depending on the requirements of the experiment. Before the assay was performed, biosensors were hydrated for 10' with 250µL of SE buffer (20mM Tris pH8, 200mM NaCl, 5% glycerol, 1mM β-mercaptoethanol). To measure the interaction kinetics between PP1 and Caspase-9 constructs, 30 µg/mL of PP1 was immobilized in the Ni-NTA biosensor as bait protein and 10µM, 5µM, 2.5µM and 1.25µM of Caspase-9 construct

CASP9C287AFL, containing a GST tag which does not bind to the sensor, were used as prey protein. Advanced kinetics experiment was set up in the device with the conditions listed in **Table 11**. The biosensor was attached onto the BLI arm to perform the baseline measurement with buffer for 30''. The second step was to pipet 4µL of the bait protein into the drop holder and low the arm to perform the binding of the bait to the biosensor for 180''. The next step consisted of a new baseline for 1'. Then, 4 µL of the prey protein were placed in the drop holder to perform its binding to the immobilized partner for 2'. Finally, the dissociation step was run by placing the arm in a new tube containing SE buffer.

In the case of the interaction between Caspase-9 and SET, 30 µg/mL of GST-Caspase-9C287A full length was immobilized in an anti-GST sensor as bait protein and 10µM and 20µM of SET full length were used as prey protein. The experiment was performed as described for Ni-NTA sensors.

After experiments, Ni-NTA biosensors were regenerated by submerging the biosensor surface in 10mM glycine pH1.7 5'', 1X PBS 5'', 10mM $NiCl_2$ to reload the biosensor 1', 1X PBS 1' and 15% sucrose dissolved in 1X PBS 5'. Anti-GST biosensors were regenerated in 10mM glycine pH1.7 5'', 1X PBS 5'' repeated five times. Finally, all biosensors were dried for 5' at room temperature before storage.

Table 11. Advanced kinetics experiment steps (Sultana and Lee, 2015).

Step	Step name	Time(s)	Step type
1	Baseline 1	30	Baseline
2	His-tagged protein	180	Loading
3	Baseline 2	60	Baseline
4	Association	120	Association
5	Dissociation	120	Dissociation

4.5.5. Isothermal titration calorimetry

Pure proteins in the case of Caspase-9, PP1cα and SET and YPP2Ah peptide were diluted in the same size exclusion buffer to perform the experiment in a Nano ITC (TA Instruments). The experiments were run at different temperatures from 8 to 25ºC, depending on the analysis. Samples were degassed for 10' using the degassing

work station. The reference cell was filled with sterile degassed MilliQ water and refilled periodically. 300µL of 20-30µM of protein were loaded in the cell (reaction volume 170µL) with a Hamilton syringe and 50µL of the second protein or YPP2Ah peptide were loaded in the titration syringe attached to the buret. The experiment was performed in 30 serial injections of 1.5µL with 210 seconds of injection interval. Data were further processed with NanoAnalyze v.3.5.0. software.

4.6.*In vitro* Caspase-9 activation assay

Caspase-9 wild type full length was purified as previously described and diluted to 2µM in the following buffers:

- Buffer S: 50mM $Na_2HPO_4 \cdot 7H_2O$, 150mM NaCl, 1.5% Sucrose, 0.05% Chaps pH 7.4, 10mM DTT.
- Buffer SC: 50mM $Na_2HPO_4 \cdot 7H_2O$, 150mM NaCl, 1.5% Sucrose, 1% Chaps, 10mM DTT, 0.7M Sodium Citrate Tribasic pH 7,4. The presence of sodium citrate in the buffer favors Caspase-9 activation, therefore Caspase-9 diluted in this buffer will be used as a positive control.

The experiment was set up in an Optiplate-96F black plate (Perkin Elmer), where Caspase-9 activation was tested in the presence of increasing concentrations of the peptide PP2Ah (from 0.037mM to 1.5mM) in buffer S. In addition, several controls were measured:

- Negative control: Caspase-9 diluted in buffer S onto buffer S.
- Activation control: Caspase-9 diluted in buffer SC onto buffer S. It is a positive control of moderate activation.
- Positive control: Caspase-9 diluted in buffer SC onto buffer SC.
- Sample control: incubating Caspase-9 with 0.5mM and 1mM of a small molecule, termed DES, which is known to activate Caspase-9.

Firstly, Caspase-9 diluted in buffer S and SC was incubated at room temperature for 20'. In this time, 83µL of reaction buffer S or SC per well were shared in the 96 wells plate and then 2µL of S buffer in the negative control, 2µL of SC buffer in the positive control and 2µL of ligand (PP2Ah or DES) in the samples were added. After 20' of incubation, 5µL of Caspase-9 in buffer SC were added to

the activation and positive control wells and 5µL of Caspase-9 in buffer S were added to the negative control, sample control with DES and samples with increasing concentrations of PP2Ah. The plate was incubated for another 20' at room temperature. 10µL of 0,4mM of the fluorogenic Caspase-9 substrate Ac-LEHD-AFC were added to each well and fluorescence was measured with a Wallac Victor^2 1420 Multilabel HTS Counter (λ_{ex} = 400 nm; λ_{em} = 510 nm), using filter FP390 at 25ºC.

4.7. Cell culture

HeLa and MDA-MB-231 cell lines were cultured in DMEM High glucose (Sigma-Aldrich) supplemented with 10% fetal bovine serum (FBS) (Lonza). Daudi and Jurkat cells were cultured in RPMI 1640 (Gibco) supplemented with 10% FBS. SH-SY5Y neuroblastoma cell line was cultured in DMEM F12 (Gibco) supplemented with 10% FBS, 1% Glutamine (Gibco) and 1% Hepes 1M (Gibco). All cell lines were grown at 37ºC and 5% CO_2 and underwent passage two or three times a week.

To force starvation conditions in order to induce PP2Acα2 expression, $5 \cdot 10^5$ cells were plated in P60 culture plates and grown under starvation conditions with 0,5% FBS and without any FBS. After 48h of incubation, total RNA was isolated for further analyses.

4.8. Mesoporous silica nanoparticles

Two types of mesoporous silica nanoparticles, one with a diameter size of 400nm and the other one with 100nm (termed MCM-41), were synthesized at COMAV facilities (Polytechnic University of Valencia) using tetraethylorthosilicate (TEOS) (Sigma-Aldrich) as a hydrolytic inorganic precursor and surfactant hexadecyltrimethyl ammonium bromide (CTAB) (Sigma-Aldrich) as the porogen species. Calcination of the mesostructured phase resulted in the starting solid. Then $[Ru(bipy)_3]^{2+}$ (Sigma-Aldrich) was added to a methanol suspension containing the 400nm or MCM-41 scaffolding for the control nanoparticles. The synthetic peptides C9h-Rhodamine B and C9hC in a DMSO suspension were loaded respectively in

400nm and MCM-41 solids and they were used for peptide delivery. The mixture was stirred for 24h to load the pores of the mesoporous support. For the attachment of ε-poly-L-lysine, excess of 3-(triethoxysilyl) propyl isocyanate was added to the loaded nanoparticles and the final suspension was stirred for 2h before adding ε-poly-L-lysine. The final solid was filtered, washed with methanol and dried (Mondragón et al., 2014). The preservation of the mesoporous structure in the final solids was confirmed by transmission electron microscopy.

4.8.1. WST-1 cell viability analysis

To determine the most appropriate amount of cells needed to perform cell viability assays, five 96 well plates were seeded with 1000, 2500, 5000, 10000 and 20000 HeLa cells in triplicates in 100µL of DMEM and 10% FBS. Plates were incubated for 2, 24, 48, 72 and 96h at 37ºC with 5% CO_2. After incubation times, 10µL of WST-1 Cell proliferation reagent (Roche) was added to each well and incubated at 37ºC for 1h30'. Absorbance was measured with a Wallac 1420 Victor^2 Multilabel HTS Counter at 450nm substracting absorbance at 690nm, using P450 and P690 filters respectively.

To test cell viability after treatment with 400nm MSNs loaded with C9h-RhodamineB or MCM-41 loaded with C9hC, 2500 HeLa cells were seeded in 100µL DMEM + 10% FBS per well in a 96 well plate and were incubated during 24h. Nanoparticles were dissolved in DMSO at the appropriate concentrations required to have a final concentration of 1% DMSO in the well and they were gently sonicated for 10' in a water bath with a Bioblock scientific Vibra Cell 75042 sonicator at 40% amplitude. Then, they were further dissolved in DMEM+10%FBS, the previous medium of the cells was removed and the new medium containing the treatment was added in triplicates for each concentration of nanoparticles. DPTmut3-C9h peptide was also dissolved in DMSO to have equivalent peptide concentrations to 400nm MSNs or MCM-41 cargo at the different doses applied and a final concentration of 1%DMSO in the well, it was further dissolved in DMEM+10%FBS and added to the cells. The wells containing cells treated with fresh DMEM+10%FBS and DMEM+10%FBS+1%DMSO were used as negative controls. After 24 and 48h of incubation, 10µL of WST-1 Cell proliferation reagent (Roche) was added to each

well, incubated at 37ºC for 1h30' and absorbance was measured as described for HeLa cells.

Toxicity of 400nm MSNs and MCM-41 was evaluated performing the same experiment with the use of empty MCM-41 (without any cargo) and 400nm MSNs loaded with the model dye molecule $[Ru(bipy)_3]^{2+}$ to verify that cell viability was not significantly reduced due to the treatment.

4.8.2. Cell penetration assay with confocal microscopy

50000 HeLa cells in 2mL of DMEM + 10% FBS per well were seeded in 6 well plates and incubated 24h at 37ºC and 5% CO_2 before being treated with 150µg/mL of MCM-41 nanoparticles loaded with $[Ru(bipy)_3]^{2+}$. After 24h of incubation, cells were mounted with Mowiol, nuclei were stained with 10ng/mL Hoechst 33342 and samples were observed in a confocal Leica microscope using a TCS SP2 system equipped with an acoustic optical beam splitter (AOBS).

4.9. FACS AnnexinV-FITC apoptosis measurement

25000 HeLa cells in 1mL of DMEM + 10% FBS per well were seeded in 24 well plates and incubated 24h at 37ºC and 5% CO_2 before being treated with different concentrations of MCM-41 nanoparticles and the equivalent cargo concentration of DPTmut3-C9h. Cells treated with 1% DMSO were used as negative control.

The apoptotic effect of bifunctional peptides DPTmut3-C9h-S4, DPTmut3-C9h-S5, DPT-mut3-SET-S1 and DPT-mut3-SET-S2 alone or combined was evaluated in MDA-MB-231 cell line. 50.000 cells in 1mL of DMEM + 10% FBS per well were seeded in 24 well plates and incubated 24h at 37ºC and 5% CO_2 before being treated with 100µM of a single peptide or 40µM of each peptide in the mixes DPTmut3-C9h-S4 + DPTmut3-C9h-S5 or DPT-mut3-SET-S1 + DPT-mut3-SET-S2. Non treated cells were used as negative control.

In both cases, after 24h of incubation, AnnexinV – FITC apoptosis detection kit I (BD) was added to the samples following the manufacturer's protocol and

samples were analyzed with a FACS Canto (BD) flow cytometer using blue laser (488nm) to measure FITC (λ_{ex}= 490nm, λ_{em}= 525nm) and PI (λ_{ex}= 536nm, λ_{em}= 617nm) fluorescence.

4.10. Study of Caspase-9b and PP2Acα2 expression in CLL

4.10.1. B-cells isolation

Fresh blood from healthy donors (HD) was obtained from the Établissement français du sang (Paris). Peripheral blood mononuclear cells (PBMC) or bone marrow cells isolated from CLL patients were obtained from UPMC Department of Hematology (Paris) and from Dr. María José Terol at Health Research Institute INCLIVA (Valencia). Mononuclear cells from peripheral blood or bone marrow were prepared by Ficoll gradient centrifugation. After 20' centrifugation at 2300rpm, PBMC were collected and washed twice with PBS. B cells were isolated using DynaI negative isolation kit (Invitrogen), reaching purity up to 98%.

4.10.2. RNA extraction and cDNA production

Total RNA from cell lines and from patients B cells was extracted with TRIzol reagent (Life Technologies), following the manufacturer protocol, and it was eluted in 20µL of DEPC water. RT-PCR was performed over up to 2 ng of RNA to obtain cDNA using High Capacity cDNA Reverse Transcription Kit (Applied Biosystems).

4.10.3. Caspase-9 and PP2Acα detection by conventional PCR

To analyze the presence of Caspase-9, Caspase-9b, PP2Acα and PP2Acα2 conventional PCR was performed using Kapa HiFi DNA polymerase (Kapa Biosystems) under the conditions shown in **Table 12** and using the primers of **Table 13.** Samples were visualized in a 2% agarose gel.

Table 12. PCR conditions to amplify Caspase-9 and PP2A splicing variants from cDNA of CLL patients.

Conditions	Reaction mix
Initial denaturation:	5µL Buffer HiFi 5X
95ºC – 3’	0.75µL dNTPs (10mM each)
30 cycles:	0.75µL Forward primer
98ºC – 20’’	0.75µL Reverse primer
55ºC – 20’’	1.25µL DMSO
72ºC – 2’	0.25µL Template DNA (cDNA)
Final extension:	0.5µL Kapa HiFi DNA polymerase (Nippon Genetics)
72ºC – 5’	15.75µL MilliQ water

Table 13. Primers used to amplify Caspase-9 and PP2Acα splicing variants from cDNA of CLL patients.

Primer name	Sequence
Caspase-9 FWD	ATGGACGAAGCGGATCGG
Caspase-9 REV	TTATGATGTTTTAAAGAAAAGTT
PP2A FWD	GACGAGAAGGTGTTCACCAA
PP2A REV	TTACAGGAAGTAGTCTGGGGTAC

4.10.4. Real Time PCR

Real Time PCR was applied to quantitatively analyze Caspase9, Caspase9b, PP2Acα and PP2Acα2 gene expression using TaqMan PCR Mastermix in a 7500 Fast Real Time Applied Biosystems device. Caspase9 and PP2Acα probes respectively corresponded to Hs00154261_m1 and Hs01003394_mH Life Technologies references. Quantitative PCR primers for Caspase9b were (Vu et al., 2013):

5’-GGATTTGGTGATGTCGAGCAG-3’ (forward)

5’-CATCTGGCTCGGGGTTACT-3’ (reverse)

5’-TTCCCCTGAAGACGAGTCCCCTGG-3’ (probe)

PP2Acα2 primers and probe were designed with the following sequences:

5’-CAAGAAGTTCCCCATGAGGGATATA-3’ (forward)

5’-CAACGATAACAATAGTTTGGAGCACT-3’ (reverse)

5’-CGTTACTACATTCCGGTCATGGCACCA-3’ (probe).

GAPDH was used as the housekeeping reference gene (Hs99999905_m1, Life Technologies). Each patient sample was analyzed in triplicates for the detection of each gene in a 96 wells Micro Amp Fast Optical reaction plate (Applied Biosystems). Each probe was diluted 1:10 in Mastermix (Applied Biosystems) and 11µL of this mix were distributed in each well. 9µL of 1:90 cDNA dilution in DEPC water were added to the wells. The reaction conditions are shown in **Table 14**. Data analysis of relative expression was calculated following the $2^{-\Delta\Delta C}{}_{T}$ method (Livak and Schmittgen, 2001).

Table 14. Real Time PCR conditions.

Steps	Temperature (ºC)	Time
Hold	95	10’
40 cycles	95	15’’
	60	1’

RESULTS

"Dimidium facti, qui coepit, habet: sapere aude, incipe" He who has begun is half done; dare to know, dare to begin! "First book of letters", Horace, 1 b.C.

5. RESULTS

5.1. Characterization of Caspase-9 – PP1α interaction

5.1.1. Overexpression and purification of Caspase-9 constructs

Both His-tagged and GST-tagged Caspase-9 constructs were overexpressed following the same protocol, optimized from (Denault and Salvesen, 2002a). In the case of His-tagged constructs, the C-terminal position of the tag resulted in higher yield of expression for Caspase-9 wild type full length (overexpressed in pET23b) and it was crucial for the expression of ΔCARD Caspase-9 C287A. All expression attempts of ΔCARD Caspase-9 using N-terminal His tag didn't allow to get soluble protein, even trying different plasmids, culture media, temperatures and IPTG concentrations. On the contrary, ΔCARD Caspase-9 cloned in C-terminal His-tagged pET21b gave satisfactory results, as it was previously demonstrated by (Chao et al., 2005). Additionally, some difficulties appeared when we wanted to overexpress Caspase-9 with N-terminal GST-tag, as expected according to the previously described constructs in the literature. Overexpression attempts using pGEX-6P-2 failed to provide soluble protein, however we managed to produce GST-Caspase-9 using the in-house modified pGKI vector. These Caspase-9 constructs in pGKI vector (GST-CARD, GST-ΔCARD Caspase-9 C287A and GST-Caspase-9 full length C287A) allowed us to get pure protein and then we could perform biolayer interferometry experiments with PP1α. This is relevant because Blitz requires that prey protein has no tag or different tag from the bait protein. As PP1 can only be overexpressed properly folded with His-tag, the tag could not be changed in this case, so we decided to change the tag in Caspase-9 constructs to GST-tag.

C-terminal His-tagged Caspase-9 wild type full length construct was purified by affinity chromatography with a 5mL HisTrap column (GE Healthcare) and in a further step by size exclusion chromatography (**Figure 27**) to be able to separate pure protein from *E. coli* contaminants that were copurified with the sample, as ArnA and Chloramphenicol acetyltransferase. The fractions containing pure protein were concentrated and used for further experiments.

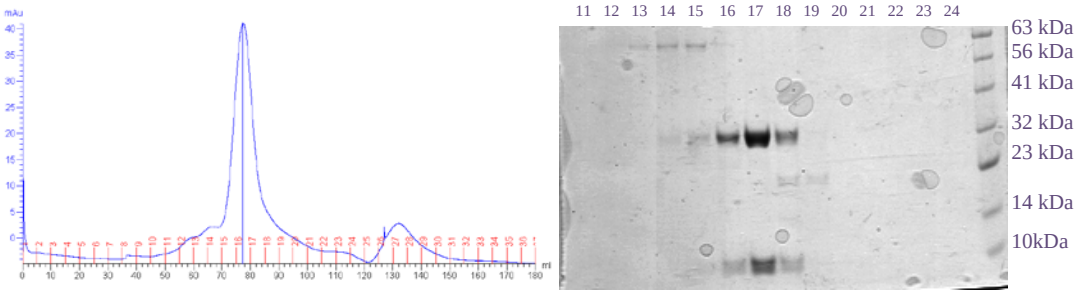

Figure 27. Superdex 200 16/60 size-exclusion chromatogram of Caspase-9 wild type full length and SDS-PAGE gel showing fractions 11-24. Fractions 16-18 contain pure protein.

Caspase-9 constructs in pGKI vector were purified by affinity chromatography using a 5mL GSTrap column (GE Healthcare). GST-ΔCARD4QC construct did not yield any interaction with PP1α in the pull-down assay, so it was not further purified at large scale for this purpose. GST-CARD and GST-ΔCARDC287A elutions are shown in **Figure 28 A.** Low yield of GST-C9C287AFL was obtained in the purification, thus results are shown in **Figure 28 B.** with the concentrate of pure protein. GSTrap columns were eluted directly with a syringe loaded with buffer B. No further purification steps were performed, as the proteins could not be detected after size exclusion chromatography step. For biolayer interferometry experiments, buffer was changed with an Amicon Ultracel concentrator, adding 10 volumes of buffer A and concentrating samples until reaching the amount required for further experiments.

5.1.2. Overexpression and purification of PP1cα

Several attempts were performed to overexpress well folded PP1cα in pGEX-6P-2, pMBKI (generated in the laboratory by Dr. Marcin Węgrecki (IBV, Valencia), an in-house modified version of the pET28-NKI/LIC 6His/3C vector (originally obtained from Dr A. Perrakis group, NKI, Amsterdam) in which the His tag was substituted by a MBP tag) and also in several His-tagged pET derived vectors. In 2013, (Peti et al., 2013) published the details of the expression protocol that allowed to obtain soluble and well folded $PP1\alpha_{7-330}$ that let us continue the studies of this protein.

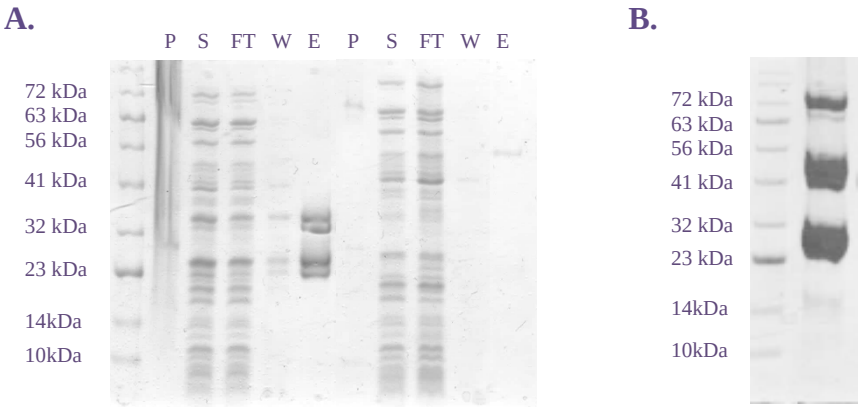

Figure 28. A. SDS-PAGE 10% gel of the affinity purification of CARD and ΔCARDC287A. Pellet (P), supernatant (S), flow-through (FT) and wash (W) were used as controls. Protein elution (E) corresponds to a band of 38,7 kDa for GST-CARD construct and 56 kDa for GST-ΔCARDC287A. The band around 26 kDa is GST alone. **B. Concentrated fraction of GST-Caspase-9 FLC287A pure protein.** The upper band at 72kDa corresponds to GST-Caspase-9 FL C287A, the band in the middle is a degradation product of this protein and the lower band at 26kDa is GST alone.

At the beginning, PP1$\alpha_{7\text{-}330}$ was purified using the buffers described in (Kelker et al., 2009), but it resulted in soluble aggregated protein. The addition in all buffers of 5% Glycerol solved the aggregation problem, obtaining pure protein.

PP1$\alpha_{7\text{-}330}$ was first purified by affinity chromatography with a 5mL HisTrap column and the fractions containing the protein were concentrated up to 2.5mL or the lowest volume before protein precipitation took place. 2.5mL of protein were injected in a Superdex 75 16/60 column for size exclusion chromatography. The chromatogram clearly shows two peaks, the first corresponding to an aggregate of the chaperones GroEL/ES which were co-expressed with PP1 $_{\alpha 7\text{-}330}$ and the second peak corresponds to a protein of a molecular weight of approximately 40 kDa. The gel of the fractions corresponding to both peaks is shown in **Figure 29**, where fractions 7 to 9 are pure PP1 $_{\alpha 7\text{-}330}$ with residual degradation. Protein yield was good and enough to perform biolayer interferometry experiments but limited for ITC. The stability of the protein diminishes rapidly with time and it cannot be concentrated more than 5µM because it precipitates, and even so, it is only stable for several

hours. For this reason, interaction assays need to be performed immediately after purification, using fresh protein.

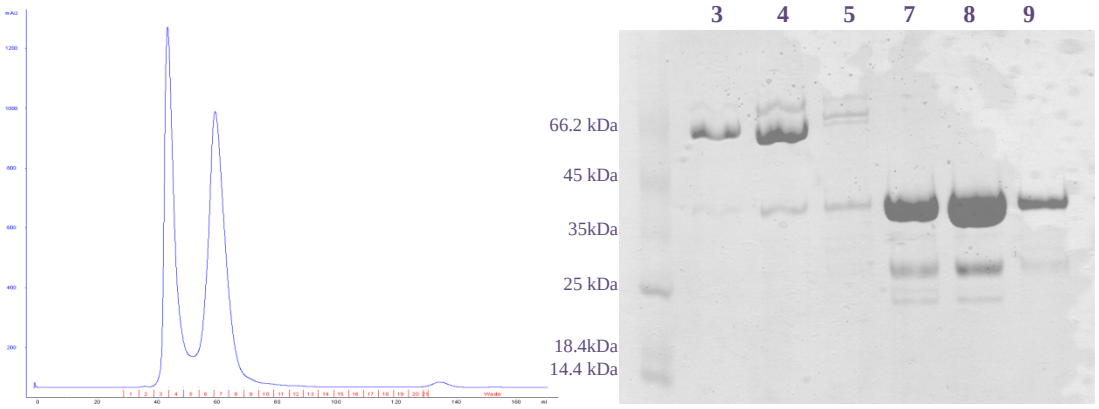

Figure 29. PP1$\alpha_{7\text{-}330}$ Size-exclusion chromatogram and SDS-PAGE gel showing fractions 3 to 9. The first peak corresponds to the chaperon coexpressed with PP1 and the second peak is pure PP1.

5.1.3. Pull-down assays

Caspase-9 and PP1 constructs were expressed in 20 mL of culture according to the previously described protocol and processed as described for low-scale purification. The supernatant of Caspase-9 constructs (GST-CARD, GST-ΔCARDC94QC, GST-ΔCARDC9C287A, GST-CASP9C287AFL) used as bait proteins was incubated for 30’ with glutathione sepharose beads at 4ºC in a nutator. Also the supernatant of PP1$\alpha_{7\text{-}330}$ was incubated with the beads to perform a negative control. Then, the mixture was centrifuged for 5 minutes at 5000g. Beads were washed three times with buffer A (100 mM Tris pH 8, 200mM NaCl) to eliminate the unspecifically bound material. Then, PP1$\alpha_{7\text{-}330}$ was incubated as prey protein for 30’ at 4ºC in a nutator. The mixture was centrifuged again and beads were washed with buffer A. Finally, the protein-protein complex was eluted with 100 µL of buffer B (100mM Tris pH8, 200mM NaCl, 20mM Reduced Glutathione). Samples were run in a SDS-PAGE and a Western Blot was performed to confirm the presence of the two proteins in the elutions. Western Blot revealed with Anti-GST let us confirm the

presence of Caspase-9 constructs bound to Glutathione sepharose 4B beads and the second Western Blot revealed with Anti-His showed that PP1$\alpha_{7\text{-}330}$ was bound to Caspase-9 to the CARD domain, the ΔCARD domain and the full length protein. PP1α didn't bind ΔCARD-C94QC construct, maybe due to dimer formation of this protein that prevents the interaction with PP1. In the construct ΔCARD-C94QC several mutations were performed to force Caspase-9 dimer formation for crystallographic studies (**Figure 30**).

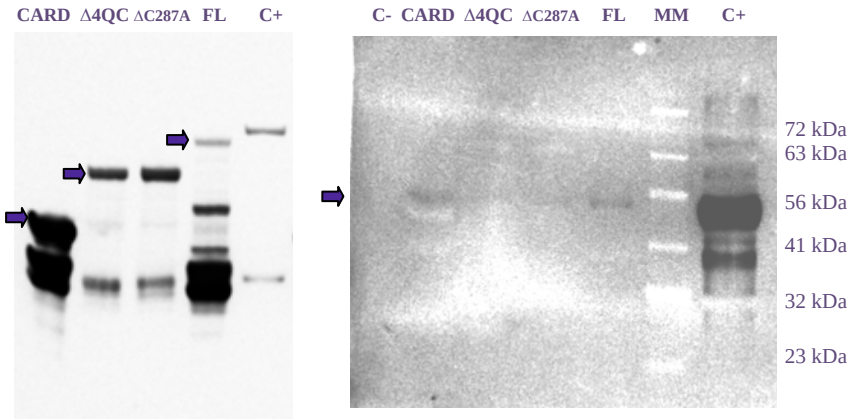

Figure 30. A. Western blot revealed with Anti-GST antibody. From left to right, the elution of PP1 $_{\alpha 7\text{-}330}$ with CARD, ΔCARDC94QC, ΔCARDC9C287A, CASP9C287AFL respectively and a positive control (a protein containing a GST tag). **B. Western blot revealed with Anti-His antibody.** From left to right, negative control, the elution of PP1 $_{\alpha 7\text{-}330}$ with CARD, ΔCARDC94QC, ΔCARDC9C287A, CASP9C287AFL respectively; molecular marker and a positive control.

Also, a pull-down assay was performed with pure GST-C9C287AFL and PP1$\alpha_{7\text{-}330}$, where PP1 and Caspase-9 coeluted. The first lane is a negative control to demonstrate that PP1 cannot interact with gluthathione sepharose beads, the second lane shows the coelution of both proteins (although Caspase-9 is degraded) and third and fourth lanes contain pure PP1$\alpha_{7\text{-}330}$ and C9C287AFL, respectively (**Figure 31**).

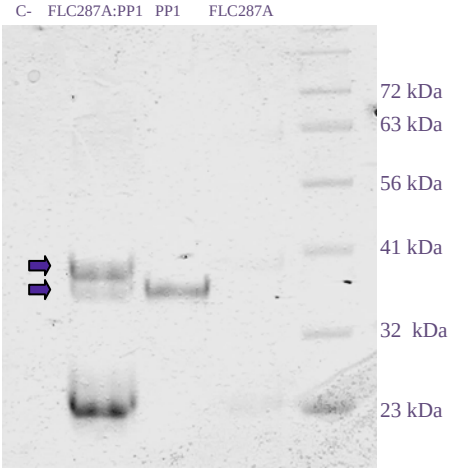

Figure 31. SDS-PAGE of pull down assay of pure GST-C9C287AFL and PP1α$_{7-330}$.

5.1.4. Biolayer interferometry

Biolayer interferometry advanced kinetics experiment was performed with Ni-NTA biosensors using PP1α$_{7-330}$ as bait protein and GST-C9C287AFL as prey protein. The assay was done three times with similar results. The resulting dissociation constant was around $3.8 \cdot 10^{-7}$, as shown in **Figure 32.**

Advanced kinetics assay between CARD and PP1 could not be properly performed because there was too much unspecific binding of CARD to the Ni-NTA sensor, thereby this method was not appropriate to measure the interaction between these two protein constructs. Another assay was performed using PP1α$_{7-330}$ as bait and ΔCARDC9C287A as prey (**Figure 33**), but the resulting dissociation constant is below the detection limit of the equipment.

Although the kinetics assay would need to be optimized to avoid residual unspecific binding, the results show that the interaction between CASP9C287AFL and PP1cα is much stronger than the interaction between ΔCARDC9C287A and PP1cα, which is below the detection limit of the technique.

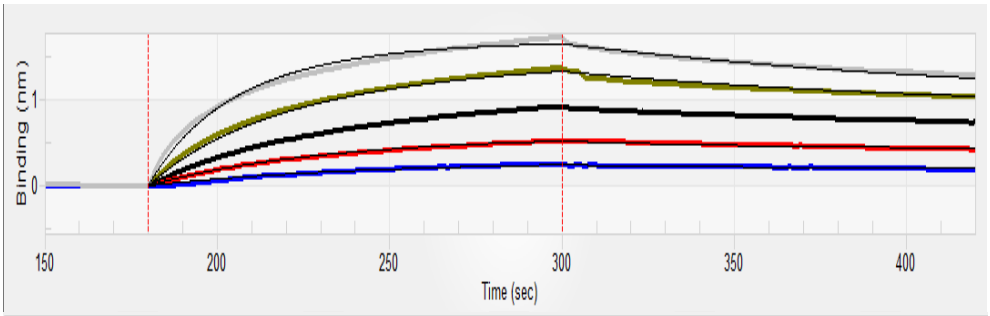

Index	Sample ID	Conc. (µM)	Information	KD (M)	ka (1/Ms)	ka Error	kd (1/s)	kd Error	Rmax	Rmax Error	R equilibrium
4	pp1 c9 5uM	5									
5	pp1 c9 2.5uM	2.5		3.779e-7	7.541e3	1.222e2	2.85e-3	5.233e-5	1.958	0.02435	1.701
6	pp1 c9 1.25uM	1.25		3.779e-7	7.541e3	1.222e2	2.85e-3	5.233e-5	2.264	0.04725	1.738
7	pp1 c9 0.625uM	0.625		3.779e-7	7.541e3	1.222e2	2.85e-3	5.233e-5	2.488	0.07307	1.55
8	pp1 c9 0.313uM	0.313		3.779e-7	7.541e3	1.222e2	2.85e-3	5.233e-5	1.999	0.06831	0.9056
9	pp1 c9 5uM	5		3.779e-7	7.541e3	1.222e2	2.85e-3	5.233e-5	1.868	0.01193	1.736

Figure 32. BLI sensorgram showing association and dissociation of increasing concentrations of GST-CASP9C287AFL to PP1α7-330 previously bound to a Ni-NTA biosensor.

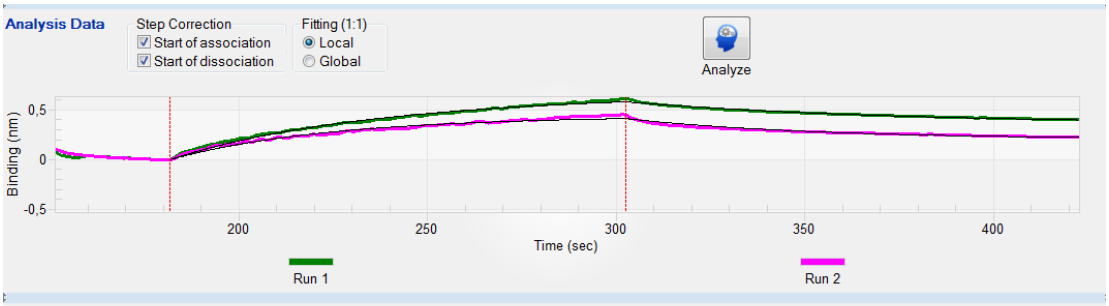

Index	Sample ID	Conc. (µM)	Information	KD (M)	ka (1/Ms)	ka Error	kd (1/s)	kd Error	Rmax	Rmax Error	R equilibrium
1	pp1 20 ug/ml	20		1.734e-5	3.071e2	3.034e1	5.325e-3	9.308e-5	2.034	0.191	1.089
2	pp1 20 ug/ml	10		2.019e-5	4.966e2	9.857e1	1.002e-2	2.098e-4	2.132	0.4053	0.7062
3	nop7 control	10									
4	nop7 control	10									

Figure 33. BLI sensorgram showing association and dissociation of 20 (green) and 10 (pink) µM of ΔCARDCASP9C287A to PP1α7-330 previously bound to a Ni-NTA biosensor.

This evidence supports the idea that Caspase-9 needs both CARD and ΔCARD domain to form a significant *in vitro* interaction with PP1. This is also consistent with the results obtained by (Dessauge et al., 2006), as it will be discussed below.

Isothermal titration calorimetry experiments were also carried out to characterize the binding affinity between Caspase-9 and PP1α. In the experiment with the highest concentration used, 20μM of PP1α were titrated with 1.7mM of Caspase-9 wild type full length; however, the interaction was not detected. It may be due to the necessity of an even higher Caspase-9 concentration, which is not possible since over this concentration the protein jellifies and is not able to be loaded in the syringe of the ITC buret. On the other hand, PP1α cannot be used as titrant, since it is very sensitive to precipitation at high concentrations.

5.2. Characterization of Caspase-9 and PP2A interaction

5.2.1. Caspase-9 and PP2Acα binding sites determination

The binding site of murine Caspase-9 to human PP2Acα has been described by pep-scan-based Far Western Blot (Frank and Overwin, 1996) as shown in **Figure 34** (Arrouss et al., 2013) and patented (Rebollo et al., 2013b, 2010). As it will be analyzed in **Figure 78**, Caspase-9 sequence is highly conserved between mouse and human. Among the synthetic dodecapeptides covering Caspase-9 sequence, four spots presented binding to PP2Acα, corresponding to residues 401-418 of murine sequence, equivalent to 363-380 residues of human Caspase-9, peptide that was termed C9h.

A

Murine Caspase-9:	Y	**I**	E	T	L	D	**G**	I	**L**	E	Q	W	A	**R**	S	E	D	L
Human Caspase-9:	Y	**V**	E	T	L	D	**D**	I	**F**	E	Q	W	A	**H**	S	E	D	L

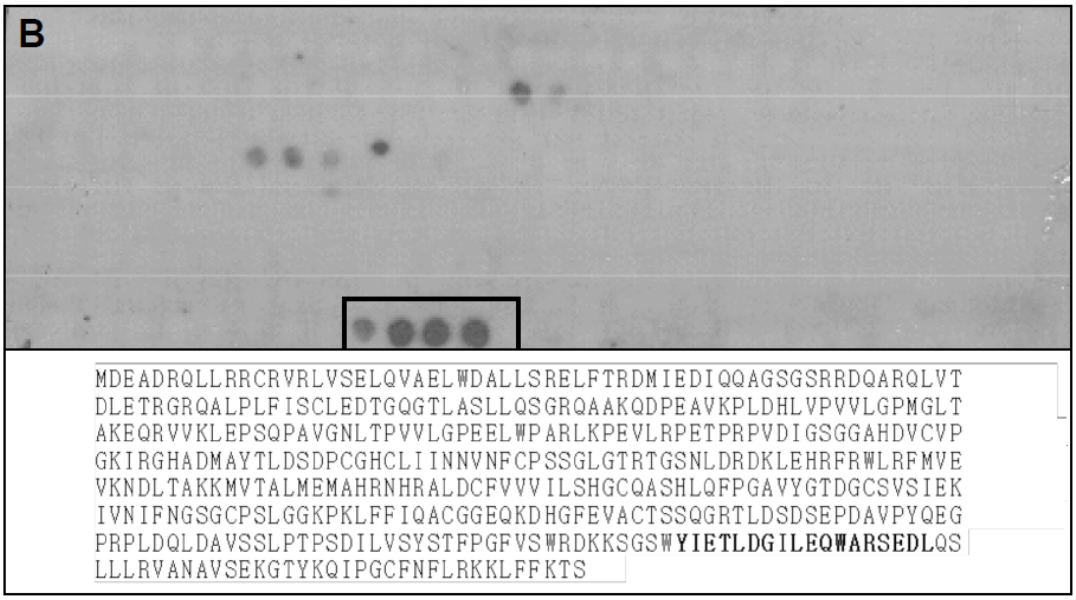

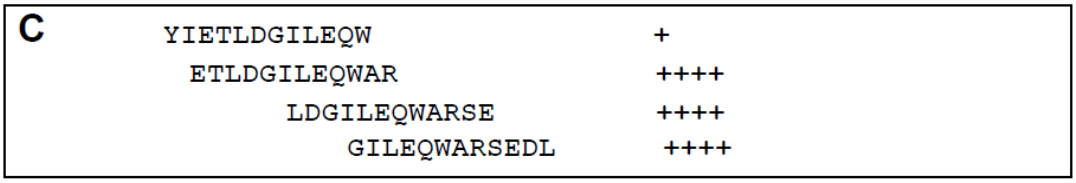

Figure 34. Pep-scan-based Far Western Blot analysis to determine Caspase-9 binding site to PP2A. A. Comparison of murine and human Caspase-9 sequences in the binding site to PP2Acα. **B.** Nitrocellulose membrane where 12 aminoacid overlapping peptides covering Caspase-9 sequence were synthesized by automated spot synthesis. Each spot corresponds to a peptide. Murine Caspase-9 sequence corresponding to PP2Acα interaction site is represented in bold. **C.** Sequences of the peptides that presented positive spots.

In the present work we have determined the sequence of PP2Acα that binds Caspase-9 by pepscan-based Far-Western Blot. Dodecapeptides covering PP2Acα sequences were synthesized in a nitrocellulose membrane, hybridized with human Caspase-9 and incubated with anti-Caspase-9, as described in materials and methods. Five spots were detected after revealing the nitrocellulose membrane with ECL System, which corresponded to residues 175-194 of PP2Acα (**Figure 35**). The peptide comprising this 175-194 residues of PP2Acα was termed PP2Ah and registered (Rebollo et al., 2013a). If we observe this region in PP2Acα structure

(PDB code 2IE3), it is located on the surface of the protein and it comprises a small α-helix and an unstructured area, which validates the possibility of this region to be the Caspase-9 interaction site. Both Caspase-9 and PP2A binding sites represented in their structures are shown in **Figure 58**.

A.

B.

MDEKVFTKELDQWIEQLNECKQLSESQVKSLCEKAKEILTKESNVQEVRCPVTVCGD
VHGQFHDLMELFRIGGKSPDTNYLFMGDYVDRGYYSVETVTLLVALKVRYRERITIL
RGNHESRQITQVYGFYDECLRKYGNAN**VWKYFTDLFDYLPLTALVDGQIFCLHGGLS**
PSI**DTLDHIRALDRLQEVPHEGP**MCDLLWSDPDDRGGWGISPRGAGYTFGQDISETF
NHANGLTLVSRAHQLVMEGYNWCHDRNVVTIFSAPNYCYRCGNQAAIMELDDTLKYS
FLQFDPAPRRGEPHVTRRTPDYFL

```
            DTLDHIRALDRL
                 LDHIRALDRLQE
                      HIRALDRLQEVP
                           RALDRLQEVPHE
                                LDRLQEVPHEGP
```

C.

```
Shuttle           : VKKKKIKREIKI
Interacting site  : DTLDHIRALDRLQEVPHEGP
DPT-PP2Ah         : VKKKKIKREIKIDTLDHIRALDRLQEVPHEGP
```

Figure 35. Pep-scan-based Far Western Blot analysis to determine PP2Acα binding site to Caspase-9. A. Nitrocellulose membrane where 12 aminoacid overlapping peptides covering PP2Acα sequence were synthesized by automated spot synthesis. Each spot corresponds to a peptide. **B.** Human PP2Acα sequence, with Caspase-9 interaction site in bold and framed. The sequences of the peptides that gave positive spots are detailed below. **C.** Bifunctional peptide composed of DPT cell penetrating peptide that acts as a shuttle and Caspase-9 interacting site of PP2Acα (PP2Ah).

5.2.2. Characterization of the residues implicated in the binding

A docking analysis was performed using Frodock software to model a rigid docking. Frodock approach was fundamented in the algorithm based on FFT (fast Fourier transform), in which molecules are represented by 3D grids, and ligand and receptor grids are correlated using FFT to efficiently scan the translational space. After this orientation search, many coupled conformations with favorable surface complementarity were obtained. The advantage of Frodock with respect to previous algorithms is the Fast Rotational Method (FRM), previously applied in electron microscopy to develop new mathematical expressions and a new methodology termed Frodock (Fast Rotational Docking). By means of this algorithm we managed to know that Caspase-9 bound PP2A only through the catalytic subunit and also that this binding didn't compete with the natural PP2A heterotrimer.

The docking model proposed some candidate residues from the binding sites of Caspase-9 and PP2A to have a crucial role in the interaction or contribute to a stronger binding affinity. The predictions are represented in **Figure 36**.

Figure 36. Candidate residues proposed by Frodock to actively participate in the interaction between Caspase-9 and PP2acα.

Simple, double and triple mutants of C9h peptide were synthesized, hybridized with PP2Acα, incubated with anti-PP2A followed by PO-conjugated secondary antibody and revealed with an ECL system in a pep-scan-based Far Western Blot assay, in the same way that was described for the peptides covering the wild type sequence. From the candidate residues in Caspase-9 sequence, only Tryptophan 374 showed to be indispensable for the interaction with PP2Acα, as its mutation to Alanine was capable of disrupting the binding between these two proteins (**Figure 37**).

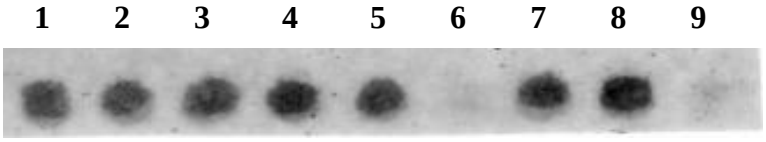

1 - Y V E T L D D I F E Q W A H S E D L (wild type)
2 - Y V E T L D **V** I F E Q W A H S E D L
3 - Y V E T L D D I F **Q** Q W A H S E D L
4 - Y V E T L D D I F **L** Q W A H S E D L
5 - Y V E T L D D I F E **L** W A H S E D L
6 - Y V E T L D D I F E Q **A** A H S E D L
7 - Y V E T L D **V** I F **Q** Q W A H S E D L
8 - Y V E T L D **V** I F E **L** W A H S E D L
9 - Y V E T L D **V** I F E **L** **A** A H S E D L

Figure 37. Sequence of Caspase-9 synthetic peptides corresponding to the binding site to PP2Ac*α*. Mutations in the peptide sequence are shown in red.

Simple, double or methylated mutants of PP2Ah peptide were carried out in a first attempt in the candidate key residues predicted by Frodock and in further experiments other mutations were also analyzed, as listed in **Table 15**. All peptides were synthesized in an amino-derivatized nitrocellulose membrane, incubated with purified Caspase-9 protein and, after washing steps, incubated with anti-Caspase-9 followed by PO-conjugated secondary antibody. Among all the mutants analyzed, only L177A and R185A PP2Ah simple mutants disrupted the interaction with Caspase-9 in Far Western Blot analysis.

Table 15. List of PP2Ah mutant peptides analyzed for Caspase-9 binding.

Number	Peptide sequence	Disrupt Caspase-9 binding
Wild type (control)	SIDTLDHIRALDRLQEVPHEGP	-
1	**A**IDTLDHIRALDRLQEVPHEGP	-
2	SID**A**LDHIRALDRLQEVPHEGP	-
3	SIDT**A**DHIRALDRLQEVPHEGP	YES
4	DTL**A**HIRALDRLQE	-
5	DTL**N**HIRALDRLQEVPHEGP	-
6	DTL**R**HIRALDRLQEVPHEGP	-
7	DTL**R**HI**D**ALDRLQEVPHEGP	-
8	SIDTLD**A**IRALDRLQEVPHEGP	-
9	SIDTLD**F**IRALDRLQEVPHEGP	-
10	DTLDH**A**RALDRLQE	-
11	DTLDHI**A**ALDRLQE	-
12	DTLDHI**V**ALDRLQE	-
13	DTLDHI**D**ALDRLQE	-
14	DTLDHI**R^{m}**ALDRLQE	-
15	DTLDHI**R^{m}**ALD**R^{m}**LQE	-
16	DTLDHIR**G**LDRLQE	-
17	DTLDHIRA**A**DRLQE	-
18	DTLDHIRAL**A**RLQE	-
19	DTLDHIRALD**A**LQE	YES
20	DTLDHIRALD**R^{m}**LQE	-
21	DTLDHIRALDR**A**QE	-
22	DTLDHIRALDR**V**QE	-
23	DTLDHIRALDR**I**QE	-
24	DTLDHIRALDRL**A**E	-
25	DTLDHIRALDRL**L**E	-
26	SIDTLDHIRALDRLQEV**D**HEGP	-

5.2.3. Role of Caspase-9 residue W374

With the aim of evaluating the possibility of the mutation in the residue W374 to Alanine to provoke a destabilization effect in Caspase-9 structure, *in silico* predictions and circular dichroism experiments were performed. FoldX software was applied to study the possible changes in the free energy between Caspase-9 wild type and the mutant in W374 residue. First of all, Caspase-9 structure (PDB code 1JXQ) was optimized with the command Repair PDB. This command verifies through 180º rotations if asparagine, glutamine and histidine residues of the PDB model present a right conformation or not, since electron density of carboxamide groups of asparagine and glutamine are almost symmetric and the right rotamer is only possible to be known by calculating the interaction with close atoms. Moreover, the same happens to histidine. In a second step, the command optimizes side chains to avoid its further movement and identifies the residues with bad energies and mutates them along with its neighbors to find a new minimal energy.

Once Caspase-9 structure was repaired, Alascan command was executed, in which every residue of the protein was mutated to Alanine, giving the ΔΔG of the mutation as a result. The value obtained for the energy change of tryptophan 374 residue mutated to alanine was -0,48539. From this result, we could deduce that this mutation didn't mean a significant change in the free energy.

In a further experiment, synthetic peptides of the binding region of Caspase-9 to PP2Acα with the wild type and the W374A mutant sequences were analyzed by circular dichroism to assess if this mutation also affected the structure of the protein. Both peptides showed to have random coil spectra when they were dissolved only in sodium phosphate buffer, so they didn't present any secondary structure. However, when TFE was added as α helix inductor, it was observed that the structure pattern shown by these peptides corresponded to an α helix in a more extent as higher concentration of TFE was added, been observed clearly from 40% TFE in the sample buffer (**Figure 38**). Spectropolarimeter raw data were generated in millidegrees and further corrected by substracting blank value to sample value and further converted to molar ellipticity units with Jasco software. From a global point of view of the analysis, no significant differences in α helix percentage were observed between wild type and W374 mutant peptides.

All together, these results let us conclude that the tryptophan 374 residue is not implicated in the structure of the protein, but plays an important role in the interaction with PP2Acα.

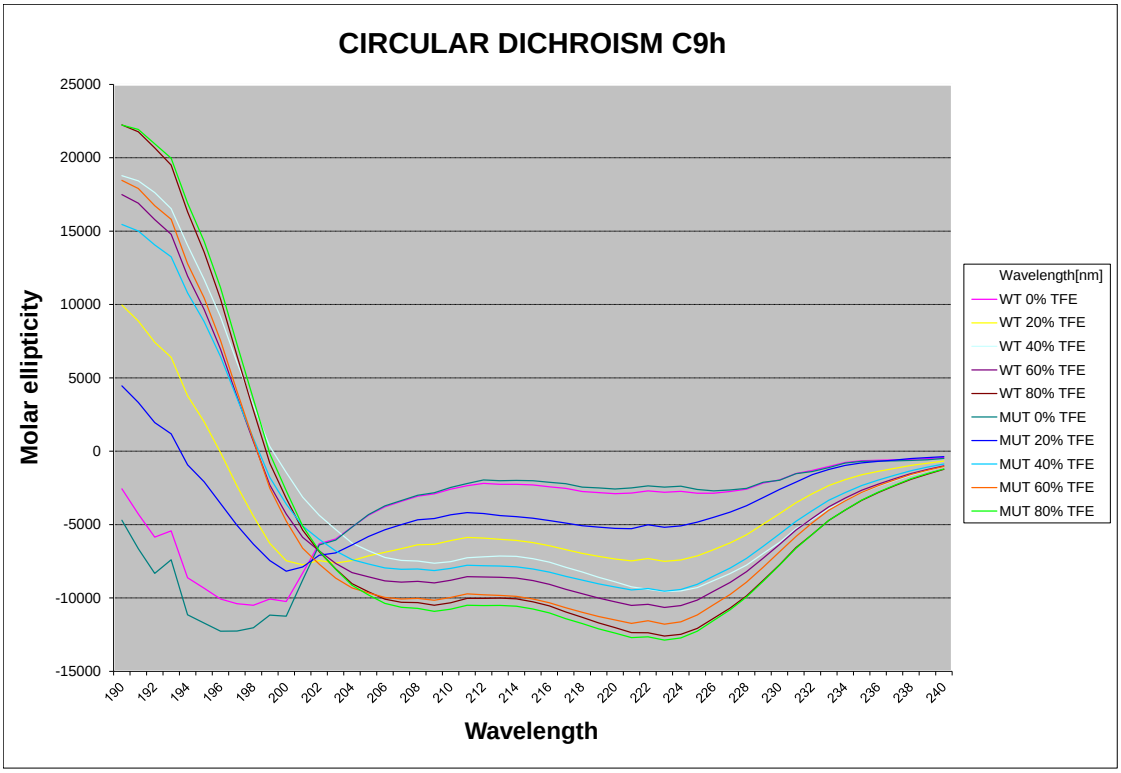

Figure 38. Circular dichroism spectra of wild type (WT) and W374A (MUT) C9h peptides with increasing concentrations of TFE.

5.2.4. Biophysical characterization of the interaction between Caspase-9 and YPP2Ah peptide

5.2.4.1. Differential scanning fluorimetry

A ThermoFluor assay was performed to analyze the linkage between Caspase-9 thermal stability and its binding to the peptide YPP2Ah. ΔCARD Caspase-9 C287A protein construct was overexpressed and purified in the same

conditions described for the full length protein. This protein eluted in size exclusion chromatography as a monomer, as shown in **Figure 39**.

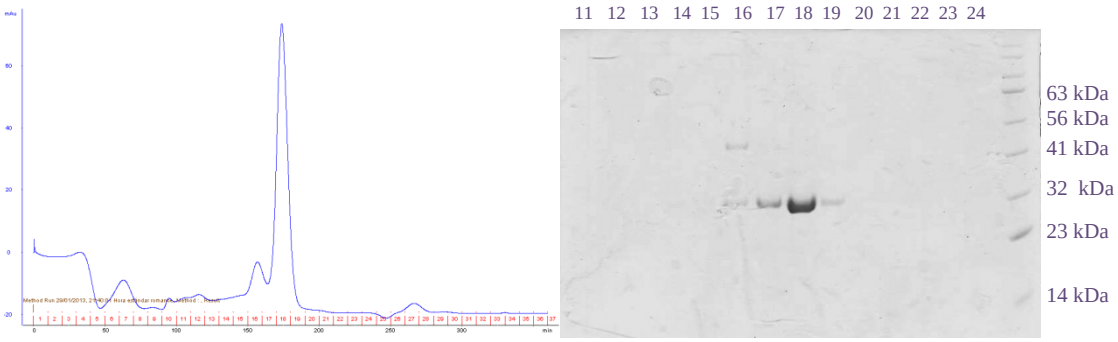

Figure 39. Superdex 200 26/60 size exclusion chromatogram of ΔCARD Caspase-9 C287A and SDS-PAGE showing fractions 11-24.

Changes in ΔCARD Caspase-9 C287A intrinsic melting temperature were observed based on the binding of increasing concentrations of YPP2Ah. This peptide showed to preferentially interact with the native form of the protein, suggesting an approximated value for the K_D in the 10^{-5} to 10^{-4} range.

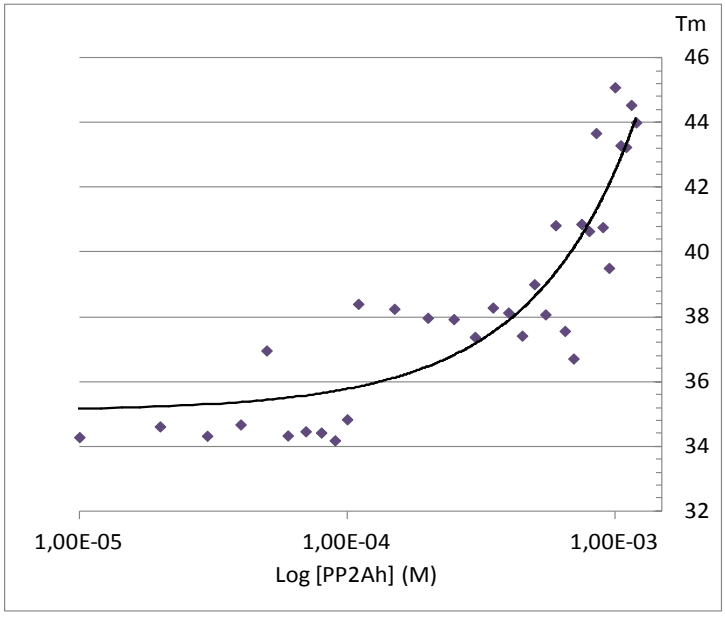

Figure 40. Thermofluor assay of ΔCARD Caspase-9 with increasing concentrations of PP2Ah peptide.

5.2.4.2. Isothermal titration calorimetry

The preliminary Thermofluor results for the binding affinity between Caspase-9 and PP2Ah allowed us to get an approximation of the optimal peptide concentrations we needed to detect the binding by isothermal titration calorimetry. Binding assays were performed using 20µM of Caspase-9 wild type full length purified protein in the cell titrated with 2.5mM YPP2Ah synthetic peptide in the buret, being both dissolved in Caspase-9 size exclusion buffer (20mM Tris pH8, 100mM NaCl, 1mM β-mercaptoethanol). Caspase-9 wild type full length was overexpressed and purified as described in 5.1.1. The experiment was repeated at 8ºC, 15ºC and 20ºC, obtaining K_D values of $2.934 \cdot 10^{-6}$M, $9.172 \cdot 10^{-6}$M and $2.335 \cdot 10^{-5}$M respectively. From these data we can conclude that the binding affinity between Caspase-9 and YPP2Ah is in the micromolar range, one order of magnitude higher than expected according to differential scanning fluorimetry results.

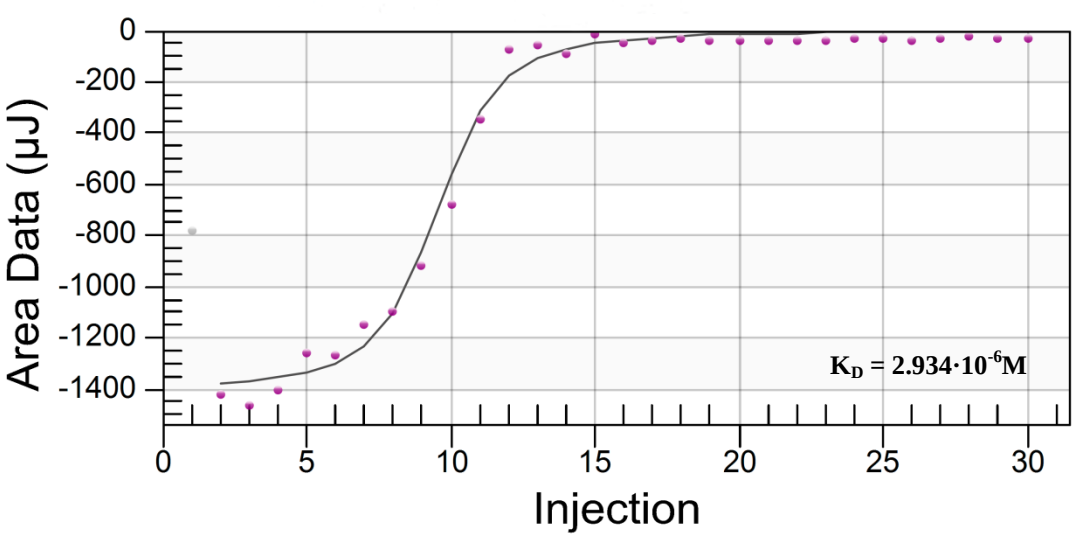

Figure 41. Caspase-9 and YPP2Ah isothermal titration calorimetry experiment performed at 8°C.

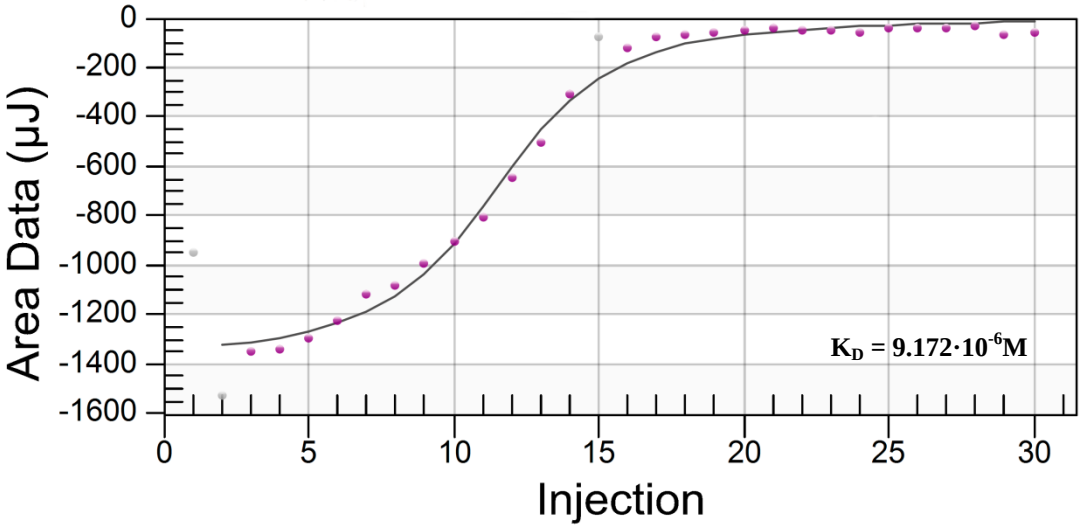

Figure 42. Caspase-9 and YPP2Ah isothermal titration calorimetry experiment performed at 15°C.

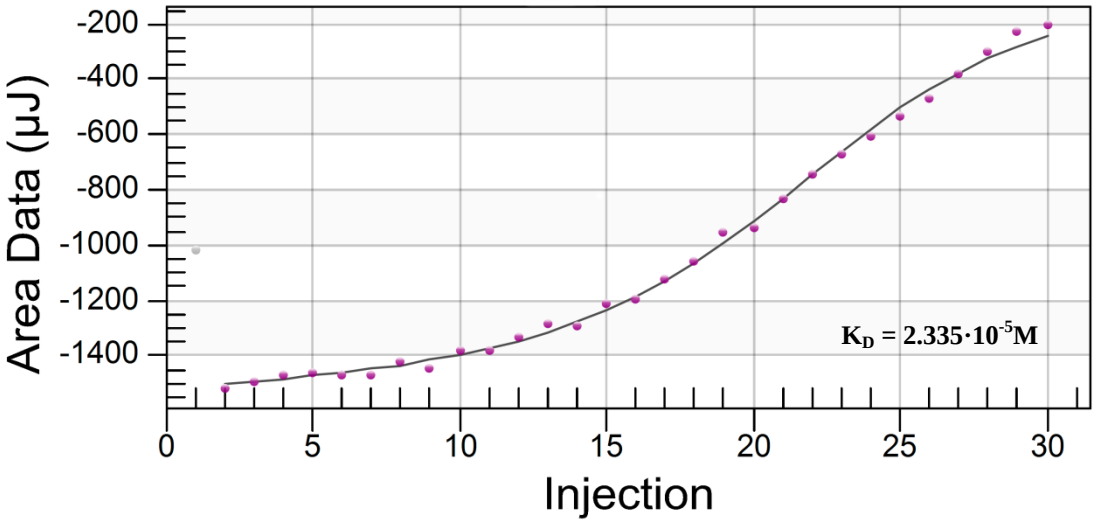

Figure 43. Caspase-9 and YPP2Ah isothermal titration calorimetry experiment performed at 20°C.

5.2.4.3. Caspase-9 is not activated by YPP2Ah

Caspase-9 activation assay is based on the detection of the fluorogenic substrate Ac-LEHD-AFC cleavage. This molecule emits blue light (λ_{max} = 400nm) and, upon Caspase-9 activation, free AFC (AFC: 7-amino-4-trifluoromethylcoumarin) emits a yellow-green fluorescence (λ_{max} = 505 nm). A buffer that provided Caspase-9 activating conditions was added to the protein, containing sodium citrate as a kosmotropic salt that artificially activates monomeric caspases. As shown in **Figure 44**, Caspase-9 was activated in the presence of a buffer containing sodium citrate (moderately activated in activation control and highly activated in positive control, as expected) and with the addition of the small molecule DES, known to activate Caspase-9. These controls demonstrate that our recombinant Caspase-9 is susceptible to be activated *in vitro*. However, the presence of YPP2Ah peptide in concentrations from 0.0625mM to 2mM didn't produce any enzymatic activation of Caspase-9 *in vitro*.

5.2.5. Overexpression and purification of PP2Acα

HA-6His-TEV-PP2Acα D88N was transfected in Sf9 insect cells. In a further step, virus was amplified in Sf9 cells and the supernatant was used to inoculate Sf9ET cells with serial dilutions to titrate the amount of virus (**Figure 45**). Usually the titer obtained was in the range of 10^8-10^9 virus. High Five cells were infected at a multiplicity of infection (m.o.i.) of 2 and the protein was further purified. Several purification conditions were tried but up to date we could only obtain the protein in soluble aggregates after size exclusion chromatography (**Figure 46**).

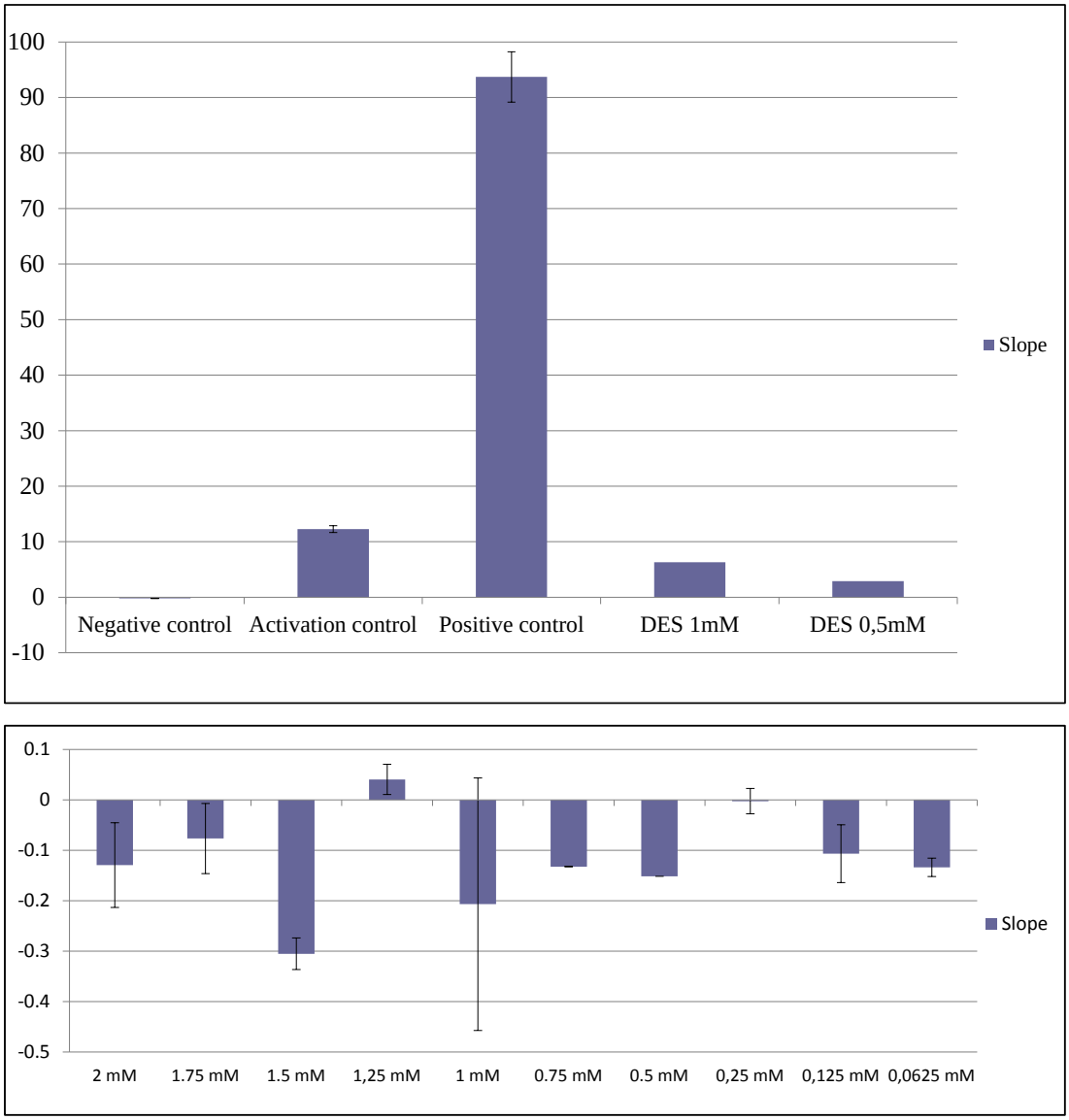

Figure 44. Slope of AFC fluorescence measured every 90 seconds during 40 minutes. In the first graph, the following controls are represented: Negative control: Caspase-9 in non-activating buffer, dissolved in the same buffer. Activation control: Caspase-9 in non-activating buffer, dissolved in activating buffer. Slope is usually about 10. Positive control: Caspase-9 in activating buffer, dissolved in activating buffer. Slope is usually very high. DES: a small molecule that is known to enzymatically activate Caspase-9. In the second graph, the concentrations show the amounts of YPP2Ah used for the assay.

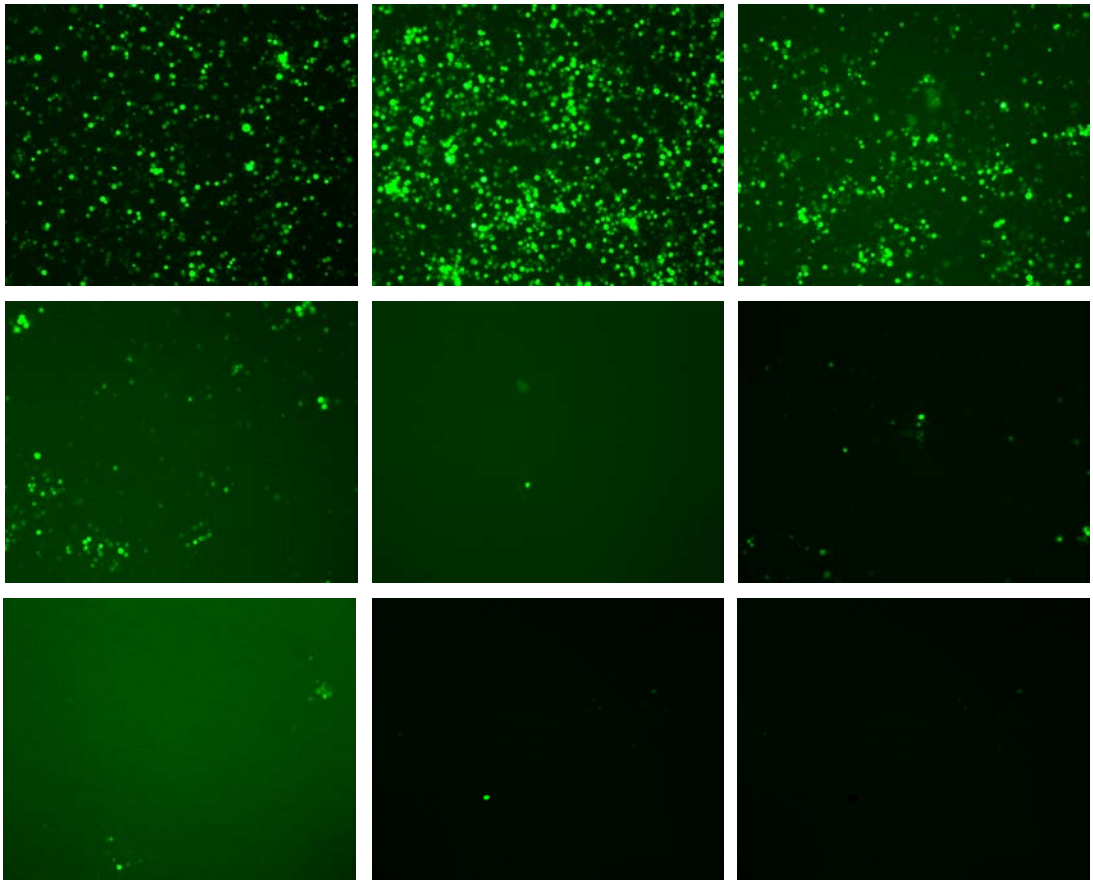

Figure 45. Fluorescence microscopy images of Sf9ET cells expressing GFP when they are infected with serial dilutions of HA-6His-PP2Acα D88N.

5.2.6. Therapeutic potential of C9h peptide for cancer therapy

5.2.6.1. Apoptotic effect of DPT-C9h and DPT-PP2Ah bifunctional peptides

Caspase-9 derived peptide C9h and PP2Acα derived peptide PP2Ah were fused to DPT cell penetrating peptide (Guergnon et al., 2006), forming DPT-C9h and DPT-PP2Ah sychnologic peptides. Several established and primary cell lines were treated with either 100µM of DPT-C9h, 100µM of DPT-PP2Ah or both peptides and

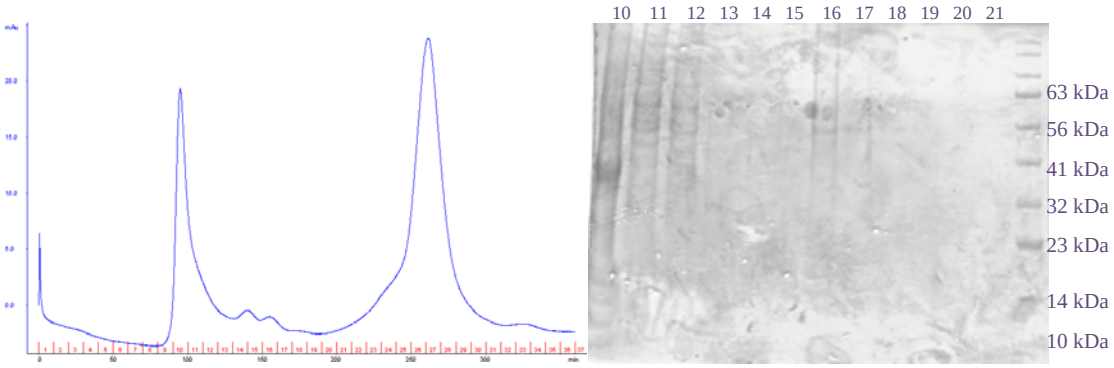

Figure 46. Size exclusion chromatogram of HA-6His-TEV-PP2Acα D88N and SDS-PAGE running fractions 10-21. The first peak is the soluble aggregate of PP2Acα (confirmed in fraction 10 of the gel) and the second peak corresponds to contaminants copurified with PP2Acα in affinity chromatography.

AnnexinV-FITC apoptosis measurement was performed by FACS. DPT-C9h showed to induce apoptosis more efficiently than DPT-PP2Ah; in addition, when cells were treated with both peptides, a synergistic effect was observed, showing a slightly higher apoptotic effect compared to DPT-C9h (Experiments performed at CIMI, UPMC, Paris; data not shown). According to these preliminary data, we decided to continue the studies with DPT-C9h to evaluate the use of its antiapoptotic effect for cancer therapy. DPT-C9h was proved to induce species specific Caspase-9 dependent apoptosis in cancer cell lines, primary human cells and primary human breast cancer xenograft models as well as CLL B cells (Arrouss et al., 2015, 2013).

5.2.6.2. Evaluation of mesoporous silica nanoparticles as a C9h vehicle

Mesoporous silica nanoparticles with a diameter size of 400nm were synthesized and the preservation of the mesoporous structure in the final solids was confirmed by transmission electron microscopy (**Figure 47**).

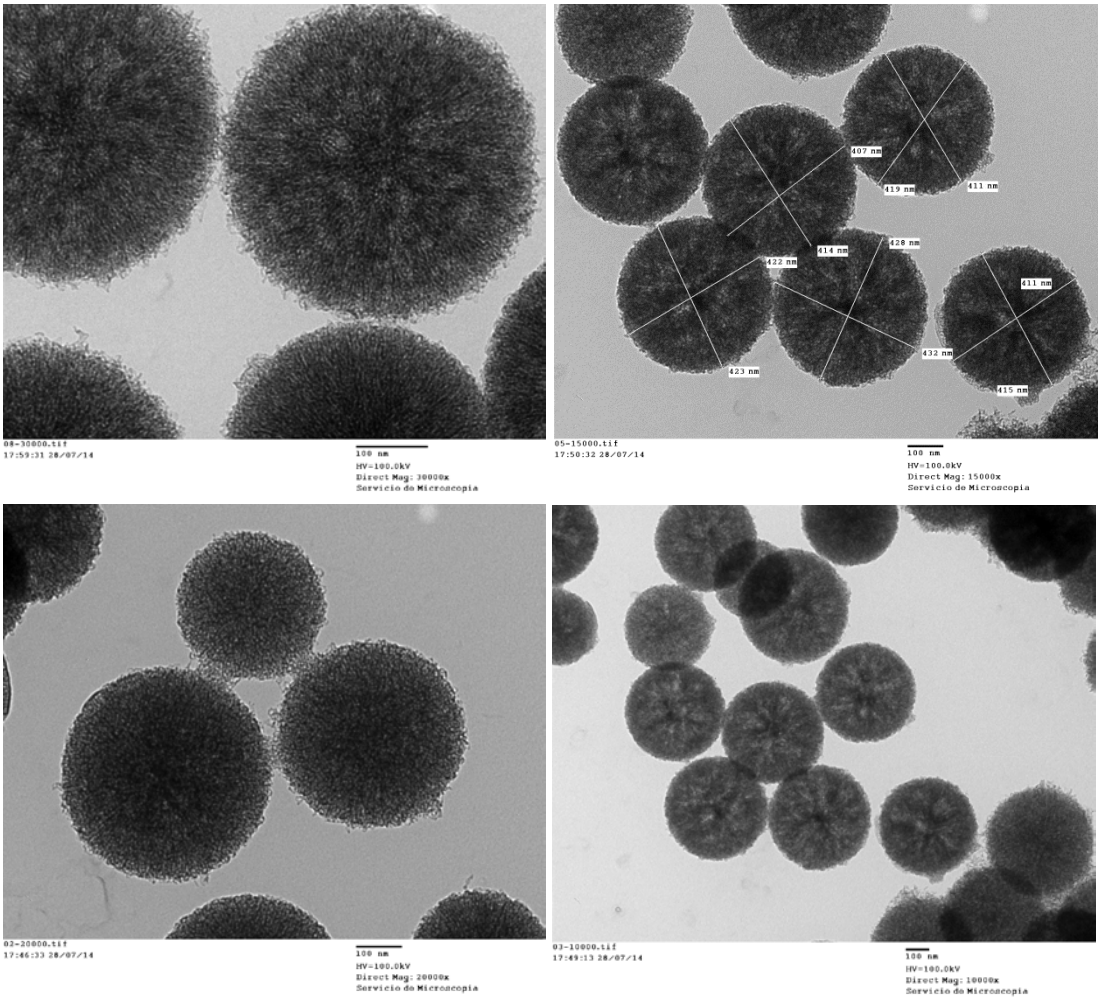

Figure 47. Transmission electron microscopy images of 400nm diameter mesoporous silica nanoparticles.

To determine the most appropriate amount of cells needed to perform cell viability assays, several concentrations of HeLa cells were tested using WST-1 Cell proliferation reagent. The cell concentration chosen to perform further experiments was 2500 cells/mL, as they remained in the exponential growth phase during the times required for the experiments (**Figure 48**).

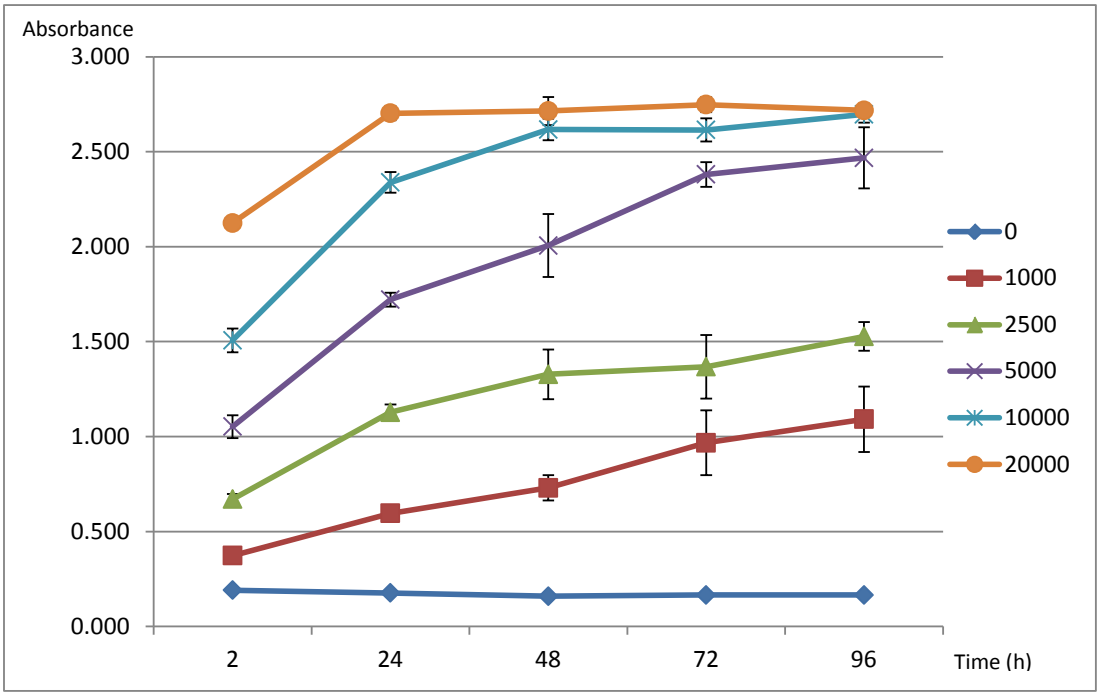

Figure 48. Cell viability assay to determine the appropriate concentration of HeLa cells to perform assays with MSNs.

2500 HeLa cells/mL were treated with 400nm diameter MSNs loaded with $[Ru(bipy)_3]^{2+}$ and analyzed by confocal microscopy to determine the localization of the nanoparticles once they entered into the cells. As it can be observed in **Figure 49**, the efficiency of entrance in the cell is high and nanoparticles are distributed in the cytoplasm, but they don't enter into nuclei, stained with Hoechst 33342.

MCM-41 nanoparticles have already been observed in a transmission electron microscope to verify the preservation of the mesoporous structure, as well as in localization assays by confocal microscopy in previous studies (de la Torre et al., 2015, 2014).

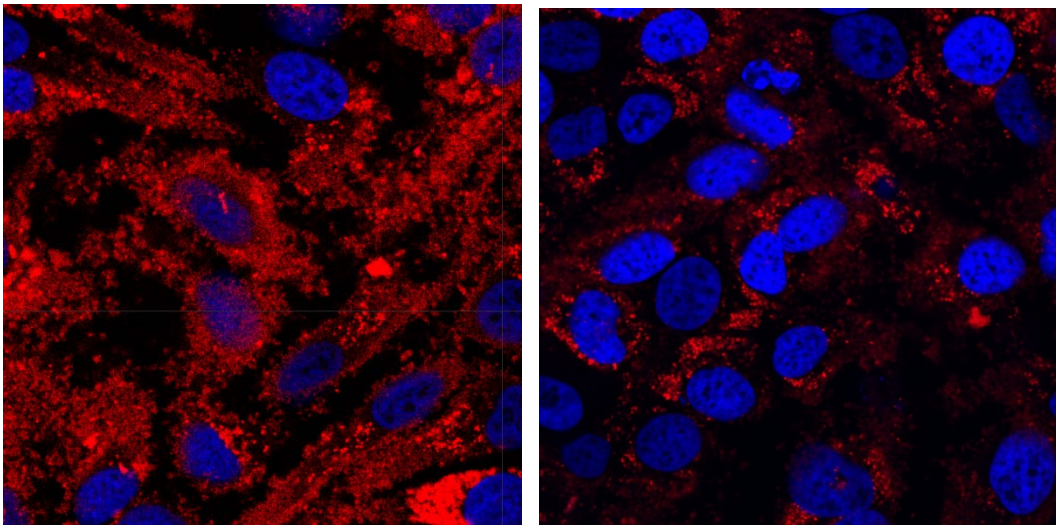

Figure 49. Confocal microscopy images of HeLa cells treated with 400nm MSNs. Nuclei are stained in blue and $Ru(bipy_3)^{2+}$ containing nanoparticles are observed in red.

The toxicity of 400nm and MCM-41 MSNs was evaluated performing a cell viability assay of 2500 HeLa cells/mL treated with increasing concentrations of 400nm or MCM-41 MSNs loaded only with $[Ru(bipy)_3]^{2+}$. As shown in **Figure 50**, even at high concentrations like 500µg/mL, any of both types of nanoparticles produce any significant toxicity in the cells after 24h of incubation.

2500 HeLa cells/mL were incubated 24h and then treated with several concentrations of 400 nm MSNs from 25 to 500µg/mL loaded with C9h-rhodamineB. Cell viability assays were performed after 24, 48 and 72h of incubation with the MSNs. No significant effect in cell viability was observed after treatment, since only a 10-20% decrease of live cells was observed in the best cases (**Figure 51**).

In a further cell viability assay, 2500 HeLa cells/mL were treated with MCM-41 MSNs ranging from 75µg/mL to 1000µg/mL, loaded with the peptide C9hC. Cell viability was measured after 24, 48 and 72h of incubation with the treatments (**Figure 52**). High concentrations (1000µg/mL and 500µg/mL) didn't produce any effect on cell viability. However, the lowest concentration tried (75µg/mL) showed a little decrease in cell viability, comparable to the effect caused by the larger 400nm MSNs. More importantly, when cells were treated with 125µg/mL or 250µg/mL

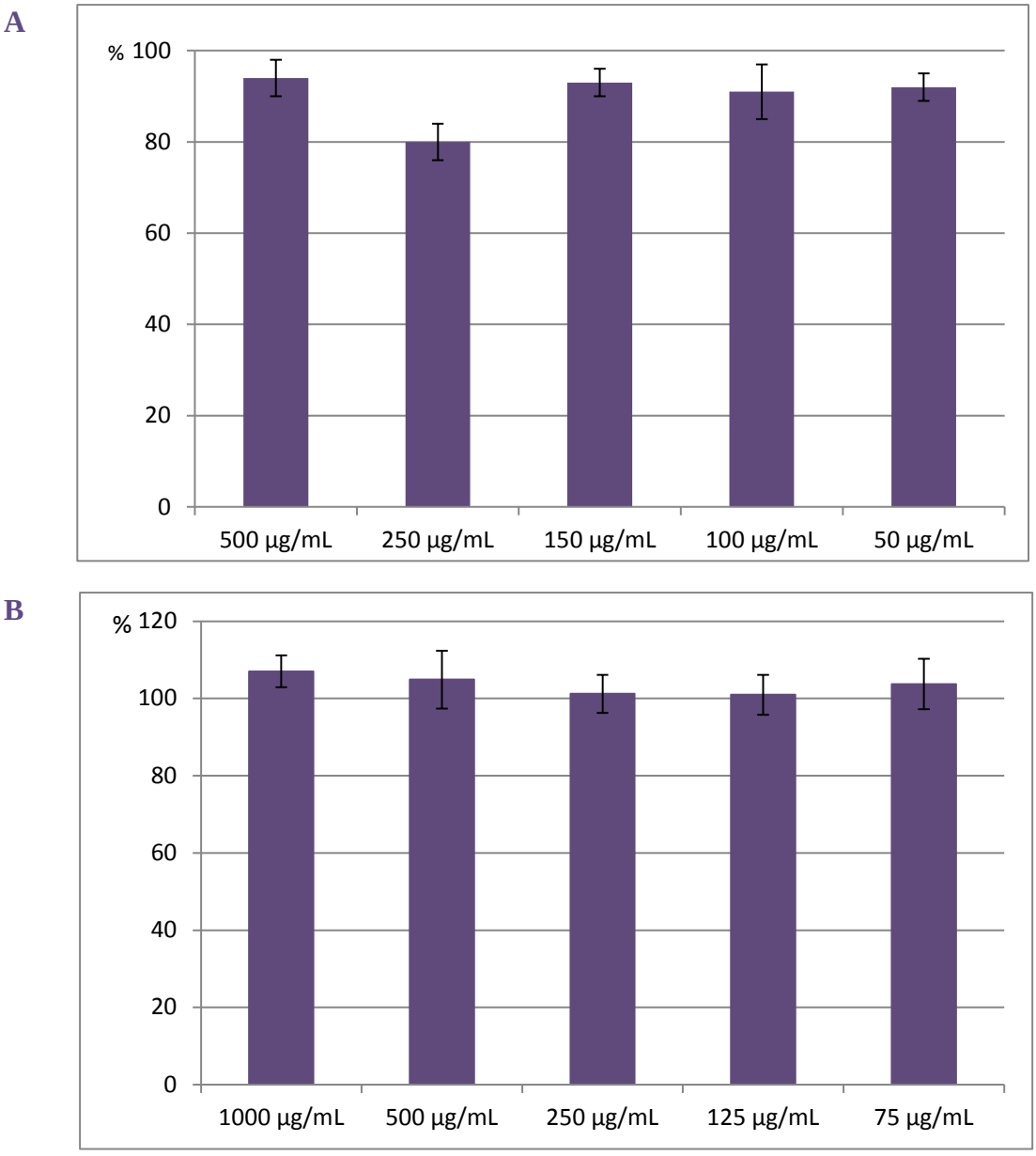

Figure 50. Cell viability assay to evaluate the toxicity of mesoporous silica nanoparticles. A. HeLa cells treated with 400nm MSNs loaded with $[Ru(bipy)_3]^{2+}$. **B.** HeLa cells treated with empty MCM-41 nanoparticles.

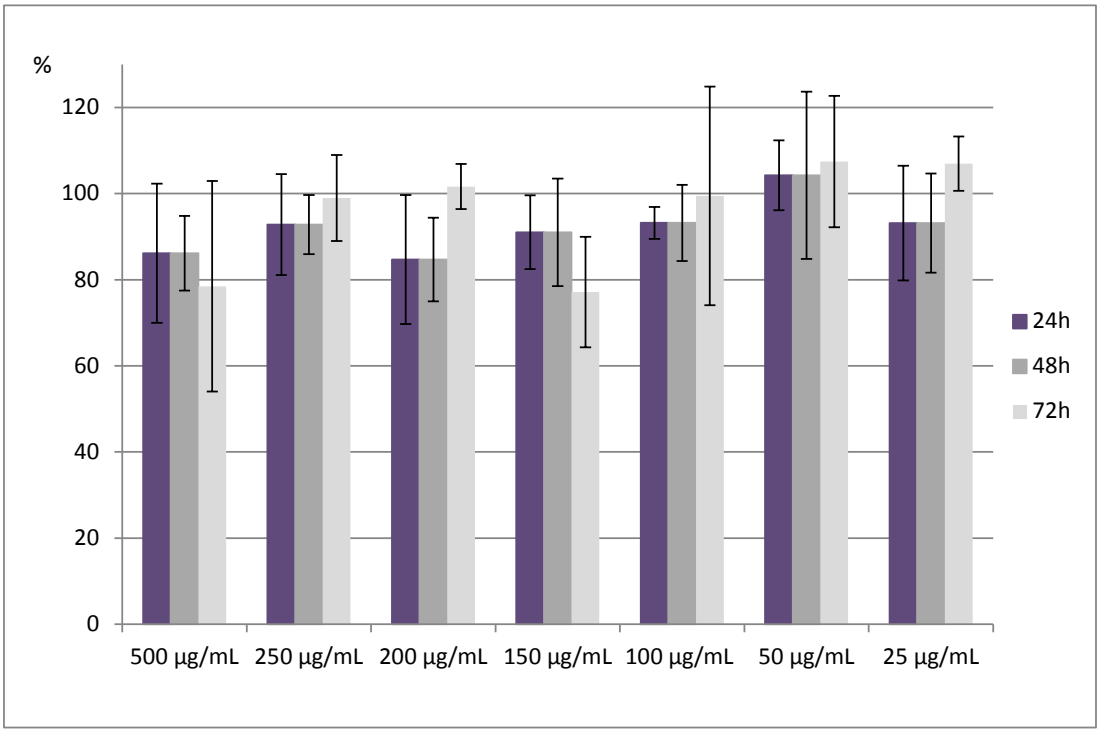

Figure 51. Cell viability assay of HeLa cells treated with 400nM MSNs loaded with C9h-RhodamineB for 24, 48 and 72h.

MCM-41-C9hC, the delivered C9hC peptide was able to induce a decrease in cell viability of 50% after 72h of incubation.

Equivalent concentrations of DPTmut3-C9h to the concentrations of C9hC delivered by the applied doses of MCM-41-C9hC were also analyzed in the same experiment as controls. If we compare the diminution of cell viability induced by DPTmut3-C9h with respect to the equivalent concentration of peptide delivered by MCM-41, we can observe an improvement in the efficiency of cell viability reduction at peptide concentrations of 5.40µM and 2.70µM when the peptide is delivered using MCM-41 nanoparticles as a vehicle. At these concentrations, DPTmut3-C9h was capable of inducing only a 10-20% decrease; in contrast, C9hC

delivered by MCM-41 induced a 50% decrease in cell viability after 72h of treatment.

In a further experiment, to get a better characterization of the apoptotic effect of C9hC delivered by MCM-41 nanoparticles, apoptosis induction measurement was performed using AnnexinV-FITC apoptosis detection kit and analyzed by FACS. 25000 HeLa cells/mL were incubated for 24h and then treated with 250µg/mL, 125µg/mL and 75µg/mL MCM-41-C9hC (two different stocks were analyzed) and the equivalent peptide concentrations of DPTmut3-C9h. Cells treated with 50µM of DPTmut3-C9h were used as positive control. As represented in **Figure 54**, control treatment with 10µM DPTmut3-C9h induced a 36% of apoptosis, while the equivalent peptide concentration delivered by 250µg/mL MCM-41 induced around 50% of apoptosis. Furthermore, lower peptide concentrations (5.405µM and 2.70µM) delivered by MCM-41 also induced apoptosis in around 60% of the cells, a value that is comparable with the effect produced by 10 times more concentration of DPTmut3-C9h peptide.

According to these results, the use of MCM-41 nanoparticles as a vehicle for the delivery of C9hC peptide has shown to be more efficient than the cell penetrating peptide DPTmut3 to deliver the cargo C9h, allowing us to observe the same apoptotic effect in HeLa cell line as with DPTmut3-C9h peptide with a dose reduction of up to ten times.

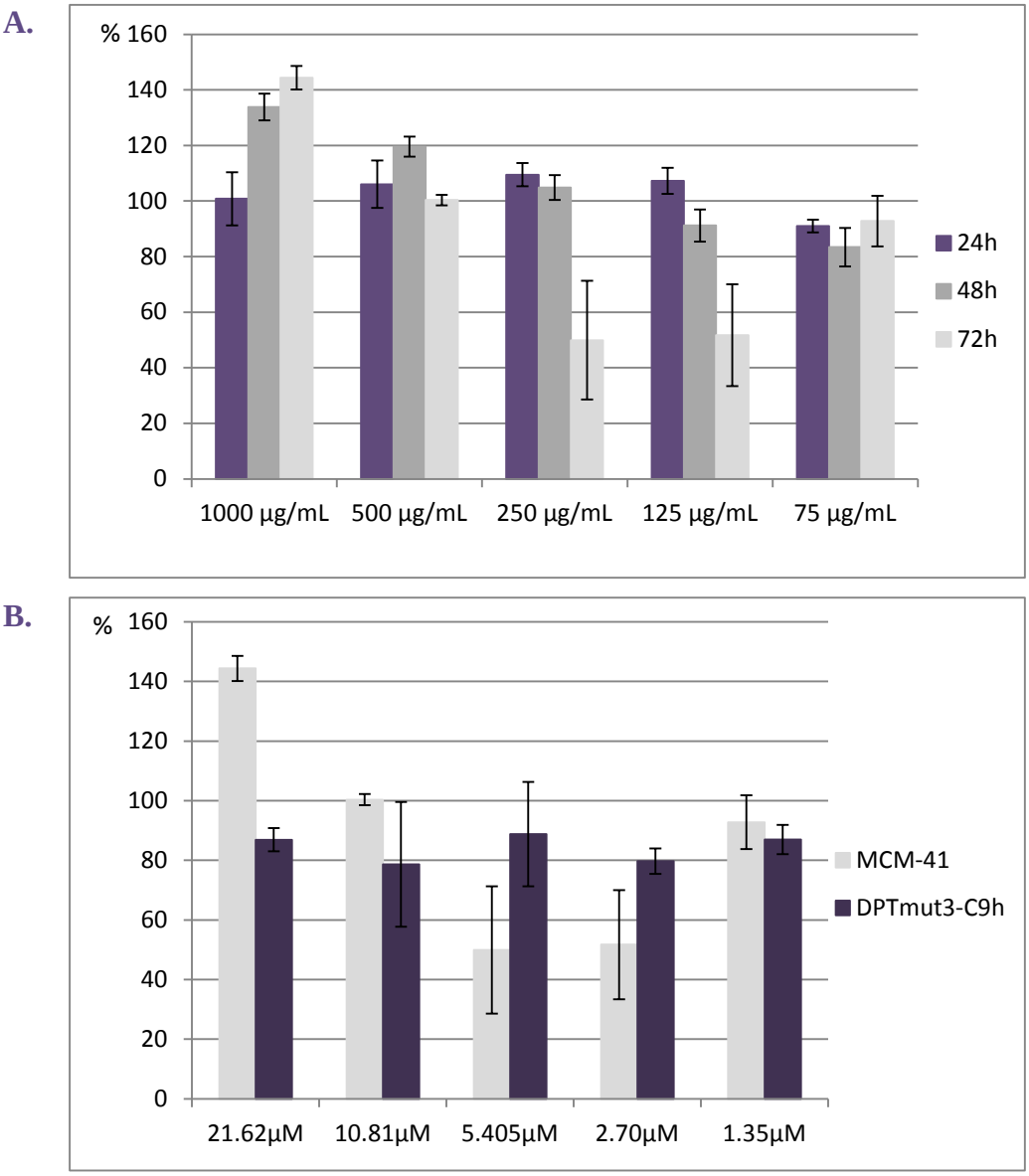

Figure 52. Cell viability assay of HeLa cells treated with MCM-41 nanoparticles loaded with the peptide C9hC. **A.** Percentage of cell viability after 24, 48 and 72h of treatment with MCM-41-C9hC is represented. **B.** Comparative percentage of cell viability after 72h of treatment with MCM-41-C9h or DPTmut3-C9h is shown.

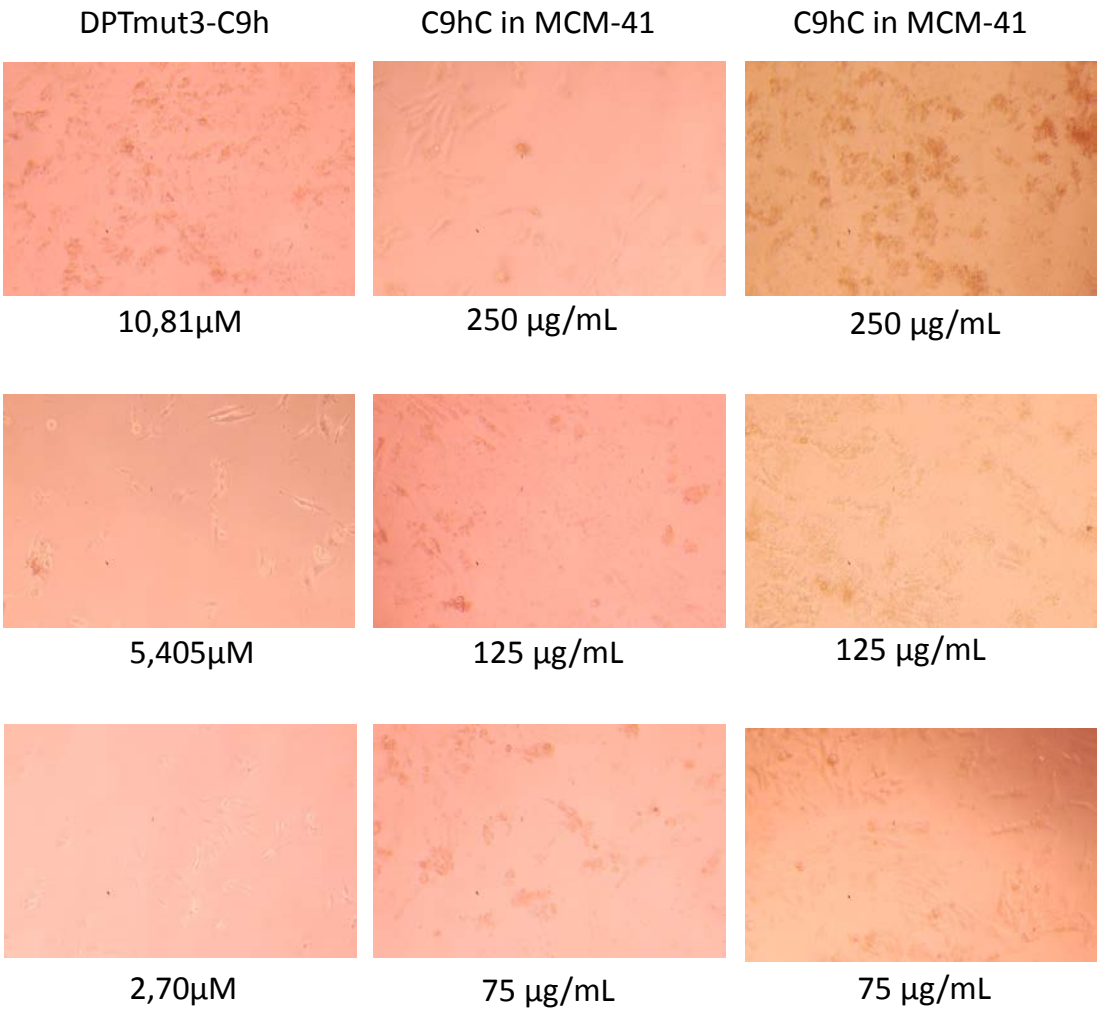

Figure 53. Microscope observation of HeLa cells treated with MCM-41 loaded with C9hC before FACS analysis was performed.

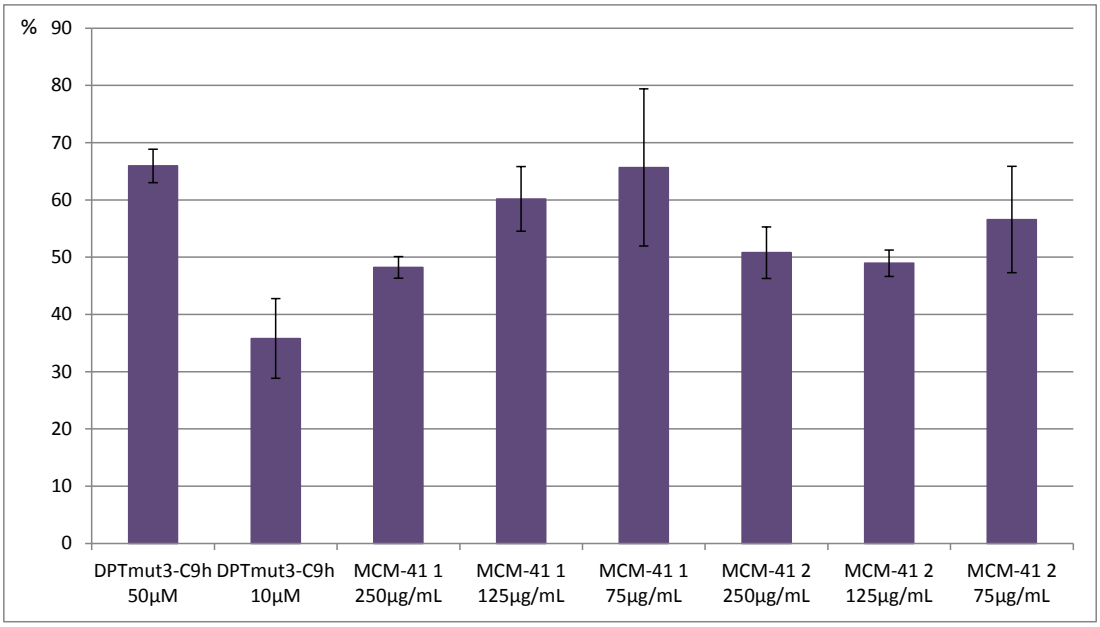

Figure 54. Percentage of apoptotic induction in HeLa cells after treatment with DPTmut3-C9h or MCM-41-C9hC.

5.3. Preliminary evidences of a the ternary complex Caspase-9/PP1cα/PP2Acα

5.3.1. Pep-scan-based Far Western Blot shows new binding sites

In a pep-scan-based Far Western Blot experiment, an amino-derivatized nitrocellulose membrane with peptides covering murine Caspase-9 was incubated first with PP1α and then with PP2Acα. Surprisingly, after incubation with anti-PP2A and revealing with ECL system, the binding sites obtained were different from the sites of each protein independently bound to Caspase-9 (**Figure 55**). Two interaction sites have been described for PP1cα in Caspase-9 (Dessauge et al., 2006), which comprise the first residues of the CARD domain, at the N terminal of the protein, and the residues 185-201 in the catalytic large subunit of the protein (both framed in red). However, when PP1 and PP2A were present, only the second PP1 binding site was maintained. On the contrary, PP2Acα binding site remained intact (framed in

blue). In addition, new binding sites were detected when the membrane was incubated with both proteins (framed in yellow). As represented in **Figure 55**, the binding sites detected when Caspase-9 was incubated with both phosphatases would be compatible with the possibility that a ternary complex takes place.

Table 16. Details of PP1 and PP2A binding sites to murine Caspase-9.

Site	Protein bound	Residues in murine Caspase-9	Murine Caspase-9 sequence	Equivalent residues in human Caspase-9
1	PP1	1-18	MDEADRQLLRRCRVRLVS	1-18
2	PP1 + PP2A	15-30	RLVSELQVAELWDALL	19-30
3	PP1 + PP2A	139-154	LTPVVLGPEELWPARL	96-116
4	PP1	223-239	LDRDKLEHRFRWLRFM	143-158
5	PP1 + PP2A	381-394	VSYSTFPGFVSWRD	381-401
6	PP1 + PP2A	388-406	FVSWRDKKSGSWYIETLD	350-368
7	PP2A	401-418	YIETLDGILEQWARSEDL	363-380

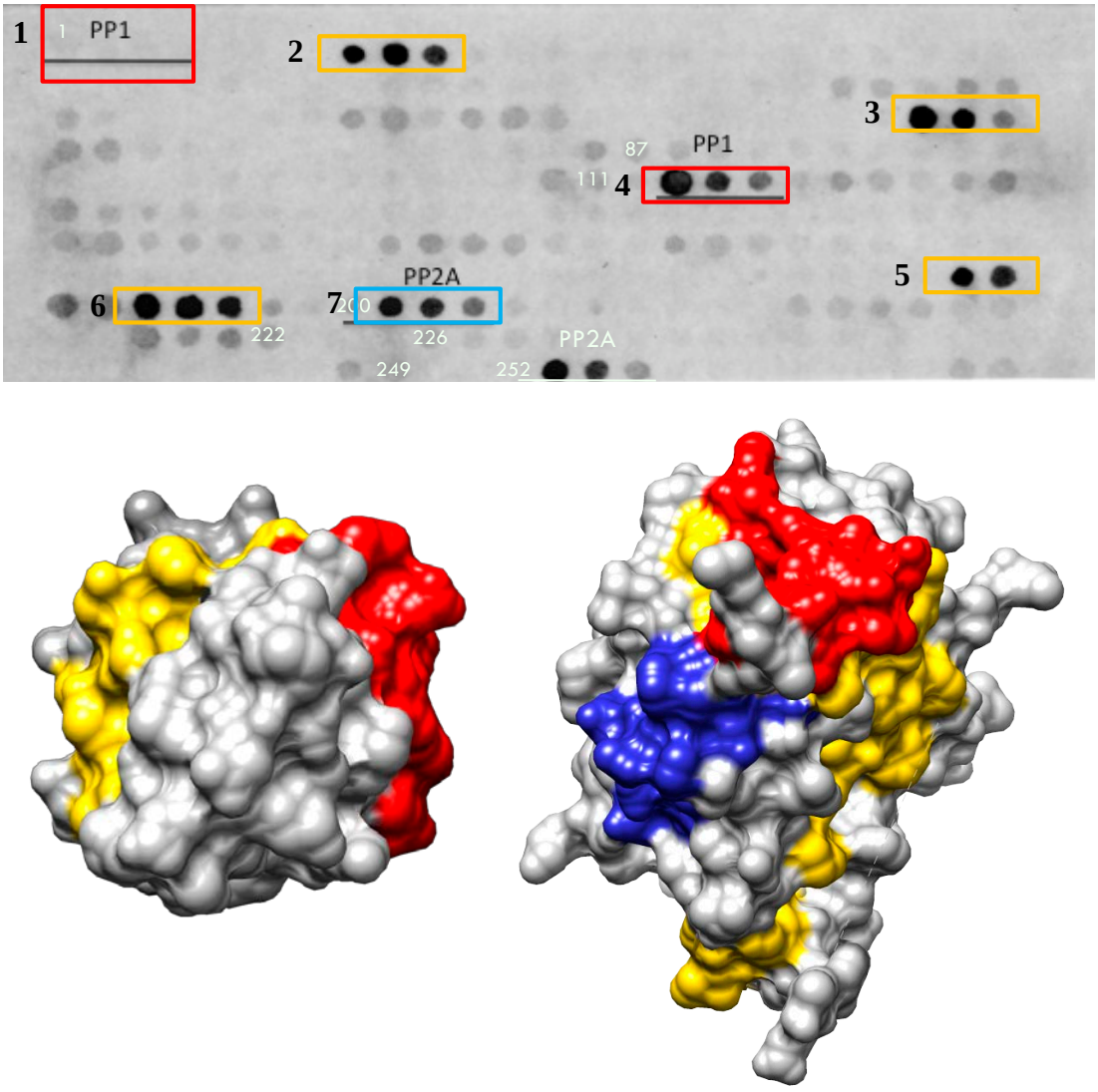

Figure 55. A. Pep-scan-based Far Western Blot analysis of Caspase-9 binding sites to PP1 and PP2A when both phosphatases were present. B. Surface representation of PP1 and PP2A binding sites in human CARD domain (PDB 4RHW) and ΔCARD Caspase-9 (PDB 1JXQ). PP1 binding sites are shown in red, PP2A binding site is shown in blue and new binding sites as a result of the coincubation are shown in yellow. According to this experiment, PP1 and PP2A would bind Caspase-9 to all the highlighted surfaces in figure B with the exception of PP1 binding site at the CARD domain (shown in red in the left figure).

5.3.2. Caspase-9b spliced variant contains PP2Acα binding site but not PP1cα binding site 2

Interestingly, Caspase-9 and PP2Acα binding sites are present either in the full length or the aberrant spliced forms. PP2Acα binding site in Caspase-9 is located in the small subunit of ΔCARD domain, near the C-terminal of the protein. This interaction site concurs with the function of the small subunit of Caspase-9 to confer substrate specificity to the protein. In the case of PP2Acα, it is remarkable that Caspase-9 binding site is found in the last residues before the deletion that takes place in PP2Acα2 (**Figure 56**), what may have a structural meaning in the hypothetical binding of DPT-C9h to PP2Acα2. Unlike PP2Acα, the second described PP1cα binding site in Caspase-9 is not present in Caspase-9b (**Figure 57**), corresponding to residues 185-201. According to this evidences, PP2Acα2 but not PP1cα would be able to hypothetically bind Caspase-9b.

```
            1                                                   50
PP2Acα      MDEKVFTKEL DQWIEQLNEC KQLSESQVKS LCEKAKEILT KESNVQEVRC
PP2Acα2     MDEKVFTKEL DQWIEQLNEC KQLSESQVKS LCEKAKEILT KESNVQEVRC
            51                                                  100
PP2Acα      PVTVCGDVHG QFHDLMELFR IGGKSPDTNY LFMGDYVDRG YYSVETVTLL
PP2Ac2      PVTVCGDVHG QFHDLMELFR IGGKSPDTNY LFMGDYVDRG YYSVETVTLL
            101                                                 150
PP2Acα      VALKVRYRER ITILRGNHES RQITQVYGFY DECLRKYGNA NVWKYFTDLF
PP2Acα2     VALKVRYRER ITILRGNHES RQITQVYGFY DECLRKYGNA NVWKYFTDLF
            151                                                 200
PP2Acα      DYLPLTALVD GQIFCLHGGL SPSIDTLDHI RALDRLQEVP HEGPMCDLLW
PP2Acα2     DYLPLTALVD GQIFCLHGGL SPSIDTLDHI RALDRLQEVP HEG.......
            201                                                 250
PP2Acα      SDPDDRGGWG ISPRGAGYTF GQDISETFNH ANGLTLVSRA HQLVMEGYNW
PP2Acα2     .......... .......... .......... .......... .......YNW
            251                                                 300
PP2Acα      CHDRNVVTIF SAPNYCYRCG NQAAIMELDD TLKYSFLQFD PAPRRGEPHV
PP2Acα2     CHDRNVVTIF SAPNYCYRCG NQAAIMELDD TLKYSFLQFD PAPRRGEPHV
            301
PP2Acα      TRRTPDYFL
PP2Acα2     TRRTPDYFL
```

Figure 56. Alignment of full length and alternative spliced form of PP2A. Caspase-9 binding site is shown in yellow.

```
           1                                                   50
Caspase-9  MDEADRRLLR RCRLRLVEEL QVDQLWDALL SRELFRPHMI EDIQRAGSGS
Caspase-9b MDEADRRLLR RCRLRLVEEL QVDQLWDALL SRELFRPHMI EDIQRAGSGS
           51                                                  100
Caspase-9  RRDQARQLII DLETRGSQAL PLFISCLEDT GQDMLASFLR TNRQAAKLSK
Caspase-9b RRDQARQLII DLETRGSQAL PLFISCLEDT GQDMLASFLR TNRQAAKLSK
           101                                                 150
Caspase-9  PTLENLTPVV LRPEIRKPEV LRPETPRPVD IGSGGFGDVG ALESLRGNAD
Caspase-9b PTLENLTPVV LRPEIRKPEV LRPETPRPVD IGSGGFGDV. ..........
           151                                                 200
Caspase-9  LAYILSMEPC GHCLIINNVN FCRESGLRTR TGSNIDCEKL RRRFSSLHFM
Caspase-9b .......... .......... .......... .......... ..........
           201                                                 250
Caspase-9  VEVKGDLTAK KMVLALLELA QQDHGALDCC VVVILSHGCQ ASHLQFPGAV
Caspase-9b .......... .......... .......... .......... ..........
           251                                                 300
Caspase-9  YGTDGCPVSV EKIVNIFNGT SCPSLGGKPK LFFIQACGGE QKDHGFEVAS
Caspase-9b .......... .......... .......... .........E QKDHGFEVAS
           301                                                 350
Caspase-9  TSPEDESPGS NPEPDATPFQ EGLRTFDQLD AISSLPTPSD IFVSYSTFPG
Caspase-9b TSPEDESPGS NPEPDATPFQ EGLRTFDQLD AISSLPTPSD IFVSYSTFPG
           351                                                 400
Caspase-9  FVSWRDPKSG SWYVETLDDI FEQWAHSEDL QSLLLRVANA VSVKGIYKQM
Caspase-9b FVSWRDPKSG SWYVETLDDI FEQWAHSEDL QSLLLRVANA VSVKGIYKQM
           401          416
Caspase-9  PGCFNFLRKK LFFKTS
Caspase-9b PGCFNFLRKK LFFKTS
```

Figure 57. Alignment of full length and alternative spliced form of Caspase-9. PP1α binding sites are shown in green and PP2A binding site is highlighted in magenta.

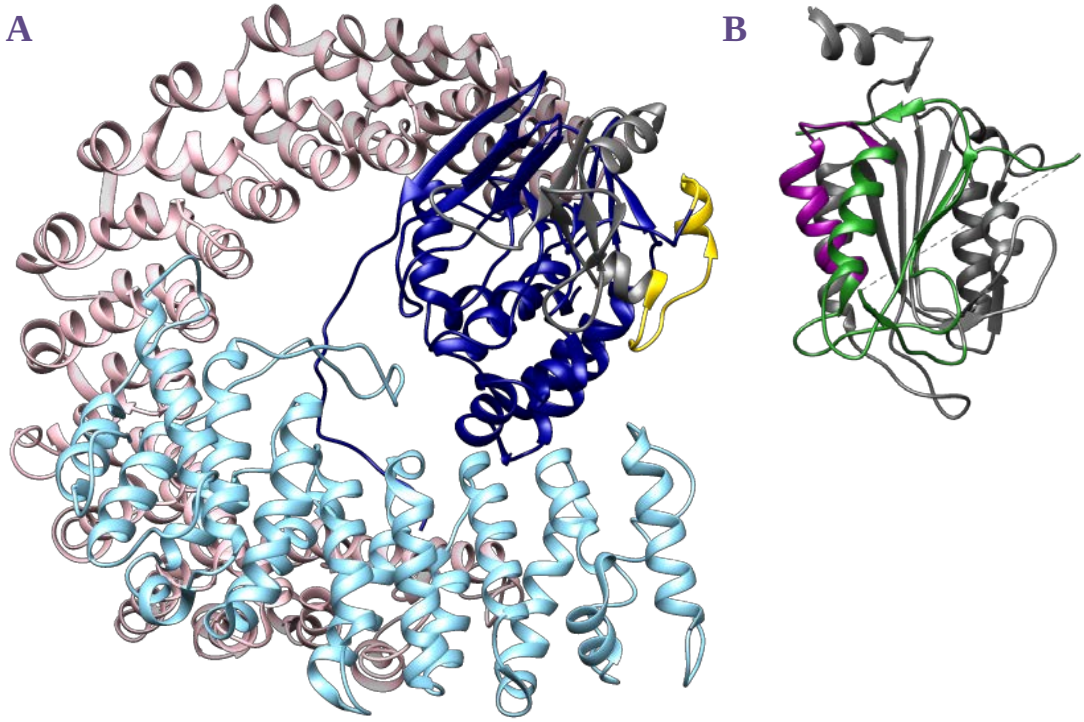

Figure 58. Model of the interaction between Caspase-9 and PP2A. A. PP2A (PDB code 2IAE) is represented showing A scaffold subunit in pink, B regulatory subunit in light blue and C catalytic subunit in dark blue. Caspase-9 binding site is colored in yellow (175-194). **B.** ΔCARD Caspase-9 (residues 140-416) (PDB 1JXQ) is shown in green, with PP2Acα binding site in magenta (residues 363-380). The deletions present in the spliced forms are shown in grey, comprising PP2Acα residues 194-247 and Caspase-9 residues 140-289.

5.4. Study of Caspase-9 and PP2Acα splicing variants

5.4.1. Caspase-9 and PP2Acα splicing variants in cell lines

cDNA of HeLa, SH-SY5Y, Daudi and Jurkat cell lines was analyzed by conventional PCR to detect the presence of Caspase-9 and PP2Acα full length and their spliced variants Caspase-9b and PP2Acα2 respectively (**Figure 59**). In a further approach, cDNA of these cell lines was analyzed by Real Time PCR to quantify the abundance of the spliced variants with respect to the full length forms (**Figure 60**).

For the cells grown under typical conditions (DMEM + 10% FBS), in the case of Caspase-9, all cell lines analyzed showed a healthy pattern of relative abundance of the spliced form Caspase-9b, with SH-SY5Y presenting the highest Caspase-9b values, at around 0.3 in the normalized value of relative abundance of the spliced form with respect to the full length Caspase-9, considered as 1. As described in the literature for non-small cell lung cancer (Shultz et al., 2010), the established limit between healthy and moderately dysregulated range is a normalized value of 0.303 for the spliced form. Surprisingly, all cell lines also possessed PP2Acα2 abundance corresponding to healthy state, obtaining very small values in Real Time PCR and a faint band in conventional PCR, when detected.

As PP2Acα2 has only been described in cells grown in the absence of serum (Migueleti et al., 2012), HeLa, SH-SY5Y, Daudi and Jurkat cell lines were incubated under starvation conditions (DMEM with 5% FBS and without serum) for 48h, total RNA was extracted and cDNA was also analyzed by Real Time PCR. As represented in **Figure 60**, in most of the cases cells showed healthy expression patterns of Caspase-9 and PP2Acα, with the exception of starved Daudi (0.5%FBS), which showed a moderate dysregulation in the relative abundance of Caspase-9b, and Jurkat (without FBS), which presented values in the limit between a moderate and a high dysregulation in the relative abundance of Caspase-9b.

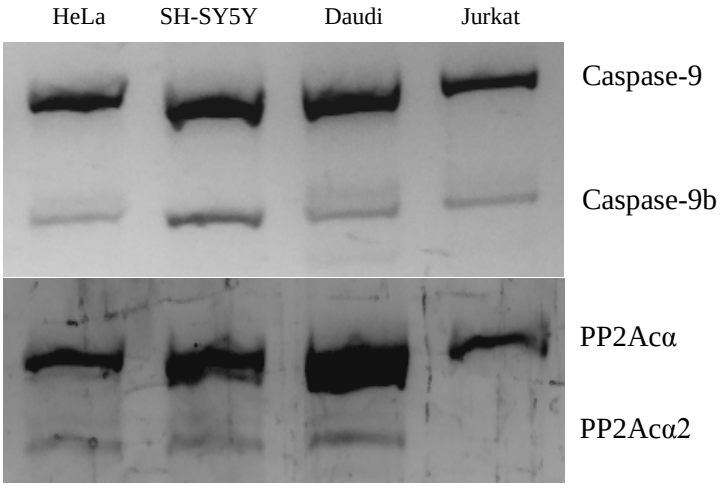

Figure 59. Conventional PCR amplification of both splicing variants of Caspase-9 and PP2Acα in cell lines grown under typical conditions, DMEM + 10% FBS.

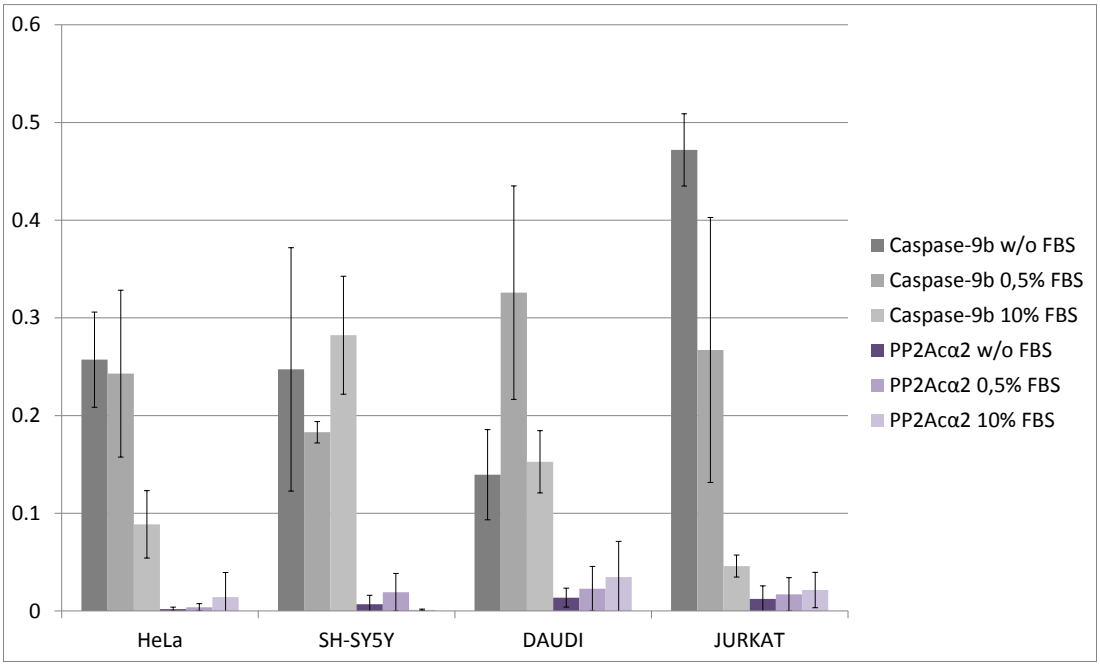

Figure 60. Real-Time PCR amplification values of spliced variants normalized with respect to the full length forms, considered as 1. Caspase-9b is represented in grey and PP2Acα in purple. The color intensity represents: dark for cells grown without FBS, medium for cells grown with 0.5%FBS and light for cells with normal conditions of 10%FBS.

5.4.2. Caspase-9 and PP2Acα splicing variants in CLL patients

cDNA from several healthy donors and CLL patients was analyzed by conventional PCR in a preliminary study to determine the presence of Caspase-9 and PP2Acα spliced variants related to the disease. Caspase-9b is slightly expressed in healthy donors, appearing as a faint band in the agarose gel (**Figure 61**); however, CLL patients showed a moderate overexpression of this shorter form in different degrees, depending on the patient. Healthy donors showed no detectable or very faint expression of PP2Acα2, but the majority of CLL patients presented from moderate to high rate overexpression of the aberrant form.

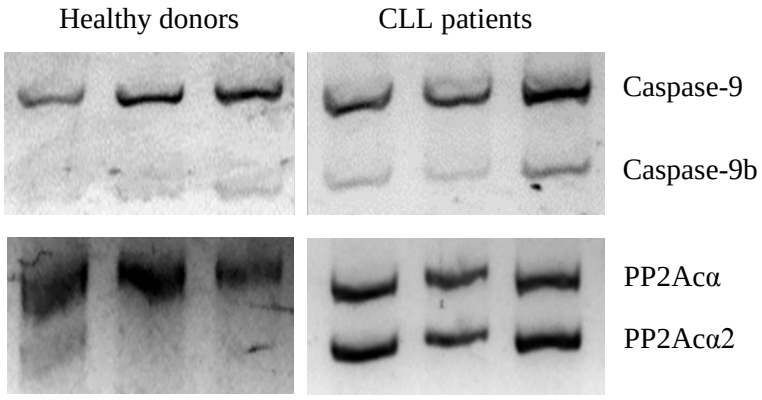

Figure 61. 2% Agarose gel showing amplification products of Caspase-9 and PP2Acα splicing variants from healthy donors and CLL patients samples.

A cohort of 24 healthy donors and 25 CLL patients from Pitié Salpêtrière and Saint Louis hospitals (Paris) was analyzed by Real Time PCR to quantify Caspase-9b and PP2Acα2 expression. Every sample was analyzed in triplicates for at least two times. As it was established by (Shultz et al., 2010), the criteria followed to classify Caspase-9b levels were normal (Caspase-9:Caspase-9b mRNA ratio 1: < 0.303), moderately dysregulated (ratio 1: 0.454 > X > 0.303) and highly dysregulated (1: > 0.454) (**Table 17**). According to this, 52% of CLL patients analyzed presented a normal level of Caspase-9b, 12% were moderately dysregulated and 28% were highly dysregulated (**Figure 64**). Moreover, 80% of healthy donors showed normal levels and the rest were slightly over the healthy ratio (**Figure 63**). Unlike the case of non-small-cell lung cancer, where 36% of the patients were moderately dysregulated and 42% were highly dysregulated, in CLL only a total of 40% of the patients had any alteration in Caspase-9b expression levels (**Figure 62**).

Considering previous data (Migueleti et al., 2012) and conventional PCR results, the expression rate expected for PP2Acα2 in healthy donors was not supposed to be very high, as no expression or very faint bands could be seen in agarose gels. Surprisingly, PP2Acα2 was expressed in healthy donors in a PP2Acα:PP2Acα2 ratio from negligible values up to 1:1.4 in 75% of the samples analyzed (**Figure 63**). With this data, we decided to formulate more stringent criteria than the ones for Caspase-9b to determine the severity of the dysregulation in

PP2Acα2 expression. We established a ratio PP2Acα:PP2Acα2 1: <0.75 for healthy expression, a ratio 1: 1.5 < X < 0.75 for moderately dysregulated and 1: > 1.5 for highly dysregulated expression. With this sorting, only 12% of CLL patients presented a normal PP2Acα2 expression pattern, 40% were moderately dysregulated and 48% were highly dysregulated (**Figure 62**, **Figure 64**). In sum, 88% of CLL patients analyzed had altered overexpression levels of PP2Acα2, what lead us to postulate the detection of this spliced form as a potential biomarker for CLL disease.

Table 17. Normalized abundance values established to sort the different levels of dysregulation in the expression of Caspase-9b and PP2Acα2.

	Normal	Moderately dysregulated	Highly dysregulated
Caspase-9: Caspase-9b	1 : < 0.303	1 : 0.454 > X > 0.303	1 : > 0.454
PP2Acα : PP2Acα2	1 : < 0.75	1 : 1.5 > X > 0.75	1 : > 1.5

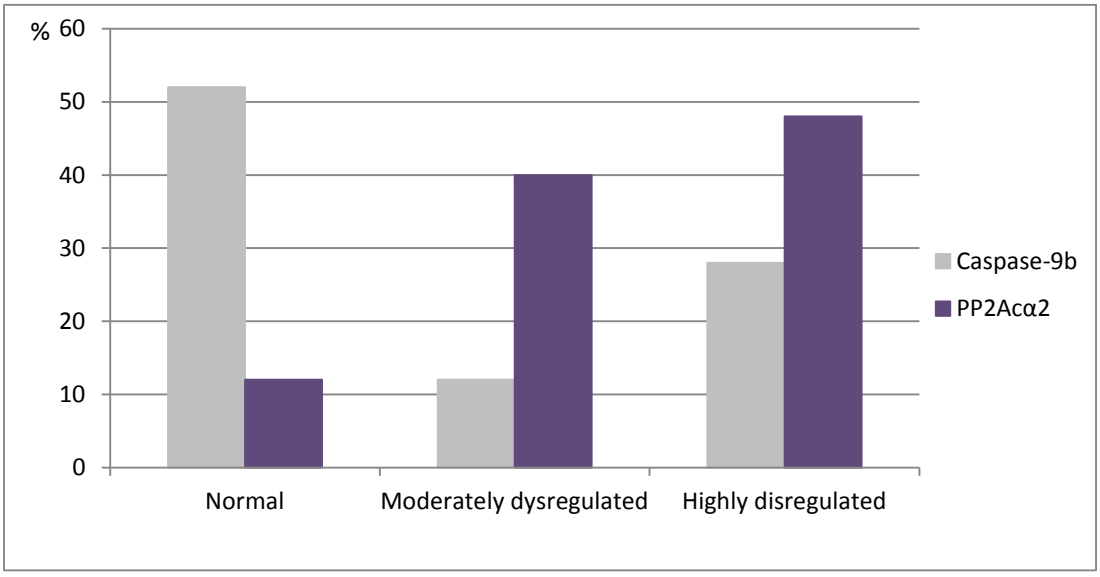

Figure 62. Percentage of CLL patients sorted by the level of dysregulation of Caspase-9b and PP2Acα2 expression.

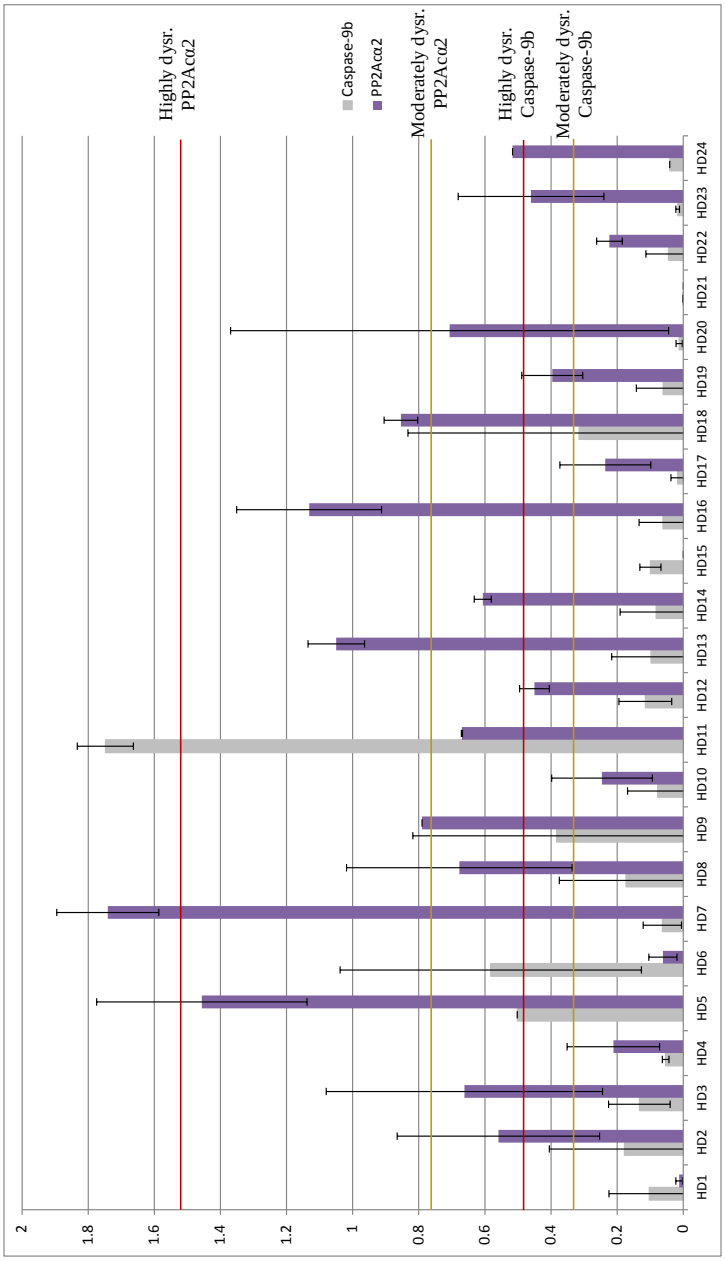

Figure 63. Real Time PCR analysis of healthy donors. Amplification values of spliced forms have been normalized with respect to full length forms, considered as 1. Caspase-9b is represented in grey and PP2Acα2 is in purple. The limits for moderately dysregulated values are marked in yellow and the limits for highly dysregulated values, in red.

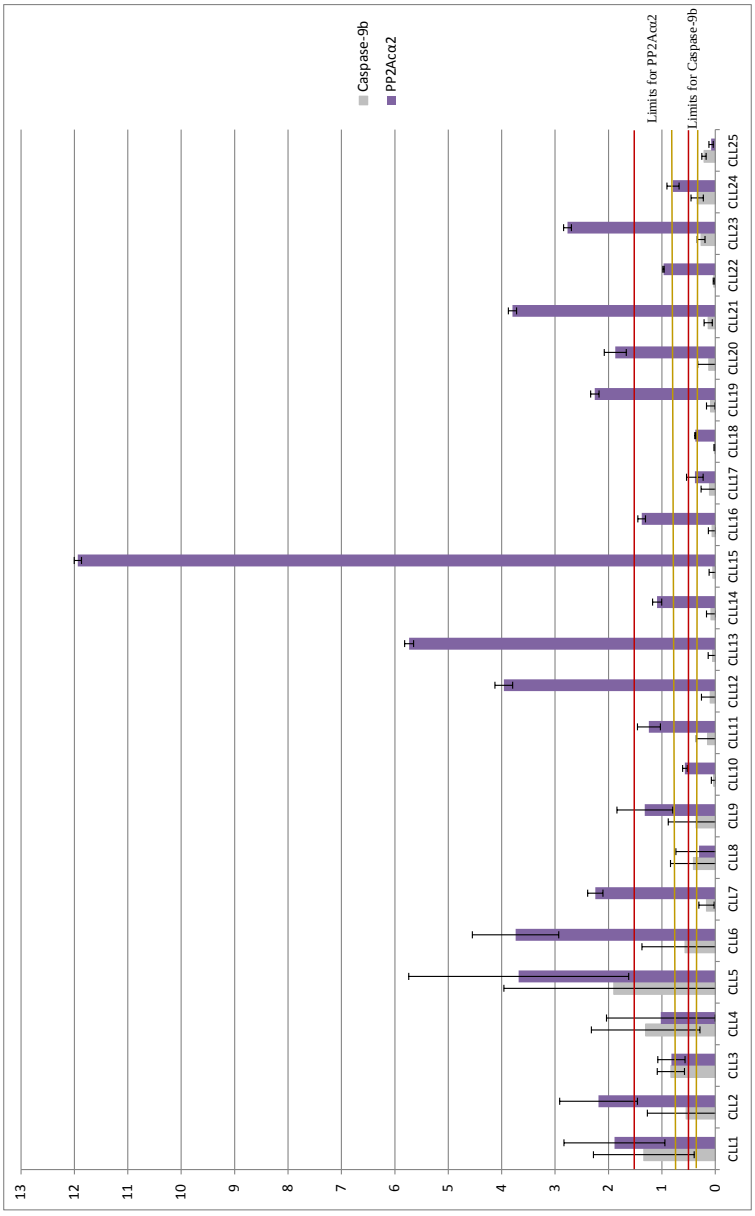

Figure 64. Real Time PCR analysis of CLL patients. Amplification values of spliced forms have been normalized with respect to full length forms, considered as 1. Caspase-9b is represented in grey and PP2Acα2 is shown in purple. The limits for moderately dysregulated values are marked in yellow and the limits for highly dysregulated values, in red.

The data of relative abundance of Caspase-9 and PP2Acα spliced variants was gathered with the medical available information of some of the CLL patients analyzed with the aim of establishing a correlation between this information and other parameters of the disease. The medical records available are listed in **Table 19**. Patients were classified according to the disease scores Binet (Binet et al., 1981) and Matutes (Matutes et al., 1994). Binet score sorts patients into three groups from less to more severe disease stages:

A. Less than three areas involved, including cervical, axilary and inguinal lymph nodes, whether unilateral or bilateral spleen and liver, hemoglobin ≥ 10 g/dL and platelets ≥ $100 \cdot 10^9$/L.

B. With at least three areas involved, hemoglobin ≥ 10 g/dL and platelets ≥ $100 \cdot 10^9$/L

C. Hemoglobin less than 10g/dL or platelets less than $100 \cdot 10^9$/L or both (independently of the areas involved).

Among the patients analyzed, all individuals classified with B or C Binet score presented highly dysregulated abundance of PP2Acα2, being the only patient analyzed which belonged to score C the one with the highest PP2Acα2 levels. Among A score patients, PP2Acα2 levels from normal to highly dysregulated values were found. Thus, the high dysregulation in the relative abundance of PP2Acα2 can be used as a potential biomarker to confirm the classification of patients at severe stages of the disease when correlated with other indicators.

Matutes score is used to establish a difference between CLL and other B cell diseases according to the reactivity of CD5, CD23 and FMC7 monoclonal antibodies and the intensity of expression of membrane immunoglobulins and CD22. When patients have 4 or 5 points of this score (**Table 18**), the disease is diagnosed as CLL. Among the patients analyzed, we couldn't establish any correlation between Matutes score 4 and 5 and the expression of the aberrant spliced forms of Caspase-9 and PP2Acα. The patient CLL19 had been treated with fludarabine, but we would need to analyze more patients to know if there is any relation between the treatment and the abundance of Caspase-9 and PP2Acα spliced variants.

Table 18. Matutes score system for CLL determination. Taken from (Matutes et al., 1994).

Membrane marker	Points	
	1	0
Smig	Weak	Moderate/strong
CD5	Positive	Negative
CD23	Positive	Negative
FMCC7	Negative	Positive
CD22	Weak/negative	Moderate/strong

Table 19. Medical records available of Pitié Salpêtrière and Saint Louis hospitals patients analyzed along with their respective Caspase-9b and PP2Acα2 expression values.

Patient	Age at diagnosis	Previous treatments	Binet score	White blood cells	Hemoglobin	Platelets	Matutes score	Caspase-9b	PP2Acα2
CLL15	71	No	C	100.000	10.2	86	4	0.05	11.93
CLL13	56	No	B	97.000	11.7	230	5	0.05	5.73
CLL12	63	No	B	85.000	12.7	116	5	0.10	3.96
CLL21	64	No	B	110.000	9.8	95	5	0.13	3.80
CLL6	82	No	B	28.000	10.6	206	5	0.57	3.74
CLL19	60	Yes	B	230.000	12.5	90	5	0.09	2.26
CLL5	72	No	A	200.000	12.9	92	5	1.90	3.68
CLL2	78	No	A	100.000	12.3	223	4	0.55	2.19
CLL1	50	No	A	130.000	10.9	189	5	1.34	1.89
CLL20	68	No	A	87.000	10.6	120	5	0.12	1.87
CLL16	43	No	A	44.000	15.0	210	5	0.06	1.38
CLL11	75	No	A	25.000	14.2	186	4	0.14	1.24
CLL4	72	No	A	27.000	14.6	250	5	1.30	1.02
CLL3	68	No	A	80.000	13.1	188	5	0.83	0.82
CLL17	87	No	A	140.000	10.1	66	5	0.11	0.38

Another cohort of 9 patients from Health Research Institute INCLIVA (Valencia) was analyzed by Real Time PCR. Patients were selected from different stages of the disease: advanced stage with relapse, tumor population with mutations in IgV_H and tumor populations without mutations in IgV_H. In the literature, tumors that present IgV_H without mutations are usually related to a worse prognosis (Chiorazzi and Ferrarini, 2003). The preliminary results shown in **Figure 65** indicate that patients at advanced stage with relapse along with patients without mutations in

IgV_H didn't present aberrant expression of Caspase-9b nor PP2Acα2. Nevertheless, patients with mutations in IgV_H seem to have a moderate dysregulation of PP2Acα2 expression.

The medical records of these patients include other parameters apart from the already mentioned Binet score. Another common score used to classify the stages of the disease is Rai score (Rai et al., 1975; Rozman and Montserrat, 1995), detailed in **Table 20**.

Table 20. Rai score classification.

Stage	Clinical features	Staging systems	Median survival (years)
0	Lymphocytosis alone	Low risk	14.5
I	Lymphocytosis, lymphadenopathy	Intermediate risk	7.5
II	Lymphocytosis, spleen or liver enlargement (or both)		
III	Lymphocytosis, anemia (hemoglobin < 11.0 g/dL)	High risk	2.5
IV	Lymphocytosis, thrombocytopenia (platelet count < 100000/mm^3)		

Patients with aggressive forms of CLL usually present unmutated IgV_H and they are positive for the 70kD-zeta-associated protein (ZAP-70), whereas in indolent disease, CLL cells usually express mutated IgV_H but don't express ZAP-70. However, aggressive disease is not always associated with unmutated IgV_H, therefore although the presence of IgV_H is associated with the expression of ZAP-70, it has been considered ZAP-70 as a stronger predictor of the need for treatment of CLL (Rassenti et al., 2004).

Initially, CD38+ B cells have appeared in higher percentages (≥30%) in patients with unmutated IgV_H with respect to the ones with mutated IgV_H. Besides, patients in both the unmutated and the ≥30% CD38+ groups responded poorly to continuous multiregimen chemotherapy and had shorter survival. On the other hand,

the mutated and the <30% CD38+ groups required minimal or no chemotherapy and had prolonged survival (Damle et al., 2007, 1999).

CD38 expression has been related to increased Ki-67 and ZAP-70 positivity, suggesting that CD38+ clones could more frequently enter cell cycle than CD38-.

Among the data available for this cohort of patients, we can observe that the patient 26960 has a Binet score C and a Rai score IV and correlates with a moderate dysregulation in PP2Acα2, appearing again associated to advanced states of the disease. In addition, among the patients with mutated forms of IgV_H, the ones that are ZAP-70 negative also show a moderate dysregulation of PP2Acα2. Notwithstanding, only 3 patients of each type were available to be analyzed in this experiment, thus to be able to establish a reliable correlation between the parameters of the disease more patients should be analyzed.

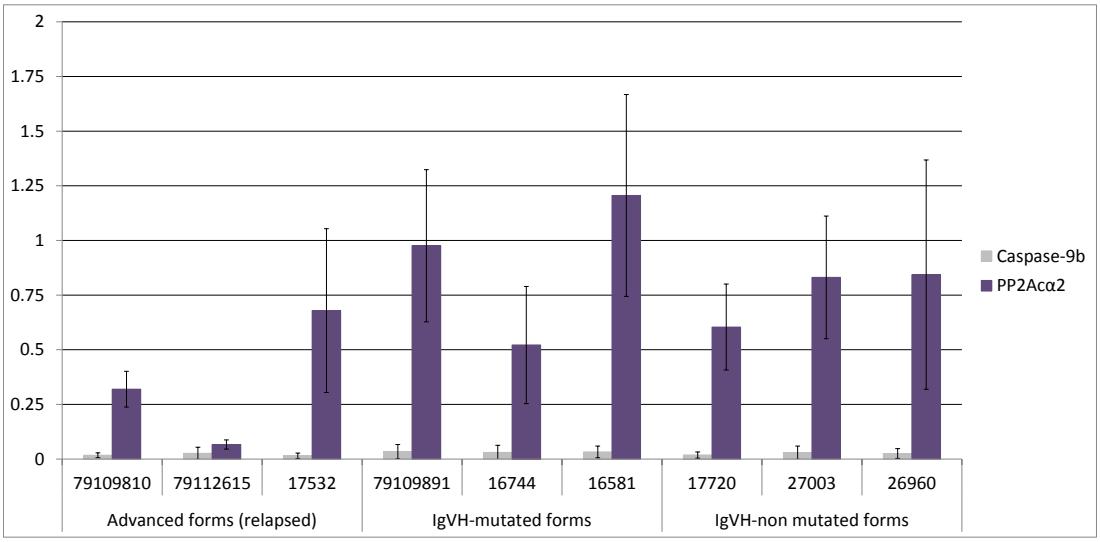

Figure 65. Real Time PCR analysis of CLL patients in advanced state, with mutations in IgV_H genes and without mutations.

Table 21. Medical records available of INCLIVA patients analyzed along with their respective Caspase-9b and PP2Acα2 expression values.

	Gender	Mutation IgVH	ZAP-70	CD38	Binet score	Rai score	Caspase-9b	PP2Acα2
79109810	Male	+	-	+			0.02	0.32
79112615	Male		+	-			0.03	0.07
17532	Male		+	+	B	II	0.01	0.68
79109891	Male	+	-	-			0.03	0.98
16744	Male	+	+	-	A	0	0.03	0.52
16581	Male	+	-	-	A	0	0.03	1.21
17720	Male	-	+	-	A	0	0.02	0.60
27003	Male	-	+	+	A	0	0.03	0.83
26960	Male	-		-	C	IV	0.03	0.84

5.4.3. Approach to production of recombinant Caspase-9b and PP2Acα2

Caspase-9b was cloned in pET23b vector and overexpressed in *E. coli* in the same conditions described for the full length protein. Overexpression levels were satisfactory, however we could only obtain soluble aggregates after size exclusion chromatography. After several purification attempts and thermal stability assays with different buffers, we could observe that the protein was more stable at pH 8.8 rather than pH8 used for other Caspase-9 constructs. Nevertheless, the conditions tried were not able to solve the aggregation problem.

HA-6His-TEV-PP2Acα2 D88N was cloned in pFastBacHTb vector and transposed to a bacmid using Bac-to-Bac system. The bacmid was transfected in Sf9 cells and further amplified. The amount of virus was titrated infecting Sf9ET cells with serial dilutions of the virus. The results of the titration are shown in **Figure 67**, obtaining very high virus titers, up to 10^{10}. High Five cells were infected at a m.o.i. of 2 and several purification attempts were performed with different conditions, but no protein could be obtained after affinity chromatography.

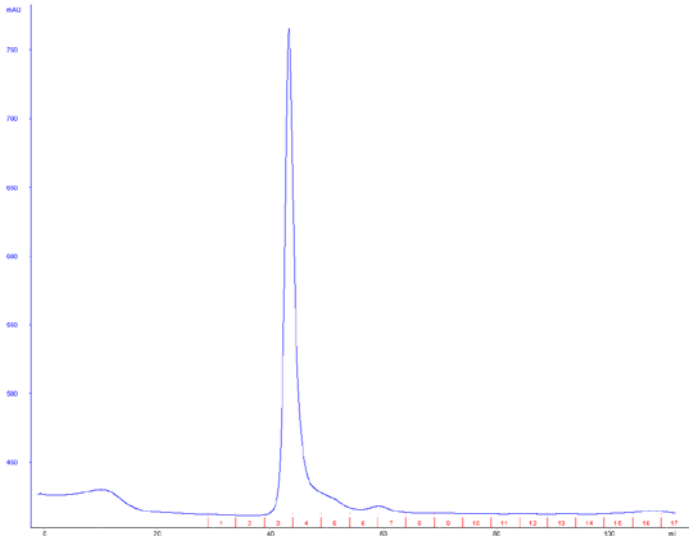

Figure 66. Size exclusion chromatogram of Caspase-9b. The peak corresponds to Caspase-9b eluting in the dead volume as it is aggregated.

5.5. Characterization of the direct interaction between Caspase-9 and PP2Acα inhibitor 2 (SET)

5.5.1. Binding sites determination

As it has been described in the introduction of the present work, it is widely known that SET is a PP2A inhibitor. Moreover, we have described and characterized the direct interaction between Caspase-9 and PP2Acα. With the aim of checking the possibility of a direct binding between SET and Caspase-9, a pep-scan-based Far-Western Blot approach was performed to map the binding sites between these two proteins. After revealing the nitrocellulose membrane where peptides covering Caspase-9 sequence were synthesized, incubated with SET, then with anti-SET and revealed with ECL System, three binding sites were detected that corresponded with the following residues in Caspase-9 sequence: Site 1 (399-416), Site 2 (347-364) and Site 3 (267-284) (**Figure 68**).

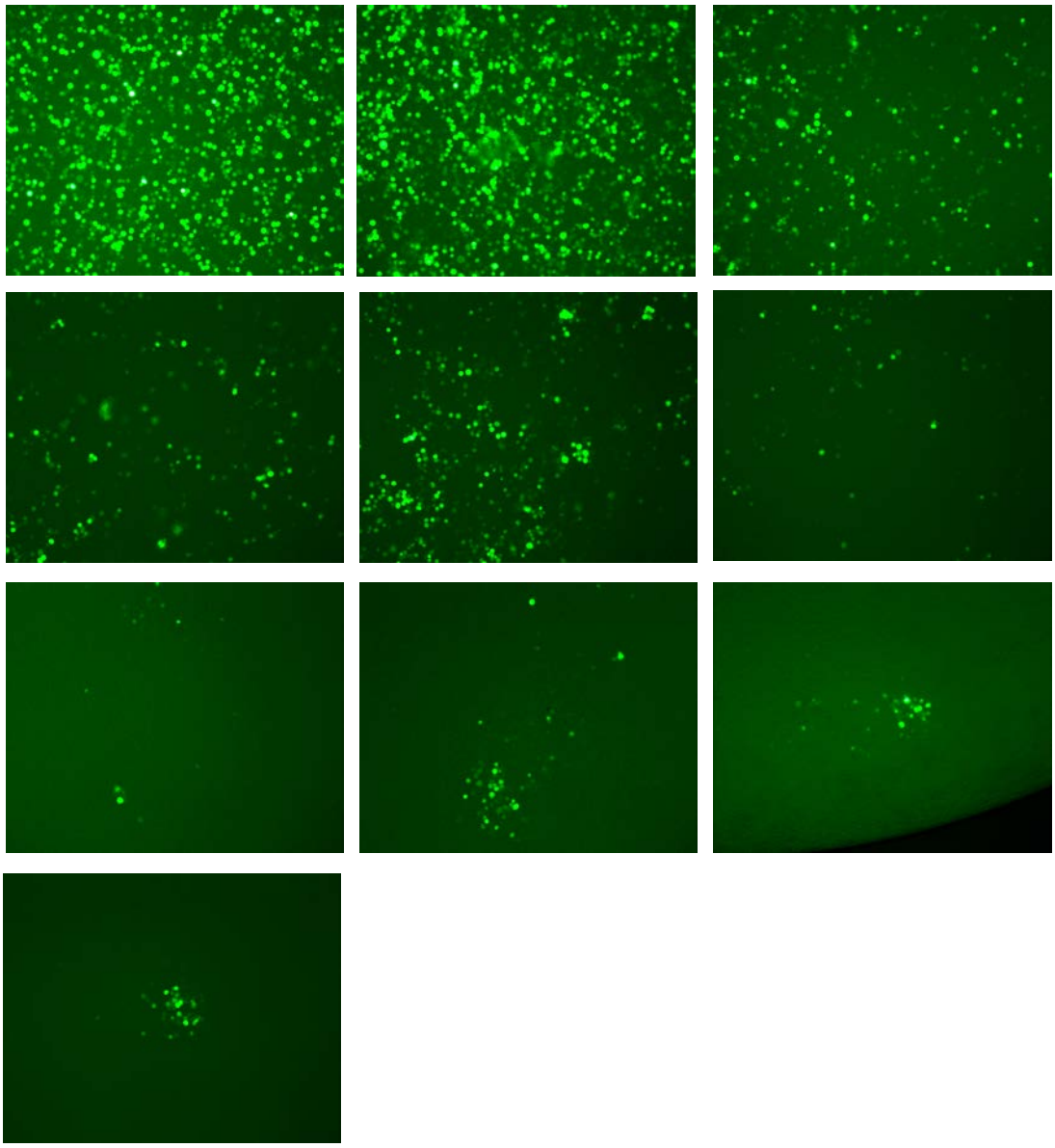

Figure 67. Fluorescence microscopy images of Sf9ET cells expressing GFP when they are infected with serial dilutions of PP2Acα2 baculovirus.

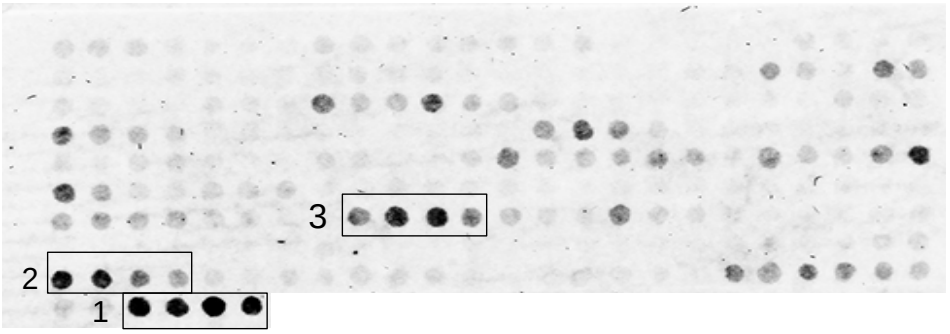

Binding site	Name	Boundaries	Sequence
Site 1	C9h-S4	399-416	QMPGCFNFLRKKLFFKTS
Site 2	C9h-S5	347-364	TFPGFVSWRDPKSGSWYV
Site 3	C9h-S6	267-284	FNGTSCPSLGGKPKLFFI

Figure 68. Pep-scan-based Far Western Blot analysis to determine Caspase-9 binding sites to SET. Nitrocellulose membrane where 12 aminoacid overlapping peptides covering human Caspase-9 sequence were synthesized by automated spot synthesis. Each spot corresponds to a peptide. The three binding sites detected are framed and their sequences are detailed below.

In the same way, a membrane where overlapping dodecapeptides covering SET sequence were synthesized, incubated with human Caspase-9, then with antiCaspase-9 and the secondary antibody and finally revealed with ECL system. In this case two binding sites in SET sequence were detected, as detailed in **Figure 69**.

Binding site	Name	Boundaries	Sequence
Site 1	SET2h-S1	53-74	ILKVEQKYNKLRQPFFQKRSEL
Site 2	SET2h-S2	169-186	RSSQTQNKASRKRQHEEP

Figure 69. Pep-scan-based Far Western Blot analysis to determine SET binding sites to Caspase-9. Nitrocellulose membrane where 12 aminoacid overlapping peptides covering human SET sequence were synthesized by automated spot synthesis. Each spot corresponds to a peptide. The two binding sites detected are framed and their sequences are detailed below.

5.5.2. Apoptosis assays

The apoptotic effect of the peptides corresponding to Caspase-9 and SET binding sites fused to the improved shuttle DPTmut3 (Fominaya et al., 2015a) was tested in MDA-MB-231 cells and measured by FACS. 100µM of DPTmut3-C9h-S4 showed a high efficiency, inducing more than 80% of apoptosis upon 24h of treatment. The incubation with DPTmut3-C9h-S5 produced a slight apoptotic effect of around 40%. A smaller dose was also tried, 40µM, of each of these peptides and the combination of both. Once again, DPTmut3-C9h-S4 resulted to be more efficient, inducing apoptosis in around 40% of the cells. DPTmut3-C9h-S5 was not able to induce apoptosis at this concentration and neither did present a synergistic effect in combination with DPTmut3-C9h-S4.

Moreover, SET derived bifunctional peptide DPTmut3-SET-S1 induced apoptosis in more than 90% of the cells upon 24h of treatment with a 100µM dose. This effect was reduced to 40% upon treatment with 40µM of this peptide. On the other hand, DPTmut3-SET-S2 didn’t produce any apoptotic effect or synergistic effect when administered with DPTmut3-SET-S1.

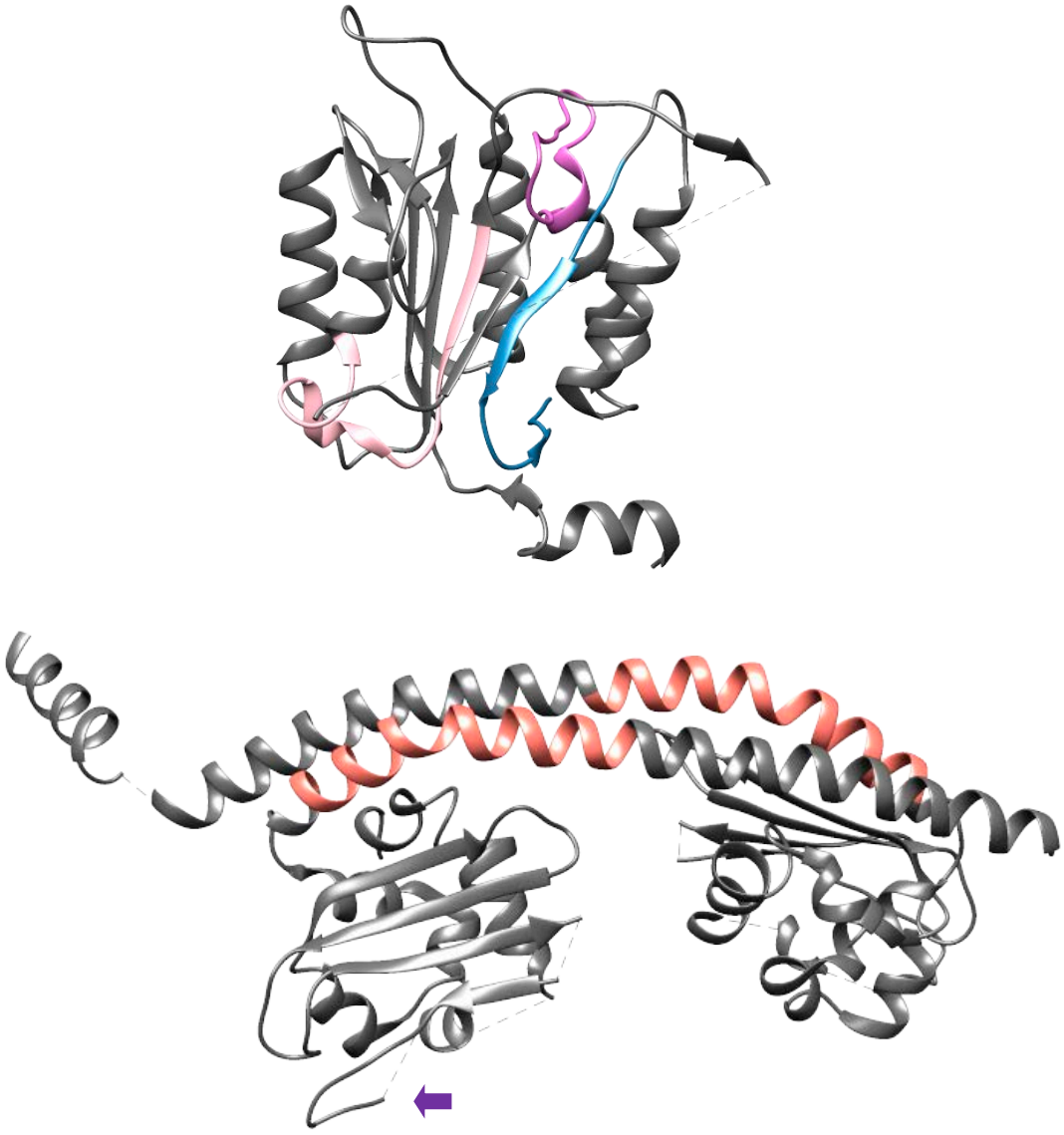

Figure 70. Caspase-9 and SET binding sites model. A. ΔCARD Caspase-9 structure (PDB 1JXQ) showing SET binding site 1 in blue, 2 in magenta and 3 in pink. **B.** SET dimer structure (PDB 2E50) showing Caspase-9 binding site 1 in coral. Binding site 2 is not visible in the structure, but the area where it should be placed is highlighted with the purple arrow.

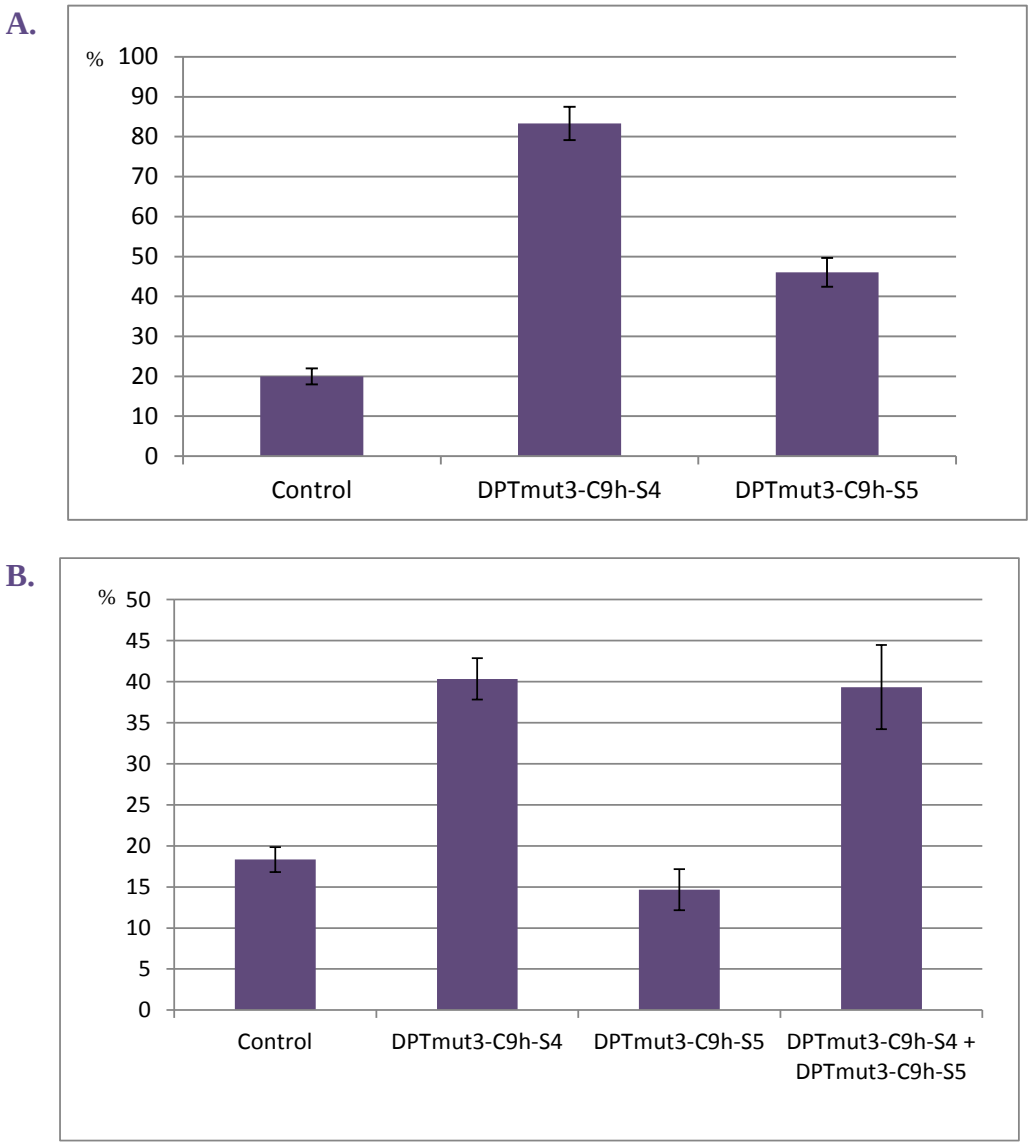

Figure 71. Percentage of apoptosis induced by Caspase-9 derived bifunctional peptides targeting SET. A. Apoptosis induced by 100µM peptide treatment. **B.** Apoptosis induced by 40µM of each peptide independently or the combination of 40µM DPTmut3-C9hS4 + 40µM DPTmut3-C9h-S.5

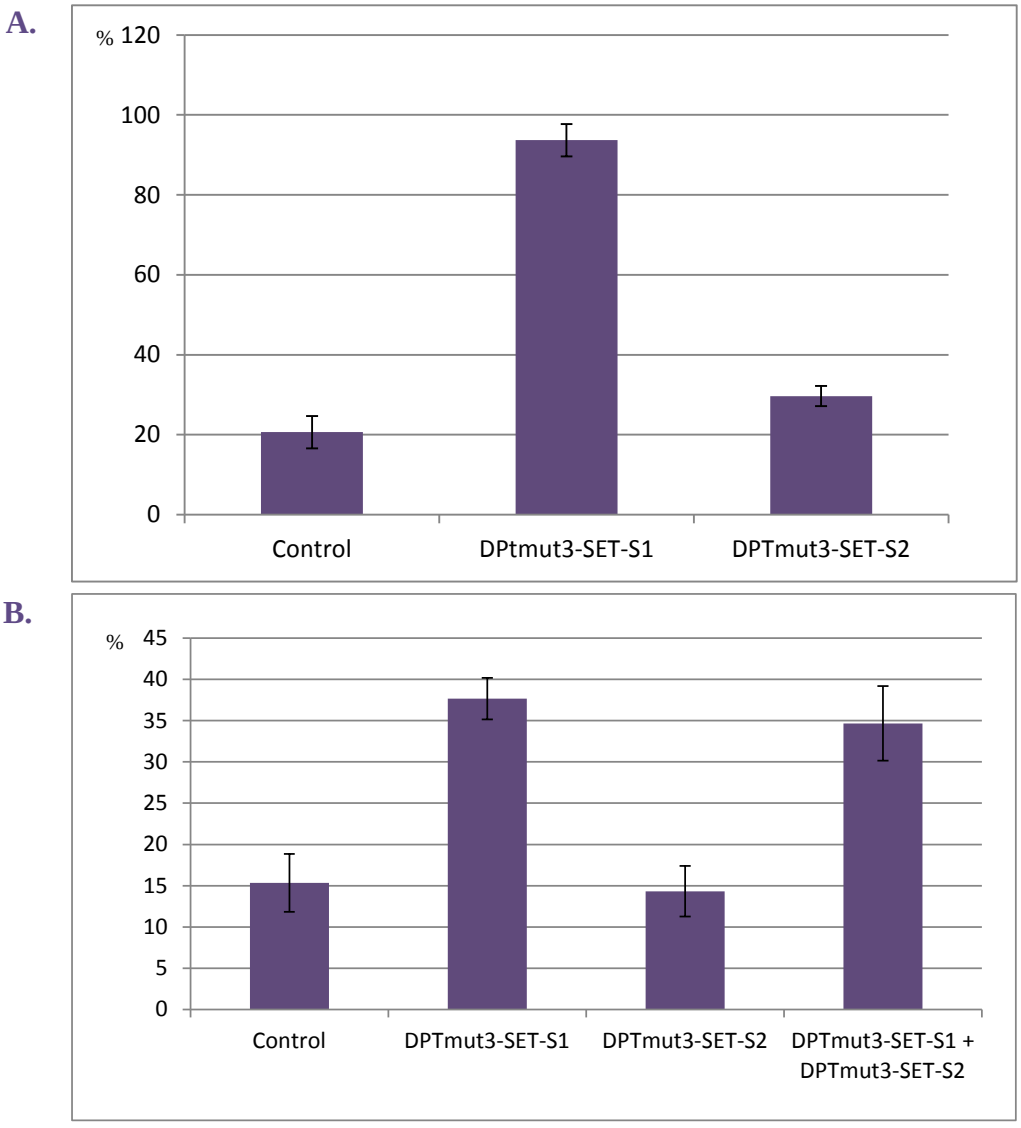

Figure 72. Percentage of apoptosis induced by SET derived bifunctional peptides targeting Caspase-9.

5.5.3. Caspase-9 overexpression and purification

Caspase-9 constructs corresponding to GST-CARD, GST-ΔCARDC94QC, GST-ΔCARDC9C287A, GST-C9WTFL and C9WTFL-His were overexpressed and purified as described in 5.1.1.

5.5.4. SET overexpression and purification

SET full length and SET 1-225 constructs were overexpressed in *E.coli* and purified by affinity chromatography with a 5mL HisTrap column. The fractions containing the protein were concentrated up to 2.5mL and injected in a Superdex 200 26/60 column. Both SET constructs elute as a dimer in size exclusion chromatography. The fractions corresponding to the peak were run in a SDS-PAGE gel and they were concentrated until the needed concentration for further experiments. The rest of the protein was frozen in liquid nitrogen and stored at -80ºC.

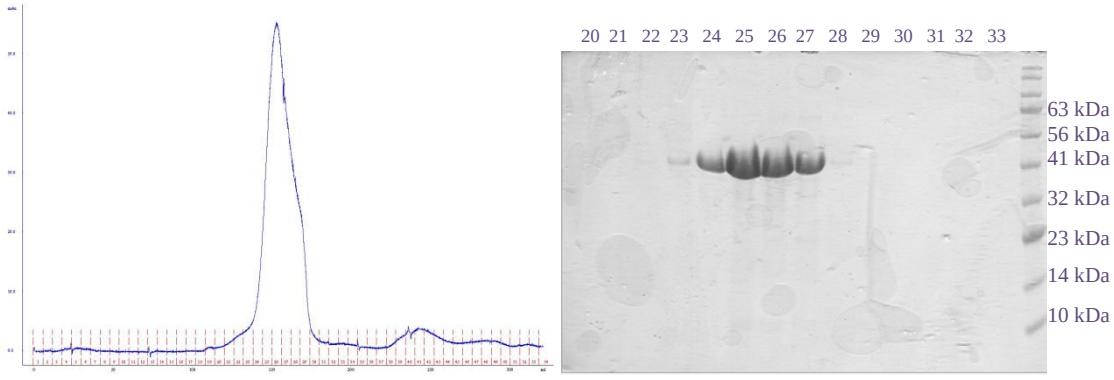

Figure 73. SET full length size exclusion chromatogram and SDS-PAGE in which fractions 20-33 were run. Pure protein was recovered from fractions 23-28.

5.5.5. Pull-down and Western Blot assays

Caspase-9 and SET constructs were overexpressed in 20 mL of culture according to the previously described protocols and processed as described for low-scale purification. The supernatant of Caspase-9 constructs (GST-CARD, GST-

ΔCARDC94QC, GST-ΔCARDC9C287A, GST-CASP9C287AFL) were used as bait proteins. Also the supernatant of SET full length and SET 1-225 were incubated with the beads to perform a negative control. Beads were washed and then, the supernatant of SET constructs (full length and 1-225) was incubated as prey protein. Finally, the protein-protein complex was eluted with buffer B and samples were run in a SDS-PAGE. After that a Western Blot was performed to confirm the presence of the two proteins in the elutions. Western Blot revealed with Anti-GST let us confirm the presence of Caspase-9 constructs bound to Glutathione sepharose 4B beads and the second Western Blot revealed with Anti-His shown that SET was bound to Caspase-9 to the CARD domain, the ΔCARD domain and the full length protein but it was also unspecifically bound to glutathione sepharose beads. It seems that SET binds stronger to the beads that contain Caspase-9 with respect to the negative control, but these data don't allow us to confirm the interaction between them.

In a further experiment, a pull-down assay was performed using Caspase-9 (GST-CARD, GST-ΔCARDC9C287A and GST-C9WTFL) and SET (full length and 1-225) pure proteins from large scale purification. GST bound to glutathione sepharose beads was used as bait protein negative control. SET presented strong unspecific binding to glutathione sepharose beads loaded with GST with almost the same intensity as it did for Caspase-9; therefore, these data don't allow us to confirm the *in vitro* interaction between SET and Caspase-9.

5.5.6. The interaction between Caspase-9 and SET is not detected *in vitro* by biophysical techniques

Biolayer interferometry technique was used to perform an advanced kinetics assay to determine the affinity of the binding between GST-CARD and GST-ΔCARDC9C287A to SET full length. Caspase-9 constructs were bound to GST sensors as bait proteins and SET was further added as prey protein in high concentrations (10 and 20μM) to try to detect an expected low K_D. In both cases, the affinity between both proteins was below the detection limit of the equipment.

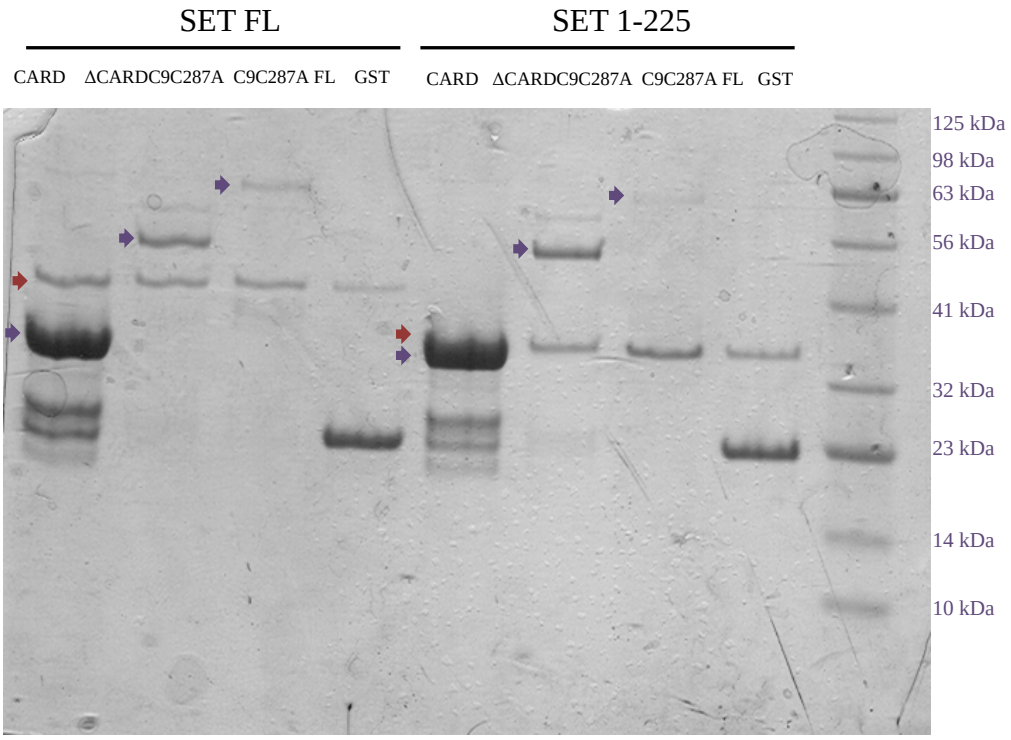

Figure 74. SDS-PAGE where the elutions of the pull down assay of Caspase-9 and SET different constructs were run. Caspase-9 constructs are marked with the purple arrow and SET constructs are indicated with the red arrow.

As isothermal titration calorimetry is a more sensitive technique to measure binding affinity, we tried to detect the interaction between Caspase-9 wild type full length and SET full length in SE buffer (20mM Tris pH8, 100mM NaCl, 1mM β-mercaptoethanol). 30µM Caspase-9 wild type full length was added to the cell and two experiments were performed with 1mM and 1.5mM SET in the buret, adding 30 injections of 1.5µL every 210 seconds at 25ºC. The interaction between both proteins could not be detected in any of these conditions.

Index	Sample ID	Conc. (μM)	Information	KD (M)	ka (1/Ms)	ka Error	kd (1/s)	kd Error	Rmax	Rmax Error	R equilibrium
1	SET 10uM	10		2.221e-5	2.585e2	1.814e1	5.74e-3	7.197e-5	2.924	0.2149	0.908
2	SET 20uM	20		2.221e-5	2.585e2	1.814e1	5.74e-3	7.197e-5	1.439	0.08342	0.6817

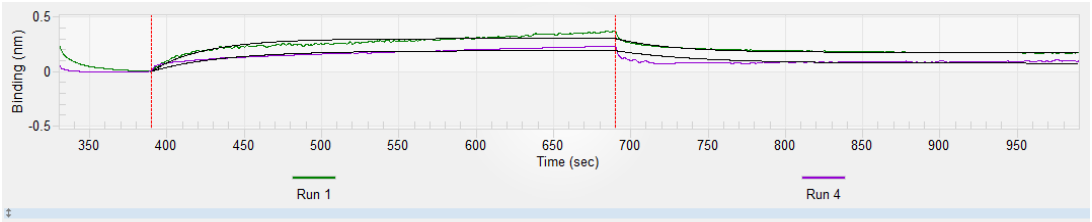

Index	Sample ID	Conc. (μM)	Information	KD (M)	ka (1/Ms)	ka Error	kd (1/s)	kd Error	Rmax	Rmax Error	R equilibrium
1	SET 20uM	20		4.871e-5	2.291e2	5.568e1	1.116e-2	2.643e-4	1.98	0.4646	0.5762
2	SET 20uM	20									
3	SET 20uM	20									
4	SET 20uM	20		4.871e-5	2.291e2	5.568e1	1.116e-2	2.643e-4	0.9112	0.1998	0.2652

Figure 75. BLItz sensorgram of advanced kinetics assays between Caspase-9 and SET. In the upper sensorgram, GST-CARD was used as a bait protein and 10μM and 20μM of SET were added as prey protein. In the lower sensorgram, GST-ΔCARDC9C287A was added as bait protein and 20μM of SET as prey protein.

DISCUSSION

"Nothing in life is to be feared, it is only to be understood. Now is the time to understand more, so that we may fear less." Marie Curie.

6. DISCUSSION

In the present work we have carried out an approach to the complex interplay that takes place at Caspase-9 level in the apoptotic pathway, in which phosphatases PP1α and PP2Acα and the inhibitor 2 of PP2A, also known as SET, actively participate in the signal transduction cascade. The network of interactions among these proteins and the known functions they exert over their partners are compiled in **Figure 76**.

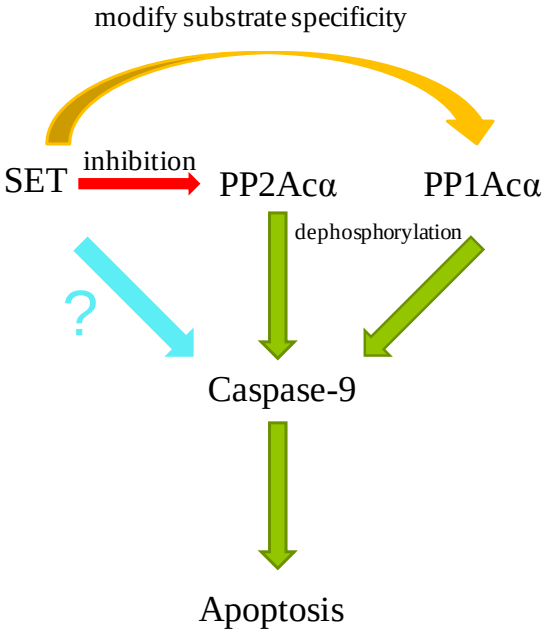

Figure 76. Scheme of the interactions among the proteins studied in the present work.

The direct interaction between PP1α and Caspase-9 was described by our collaborators several years ago (Dessauge et al., 2006). It was also known before the start of this project that SET bound PP1α, modifying its substrate specificity (Katayose et al., 2000), but this interaction still remains uncharacterized.

In a project developed in tight collaboration with the laboratory of Dr. Angelita Rebollo at CIMI-UPMC (Paris), we have described for the first time the direct interaction between PP2Acα and Caspase-9 (Arrouss et al., 2013), which has been characterized in the present work.

It is widely known that SET is a potent PP2Acα inhibitor (Li et al., 1996). Remarkably, in this work we have determined three potential SET binding sites in Caspase-9 sequence and two binding sites in SET to Caspase-9. Unfortunately, the interaction could not be characterized *in vitro* with our recombinant proteins from bacterial source. However, the interaction was proved to take place, as the peptides corresponding to Caspase-9 binding site 1 and SET binding site 1 were able to induce apoptosis.

In this section we will go through this complex protein interplay, scrutinizing the particularities of each association and evaluating the applications that we are developing for cancer therapy based on these proteins as potential targets.

6.1. Interaction between Caspase-9 and PP1cα

In the study where this interaction was firstly described, Dessauge et al., 2006 determined two binding sites in Caspase-9 for the interaction with PP1: one located at CARD domain and the other one at the catalytic domain. When they performed a competition binding assay between PP1α and Caspase-9 binding site 1 and 2 peptides, they observed that the amount of PP1α associated to Caspase-9 decreased after competition with site 1 peptide or site 2 peptide but the binding was undetectable upon competition with both peptides together, suggesting that both domains were indispensable for a complete interaction.

Furthermore, the need of the full length Caspase-9 protein for the interaction has an important biological significance and it is consistent with the molecular mechanism of Caspase-9 in the context of apoptosis. If PP1 preferentially binds to full length Caspase-9, this means that the dephosphorylation and subsequent activation occurs before procaspase-9 is processed in the apoptosome. Thus, the kinase/phosphatase crosstalk is a control point before the procaspase-9 processing as a mature protein and the activation of its protease activity. This hypothesis is also supported by (Dessauge et al., 2006) experiments, in which upon PP1α depletion from cytosol, procaspase-9 processing was inhibited, suggesting a requirement of PP1α activity for cytochrome c – dependent activation of Caspase-9.

Another piece of evidence from our kinetics results is that the *in vitro* interaction between these two proteins is weak. This was somehow expected because these proteins form transient interactions in the cell that are crucial for signal transduction in apoptosis. Also, they are regulated by protein reversible phosphorylation which may have an important role in the modulation of the affinity between these two proteins. In line with these results, Dessauge et al., 2006 observed that upon 6h of IL-2 deprivation, the level of PP1α and procaspase-9 phosphorylation strongly decreased, probably because once PP1α dephosphorylated procaspase-9, it was dispensable for the complex that leaded to Caspase-9 activation, suggesting either a dynamic association or a conformational change in procaspase-9 once it is dephosphorylated, inducing PP1α release.

Notwithstanding, it has to be taken into account that this interaction *in vivo* occurs under certain stimuli and works under complicated regulatory mechanisms in which many proteins are involved. It is possible that these two proteins, as it is usually the case for PP1, need regulatory additional proteins to control their binding or additional post-translational modifications that are not present in our recombinant proteins. The phosphorylation event might be crucial in the recognition of procaspase-9 by PP1 and also it might increase the affinity of the interaction.

6.2. Potential PP1 dephosphorylation sites in Caspase-9

In the present project, we have selected several Caspase-9 phosphorylation sites and designed phosphomimetic mutants and we will study whether the affinity of the interaction is affected. These candidates have been selected as PP1 targets, given that all of them have known kinases that phosphorylate them in the context of the apoptotic pathway.

(Parrish et al., 2013) highlighted Thr 125 as an important target residue for post-translational modifications, since it is conserved among evolution and it is regulated by different signaling pathways. ERK kinase, the cycling dependent kinase (CDK1), DYRK1A and p38α can phosphorylate this residue, decreasing Caspase-9 activation and its proteolytic activity. However, there is no known phosphatase

targeting this threonine located in the linker between CARD and the catalytic domain of Caspase-9.

Furthermore, S196 is another potential target for PP1, as it is surrounded by a RVxF motif, as it will be detailed in **Figure 79**. (Bollen et al., 2010) reviewed that for some PP1-binding partners, a phosphorylation event near or within a RVxF motif strengthens their interaction with PP1. This residue is also an Akt target (Cardone et al., 1998), an anti-apoptotic kinase that inactivates the pathway by phosphorylation of pro-apoptotic factors such as Bad or procaspase-9, which are also PP1 target proteins. Most importantly, this residue is located in the second PP1 binding site of Caspase-9 sequence described by (Dessauge et al., 2006). Moreover, Akt is negatively regulated upstream of the apoptotic pathway by PP1. All in all, this suggests the hypothesis that Ser 196 residue of Caspase-9 might be dephosphorylated by PP1, completing a perfect interplay between the anti-apoptotic kinase and the pro-apoptotic phosphatases PP1 and PP2A in the regulation of Caspase-9 activation, as it is represented in **Figure 77**.

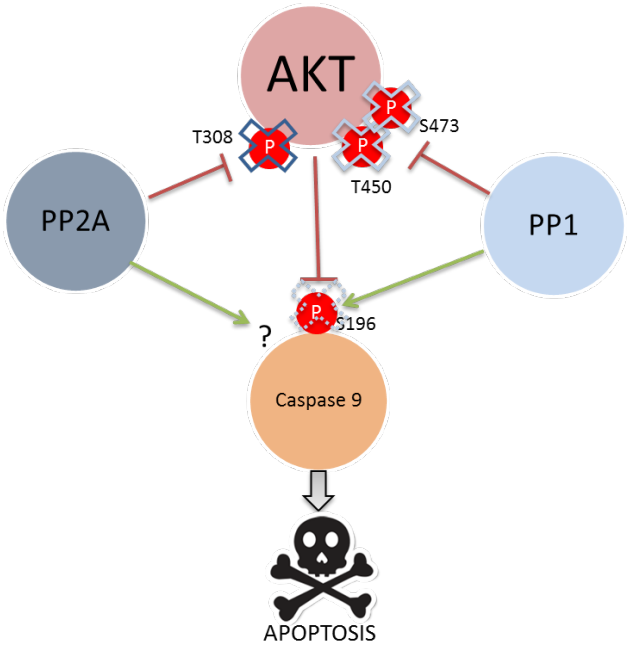

Figure 77. Schematic representation of the interplay between the kinase AKT, phosphatases PP1 and PP2A and Caspase-9. AKT is a kinase that directly

phosphorylates Caspase-9 by targeting Ser 196 residue. As a result, the proteolytic activity of Caspase-9 is significantly reduced, preventing further proapoptotic signaling. On the other hand, two proteins inactivate AKT by dephosphorylating particular residues: T450 and S473 are targets of PP1 and T308 of PP2A. It is also known that both phosphatases directly interact with Caspase-9 but their dephosphorylation target residues remain unknown. Since Caspase-9 has a PP1 RVxF binding motif surrounding S196 and PP1 acts as an inhibitor of AKT action, we hypothesize that this phosphatase might be responsible for S196 dephosphorylation, antagonizing AKT antiapoptotic signaling.

Further experiments with Caspase-9 phosphomimicking mutants (T125E, S196D, S310D) designed during the present project should be performed to elucidate the candidate residue to be phosphorylated by PP1, shedding light into the activation of Caspase-9 in the apoptotic pathway.

6.3. Caspase-9 binding site 2 to PP1cα is a degenerated RVxF binding site

(Bollen et al., 2010) proposed a combinatorial control of PP1 in which the binding of PIPs (PP1 interacting proteins) to this phosphatase is mediated by multiple, degenerated short sequence motifs functioning as interacting sites. The primary PP1-binding motif in PIPs is the RVxF motif, which functions as an anchor for PP1 and allows its partner protein to make additional interactions with the phosphatase. These additional contacts can be weak but the multiple binding sites ensure a tight interaction. PIPs differ in the number and type of the PP1-docking sites and, as they are degenerated, some sequence variants considerably affect the affinity for PP1. Hence, the disruption of only a single motif can be enough to weaken (Beullens et al., 2000) or even break the interaction (Aggen et al., 2000).

If we compare human and mouse Caspase-9 sequence, we can observe the high level of conservation between them. The first PP1 binding site characterized in Caspase-9 sequence (Dessauge et al., 2006) is totally conserved; however the second binding site presents several aminoacid changes, as shown in **Figure 78**. In the last years, many RVxF motifs for PIPs have been determined, which has allowed to establish a degenerated code for the aminoacids composing these binding sites. Unlike (Dessauge et al., 2006), who didn't consider the second PP1 binding site in murine Caspase-9 sequence an RVxF motif, we have reanalyzed this binding site in human and mouse and we have observed that this interaction region contains a RVxF

motif comprising residues 196-199 in human Caspase-9, as it is shown in **Table 22**, with the sequence SLHF, whose characteristics are also detailed in **Figure 79**.

The wide structural knowledge about PP1, its specific binding motifs and the increasing number of PIPs constitute a valuable guidance to design therapeutic approaches targeting these interactions. As we have developed in the present work for other targets as PP2A and SET, we already know small molecule compounds such as peptides that can compete with specific binding motifs and disrupt the interaction between PP1 and procaspase-9. A deeper knowledge of the binding kinetics and the dephosphorylation event at this point will help us to elucidate potential applications for these peptides as a targeted therapy.

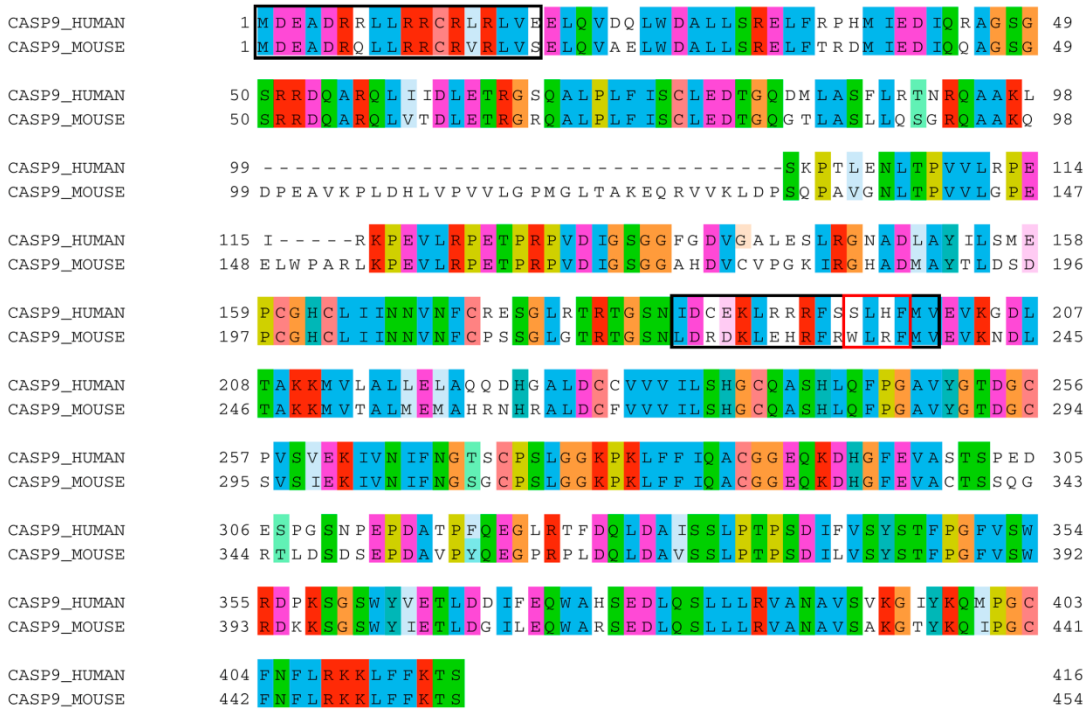

Figure 78. Alignment of human and mouse Caspase-9 sequence. PP1 binding sites are framed in black and RVxF motif is framed in red inside the second PP1 binding site. As it can be seen in the alignment, this motif is not conserved between human and mouse.

Table 22. RVxF degenerated code for PIPs binding site to PP1. Human Caspase-9 matches totally with the aminoacids described as RVxF binding site. Mouse Caspase-9 shows a W residue at R position of the RVxF motif.

	R	V	X	F
RVxF motif consensus	K/R/H/N/S	V/I/L	any residue except F/I/M/Y/D/P	F/W/Y
Caspase-9 human (196-199)	S	L	H	F
Caspase-9 mouse (223-239)	W	L	R	F

Figure 79. Detailed analysis of Caspase-9 sequence comprising residues 189-204. S196 is phosphorylated by Akt (Cardone et al., 1998) because it recognizes a motif surrounding this residue (blue frame). Also, Caspase-9 sequence has a PP1-binding RVxF motif surrounding S196 (orange frame). This motif usually is flanked by N-terminal basic residues (highlighted in green) and C-terminal acidic residues (shown in red).

6.4. Interaction between Caspase-9 and PP2Acα

The starting point of the present work was the determination of Caspase-9 binding site to PP2Acα and the description for the first time of a direct interaction between them (Arrouss et al., 2013). In the same way, we have determined Caspase-9 binding site in PP2Acα sequence and we have further characterized the residues of both proteins whose mutation disrupts the interaction. From these binding sites, peptides have been designed and fused to a cell-penetrating peptide sequence termed DPT to target this interaction. The therapeutic effect and technical development of the peptide C9h will be discussed below.

The peptides C9h and PP2Ah were characterized, showing that tryptophan 374 of Caspase-9 was implicated in the function of the protein and its mutation didn't produce any change in the free energy nor the secondary structure of the peptide. Moreover, PP2Ah bound Caspase-9 with a K_D in the micromolar range,

suggesting that the interaction between Caspase-9 and PP2Acα is transient. However, the peptide YPP2Ah was not able to *in vitro* activate Caspase-9.

Historically, PP2A structural studies have been very difficult to accomplish because of the very low level of PP2Acα that can be obtained even from insect cells infected with baculovirus or mammalian expression systems (Cho and Xu, 2007). In the present work, we have overexpressed PP2Acα in Sf9 insect cells fused to an HA tag at the N-terminal part that was described to increase protein stability (Wadzinski et al., 1992). The mutation at the active site D88N was performed to improve expression levels (Myles et al., 2001), and a cleavable His-tag was also added at the N-terminal of the protein. Baculovirus containing the sequence codifying for this construct were transfected into Sf9 cells and virus amplification provided satisfactory virus titers, quantified by GFP expression of infected Sf9ET cells. However, after infection in High Five insect cells, very low yield of protein was recovered and furthermore it was purified as soluble aggregates when it was detectable after size exclusion. Several purification buffers have been tried, but up to date we couldn't obtain pure and well folded PP2Acα, which has strongly limited this work, preventing the biophysical and structural characterization of the protein-protein interaction between PP2Acα and Caspase-9 and the protein-peptide interaction PP2Acα – C9h.

6.5. Therapeutic strategies for the use of C9h in cancer

Once Caspase-9 derived peptide (C9h) and PP2Acα derived peptide (PP2Ah) were determined as the binding sites of the interaction, they were fused to a cell-penetrating peptide sequence termed DPT, to act as a shuttle for the entry of the peptide in the cells. The cell-penetrating peptide DPT-sh1 (drug phosphatase technology) was designed based on the concept of blocking the interaction of the Ser/Thr phosphatases PP1 and PP2A core catalytic subunits with their local regulatory partners using intracellular delivery of peptides to prevent specific substrate dephosphorylation. A new cell-penetrating sequence was identified in *Theileria parva* casein kinase 2α and was used as a new nontoxic shuttle for *ex vivo* and *in vivo* intracellular delivery of sequences interfering with PP2A or PP1

holoenzymes (Guergnon et al., 2006). Applying this technology, the sychnologic peptides DPT-C9h and DPT-PP2Ah were generated.

DPT-C9h showed to induce apoptosis more efficiently than DPT-PP2Ah; in addition, when cells were treated with both peptides, a synergistic effect was observed, showing a slightly higher apoptotic effect compared to DPT-C9h. According to these preliminary data, we decided to continue the studies with DPT-C9h to evaluate the use of its antiapoptotic effect for cancer therapy. DPT-C9h was proved to induce species specific Caspase-9 dependent apoptosis in cancer cell lines, primary human cells and primary human breast cancer xenograft models (Arrouss et al., 2013). DPT-C9h had a specific effect on transformed B cells isolated from chronic lymphocytic leukemia patients without any effect on primary healthy cells, confirming its tumor specificity. Moreover, DPT-C9h was also specific for B cells, not inducing any apoptotic effect on T-cells, NK-cells or monocytes (Arrouss et al., 2015).

In another study, DPT-sh1 cell-penetrating peptide resulted to be more efficient than the classical CPP Tat when bound to a peptide that interacts with PP2A-Bα. This peptide was obtained from the 23-46 aminoacids of canine adenoviral E4orf4 protein with the aim of mimicking E4orf4 anticancer signal. E4orf4 binds PP2A-Bα to specifically induce p53-independent death of human cancer cells. DPT-E4orf4$_4$ adopted an α-helical structure and inhibited survival of HeLa cells. All together, these results suggest that α-helical structured DPT bound peptides specifically interacting with PP2A could be a valuable anti-cancer drug design scaffold (Galioot *et al*., 2013).

Either for DPT-C9h or DPT-E4orf4$_4$ treatments, doses up to 100µM were utilized in the experiments, which is a high concentration to satisfactorily face preclinical trials. Frequently, high biodegradability and low bioavailability have been limiting obstacles for the therapeutic use of peptides (Vlieghe et al., 2010). In addition, blood plasma contains more than 120 proteins, among which are present numerous proteolytic enzymes involved in peptide degradation (Kumar and Bhalla, 2005). A serum protease cleavage site was detected in the sequence of DPT-sh1 cell-penetrating peptide at the R residue. The mutation to Alanine in this aminoacid seemed to solve the degradation problem, as DPTmut3-C9h presented enhanced

stability while keeping the apoptotic function. Hence, the improved sychnologic peptide showed higher bioaccumulation in tumors with respect to the parental DPT-C9h (Fominaya et al., 2015a).

In parallel with this last study, the use of mesoporous silica nanoparticles was evaluated in the present work as a potential vehicle for the delivery of C9h. Mesoporous silica nanoparticles have emerged as promising candidates to deliver therapeutic agents to the target site in a controlled manner and they also possess favorable chemical properties, thermal stability and biocompatibility. Hence, this local delivery of the cargo reduces potential side effects and maximizes therapeutic effects obtaining the optimal concentration of biologically active agents in local sites, which permits a dose reduction in the treatment. MSNs have also shown to be useful carriers for the delivery of unspecific drugs that require high doses to be effective and also for the delivery of hydrophobic molecules (Kwon et al., 2013).

In the present work two types of MSNs have been used as drug carriers for C9h with different results. 400nm diameter MSNs showed poor efficiency in the controlled delivery of C9h, as they were not capable of inducing apoptosis as expected when cells are treated with C9h. Severe resuspension problems were experimented with these nanoparticles, as they were not resuspendable in PBS or other solvents, and even when resuspended in DMSO they formed aggregates that were very difficult to dislodge and after administration, aggregates were also observed in the wells, avoiding that part of the MSNs entered into the cells.

On the contrary, MCM-41 nanoparticles were mostly resuspended in DMSO after sonication and aggregates were barely observed in the wells after treatment. MCM-41 loaded with C9hC were able to reduce cell viability with an efficiency of 30% more than the equivalent peptide dose of DPTmut3-C9h, as well as to induce apoptosis in a percentage equivalent to up to 10 times less amount of peptide. Comparatively, at a peptide dose of 10μM, when the peptide was delivered with MCM-41 it was able to induce 15% more apoptosis than when fused to the cell-penetrating peptide DPTmut3. Moreover, at 5μM dose, C9hC loaded in MCM-41 induced apoptosis at a range equivalent to the effect produced by 50μM DPTmut3-C9h. In conclusion, MCM-41 nanoparticles constitute a promising tool for C9h

delivery in cancer cells, allowing a dose reduction in the treatment without losing its apoptotic effect.

Notwithstanding, upon facing preclinical trials there is still much work to do to better characterize some features of mesoporous silica nanoparticles. Silica is widespread in the nature and has better biocompatibility than other metal oxides such as titanium and iron oxide, and silica can be safely taken up by living cells through endocytosis, due to the affinity of its silanol groups for cell phospholipids. However, more studies need to be addressed to evaluate the biodegradability and long-term biocompatibility of MSNs. Most of the nanomedicines applying inorganic nanocarriers are still at the stage of preclinical or basic research, nevertheless Cornell Dot gold and silica cancer selective nanoparticles have been approved by FDA for first-in-human clinical trials (Benezra et al., 2011).

To date, the French company Pep-therapy (www.pep-therapy.com) is in charge of carrying out the preclinical trials of DPTmut3-C9h for its use in cancer therapy, since cell-penetrating peptide technology has longer been evaluated for clinical trials with relative success (Chen and Harrison, 2007), but in the future other options may be taken into account to further optimize cancer treatment with C9h peptide.

6.6. Preliminary evidences for the ternary complex PP1α-PP2Acα-Caspase-9

PP1 and PP2A share many protein partners, as members of Bcl-2 and Retinoblastoma families, whose phosphorylation status is regulated by these protein phosphatases, in a cross-talk between PP1 and PP2A that controls cell survival (Garcia et al., 2003; Kolupaeva and Janssens, 2013). According to the preliminary results obtained in the present work, PP1α and PP2Acα would be able to bind simultaneously to Caspase-9. The way in which this ternary interaction is happening still remains unknown and further experiments are required to elucidate this mechanism, but pep-scan-based Far Western Blot experiments suggest that the binding sites for each of these proteins separately are different than when both phosphatases are present, and also new binding sites take place in the ternary complex. In fact, the first PP1 binding site in Caspase-9 is not maintained in the

ternary complex, but either PP1 binding site 2 or PP2A binding site remain participating in the interaction. This evidence may have significance at the point of Caspase-9 regulation when the complex is taking place, as new binding sites appear in the ΔCARD domain and PP1 binding site 1 at the CARD domain is not participating in the interaction of the ternary complex, suggesting that the ternary complex may occur with mature Caspase-9 after CARD domain cleavage. The perspective of this possible ternary complex opens the possibility to integrate the Caspase-9 dephosphorylation events mediated by Ser/Thr phosphatases PP1 and PP2A, which might work in a different way in cancer cells with respect to healthy cells, opening a promising research line for the future.

6.7. Caspase-9b and PP2Acα2 in CLL

Disruption of alternative splicing has been related to hematological malignancies and cancer, among other diseases (Cooper et al., 2009; Makishima et al., 2012; Venables, 2006). Several mutations have been described that affect the splicing of oncogenes, tumor suppressors and other relevant genes in cancer (Srebrow and Kornblihtt, 2006); however, many alternative splicing events that take place in cancer occur in the absence of mutations in the affected genes. In some cases, spliceosome machinery elements could act as oncogenes, since abnormally expressed splicing factors in tumor cells induce the production of mRNA isoforms that are nonexistent or less abundant in normal cells, thus contributing to cancer development, progression and different response to therapy (Karni et al., 2007). These aberrant spliced forms confer some advantageous characteristics to tumor cells, showing an increased proliferation, anti-apoptotic or pro-angiogenic effect, as well as enhanced cell motility or tumor cell survival (Grosso et al., 2008).

The Serine/Threonine protein phosphatases PP1 and PP2A have an essential role also in the regulation of protein factors involved in the mechanisms of alternative mRNA processing, as SR proteins (Chalfant & Hannun, 2000). PP1 and PP2A participate in splicing as regulators of the second step of pre-mRNA splicing, dephosphorylating specific U2 and U5 snRNP proteins SAP155 and U5-116kDa (Shi et al., 2006). In another study it has been shown that endogenous ceramide produced via the *de novo* sphingolipid pathway regulates alternative pre-mRNA

splicing of Caspase-9 and Bcl-x in a mechanism mediated by PP1 (Chalfant et al., 2002; Pan et al., 2011).

In the present work we have studied the abundance of Caspase-9 and PP2Acα aberrant splicing variants in CLL, which possess an antiapoptotic and inactive function respectively.

Caspase-9b is dysregulated in several subtypes of non-small-cell lung cancer (NSCLC) patient tumors, including adenocarcinomas, squamoid carcinomas and large-cell carcinomas, and it is known to be responsible of maintaining the tumorigenic capacity of NSCLC cells and make cells resistant to erlotinib treatment (Shultz et al., 2011). Targeting the alternative splicing of Caspase-9 would sensitize NSCLC cells to already available chemotherapies, increasing their efficiency and thereby limiting their toxic side-effects (Shultz & Chalfant, 2011). In other studies it was described that the main regulatory factors of Caspase-9 alternative splicing were endogenous ceramide (Chalfant et al., 2002), SRSF1 (SRp30a or ASF/SF2) (Massiello and Chalfant, 2006; Shultz et al., 2011, 2010) and Ser52 phosphorylation of hnRNP L splicing factor. This Akt-mediated phosphorylation regulated the interaction of hnRNP L with Caspase-9 RNA influencing the differential mRNA processing, establishing hnRNP L phosphorylation as the tumor cause and evaluating its potential as biomarker and target for cancer therapy (Goehe et al., 2010; Shankarling & Lynch, 2010).

In the case of NSCLC, 78% of the patients analyzed presented a dysregulation in Caspase-9b relative abundance whereas for CLL patients analyzed in this work, only a total of 40% of the patients had moderate or high dysregulated abundance of Caspase-9b. Comparing these data with the accessible medical records of some patients, we couldn’t establish a correlation between the dysregulation in Caspase-9b and any characteristic of the disease, but we don’t discard that it may be related to any feature of this malignancy. In this sense, it will be desirable to analyze more patients and compare the data of Caspase-9b relative abundance with other parameters of the disease, as stage, prognosis, chemotherapy response, etc.

On the other hand, we have found a clear association between the dysregulation in PP2Acα2 relative abundance and CLL, as 88% of the patients analyzed showed aberrant amounts of this truncated protein. These data are

especially relevant, because for the first time PP2Acα2 overexpression is associated to a disease state, more precisely to CLL. The role of this protein is still unknown since little information is available of this spliced form in the only paper published describing its existence and inactivity (Migueleti et al., 2012). Therefore, we consider that PP2Acα2 can constitute an interesting biomarker for CLL to be implemented among clinicians for a more accurate diagnose and treatment. Comparing these results with the available medical records, we can associate a high dysregulation in PP2Acα2 to advanced stages of the disease, as all patients analyzed classified as Binet B and C, but also some patients at Binet A stage also presented a high dysregulation. Again, more patients should be analyzed to establish a tighter correlation with the disease stage and also be able to analyze the relation with other parameters of the disease.

We are also at the very preliminary stage of the analysis of other cohort belonging to different populations of CLL patients, as advanced stage patients with relapse and patients with and without mutations in IgV_H genes, among which the lack of mutations in IgV_H genes is associated to a worse prognosis. The very first results obtained in this work suggest a moderate dysregulation in patients with mutations in IgV_H genes, and therefore with better prognosis. Comparing our data with the medical records available, we can observe that a patient has a Binet score C and a Rai score IV and correlates with a moderate dysregulation in PP2Acα2, appearing again associated to advanced states of the disease. Besides, among the patients with mutated forms of IgV_H, the ones that are ZAP-70 negative also show a moderate dysregulation of PP2Acα2. In any case, we need to further analyze more patients of each group to extract reliable correlations.

In the same way as we have postulated PP2Acα2 overexpression as a biomarker of CLL, in a recent study it was described that an aberrant splicing variant of SET (SET-α) was expressed at the same level as SET-β in CLL and non-Hodgkin lymphoma cell lines and in CLL patients, correlating to more aggressive disease states (Christensen et al., 2011a).

Due to CLL molecular heterogeneity (Landau and Wu, 2013), it would be desired to analyze in further studies CLL patients at all stages of the disease, to compare genomes of patients before treatment, after treatment and relapsed cases,

what would shed light on specific lesions or mutations selected *in vivo* in the application of therapies. Moreover, study of samples across the disease and treatment process would provide useful information about different cell subpopulations and the evolution of the disease as well as the capacity to evaluate the impact of the treatment in early lesions compared to later aggressive subclones.

In the present work, we have also tried to develop an *in vitro* approach to the spliced variants Caspase-9b and PP2Acα2 to be able to characterize these proteins independently of the amount of sample, which is always a bottleneck when working with patients. Caspase-9b was cloned in pET23b vector and overexpressed in *E.coli* in the same conditions as the full length protein. Several purification conditions were tried but up to date we could only obtain soluble aggregates. Similar results were obtained for PP2Acα2, cloned as described for the full length protein, transfected in Sf9 cells, infected in High Five cells and purified under several conditions. Although it has been suggested in the literature that proteins seem to be more tolerant to structural deletions, insertions and replacements than expected (Birzele et al., 2008), we were not able to get pure well folded Caspase-9b and PP2Acα2.

6.8. Interaction between Caspase-9 and SET

As described in the introduction, Granzyme A cleaves and inactivates the SET complex, leading to a caspase-independent apoptotic pathway (Lieberman, 2010). In the present work, we have determined the binding sites of a direct interaction between Caspase-9 and SET. The interaction couldn't be confirmed *in vitro* through biophysical techniques, as it may be a transient weak interaction that was only detected by more sensitive techniques as pep-scan-based Far Western Blot assays. The interaction may not be detected also due to the lack of posttranslational modifications in the recombinant proteins from bacterial source that were necessary for the binding to take place. In this way, a further step to characterize this interaction *in vitro* would be the overexpression of Caspase-9 and SET in eukaryotic systems that would include eukaryotic posttranslational modifications in the proteins.

Despite this, we could confirm the interaction *ex vivo*, as the synthetic peptides of binding site 1 of Caspase-9 and binding site 1 of SET are capable of

inducing apoptosis in a very efficient way, blocking this interaction, albeit the function of this direct association still remains unknown.

According to the localization of the binding sites, SET would bind Caspase-9 through the small subunit of the catalytic part, responsible for substrate specificity. The third binding site located in the interdomain linker between the large and the small subunit was discarded for apoptotic assays as it was not exposed in the surface of the protein and Caspase-9 was more likely to be interacting through the small subunit. As the CARD domain is not implicated in the interaction, it may indicate that the interaction takes place with mature cleaved Caspase-9. We don't discard either that the association occurs also in the presence of PP2Acα, which is inhibited by SET in a high affinity interaction. Further experiments should be performed to elucidate if this ternary complex is binding, if they do so before or after Caspase-9 processing and eventually if SET is connecting the caspase-independent and the caspase-dependent apoptotic pathways through the direct binding to Caspase-9.

6.9. Concluding remarks

The search of new therapeutic approaches in the fight against cancer requires an understanding of the molecular events that trigger the uncontrolled proliferation and alterations in apoptosis of tumor cells. The knowledge of the protein-protein interactions that rule these processes is essential for the development of rational tools against the disease.

In the present work, we have mapped two of these interactions that regulate Caspase-9, either by dephosphorylation in the case of PP2A or with a function that still remains unknown, in the case of Inhibitor 2 of PP2A (SET). The previously described interaction between Caspase-9 and PP1 has also been revised and characterized in this work. With all this information, we have proved that targeting protein-protein interactions in this system can be achieved with the generation of competing peptides. Our experiments have also shown the validity of two independent peptide delivery methods inside the cell that constitute a valuable tool as drug carriers, obtaining promising results with the application of bifunctional peptides composed of a bioactive peptide fused to the cell-penetrating peptide DPT

and also mesoporous silica nanoparticles loaded with the bioactive peptide as a cargo.

We have also analyzed for the first time the relative abundance of the aberrant splicing variants of Caspase-9 and PP2Acα, finding that the overexpression of PP2Acα2 is present in 88% of CLL patients analyzed and is related to B and C Binet stages of the disease. Therefore, it could be used as a potential biomarker for CLL diagnose.

Finally, the knowledge of the functional significance of the aberrant splicing variant PP2Acα2 along with the optimization of the therapeutic peptides designed in this work to target protein-protein interactions and induce apoptosis specifically in tumor cells will approach us to a better scenario against cancer.

CONCLUSIONS

A great discovery does not leap completely achieved from the brain of the scientist, as Minerva sprang, all panoplied, from the head of Jupiter; it is the fruit of accumulated preliminary work. Between the days of fecund productivity are inserted days of uncertainty when nothing seems to succeed, and when even matter itself seems hostile; and it is then that one must hold out against discouragement. This without ever forsaking his inexhaustible patience, Pierre Curie used sometimes to say me: "It is nevertheless hard, this life that we have chosen". From "Pierre Curie" (1923), Marie Curie.

7. CONCLUSIONS

1. Procaspase-9 and PP1α bind directly in a transient interaction. The K_D of the binding is in the high micromolar range. Both CARD and ΔCARD Caspase-9 domains are necessary for the interaction. The second binding site in Caspase-9 sequence to PP1α is a RVxF PP1 binding motif in the human protein, but is not conserved in the murine sequence.
2. Caspase-9 and PP2Acα also present a direct interaction. Caspase-9 binds PP2Acα through the residues 363-380. The synthetic peptide covering these residues has been termed C9h. The mutation W374A disrupts the interaction with PP2Acα. W374A mutation doesn't produce any significant change in the free energy and this residue is not implicated in the stability of the protein.
3. PP2Acα binds Caspase-9 through the residues 175-194. The synthetic peptide comprising these residues has been termed PP2Ah. The single mutants L177A and R185A disrupt the interaction with Caspase-9.
4. Caspase-9 interacts with YPP2Ah with a binding affinity in the micromolar range, but this peptide is not able to activate Caspase-9 wild type full length *in vitro*.
5. 400nm mesoporous silica nanoparticles are localized in the cytoplasm when they penetrate in HeLa cells and don't present any significant toxicity upon 24h of incubation. When these nanoparticles are loaded with C9h-RhodamineB peptide, they only are capable of inducing a 10-20% reduction of cell viability upon 24h of treatment.
6. MCM-41 nanoparticles don't present any significant toxicity in HeLa cells upon 24h of incubation. MCM-41 loaded with C9hC induce a 50% reduction of cell viability after 72h of incubation, showing to be more efficient than equivalent doses of DPTmut3-C9h. Moreover, apoptosis induced by MCM-41 loaded with C9hC is equivalent to a dose up to ten times higher of DPTmut3-C9h; therefore, MCM-41 is considered a valuable tool for dose reduction and cargo delivery for cancer treatment with C9h.

7. PP1α and PP2Acα bind simultaneously to Caspase-9. In the ternary complex, PP1α doesn't bind Caspase-9 through the binding site 1, but it does so through the binding site 2. PP2Acα binding site is also maintained. In addition, new binding sites at Caspase-9 interface have been detected that support the formation of the ternary complex.

8. Among the CLL patients analyzed, 40% possess a moderate or high dysregulation in the relative abundance of Caspase-9b. More importantly, only 12% present healthy levels of PP2Acα2, 40% are moderately dysregulated and 42%, highly dysregulated. All patients belonging to disease stage Binet B or C show highly dysregulated PP2Acα2 levels. Thus, the dysregulation in PP2Acα2 expression levels constitute a potential biomarker for CLL diagnose.

9. Caspase-9 and SET (inhibitor 2 of PP2A) present a direct interaction. Three binding sites have been detected in Caspase-9 and two in SET sequence; however, the interaction has not been detected *in vitro*. The bifunctional peptides DPTmut3-C9hS4 (Caspase-9 binding site 1 to SET) and DPTmut3-SET-S1 (SET binding site 1 to Caspase-9) induce more than 80% apoptosis upon 24h of treatment, confirming the interaction and suggesting this target and these peptides as promising candidates for cancer therapy.

CONCLUSIONES

8. CONCLUSIONES

1. Procaspasa-9 y PP1α se unen directamente en una interacción transitoria. La K_D de la interacción está en el rango de micromolar bajo. Tanto el dominio CARD como el ΔCARD de Caspasa-9 son necesarios para la interacción. El segundo sitio de unión a PP1α en la secuencia de Caspasa-9 es un motivo de unión a PP1 RVxF en la proteína humana, pero no está conservado en la secuencia de ratón.
2. Caspasa-9 y PP2Acα también presentan una interacción directa. Caspasa-9 se une a PP2Acα por los residuos 363-380. El péptido sintético que abarca estos residuos se ha denominado C9h. La mutación W374A interrumpe la interacción con PP2Acα. La mutación W374A no produce ningún cambio significativo en la energía libre y este residuo no está implicado en la estabilidad de la proteína.
3. PP2Acα se une a Caspasa-9 a través de los residuos 175-194. El péptido sintético que comprende estos residuos se ha llamado PP2Ah. Los mutantes simples L177A y R185A interrumpen la interacción con Caspasa-9.
4. Caspasa-9 interacciona con YPP2Ah con una afinidad de unión en el rango de micromolar, pero este péptido no es capaz de activar a Caspasa-9 tipo silvestre completa *in vitro*.
5. Las nanopartículas mesoporosas de sílice de 400nm se localizan en el citoplasma cuando penetran en células HeLa y no presentan toxicidad significativa tras 24h de incubación. Cuando estas nanopartículas están cargadas con el péptido C9h-RhodamineB, sólo son capaces de inducir una reducción del 10-20% de la viabilidad celular tras 24h de tratamiento.
6. Las nanopartículas MCM-41 no presentan toxicidad significativa en células HeLa a las 24h de incubación. MCM-41 cargadas con C9hC inducen una reducción del 50% de la viabilidad celular a las 72h de incubación, demostrando ser más eficientes que las dosis equivalentes de DPTmut3-C9h. Además, la apoptosis inducida por MCM-41 cargadas con C9hC es equivalente a dosis hasta diez veces mayores de DPTmut3-C9h; por ello, MCM-41 se considera una herramienta valiosa para la reducción de dosis y la liberación de cargo para el tratamiento de cáncer con C9h.

7. PP1α y PP2Acα se unen simultáneamente a Caspasa-9. En el complejo ternario, PP1α no se une a Caspasa-9 a través del sitio de unión 1, pero sí lo hace a través del sitio de unión 2. El sitio de unión de PP2Acα también se mantiene. Además, se han detectado nuevos sitios de unión en la interfaz de Caspasa-9 que apoyan la formación del complejo ternario.
8. Entre los pacientes de CLL analizados, el 40% posee una desregulación moderada o alta de la abundancia relativa de Caspasa-9b. Lo que es más importante, sólo el 12% presenta niveles sanos de PP2Acα2, el 40% está moderadamente desregulado y el 42%, altamente desregulado. Todos los pacientes pertenecientes a los estadíos de la enfermedad Binet B o C muestran niveles de PP2Acα2 altamente desregulados. Por tanto, la desregulación en los niveles de expresión de PP2Acα2 constituye un potencial biomarcador para el diagnóstico de CLL.
9. Caspasa-9 y SET (inhibidor 2 de PP2A) presentan una interacción directa. Se han detectado tres sitios de unión en la secuencia de Caspasa-9 y dos en la de SET; sin embargo, no se ha detectado la interacción *in vitro*. Los péptidos bifuncionales DPTmut3-C9hS4 (sitio de unión 1 de Caspasa-9 a SET) y DPTmut3-SET-S1 (sitio de unión 1 de SET a Caspasa-9) inducen más de un 80% de apoptosis tras 24h de tratamiento, confirmando la interacción y sugiriendo esta diana y estos péptidos como candidatos prometedores para una terapia anticáncer.

9. REFERENCES

Aggen, J.B., Nairn, A.C., Chamberlin, R., 2000. Regulation of protein phosphatase-1. Chem. Biol. 7, R13–R23. doi:10.1016/S1074-5521(00)00069-7

Agostini, A., Mondragón, L., Bernardos, A., Martínez-Máñez, R., Dolores Marcos, M., Sancenón, F., Soto, J., Costero, A., Manguan-García, C., Perona, R., Moreno-Torres, M., Aparicio-Sanchis, R., Murguía, J.R., 2012. Targeted cargo delivery in senescent cells using capped mesoporous silica nanoparticles. Angew. Chemie - Int. Ed. 51, 10556–10560. doi:10.1002/anie.201204663

Alberts, B., Johnson, A., Lewis, J., Raff, M., Roberts, K., Walter, P., 2004. Biología molecular de la célula, 4th ed.

Allan, L. a., Clarke, P.R., 2009. Apoptosis and autophagy: Regulation of caspase-9 by phosphorylation. FEBS J. 276, 6063–6073. doi:10.1111/j.1742-4658.2009.07330.x

Allan, L.A., Morrice, N., Brady, S., Magee, G., Pathak, S., Clarke, P.R., 2003. Inhibition of caspase-9 through phosphorylation at Thr 125 by ERK MAPK 5, 647–655.

Alnemri, E.S., Livingston, D.J., Nicholson, D.W., Salvesen, G.S., Thornberry, N.A., Wong, W.W., Yuan, J., 1996. Human ICE/CED-3 protease nomenclature. Cell 87, 171.

Arino, J., Woon, C.W., Brautigan, D.L., Miller, T.B., Johnson, G.L., 1988. Human liver phosphatase 2A: cDNA and amino acid sequence of two catalytic subunit isotypes. Proc. Natl. Acad. Sci. U. S. A. 85, 4252–4256. doi:10.1073/pnas.85.12.4252

Arnaud, L., Chen, S., Liu, F., Li, B., Khatoon, S., Grundke-Iqbal, I., Iqbal, K., 2011. Mechanism of inhibition of PP2A activity and abnormal hyperphosphorylation of tau by I2\nPP2A/SET. FEBS Lett. 585, 2653–2659. doi:10.1016/j.febslet.2011.07.020

Arrouss, I., Decaudin, D., Choquet, S., Azar, N., Parizot, C., Zini, J.M., Nemati, F., Rebollo, A., 2015. Cell penetrating peptides as a therapeutic strategy in chronic lymphocytic leukemia. Protein Pept. Lett. 22, 539–46.

Arrouss, I., Nemati, F., Roncal, F., Wislez, M., Dorgham, K., Vallerand, D., Rabbe, N., Karboul, N., Carlotti, F., Bravo, J., Mazier, D., Decaudin, D., Rebollo, A., 2013. Specific Targeting of Caspase-9/PP2A Interaction as Potential New Anti-Cancer Therapy. PLoS One 8, e60816. doi:10.1371/journal.pone.0060816

Arya, R., White, K., 2015. Cell death in development: Signaling pathways and core mechanisms. Semin. Cell Dev. Biol. 39, 1–8. doi:10.1016/j.semcdb.2015.02.001

Ashkenazi, A., Salvesen, G., 2014. Regulated cell death: signaling and mechanisms. Annu. Rev. Cell Dev. Biol. 30, 337–356. doi:10.1146/annurev-cellbio-100913-013226

Ayllón, V., Cayla, X., García, A., Fleischer, A., Rebollo, A., 2002. The anti-apoptotic molecules Bcl-xL and Bcl-w target protein phosphatase 1α to Bad. Eur. J. Immunol. 32, 1847–1855. doi:10.1002/1521-4141(200207)32:7<1847::AID-IMMU1847>3.0.CO;2-7

Ayllón, V., Martínez-A, C., García, a, Cayla, X., Rebollo, a, 2000. Protein phosphatase 1alpha is a Ras-activated Bad phosphatase that regulates interleukin-2 deprivation-induced apoptosis. EMBO J. 19, 2237–2246. doi:10.1093/emboj/19.10.2237

Barry, M., Bleackley, R.C., 2002. Cytotoxic T lymphocytes: all roads lead to death. Nat. Rev. Immunol. 2, 401–409. doi:10.1038/nri819

Batata, a., Shen, B., 1992. Immunophenotyping of subtypes of B-chronic (mature) lymphoid leukemia: A study of 242 cases. Cancer 70, 2436–2443. doi:10.1002/1097-0142

Benezra, M., Penate-medina, O., Zanzonico, P.B., Schaer, D., Ow, H., Burns, A., Destanchina, E., Longo, V., Herz, E., Iyer, S., Wolchok, J., Larson, S.M., Wiesner, U., Bradbury, M.S., 2011. Multimodal silica nanoparticles are effective cancer-targeted probes in a model of human melanoma. J. Clin. Invest. 121, 2768–2780. doi:10.1172/JCI45600.2768

Beullens, M., Vulsteke, V., Van Eynde, A., Jagiello, I., Stalmans, W., Bollen, M., 2000. The C-terminus of NIPP1 (nuclear inhibitor of protein phosphatase-1) contains a novel binding site for protein phosphatase-1 that is controlled by tyrosine phosphorylation and RNA binding. Biochem J 352, 651–658.

Binet, J.L., Auquier, A., Dighiero, G., Chastang, C., Piguet, H., Goasguen, J., Vaugier, G., Potron, G., Colona, P., Oberling, F., Thomas, M., Tchernia, G., Jacquillat, C., Boivin, P., Lesty, C., Duault, M.T., Monconduit, M., Belabbes, S., Gremy, F., 1981. A new prognostic classification of chronic lymphocytic leukemia derived from a multivariate survival analysis. Cancer 48, 198–206. doi:10.1002/1097-0142

Birzele, F., Csaba, G., Zimmer, R., 2008. Alternative splicing and protein structure evolution. Nucleic Acids Res. 36, 550–558. doi:10.1093/nar/gkm1054

Bollen, M., Peti, W., Ragusa, M.J., Beullens, M., 2010. The extended PP1 toolkit: Designed to create specificity. Trends Biochem. Sci. 35, 450–458. doi:10.1016/j.tibs.2010.03.002

Bononi, a, Agnoletto, C., De Marchi, E., Marchi, S., Patergnani, S., Bonora, M., Giorgi, C., Missiroli, S., Poletti, F., Rimessi, a, Pinton, P., 2011. Protein kinases and phosphatases in the control of cell fate. Enzym. Res 2011, 329098. doi:10.4061/2011/329098

Bonsor, D., Butz, S.F., Solomons, J., Grant, S., Fairlamb, I.J.S., Fogg, M.J., Grogan, G., 2006. Ligation independent cloning (LIC) as a rapid route to families of recombinant biocatalysts from sequenced prokaryotic genomes. Org. Biomol. Chem. 4, 1252–1260. doi:10.1039/b517338h

Brady, S.C., Allan, L. a, Clarke, P.R., 2005. Regulation of Caspase 9 through Phosphorylation by Protein Kinase C Zeta in Response to Hyperosmotic Stress Regulation of Caspase 9 through Phosphorylation by Protein Kinase C Zeta in Response to Hyperosmotic Stress 25, 10543–10555. doi:10.1128/MCB.25.23.10543

Bratton, S.B., Salvesen, G.S., 2010. Regulation of the Apaf-1-caspase-9 apoptosome. J. Cell Sci. 123, 3209–3214. doi:10.1242/jcs.073643

Cardone, M.H., Roy, N., Stennicke, H.R., Salvesen, G.S., Franke, T.F., Stanbridge, E., Frisch, S., Reed, J.C., 1998. Regulation of cell death protease caspase-9 by phosphorylation. Science 282, 1318–1321. doi:10.1126/science.282.5392.1318

Chakravarti, D., Hong, R., 2003. SET-ting the Stage for Life and Death. Cell 112, 589–593.

Chalfant, C.E., Hannun, Y.A., 2000. The Role of Serine/Threonine Protein Phosphatases in Ceramide Signaling, in: Madame Curie Bioscience Database. Austin (TX) Landes Bioscience.

Chalfant, C.E., Rathman, K., Pinkerman, R.L., Wood, R.E., Obeid, L.M., Ogretmen, B., Hannun, Y. a., 2002. De novo ceramide regulates the alternative splicing of caspase 9 and Bcl-x in A549 lung adenocarcinoma cells. Dependence on protein phosphatase-1. J. Biol. Chem. 277, 12587–12595. doi:10.1074/jbc.M112010200

Chao, Y., Shiozaki, E.N., Srinivasula, S.M., Rigotti, D.J., Fairman, R., Shi, Y., 2005. Engineering a dimeric caspase-9: A re-evaluation of the induced proximity model for caspase activation. PLoS Biol. 3, 1079–1087. doi:10.1371/journal.pbio.0030183

Chen, L., Harrison, S.D., 2007. Cell-penetrating peptides in drug development: enabling intracellular targets. Biochem. Soc. Trans. 35, 821–825. doi:10.1042/BST0350821

Chinnaiyan, a M., 1999. The apoptosome: heart and soul of the cell death machine. Neoplasia 1, 5–15. doi:10.1038/sj.neo.7900003

Chiorazzi, N., Ferrarini, M., 2003. B cell chronic lymphocytic leukemia: lessons learned from studies of the B cell antigen receptor. Annu. Rev. Immunol. 21, 841–894. doi:10.1146/annurev.immunol.21.120601.141018

Chiorazzi, N., Rai, K.R., Ferrarini, M., 2005. Chronic lymphocytic leukemia. N. Engl. J. Med. 352, 804–815.

Cho, U. soo, Xu, W., 2007. Crystal structure of a protein phosphatase 2A heterotrimeric holoenzyme. Nature 445, 53–57. doi:10.1038/nature05351

Christensen, D.J., Chen, Y., Oddo, J., Matta, K.M., Neil, J., Davis, E.D., Volkheimer, D., Lanasa, M.C., Friedman, D.R., Goodman, B.K., Gockerman, J.P., Diehl, L.F., Castro, C.M. De, Moore, J.O., Vitek, M.P., Weinberg, J.B., Volkheimer, A.D., 2011a. SET oncoprotein overexpression in B-cell chronic lymphocytic leukemia and non-Hodgkin lymphoma: a predictor of aggressive disease and a new treatment target. Blood 118, 4150–4158. doi:10.1182/blood-2011-04-351072

Christensen, D.J., Ohkubo, N., Oddo, J., Van Kanegan, M.J., Neil, J., Li, F., Colton, C. a, Vitek, M.P., 2011b. Apolipoprotein E and peptide mimetics modulate inflammation by binding the SET protein and activating protein phosphatase 2A. J. Immunol. 186, 2535–42. doi:10.4049/jimmunol.1002847

Cohen, P., Brewis, N.D., Hughes, V., Mann, D.J., 1990. Protein serine / threonine an expanding family. Febs 268, 355–359.

Cooper, T. a., Wan, L., Dreyfuss, G., 2009. RNA and Disease. Cell 136, 777–793. doi:10.1016/j.cell.2009.02.011

Damle, R.N., Temburni, S., Calissano, C., Yancopoulos, S., Banapour, T., Sison, C., Allen, S.L., Rai, K.R., Chiorazzi, N., 2007. CD38 expression labels an activated subset within chronic lymphocytic leukemia clones enriched in proliferating B cells. Blood 110, 3352–3359. doi:10.1182/blood-2007-04-083832

Damle, R.N., Wasil, T., Fais, F., Ghiotto, F., Valetto, a, Allen, S.L., Buchbinder, a, Budman, D., Dittmar, K., Kolitz, J., Lichtman, S.M., Schulman, P., Vinciguerra, V.P., Rai, K.R., Ferrarini, M., Chiorazzi, N., 1999. Ig V gene mutation status and CD38 expression as novel prognostic indicators in chronic lymphocytic leukemia. Blood 94, 1840–1847.

Dancheck, B., Ragusa, M.J., Allaire, M., Nairn, A.C., Page, R., Peti, W., 2011. Molecular Investigations of the Structure and Function of the Protein Phosphatase 1−Spinophilin−Inhibitor 2 Heterotrimeric Complex. Biochemistry 50, 1238–1246. doi:10.1021/bi101774g

David, C.J., Manley, J.L., 2010. Alternative pre-mRNA splicing regulation in cancer: Pathways and programs unhinged. Genes Dev. 24, 2343–2364. doi:10.1101/gad.1973010

De la Torre, C., Mondragón, L., Coll, C., García-Fernández, A., Sancenón, F., Martínez-Máñez, R., Amorós, P., Pérez-Payá, E., Orzáez, M., 2015. Caspase 3 targeted cargo delivery in apoptotic cells using capped mesoporous silica nanoparticles. Chem. - A Eur. J. 21, 15506–15510. doi:10.1002/chem.201502413

De la Torre, C., Mondragon, L., Coll, C., Sancenon, F., Marcos, M.D., Martinez-Manez, R., Amoros, P., Perez-Paya, E., Orzaez, M., 2014. Cathepsin-B Induced Controlled Release from Peptide-

Capped Mesoporous Silica Nanoparticles. Chem. Eur. J. 20, 15309–15314. doi:10.1002/chem.201404382

Denault, J.-B., Salvesen, G.S., 2002a. Caspases, in: Wiley (Ed.), Current Protocols in Protein Science.

Denault, J.-B., Salvesen, G.S., 2002b. Expression, purification and characterization of Caspases, in: Wiley (Ed.), Current Protocols in Protein Science. pp. 1–15.

Dessauge, F., Cayla, X., Albar, J.P., Fleischer, A., Ghadiri, A., Duhamel, M., Rebollo, A., 2006. Identification of PP1alpha as a caspase-9 regulator in IL-2 deprivation-induced apoptosis. J. Immunol. 177, 2441–2451. doi:10.4049/jimmunol.177.4.2441

Du, C., Fang, M., Li, Y., Li, L., Wang, X., 2000. Smac, a mitochondrial protein that promotes cytochrome c-dependent caspase activation by eliminating IAP inhibition. Cell 102, 33–42. doi:10.1016/S0092-8674(00)00008-8

Earnshaw, W.C., Martins, L.M., Kaufmann, S.H., 1999. Mammalian caspases: structure, activation, substrates, and functions during apoptosis. Annu. Rev. Biochem. 68, 383–424.

Egloff, M.P., Cohen, P.T., Reinemer, P., Barford, D., 1995. Crystal structure of the catalytic subunit of human protein phosphatase 1 and its complex with tungstate. J. Mol. Biol. 254, 942–959. doi:10.1006/jmbi.1995.0667

Egloff, M.-P., Johnson, D.F., Moorhead, G., Cohen, P.T.W., Cohen, P., Barford, D., 1997. Structural basis for the recognition of regulatory subunits by the catalytic subunit of protein phosphatase 1. EMBO J. 16, 1876–87. doi:10.1093/emboj/16.8.1876

Elmore, S., 2007. Apoptosis: A review of programmed cell death. Toxicol Pathol 35, 495–516. doi:10.1037/a0030561.Striving

Fan, Z., Beresford, P.J., Zhang, D., Xu, Z., Novina, C.D., Yoshida, A., Pommier, Y., Lieberman, J., 2003. Cleaving the oxidative repair protein Ape1 enhances cell death mediated by granzyme A. Nat. Immunol. 4, 145–153. doi:10.1038/ni885

Fernald, K., Kurokawa, M., 2013. Evading apoptosis in cancer. Trends Cell Biol. 23, 620–633. doi:10.1016/j.tcb.2013.07.006

Fominaya, J., Bravo, J., Decaudin, D., Brossa, J.Y., Nemati, F., Rebollo, A., 2015a. Enhanced serum proteolysis resistance of cell-penetrating peptides. Ther. Deliv. 6, 139–147. doi:10.4155/tde.14.100

Fominaya, J., Bravo, J., Rebollo, A., 2015b. Strategies to stabilize cell penetrating peptides for in vivo applications. Ther. Deliv. 5, tde.15.51. doi:10.4155/tde.15.51

Frank, R., Overwin, H., 1996. Spot synthesis. Epitope analysis with arrays of synthetic peptides prepared on cellulose membranes., in: Morris, G.E. (Ed.), Epitope Mapping Protocols. Methods in Molecular Biology. pp. 149–170.

Garcia, A., Cayla, X., Guergnon, J., Dessauge, F., Hospital, V., Rebollo, M.P., Fleischer, A., Rebollo, A., 2003. Serine/threonine protein phosphatases PP1 and PP2A are key players in apoptosis. Biochimie 85, 721–726. doi:10.1016/j.biochi.2003.09.004

Garrido, C., Galluzzi, L., Brunet, M., Puig, P.E., Didelot, C., Kroemer, G., 2006. Mechanisms of cytochrome c release from mitochondria. Cell Death Differ. 13, 1423–1433. doi:10.1038/sj.cdd.4401950

Garzon, J.I., Lopéz-Blanco, J.R., Pons, C., Kovacs, J., Abagyan, R., Fernandez-Recio, J., Chacon, P., 2009. FRODOCK: A new approach for fast rotational protein-protein docking. Bioinformatics 25, 2544–2551. doi:10.1093/bioinformatics/btp447

Ghia, P., Ferreri, A.J.M., Caligaris-Cappio, F., 2007. Chronic lymphocytic leukemia. Crit. Rev. Oncol. Hematol. 64, 234–246. doi:10.1016/j.critrevonc.2007.04.008

Giménez, C., de la Torre, C., Gorbe, M., Aznar, E., Sancenón, F., Murguía, J.R., Martínez-Máñez, R., Marcos, M.D., Amorós, P., 2015. Gated mesoporous silica nanoparticles for the controlled delivery of drugs in cancer cells. Langmuir 31, 3753–62. doi:10.1021/acs.langmuir.5b00139

Goehe, R.W., Shultz, J.C., Murudkar, C., Usanovic, S., Lamour, N.F., Massey, D.H., Zhang, L., Camidge, D.R., Shay, J.W., Minna, J.D., Chalfant, C.E., 2010. hnRNP L regulates the tumorigenic capacity of lung cancer xenografts in mice via caspase-9 pre-mRNA processing. J. Clin. Invest. 120, 3923–3939. doi:10.1172/JCI43552

Goldberg, J., Huang, H., Kwon, Y., Greengard, P., Nairn, A.C., Kuriyan, J., 1995. Three-dimensional structure of the catalytic subunit of protein serine/threonine phosphatase-1. Nature 376, 745–753.

Goodwin, D., Simerska, P., Toth, I., 2012. Peptides As Therapeutics with Enhanced Bioactivity. Curr. Med. Chem. 19, 4451–4461. doi:10.2174/092986712803251548

Grosso, A.R., Martins, S., Carmo-Fonseca, M., 2008. The emerging role of splicing factors in cancer. EMBO Rep. 9, 1087–1093. doi:10.1038/embor.2008.189

Guergnon, J., Dessauge, F., Dominguez, V., Viallet, J., Bonnefoy, S., Yuste, V.J., Mercereau-Puijalon, O., Cayla, X., Rebollo, A., Susin, S. a, Bost, P.-E., Garcia, A., 2006. Use of penetrating peptides interacting with PP1/PP2A proteins as a general approach for a drug phosphatase technology. Mol. Pharmacol. 69, 1115–1124. doi:10.1124/mol.105.019364

Hamblin, B.T.J., Davis, Z., Gardiner, A., Oscier, D.G., Stevenson, F.K., 1999. Unmutated Ig VH genes are associated with a more aggresive form of chronic lymphocytic leukemia. Blood 94, 1848–1854.

Hassan, M., Watari, H., AbuAlmaaty, A., Ohba, Y., Sakuragi, N., 2014. Apoptosis and molecular targeting therapy in cancer. Biomed Res. Int. 2014, 150845. doi:10.1155/2014/150845

He, Q., Shi, J., 2014. MSN anti-cancer nanomedicines: Chemotherapy enhancement, overcoming of drug resistance, and metastasis inhibition. Adv. Mater. 26, 391–411. doi:10.1002/adma.201303123

Hemmings, B. a, Adams-Pearson, C., Maurer, F., Müller, P., Goris, J., Merlevede, W., Hofsteenge, J., Stone, S.R., 1990. alpha- and beta-forms of the 65-kDa subunit of protein phosphatase 2A have a similar 39 amino acid repeating structure. Biochemistry 29, 3166–73. doi:10.1021/bi00465a002

Hendrickx, A., Beullens, M., Ceulemans, H., Den Abt, T., Van Eynde, A., Nicolaescu, E., Lesage, B., Bollen, M., 2009. Docking Motif-Guided Mapping of the Interactome of Protein Phosphatase-1. Chem. Biol. 16, 365–371. doi:10.1016/j.chembiol.2009.02.012

Hsu, H., Xiong, J., Goeddel, D. V, 1995. The TNF receptor I-associated protein TRADD signals cell death and NF-kB activation. Cell 81, 495–504.

Inamdar, K. V., Bueso-Ramos, C.E., 2007. Pathology of chronic lymphocytic leukemia: an update. Ann. Diagn. Pathol. 11, 363–389. doi:10.1016/j.anndiagpath.2007.08.002

Ito, A., Koma, Y., Watabe, K., Nagano, T., Endo, Y., Nojima, H., Kitamura, Y., 2003. A Truncated Isoform of the Protein Phosphatase 2A B56γ Regulatory Subunit May Promote Genetic Instability and Cause Tumor Progression. Am. J. Pathol. 162, 81–91. doi:10.1016/S0002-9440(10)63800-X

Janssens, V., Goris, J., 2001. Phosphatases Implicated in Cell Growth and Signalling. Society 439, 417–439.

Janssens, V., Goris, J., Van Hoof, C., 2005. PP2A: The expected tumor suppressor. Curr. Opin. Genet. Dev. 15, 34–41. doi:10.1016/j.gde.2004.12.004

Kang, H.S., Choi, I., 2001. Protein phosphatase 2A modulates the proliferation of human multiple myeloma cells via regulation of the production of reactive oxygen intermediates and anti-apoptotic factors. Cell. Immunol. 213, 34–44. doi:10.1006/cimm.2001.1861

Karni, R., de Stanchina, E., Lowe, S.W., Sinha, R., Mu, D., Krainer, A.R., Wang, G.-S., Cooper, T. a, 2007. The gene encoding the splicing factor SF2/ASF is a proto-oncogene. Nat. Rev. Genet. 14, 749–761. doi:10.1038/nrg2164

Katayose, Y., Li, M., Al-murrani, S.W.K., Shenolikar, S., Damuni, Z., 2000. Protein Phosphatase 2A Inhibitors , I PP2A and I PP2A , Associate with and Modify the Substrate Specificity of Protein Phosphatase 1. Biochemistry 275, 9209 –9214. doi:10.1074/jbc.275.13.9209

Kelker, M.S., Page, R., Peti, W., 2009. Crystal Structures of Protein Phosphatase-1 Bound to Nodularin-R and Tautomycin: A Novel Scaffold for Structure-based Drug Design of Serine/Threonine Phosphatase Inhibitors. J. Mol. Biol. 385, 11–21. doi:10.1016/j.jmb.2008.10.053

Kerr, J.F.R., Wyllie, A.H., Currie, A.R., 1972. Apoptosis: A basic biological phenomenon with wide-ranging implications in tissue kinetics. Br. J. Cancer 26, 239–257.

Kischkel, F.C., Hellbardt, S., Behrmann, I., Germer, M., Pawlita, M., Krammer, P.H., Peter, M.E., 1995. Cytotoxicity-dependent APO-1 (Fas/CD95)-associated proteins form a death-inducing signaling complex (DISC) with the receptor. EMBO J. 14, 5579–88.

Kitada, S., Andersen, J., Akar, S., Zapata, J.M., Takayama, S., Krajewski, S., Wang, H.G., Zhang, X., Bullrich, F., Croce, C.M., Rai, K., Hines, J., Reed, J.C., 1998. Expression of apoptosis-regulating proteins in chronic lymphocytic leukemia: correlations with In vitro and In vivo chemoresponses. Blood 91, 3379–3389.

Klein, a, Miera, O., Bauer, O., Golfier, S., Schriever, F., 2000. Chemosensitivity of B cell chronic lymphocytic leukemia and correlated expression of proteins regulating apoptosis, cell cycle and DNA repair. Leukemia 14, 40–46. doi:10.1038/sj.leu.2401636

Kola, I., Landis, J., 2004. Can the pharmaceutical industry reduce attrition rates? Nat. Rev. Drug Discov. 3, 711–715. doi:10.1038/nrd1470

Kolupaeva, V., Janssens, V., 2013. PP1 and PP2A phosphatases - Cooperating partners in modulating retinoblastoma protein activation. FEBS J. 280, 627–643. doi:10.1111/j.1742-4658.2012.08511.x

Koma, Y., Ito, A., Watabe, K., Kimura, S.H., Kitamura, Y., 2004. A truncated isoform of the PP2A B56γ regulatory subunit reduces irradiation-induced Mdm2 phosphorylation and could contribute to metastatic melanoma cell radioresistance. Histol. Histopathol. 19, 391–400.

Kresge, C.T., Leonowicz, M.E., Roth, W.J., Vartuli, J.C., Beck, J.S., 1992. Ordered mesoporous molecular sieves synthesized by a liquid crystal template mechanism. Nature 359, 710–712.

Kumar, D., Bhalla, T.C., 2005. Microbial proteases in peptide synthesis: approaches and applications. Appl. Microbiol. Biotechnol. 68, 726–736. doi:10.1007/s00253-005-0094-7

Kuo, Y., Huang, K., Chiang, C.-W., Yang, C.-H., Yang, Y.-S., Lee, W.-Y., 2008. Regulation of phosphorylation of Thr-308 of Akt, cell proliferation, and survival by the B55alpha regulatory

subunit targeting of the protein phosphatase 2A holoenzyme to Akt. J. Biol. Chem. 283, 1882–92. doi:10.1074/jbc.M709585200

Kwon, S., Singh, R.K., Perez, R. a., Abou Neel, E. a., Kim, H.-W., Chrzanowski, W., 2013. Silica-based mesoporous nanoparticles for controlled drug delivery. J. Tissue Eng. 4. doi:10.1177/2041731413503357

Landau, D. a, Wu, C.J., 2013. Chronic lymphocytic leukemia: molecular heterogeneity revealed by high-throughput genomics. Genome Med. 5, 47. doi:10.1186/gm451

Lechward, K., Awotunde, O.S., ŚwiąTek, W., Muszyńska, G., 2001. Protein phosphatase 2A: Variety of forms and diversity of functions. Acta Biochim. Pol. 48, 921–933.

Li, M., Makkinje, A., Damuni, Z., 1996. The Myeloid Leukemia- associated Protein SET Is a Potent Inhibitor of Protein Phosphatase 2A. J. Biol. Chem. 271, 11059–11062.

Li, Z., Barnes, J.C., Bosoy, A., Stoddart, J.F., Zink, J.I., 2012. Mesoporous silica nanoparticles in biomedical applications. Chem. Soc. Rev. 41, 2590. doi:10.1039/c1cs15246g

Lieberman, J., 2010. Granzyme A activates another way to die. Immunol. Rev. 235, 93–104. doi:10.1111/j.0105-2896.2010.00902.x

Lieberman, J., Fan, Z., 2003. Nuclear war: the granzyme A-bomb. Curr. Opin. Immunol. 15, 553–559. doi:10.1016/S0952-7915(03)00108-0

Livak, K.J., Schmittgen, T.D., 2001. Analysis of Relative Gene Expression Data Using Real-Time Quantitative PCR and the 2−ΔΔCT Method. Methods 25, 402–408. doi:10.1006/meth.2001.1262

Locksley, R.M., Killeen, N., Lenardo, M.J., 2001. The TNF and TNF receptor superfamilies: Integrating mammalian biology. Cell 104, 487–501. doi:10.1016/S0092-8674(01)00237-9

Lu, J., Liong, M., Li, Z., Zink, J.I., Tamanoi, F., 2010. Biocompatibility, biodistribution, and drug-delivery efficiency of mesoporous silica nanoparticles for cancer therapy in animals. Small 6, 1794–1805. doi:10.1002/smll.201000538

Makishima, H., Visconte, V., Sakaguchi, H., Jankowska, A.M., Kar, S.A., Jerez, A., Przychodzen, B., Bupathi, M., Guinta, K., Afable, M.G., Sekeres, M. a., Padgett, R. a., Tiu, R. V., Maciejewski, J.P., 2012. Mutations in the spliceosome machinery, a novel and ubiquitous pathway in leukemogenesis. Blood 119, 3203–3210. doi:10.1182/blood-2011-12-399774

Martin, M.C., Allan, L. a., Lickrish, M., Sampson, C., Morrice, N., Clarke, P.R., 2005. Protein Kinase A Regulates Caspase-9 Activation by Apaf-1 Downstream of Cytochrome c. J. Biol. Chem. 280, 15449–15455. doi:10.1074/jbc.M414325200

Martinvalet, D., Zhu, P., Lieberman, J., 2005. Granzyme A Induces Caspase-Independent Mitochondrial Damage, a Required First Step for Apoptosis. Immunity 22, 355–370. doi:10.1016/j.immuni.2005.02.004

Mas, N., Galiana, I., Mondragón, L., Aznar, E., Climent, E., Cabedo, N., Sancenõn, F., Murguía, J.R., Martínez-Máñez, R., Marcos, M.D., Amorós, P., 2013. Enhanced efficacy and broadening of antibacterial action of drugs via the use of capped mesoporous nanoparticles. Chem. - A Eur. J. 19, 11167–11171. doi:10.1002/chem.201302170

Massiello, A., Chalfant, C.E., 2006. SRp30a (ASF/SF2) regulates the alternative splicing of caspase-9 pre-mRNA and is required for ceramide-responsiveness. J. Lipid Res. 47, 892–897. doi:10.1194/jlr.C600003-JLR200

Matutes, E., Owusu-Ankomah, K.A., Morilla, R.M., García Marco, J., Houlihan, A., Que, T.H., Catovsky, D., 1994. The immunological profile of B-cell disorders and proposal of a scoring system for the diagnosis of CLL. Leukemia 8, 1640–1645.

McDonnell, M. a., Abedin, M.J., Melendez, M., Platikanova, T.N., Ecklund, J.R., Ahmed, K., Kelekar, a., 2008. Phosphorylation of Murine Caspase-9 by the Protein Kinase Casein Kinase 2 Regulates Its Cleavage by Caspase-8. J. Biol. Chem. 283, 20149–20158. doi:10.1074/jbc.M802846200

Migueleti, D.L.S., Smetana, J.H.C., Nunes, H.F., Kobarg, J., Zanchin, N.I.T., 2012. Identification and Characterization of an Alternatively Spliced Isoform of the Human Protein Phosphatase 2A Catalytic Subunit. J. Biol. Chem. 287, 4853–4862. doi:10.1074/jbc.M111.283341

Mondragón, L., Mas, N., Ferragud, V., de la Torre, C., Agostini, A., Martínez-Máñez, R., Sancenón, F., Amorós, P., Pérez-Payá, E., Orzáez, M., 2014. Enzyme-Responsive Intracellular-Controlled Release Using Silica Mesoporous Nanoparticles Capped with ε-Poly-L-lysine. Chem. - A Eur. J. 20, 5271–5281. doi:10.1002/chem.201400148

Moreau, E.J., Matutes, E., A'Hern, R.P., Morilla, A.M., Morilla, R.M., Owusu-Ankomah, K.A., Seon, B.K., Catovsky, D., 1997. Improvement of the chronic lymphocytic leukemia scoring system with the monoclonal antibody SN8 (CD79b). Am. J. Clin. Pathol. 108, 378–382.

Mumby, M., 2007a. PP2A: Unveiling a Reluctant Tumor Suppressor. Cell 130, 21–24. doi:10.1016/j.cell.2007.06.034

Mumby, M., 2007b. The 3D Structure of Protein Phosphatase 2A: New Insights into a Ubiquitous Regulator of Cell Signaling. ACS Chem. Biol. 2, 99–103. doi:10.1021/cb700021z

Muto, S., Senda, M., Akai, Y., Sato, L., Suzuki, T., Nagai, R., Senda, T., Horikoshi, M., 2007. Relationship between the structure of SET/TAF-Ibeta/INHAT and its histone chaperone activity. Proc. Natl. Acad. Sci. U. S. A. 104, 4285–4290. doi:10.1073/pnas.0603762104

Myles, T., Schmidt, K., Evans, D.R.H., Cron, P., Hemmings, B.A., 2001. Active-site mutations impairing the catalytic function of the catalytic subunit of human protein phosphatase 2A permit baculovirus-mediated overexpression in insect cells. Biochem J 357, 225–232.

Nikoletopoulou, V., Markaki, M., Palikaras, K., Tavernarakis, N., 2013. Crosstalk between apoptosis, necrosis and autophagy. Biochim. Biophys. Acta - Mol. Cell Res. 1833, 3448–3459. doi:10.1016/j.bbamcr.2013.06.001

Packham, G., Stevenson, F.K., 2005. Bodyguards and assassins: Bcl-2 family proteins and apoptosis control in chronic lymphocytic leukaemia. Immunology 114, 441–449. doi:10.1111/j.1365-2567.2005.02117.x

Pan, D., Boon-Unge, K., Govitrapong, P., Zhou, J., 2011. Emetine regulates the alternative splicing of caspase 9 in tumor cells. Oncol. Lett. 2, 1309–1312. doi:10.3892/ol.2011.395

Parrish, A.B., Freel, C.D., Kornbluth, S., 2013. Cellular mechanisms controlling caspase activation and function. Cold Spring Harb. Perspect. Biol. 5. doi:10.1101/cshperspect.a008672

Peti, W., Nairn, A.C., Page, R., 2013. Structural basis for protein phosphatase 1 regulation and specificity. FEBS J. 280, 596–611. doi:10.1111/j.1742-4658.2012.08509.x

Peti, W., Page, R., 2007. Strategies to maximize heterologous protein expression in Escherichia coli with minimal cost. Protein Expr. Purif. 51, 1–10. doi:10.1016/j.pep.2006.06.024

Quesada, V., Conde, L., Villamor, N., Ordóñez, G.R., Jares, P., Bassaganyas, L., Ramsay, A.J., Beà, S., Pinyol, M., Martínez-Trillos, A., López-Guerra, M., Colomer, D., Navarro, A., Baumann, T., Aymerich, M., Rozman, M., Delgado, J., Giné, E., Hernández, J.M., González-Díaz, M., Puente, D. a, Velasco, G., Freije, J.M.P., Tubío, J.M.C., Royo, R., Gelpí, J.L., Orozco, M., Pisano, D.G., Zamora, J., Vázquez, M., Valencia, A., Himmelbauer, H., Bayés, M., Heath, S., Gut, M., Gut, I., Estivill, X., López-Guillermo, A., Puente, X.S., Campo, E., López-Otín, C., 2011. Exome sequencing identifies recurrent mutations of the splicing factor SF3B1 gene in chronic lymphocytic leukemia. Nat. Genet. 44, 47–52. doi:10.1038/ng.1032

Rai, K.R., Sawitsky, A., Cronkite, E.P., Chanana, A.D., N, L.R., S, P.B., 1975. Clinical staging of chronic lymphocytic leukemia. Blood 46, 219–234.

Raina, D., Pandey, P., Ahmad, R., Bharti, a., Ren, J., Kharbanda, S., Weichselbaum, R., Kufe, D., 2005. c-Abl Tyrosine Kinase Regulates Caspase-9 Autocleavage in the Apoptotic Response to DNA Damage. J. Biol. Chem. 280, 11147–11151. doi:10.1074/jbc.M413787200

Rassenti, L.Z., Huynh, L., Toy, T.L., Chen, L., Keating, M.J., Gribben, J.G., Neuberg, D.S., Flinn, I.W., Rai, K.R., Byrd, J.C., Kay, N.E., Greaves, A., Weiss, A., Kipps, T.J., 2004. ZAP-70 compared with immunoglobulin heavy-chain gene mutation status as a predictor of disease

progression in chronic lymphocytic leukemia. N. Engl. J. Med. 351, 893–901. doi:10.1056/NEJMoa040857

Ray, R.M., Bhattacharya, S., Johnson, L.R., 2005. Protein phosphatase 2A regulates apoptosis in intestinal epithelial cells. J. Biol. Chem. 280, 31091–31100. doi:10.1074/jbc.M503041200

Rebollo, A., Decaudin, D., Nemati, F., 2013a. Chimeric peptides including a penetrating peptide and a binding domain of pp2a catalytic subunit to caspase-9. EP2621944 A2.

Rebollo, A., García, A., Cayla, X., Arrouss, I., Billot, K., Godet, A.N., 2010. Pro-apoptotic peptides. WO2010/112471 A1.

Rebollo, A., Nemati, F., Decaudin, D., Bravo, J., Fominaya, J., 2013b. Cell-penetrating peptides. WO2013/098337 A1.

Renatus, M., Stennicke, H.R., Scott, F.L., Liddington, R.C., Salvesen, G.S., 2001. Dimer formation drives the activation of the cell death protease caspase 9. Proc. Natl. Acad. Sci. U. S. A. 98, 14250–14255. doi:10.1073/pnas.231465798

Riedl, S.J., Fuentes-Prior, P., Renatus, M., Kairies, N., Krapp, S., Huber, R., Salvesen, G.S., Bode, W., 2001. Structural basis for the activation of human procaspase-7. Proc. Natl. Acad. Sci. U. S. A. 98, 14790–5. doi:10.1073/pnas.221580098

Ringshausen, I., Schneller, F., Bogner, C., Hipp, S., Duyster, J., Peschel, C., Decker, T., 2002. Constitutively activated phosphatidylinositol-3 kinase (PI-3K) is involved in the defect of apoptosis in B-CLL: Association with protein kinase Cδ. Blood 100, 3741–3748. doi:10.1182/blood-2002-02-0539

Rossi, D., Bruscaggin, A., Spina, V., Rasi, S., Khiabanian, H., Messina, M., Fangazio, M., Vaisitti, T., Monti, S., Chiaretti, S., Guarini, A., Giudice, I. Del, Cerri, M., Cresta, S., Deambrogi, C., Gargiulo, E., Gattei, V., Bertoni, F., Deaglio, S., Rabadan, R., Pasqualucci, L., Foà, R., Forconi, F., Foa, R., 2011. Mutations of the SF3B1 splicing factor in chronic lymphocytic leukemia: association with progression and fludarabine-refractoriness 118, 6904–6908. doi:10.1182/blood-2011-08-373159

Rozman, C., Montserrat, E., 1995. Chronic lymphocytic leukemia. N. Engl. J. Med. 333, 1052–1057.

Rozovski, U., Keating, M., Estrov, Z., 2013. The significance of spliceosome mutations in chronic lymphocytic leukemia. Leuk. Lymphoma 54, 1364–1366. doi:10.3109/10428194.2012.742528

Rubin, E., Mittnacht, S., Villa-Moruzzi, E., Ludlow, J.W., 2001. Site-specific and temporally-regulated retinoblastoma protein dephosphorylation by protein phosphatase type 1. Oncogene 20, 3776–3785. doi:10.1038/sj.onc.1204518

Ruediger, R., Pham, H.T., Walter, G., 2001. Disruption of protein phosphatase 2A subunit interaction in human cancers with mutations in the A alpha subunit gene. Oncogene 20, 10–15.

Russell, J.H., Ley, T.J., 2002. Lymphocyte-mediated cytotoxicity. Annu. Rev. Immunol. 20, 323–370. doi:10.1146/annurev.immunol.20.100201.131730

Saelens, X., Festjens, N., Walle, L. Vande, Gurp, M. Van, Loo, G. Van, Vandenabeele, P., 2004. Toxic proteins released from mitochondria in cell death. Oncogene 23, 2861–2874. doi:10.1038/sj.onc.1207523

Salvesen, G.S., Ashkenazi, A., 2011. SnapShot: Caspases. Cell 147, 476–476.e1. doi:10.1016/j.cell.2011.09.030

Schwerk, C., Schulze-Osthoff, K., 2005. Regulation of apoptosis by alternative pre-mRNA splicing. Mol. Cell 19, 1–13. doi:10.1016/j.molcel.2005.05.026

Schymkowitz, J., Borg, J., Stricher, F., Nys, R., Rousseau, F., Serrano, L., 2005. The FoldX web server: An online force field. Nucleic Acids Res. 33, 382–388. doi:10.1093/nar/gki387

Seifert, A., Clarke, P.R., 2009. p38 α - and DYRK1A-dependent phosphorylation of caspase-9 at an inhibitory site in response to hyperosmotic stress. Cell. Signal. 21, 1626–1633. doi:10.1016/j.cellsig.2009.06.009

Seol, D.W., Billiar, T.R., 1999. A caspase-9 variant missing the catalytic site is an endogenous inhibitor of apoptosis. J. Biol. Chem. 274, 2072–2076. doi:10.1074/jbc.274.4.2072

Shankarling, G., Lynch, K.W., 2010. Living or dying by RNA processing: Caspase expression in NSCLC. J. Clin. Invest. 120, 3798–3801. doi:10.1172/JCI45037

Shi, Y., Reddy, B., Manley, J.L., 2006. PP1/PP2A Phosphatases Are Required for the Second Step of Pre-mRNA Splicing and Target Specific snRNP Proteins. Mol. Cell 23, 819–829. doi:10.1016/j.molcel.2006.07.022

Shultz, J.C., Chalfant, C.E., 2011. Caspase 9b: a new target for therapy in non-small-cell lung cancer. Expert Rev. Anticancer Ther. 11, 499–502. doi:10.1586/era.11.23

Shultz, J.C., Goehe, R.W., Murudkar, C.S., Wijesinghe, D.S., Mayton, E.K., Massiello, A., Hawkins, A.J., Mukerjee, P., Pinkerman, R.L., Park, M. a, Chalfant, C.E., 2011. SRSF1 regulates the alternative splicing of caspase 9 via a novel intronic splicing enhancer affecting the chemotherapeutic sensitivity of non-small cell lung cancer cells. Mol. Cancer Res. 9, 889–900. doi:10.1158/1541-7786.MCR-11-0061

Shultz, J.C., Goehe, R.W., Wijesinghe, D.S., Murudkar, C., Hawkins, A.J., Shay, J.W., Minna, J.D., Chalfant, C.E., 2010. Alternative splicing of caspase 9 is modulated by the phosphoinositide 3-

kinase/Akt pathway via phosphorylation of SRp30a. Cancer Res. 70, 9185–9196. doi:10.1158/0008-5472.CAN-10-1545

Silke, J., Meier, P., 2013. Inhibitor of Apoptosis (IAP) Proteins – Modulators of Cell Death and Inflammation. Cold Spring Harb Perspect Biol 5. doi:10.1101/cshperspect.a008730

Singh, K., Communal, C., Colucci, W.S., 2000. Inhibition of protein phosphatase 1 induces apoptosis in neonatal rat cardiac myocytes: role of adrenergic receptor stimulation. Basic Res. Cardiol. 95, 389–396.

Srebrow, A., Kornblihtt, A.R., 2006. The connection between splicing and cancer. J. Cell Sci. 119, 2635–2641. doi:10.1242/jcs.03053

Srinivasula, S.M., Ahmad, M., Fernandes-Alnemri, T., Alnemri, E.S., 1998. Autoactivation of procaspase-9 by Apaf-1-mediated oligomerization. Mol. Cell 1, 949–957. doi:10.1016/S1097-2765(00)80095-7

Srinivasula, S.M., Ahmad, M., Guo, Y., Zhan, Y., Lazebnik, Y., Fernandes-Alnemri, T., Alnemri, E.S., 1999. Identification of an endogenous dominant-negative short isoform of caspase-9 that can regulate apoptosis. Cancer Res. 59, 999–1002.

Sultana, A., Lee, J.E., 2015. Measuring Protein-Protein and Protein-Nucleic Acid Interactions by Biolayer Interferometry, in: Current Protocols in Protein Science. John Wiley & Sons, Inc., Hoboken, NJ, USA, pp. 19.25.1–19.25.26. doi:10.1002/0471140864.ps1925s79

Suzuki, K., Takahashi, K., 2003. Reduced expression of the regulatory A subunit of serine/threonine protein phosphatase 2A in human breast cancer MCF-7 cells. Int J Oncol 23, 1263–1268.

Switzer, C.H., Cheng, R.Y.S., Vitek, T.M., Christensen, D.J., Wink, D. a, Vitek, M.P., 2011. Targeting SET/I(2)PP2A oncoprotein functions as a multi-pathway strategy for cancer therapy. Oncogene 30, 2504–13. doi:10.1038/onc.2010.622

Takagi, Y., Futamura, M., Yamaguchi, K., Aoki, S., Takahashi, T., Saji, S., 2000. Alterations of the PPP2R1B gene located at 11q23 in human colorectal cancers. Gut 47, 268–71. doi:10.1136/gut.47.2.268

Thundimadathil, J., 2012. Cancer treatment using peptides: current therapies and future prospects. J. Amino Acids 2012, 967347. doi:10.1155/2012/967347

Török, N.J., Higuchi, H., Bronk, S., Caspase, N., To, N.J., 2002. Nitric Oxide Inhibits Apoptosis Downstream of Cytochrome c Release by Nitrosylating Caspase 9 Nitric Oxide Inhibits Apoptosis Downstream of Cytochrome c Release by 1648–1653.

Vallet-Regí, M., 2006. Ordered Mesoporous Materials in the Context of Drug Delivery Systems and Bone Tissue Engineering. Chem. - A Eur. J. 12, 5934–5943. doi:10.1002/chem.200600226

Vallet-Regí, M., Rámila, A., Del Real, R.P., Pérez-Pariente, J., 2001. A new property of MCM-41: Drug delivery system. Chem. Mater. 13, 308–311. doi:10.1021/cm0011559

Van Hoof, C., Goris, J., 2003. Phosphatases in apoptosis: To be or not to be, PP2A is in the heart of the question. Biochim. Biophys. Acta - Mol. Cell Res. 1640, 97–104. doi:10.1016/S0167-4889(03)00029-6

Vandomme, A., 2014. Caractérisation fonctionnelle du PhosphoTyrosyl Phosphatase Activator chez Plasmodium falciparum : rôle dans la régulation de PP2A et de PP1. Université de Lille II.

Venables, J.P., 2006. Unbalanced alternative splicing and its significance in cancer. BioEssays 28, 378–386. doi:10.1002/bies.20390

Vlieghe, P., Lisowski, V., Martinez, J., Khrestchatisky, M., 2010. Synthetic therapeutic peptides: science and market. Drug Discov. Today 15, 40–56. doi:10.1016/j.drudis.2009.10.009

Von Lindern, M., Baal, S. Van, Wiegant, J., Raap, A., Hagemeijer, A., Grosveldl, G., 1992. Putative Oncogene Associated with Myeloid 12, 3346–3355.

Vu, N.T., Park, M. a., Shultz, J.C., Goehe, R.W., Hoeferlin, L.A., Shultz, M.D., Smith, S. a., Lynch, K.W., Chalfant, C.E., 2013. HnRNP U enhances caspase-9 splicing and is modulated by AKT-dependent phosphorylation of hnRNP L. J. Biol. Chem. 288, 8575–8584. doi:10.1074/jbc.M112.443333

Wadzinski, B.E., Eisfelder, B.J., Peruski, L.F., Mumby, M.C., Johnson, G.L., 1992. NH2-terminal modification of the phosphatase 2A catalytic subunit allows functional expression in mammalian cells. J. Biol. Chem. 267, 16883–16888.

Wajant, H., 2002. The Fas signaling pathway: more than a paradigm. Science 296, 1635–1636. doi:10.1126/science.1071553

Wang, L., Lawrence, M.S., Wan, Y., Stojanov, P., Sougnez, C., Stevenson, K., Werner, L., Sivachenko, A., DeLuca, D.S., Zhang, L., Zhang, W., Vartanov, A.R., Fernandes, S.M., Goldstein, N.R., Folco, E.G., Cibulskis, K., Tesar, B., Sievers, Q.L., Shefler, E., Gabriel, S., Hacohen, N., Reed, R., Meyerson, M., Golub, T.R., Lander, E.S., Neuberg, D., Brown, J.R., Getz, G., Wu, C.J., 2011. and Other Novel Cancer Genes in Chronic Lymphocytic Leukemia. N. Engl. J. Med. 365, 2497–2506. doi:10.1056/NEJMoa1109016

Wang, S., Xie, W., Wang, D., Peng, Z., Zheng, Y., 2015. Discovery of a small molecule targeting SET-PP2A interaction to overcome BCR-ABL T315I mutation of chronic myeloid leukemia 6, 1–13.

Wang, S.S., Esplin, E.D., Li, J.L., Huang, L., Gazdar, A., Minna, J., Evans, G.A., 1998. Alterations of the PPP2R1B Gene in Human Lung and Colon Cancer 282, 284–288.

Wong, L.L., Zhang, D., Chang, C.F., Koay, E.S.C., 2010. Silencing of the PP2A catalytic subunit causes HER-2/neu positive breast cancer cells to undergo apoptosis. Exp. Cell Res. 316, 3387–3396. doi:10.1016/j.yexcr.2010.06.007

Wu, S.-H., Hung, Y., Mou, C.-Y., 2011. Mesoporous silica nanoparticles as nanocarriers. Chem. Commun. 47, 9972. doi:10.1039/c1cc11760b

Xiao, L., Gong, L.-L., Yuan, D., Deng, M., Zeng, X.-M., Chen, L.-L., Zhang, L., Yan, Q., Liu, J.-P., Hu, X.-H., Sun, S.-M., Liu, J., Ma, H.-L., Zheng, C.-B., Fu, H., Chen, P.-C., Zhao, J.-Q., Xie, S.-S., Zou, L.-J., Xiao, Y.-M., Liu, W.-B., Zhang, J., Liu, Y., Li, D.W.-C., 2010. Protein phosphatase-1 regulates Akt1 signal transduction pathway to control gene expression, cell survival and differentiation. Cell Death Differ. 17, 1448–1462. doi:10.1038/cdd.2010.16

Xing, Y., Xu, Y., Chen, Y., Jeffrey, P.D., Chao, Y., Lin, Z., Li, Z., Strack, S., Stock, J.B., Shi, Y., 2006. Structure of Protein Phosphatase 2A Core Enzyme Bound to Tumor-Inducing Toxins. Cell 127, 341–353. doi:10.1016/j.cell.2006.09.025

Yuan, S., Yu, X., Asara, J.M., Heuser, J.E., Ludtke, S.J., Akey, C.W., 2011. The holo-apoptosome: Activation of procaspase-9 and interactions with caspase-3. Structure 19, 1084–1096. doi:10.1016/j.str.2011.07.001

Yuan, S., Yu, X., Topf, M., Ludtke, S.J., Wang, X., Akey, C.W., 2010. Structure of an apoptosome-procaspase-9 CARD complex. Structure 18, 571–583. doi:10.1016/j.str.2010.04.001

Zinzalla, G., Thurston, D.E., 2009. Targeting protein-protein interactions for therapeutic intervention: a challenge for the future. Future Med. Chem. 1, 65–93. doi:10.4155/fmc.09.12

Zonta, F., Pagano, M.A., Trentin, L., Tibaldi, E., Frezzato, F., Trimarco, V., Facco, M., Zagotto, G., Pavan, V., Ribaudo, G., Bordin, L., Semenzato, G., Brunati, A.M., Lyn, C.H., 2015. Lyn sustains oncogenic signaling in chronic lymphocytic leukemia by strengthening SET-mediated inhibition of PP2A 125, 3747–3756. doi:10.1182/blood-2014-12-619155.F.Z.

Zou, H., Li, Y., Liu, X., Wang, X., 1999. An APAf-1·cytochrome C multimeric complex is a functional apoptosome that activates procaspase-9. J. Biol. Chem. 274, 11549–11556. doi:10.1074/jbc.274.17.11549